

**Biogeochemical cycling through the  
Neoproterozoic-Cambrian transition in China:  
an integrated study of redox-sensitive  
elements**

**Ph.D.-Thesis**

by

**Lawrence Michael Och**

**Supervised by**

**Dr. Graham A. Shields-Zhou and Prof. John McArthur**

**University College London (UCL)**

**Department of Earth Sciences**

**April 5, 2011**

I, Lawrence Och confirm that the work presented in this thesis is my own. Where information has been derived from other sources, I conform that this has been indicated in the thesis.

## Abstract

I investigated changes in biogeochemical cycling during the Precambrian-Cambrian transition on the Yangtze Platform in South China by analyzing about 350 predominantly black shale samples from several sedimentary successions deposited during the interval from the Late Cryogenian to the Lower Cambrian. I focused on redox-sensitive trace-metal concentrations in these sediments, whereby special attention is paid to molybdenum, vanadium and uranium to try to pinpoint the onset of increasing atmospheric oxygen levels and the transition from widespread euxinia to a pervasively oxygenated deep ocean. The measurements have been carried out using X-ray fluorescence analysis (XRF) and inductively coupled plasma mass spectrometry (ICP-MS). Besides that, total organic carbon and total sulphur contents have been measured for all samples. This approach is completed by iron speciation analysis which is considered to be a reliable redox proxy. I also conducted extended literature research on trace-metal enrichments in anoxic sediments throughout Earth history as well as a major review (which will be included as an extended introduction) on all currently available lines of evidence for a major Neoproterozoic Oxygenation Event, including carbon, sulphur, strontium, molybdenum and chromium isotope studies.

I show that the well preserved sedimentary succession from the Precambrian-Cambrian transition on the Yangtze Platform might represent a unique archive of ancient geochemical conditions on the Earth's surface, based on a significant increase of Mo, V and U enrichment in black shales across the Pc-C boundary. The evidence for predominantly anoxic-ferruginous and even intermittently euxinic conditions in the water column across the Pc-C boundary and significant regional variations in geochemical parameters unravel complex interactions between ocean chemistry, platformal configuration and paleontology.

# Contents

<b>Outline</b>	<b>10</b>
<b>1. Introduction</b>	<b>11</b>
<b>1.1. The oxygenation of the Earth's surface: an overview of the last 4 billion years</b>	<b>11</b>
<b>1.2. Tectonics and climate during the Neoproterozoic - Cambrian Transition</b>	<b>24</b>
1.2.1. Tectonic reorganization from the mid-Neoproterozoic to Early Cambrian (825 - 530 Ma)	24
1.2.2. Climatic shifts in the Neoproterozoic 750 – 580 Ma	30
<b>1.3. Biological innovations during the Neoproterozoic – Cambrian Interval</b>	<b>35</b>
1.3.1. The origin of life on Earth, the advent of photosynthesis and the animal revolution	35
1.3.2. The oxygen requirements of early animals	41
<b>1.4. Isotopic evidence in support of the Neoproterozoic Oxygenation Event</b>	<b>45</b>
<b>1.4.1. Carbon isotopes</b>	<b>45</b>
1.4.1.1. The biogeochemical carbon cycle	45
1.4.1.2. The carbon isotopic record	47
1.4.1.3. The carbon isotopic record during the Neoproterozoic	48
1.4.1.4. Total organic carbon content in sedimentary rocks throughout Earth's history	53
<b>1.4.2. Strontium isotopes</b>	<b>55</b>
1.4.2.1. The $^{87}\text{Sr}/^{86}\text{Sr}$ ratio of the ocean	55
1.4.2.2. Changes in the seawater $^{87}\text{Sr}/^{86}\text{Sr}$ ratio during the Neoproterozoic	57

<b>1.4.3. Sulphur isotopes</b>	<b>60</b>
1.4.3.1. The sedimentary sulphur cycle	60
1.4.3.2. Sulphur isotope fractionation	61
1.4.3.3. The sedimentary sulphur isotope record	66
1.4.3.4. The sulphur isotopic record during the Precambrian	67
1.4.3.5. Temporal changes in total sulphur and pyrite content in sedimentary rocks	71
<b>1.4.4. Chromium isotopes</b>	<b>73</b>
<b>1.4.5. Molybdenum isotopes</b>	<b>75</b>
<b>1.5. Rare Earth Element (REE) patterns as paleoredox proxies: the cerium anomaly</b>	<b>77</b>
<b>2. Redox-sensitive trace-metals and iron speciation</b>	<b>80</b>
<b>2.1. Redox-sensitive trace metals</b>	<b>80</b>
<b>2.2. The redox-sensitive trace metals Mo, V and U as paleoredox proxies for the Neoproterozoic - Cambrian transition</b>	<b>82</b>
2.2.1. Uranium	84
2.2.2. Molybdenum	86
2.2.3. Vanadium	90
2.2.4. Other trace-elements and biological productivity	92
<b>2.3. Iron speciation: A proxy for the oxygenation of the deep ocean</b>	<b>96</b>
<b>2.4. Redox-sensitive trace-metals and iron speciation in black shales on the Yangtze Platform</b>	<b>100</b>
<b>3. Geological setting</b>	<b>101</b>
<b>3.1. The geological evolution of the Yangtze Platform during the Neoproterozoic and Early Cambrian</b>	<b>101</b>

<b>3.2. The Cryogenian</b>	<b>103</b>
3.2.1. The interglacial Datangpo Formation	103
<b>3.3. The Ediacaran</b>	<b>104</b>
3.3.1. The Doushantuo Formation (ca. 635 – 551 Ma)	104
3.3.2. The Dengying and Liuchapo formation (ca. 551 – 542 Ma)	112
<b>3.4. The Early Cambrian</b>	<b>116</b>
3.4.1. The Zhujiqing Formation (ca. 542 – 526 Ma)	116
3.4.2. The Niutitang Formation (ca. 542 – 520? Ma)	118
3.4.3. The Jiumenchong Formation (ca. 542 – 520? Ma)	119
3.4.4. The Yanjiahe and Shuijingtuo formations (ca. 542 – 521 Ma)	122
3.4.5. The Xiaotan section: probably the best Precambrian – Cambrian succession in the world!	124
<b>4. Materials and Methods</b>	<b>128</b>
<b>4.1. Instrumental analysis</b>	<b>128</b>
4.1.1. X-ray fluorescence spectrometry (XRF)	128
4.1.2. Inductively coupled plasma mass spectrometry (ICP-MS)	130
4.1.3. Laser Ablation ICP-MS (LA-ICP-MS)	132
<b>4.2. A comparison between XRF and ICP-MS analytical results</b>	<b>136</b>
<b>4.3. Iron speciation analysis</b>	<b>140</b>
4.3.1. The procedure	140
4.3.2. Comparing total iron measurements (XRF and AAS)	142
<b>4.4. Carbon and sulphur analysis</b>	<b>143</b>
4.4.1. C/S analyser	143
4.4.2. Sulphide isotopes	144
<b>4.5. Trace-metal normalisation</b>	<b>144</b>

<b>5. Results and interpretation of the investigated sections</b>	<b>146</b>
<b>5.1. The Cryogenian</b>	<b>146</b>
5.1.1. The Datangpo Formation: a profile from the manganese mine at Changxingpo, Guizhou Province	146
5.1.2. Discussion	148
<b>5.2. The Ediacaran and Precambrian – Cambrian boundary sections</b>	<b>150</b>
5.2.1. The Maoshi section, Guizhou Province: A Doushantuo/Dengying boundary succession	150
5.2.2. The geochemistry of the Doushantuo Formation in the Three Gorges Area, Hubei Province	151
5.2.2.1. Member II of the Doushantuo Formation at Jiulongwan	151
5.2.2.2. The Miaohe Member (Mb. IV) at Jiulongwan	153
5.2.2.3. Member II and the Miaohe Member at Jijiawan	156
5.2.3. Ocean chemistry and platform evolution during the Ediacaran	157
5.2.4. A high-resolution profile from the top of the Miaohe Member at Jiulongwan	161
5.2.4.1. Results	161
5.2.4.2. Discussion	164
5.2.5. The Miaohe Member at Baiguoyuan, Hubei Province: A comparison	166
5.2.5.1. Results	166
5.2.5.2. Discussion	168
5.2.6. The Dengying and Liuchapo formations	170
5.2.6.1. The geochemical profile at Wuhe (Shibantan Mb. of the Dengying Fm.)	170
5.2.6.2. The Huanglian section (Liuchapo and Jiumenchong formations)	171
5.2.6.3. The Longbizui section (Liuchapo and Jiumenchong formations)	173
5.2.6.4. Discussion	175

<b>5.3. The Early Cambrian</b>	<b>179</b>
<b>5.3.1. The Early Cambrian in the Three Gorges Area (Shuijingtuo and Yangjiahe formations)</b>	<b>179</b>
5.3.1.1. The redox geochemistry during the Early Cambrian at the Jijiawan section	179
5.3.1.2. The redox geochemistry during the Early Cambrian at the Wuhe section	180
5.3.1.3. Ocean chemistry and platform evolution during the Early Cambrian: a sequel	182
<b>5.3.2. The Zhongnan section (Niutitang Formation): A highly condensed succession on the platform margin</b>	<b>186</b>
5.3.2.1. Geochemical analysis	186
5.3.2.2. Discussion	187
The Phosphorite	187
The Ni-Mo sulphide ore horizon	188
<b>5.3.3. The Xiaotan section</b>	<b>190</b>
5.3.3.1. The redox geochemistry of its black shale successions	190
1 <sup>st</sup> black shale (lower Shiyantou Fm.)	190
2 <sup>nd</sup> black shale succession (upper Shiyantou Fm.)	192
3 <sup>rd</sup> black shale succession and beyond (Yuanshan Fm.)	195
5.3.3.2. High resolution sampling: results and discussion	195
<b>5.3.4. Other Early Cambrian sections on the southwestern platform (Yunnan Province)</b>	<b>197</b>
5.3.4.1. The Deze Section (Zhongyicun Fm., Dahai Mb.)	197
5.3.4.2. The Meishucun Section (lower Shiyantou Fm.)	198
<b>5.3.5. Discussion: Biogeochemical cycling during the Early Cambrian on the southwestern Yangtze Platform</b>	<b>199</b>
<b>5.4. Biogeochemical cycling across the Precambrian – Cambrian Transitions on the Yangtze Platform: summary and global perspective</b>	<b>209</b>



<b>6. Conclusions</b>	<b>222</b>
<b>6.1. The biogeochemical cycling of redox-sensitive trace-metals during the Precambrian-Cambrian transition on the Yangtze Platform</b>	<b>222</b>
<b>6.2. A multi-proxy approach to investigate ancient paleoredox conditions</b>	<b>223</b>
<b>6.3. Future Challenges</b>	<b>224</b>

## **Appendices**

Formal Acknowledgements	226
Personal Acknowledgements	226
References	228
References used for trace-metal, TOC and S compilations	262

## **Supplement (CD-ROM attached at the back)**

Electronic version of the present PhD thesis
Stratigraphic correlation of the analysed sections
Correlation coefficients ( $R^2$ ) in some black shale successions
Raw elemental and isotopic data
Full LA-ICP-MS dataset
High resolution geochemical profiles from the LA-ICP-MS analysis

## Outline

For the present study, I investigated the biogeochemical cycling of redox-sensitive trace-metals focussing on molybdenum, vanadium and uranium alongside the redox conditions during the Precambrian – Cambrian transition on the Yangtze Platform, South China, within the framework of the second great Oxygenation Event, herewith termed the Neoproterozoic Oxygenation Event. I therefore begin with an extended review of the present knowledge on the history of the Earth's surface oxygenation, the major climatic, tectonic and biological events that occurred during the Precambrian – Cambrian transition and the lines of evidence for the Neoproterozoic Oxygenation Event, including compilations of a few key geochemical parameters involving carbon and sulphur cycling throughout Earth's history. The second chapter focuses on redox-sensitive trace-metals and the temporal changes in the concentration of Mo, V and U in black shales and their potential to better constrain the Neoproterozoic Oxygenation Event in time. Chapter 3 intends to outline the geological context on the Yangtze Platform and presents the studied sedimentary successions before briefly introducing the analytical techniques used during the present study in chapter 4. The results and their interpretation are presented for the different localities and formations, followed by the conclusions which can be drawn for the biogeochemical evolution of the marine environment on the Yangtze Platform during the Precambrian – Cambrian transition.

The generated datasets for elemental analysis and sulphide isotopes can be found in the appendix together with the used references and acknowledgements.

A review on the Neoproterozoic Oxygenation Event has been accepted with minor revisions by the journal *Earth Science Reviews* as well as a paper on biogeochemical cycling during the Early Cambrian on the southwestern Yangtze Platform (Precambrian Research).

# 1. Introduction

## 1.1. The oxygenation of the Earth's surface: an overview of the last 4 billion years

Throughout Earth history, the content of oxygen in the atmosphere and the oceans has played a crucial role in shaping our planet. The emergence of oxygen on the Earth's surface and its concentration through time is strongly linked to several major changes on Earth such as tectonic reorganisation, climatic switches and biological evolution (see Fig. 1.1). On the other hand, its presence in the atmosphere and the oceans has also influenced planetary interactions between the biosphere and its environment, allowing the Earth system to cross irreversible thresholds towards the modern Earth system, characterised by the presence of metazoans, soil biota, more equable climates, and persistently high levels of oxygen in the oceans and atmosphere.

Despite the fact that oxygen is the third most abundant element in the universe (after H and He; Anders and Grevesse, 1989) and the most abundant element by weight in the Earth's crust (Barrow and Tipler, 1986), O<sub>2</sub> was not or only sparsely available during most of Earth history and is expected to have risen to near present atmospheric levels for the first time towards the Neoproterozoic - Cambrian transition (Nursall, 1959; Canfield, 2005; Berner et al., 2003; Berner, 2006). However, the extent and timing of this suspected major oxygenation event is controversial and has crucial implications for the understanding of our Earth system. The purpose of this introductory review is to present the current state of knowledge on the timing, extent and possible causes and consequences of the Neoproterozoic Oxygenation Event (NOE) based on geochemical and paleontological lines of evidence.

First of all, oxygen is a major oxidant whose accumulation in the atmosphere forever changed the surface chemistry of the Earth (e.g. Cloud, 1972; Garrels et al., 1973; Holland, 1984, 1994, 2002, 2004; Canfield, 2005). In its role as an electron acceptor, oxygen is the most feasible and most energetic source for driving the metabolism and growth of advanced life (Catling et al., 2005). The development of the Earth's surface and the evolution of life is

therefore a direct consequence of the appearance of the photosynthesizing cyanobacteria at least 2.7 billion years ago (e.g. Buick, 1992; Brocks et al., 1999, 2003), oxygenic photosynthesis being the only plausible oxygen producing mechanism which can sustain significant levels of O<sub>2</sub> (e.g. Walker, 1977), i.e. the only source which can overwhelm the various sinks of oxygen such as oxidation of organic material and/or reducing gases.

According to a recent review by Holland (2006), the subsequent evolution of the atmosphere and oceans can be divided into five stages, based on major changes in atmospheric O<sub>2</sub> levels which arguably occurred during the last 3.82 Ga of Earth's history (see Fig. 1.1). Despite the paradigmatic status of this interpretation, it must be emphasized that the timing and extent of Earth's surface oxygenation has been subject to vigorous debate since the 1950's and no firm consensus has been reached so far (Yamaguchi, 2005). One school postulates essentially constant atmospheric O<sub>2</sub> levels since at least 3.8 Ga (e.g. Dimroth and Kimberley, 1976; Ohmoto, 1997; Yamaguchi, 2003; Watanabe et al., 2005; Ohmoto et al., 2006) whereas the other one, far more favoured amongst the scientific community, advocates a stepwise oxygenation of the Earth's surface (e.g. Cloud, 1968; Walker, 1977; Holland, 1984; Kasting, 1987).

The first stage, lasting from 3.85 to 2.45 Ga saw the emergence of oxygenic photosynthesis, but the atmosphere and the oceans remained largely anoxic, allowing Fe(II) and Mn(II) to accumulate in seawater (Roy, 2006; Holland, 2006). However, some pockets, i.e. spatially limited and transient accumulation of oxygen might have been present in the Archean ocean (Kasting, 1993; Anbar et al., 2007; Hoashi et al., 2009; Kendall et al., 2010). Kato et al. (2006), for example, demonstrated that some Precambrian BIFs exhibit cerium depletion indicating cerium (III) oxidation in Archean seawater. The discovery of significant mass-independent fractionation (MIF) of sulphur isotopes in sulphides and sulphates before and during the Great Oxidation Event (2.4-2.0 Ga; e.g. Holland et al., 2006) interval suggest that the O<sub>2</sub> concentration in the atmosphere was generally less than 10<sup>-5</sup> present atmospheric level (PAL) before ca. 2.4 Ga (Farquhar et al., 2000; Farquhar and Wing, 2003; Bekker et al., 2004; Kasting et al., 2001; Pavlov and Kasting, 2002), with possibly elevated concentrations between 3.0 and

2.8 Ga (Watanabe et al., 2005) which has been related to the first known ice age at around 2.9 Ga (Young et al., 1998; Kasting and Ono, 2006).

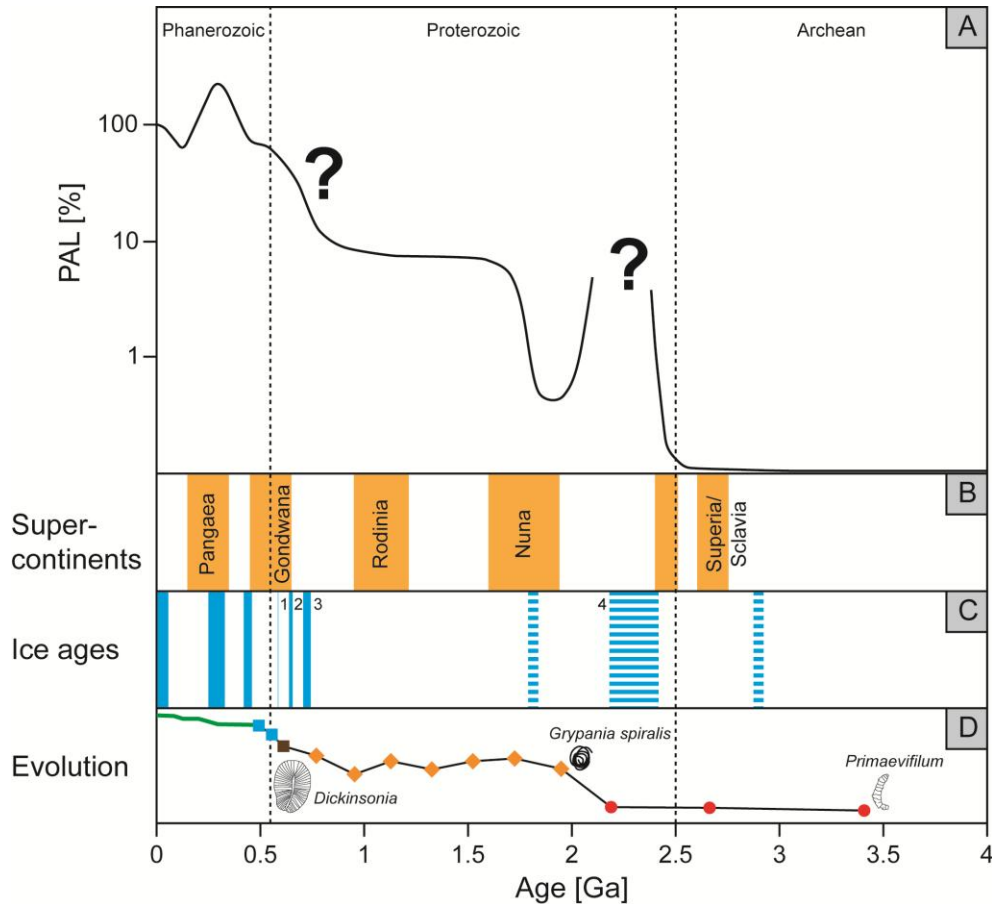


**Figure 1.1:** A) Proposed reconstruction of the atmospheric O<sub>2</sub> content through time expressed as the percentage of present atmospheric level of oxygen (after Canfield, 2005, with Phanerozoic estimates from Berner et al., 2003). Note that the uncertainty is quite high (see text). B) Periods of supercontinent formation (modified after Campbell and Allen, 2008). C) Precambrian glaciations whereby the numbered blue bars are of presumably global extent: 1) Gaskiers glaciation, 2) Marinoan glaciation, 3) Sturtian glaciation, 4) Makganyene/Huronian glaciation. The thickness of the Neoproterozoic glaciations correspond to their duration (e.g. Halverson et al., 2005, 2007); Archean and Paleoproterozoic glaciations with unknown duration are shown with dashed lines (Evans, 2003a and references therein; Reddy and Evans, 2009). The duration of the icehouse periods in the Phanerozoic are by Veizer et al. (2000). D) Biological innovations exemplified through increase of maximum size of organisms throughout Earth history. Red dots: prokaryotes, orange diamonds:

**protists, brown square: vendobiont (probable multicellular eukaryote, e.g. *Dickinsonia*), blue squares: animals, green line: vascular plants (modified after Payne et al., 2009).**

The persistence of very low oxygen levels prior to 2.45 Ga, despite the establishment of oxygenic photosynthesis at least 300 My earlier (e.g. Brocks et al., 2003), may be explained by the flux of reducing volcanic gases from submarine volcanoes ( $H_2$ ,  $H_2S$ ) which scavenged available oxygen (Kasting et al., 1993; Sleep and Zahnle, 2001; Holland, 2002; Li and Lee, 2004; Kump and Barley, 2007). At the Archean-Proterozoic boundary, continents became larger and more stable, resulting in volcanoes on land being more common with eruptions dominated by more oxidized gases (e.g.  $CO_2$ ), thus decreasing the reducing power on the Earth's surface environment (Kump and Barley, 2007; Reddy and Evans, 2009). A recent model by Holland (2009) attributes the gradual increase in the oxidation state of the atmosphere to an increase in the  $CO_2/H_2O$  and/or the  $SO_2/H_2O$  ratio of volcanic gases due to a greater portion of recycled gasses in the volcanic mix resulting from the subduction of carbonates, evaporites and sulphides, not or less active earlier in Earth history (see chapter 1.2.1.). A further possible reason for the delay could be that the nitrogen cycle, which would have been extended by involving nitrification and denitrification reactions after the emergence of oxygenic photosynthesis, exerted a negative feedback on the oxygenation of the atmosphere and ocean because coupled nitrification and denitrification drove the loss of fixed inorganic nitrogen, leading to nitrogen limitation which limited the growth of oxygen-producing organisms (Fennel et al., 2005; Falkowski and Godfrey, 2008; Godfrey and Falkowski, 2009). However, despite rampant but intriguing speculations, the question of what triggered the initial rise of oxygen to significant levels is still surrounded by much uncertainty.

The second stage, the irreversible appearance of atmospheric  $O_2$ , commonly referred to as the Great Oxygenation Event (GOE; see Table 1.2), occurred between 2.4 and 2.0 Ga (e.g. Bekker et al., 2004), during an episode of major tectonic, climatic and biological upheaval (see Fig. 1.1 and Table 1.1; Kirschvink et al., 2000; Barley et al., 2005; Reddy and Evans, 2009). The GOE led to major changes in the biogeochemical cycling of most elements which represent key factors in Earth's surface chemistry, most importantly iron, carbon, sulphur and phosphorus

and led to a diversification of mineral types (e.g. Groves et al., 2005; Hazen et al., 2008; Sverjensky and Lee, 2010). Increasing oxygen levels likely led to the extensive deposition of banded iron formations (see Fig. 1.2a; e.g. Isley and Abbott, 1999) and the more modest deposition of manganese deposits in shallow marine environments (see Fig. 1.2b; Roy, 1997, 2006; Maynard, 2010). The emergence of significant amounts of O<sub>2</sub> in the atmosphere coincides with the ending of continuous precipitation of BIFs ca. 2.4 Ga, indicating that the cessation of BIF deposition, representing a large sink for oxygen, effectively sustained long term accumulation of atmospheric O<sub>2</sub> (e.g. Holland, 2006). BIFs only reappear in the Paleoproterozoic towards the end of the GOE, between 2.0 and 1.8 Ga (Isley and Abbott, 1999), leading to the possibility that oxygen levels significantly decreased again to as low as 0.1% PAL in the meantime (Holland, 2004; Canfield, 2005). An increase in the weight ratio of Fe<sub>2</sub>O<sub>3</sub>/FeO also indicates major changes in the redox state of Fe during the GOE (Yamaguchi, 2002; Bekker et al., 2003).

Large positive excursions of  $\delta^{13}\text{C}$  between 2.3 and 2.0 Ga suggest that the carbon cycle was not in steady state and implies increased carbon burial which might have enhanced the oxygenation of the Earth's surface (Des Marais et al., 1992; Karhu, 1993; Karhu and Holland, 1996; Melezhik et al., 1999b; Schidlowski, 2001). Furthermore, the first evaporitic sediments containing sulphates indicate that the concentration of SO<sub>4</sub><sup>2-</sup> in seawater increased (Strauss, 2004; Melezhik et al., 2005c; Gellatly and Lyons, 2005; Farquhar et al., 2010b), a conclusion which is also supported through the analysis of sulphur isotopes, notably by an increase in S isotope fractionation between coeval sulphates and sulphides ( $\Delta^{34}\text{S}$ ; e.g. Bekker et al., 2004, Canfield, 2005). The period of the GOE also saw the first marine phosphorite deposits (Cook and Shergold, 1986, Nothold and Sheldon, 1986; Papineau, 2010). The mechanism behind widespread phosphate concretions and phosphorite deposition during the GOE is not only linked to organic matter that carries phosphate concentrated by biological activity (Knudsen and Gunter, 2002) but perhaps also to a major change in diagenetic mineralization of organic matter due to increased diagenetic sulphate reduction promoted by an overlying sulphate enriched ocean (Canfield and Raiswell, 1999) which in turn would have elevated the concentration of interstitial phosphate (Melezhik et al., 2005c). The level of atmospheric

oxygen during the GOE is rather uncertain but certainly increased considerably from the beginning to the end of this period, presumably within the broad range of 0.1% to 15% PAL (Yang and Holland, 2003; Holland, 2006), or perhaps even as high as today's oxygen levels (Beukes et al., 2002); both estimates are based on interpretations of the 2.2 Hekpoort paleosol of the Transvaal Supergroup, South Africa.

**Table 1.1: Major tectonic, climatic and biological events during the major steps in the oxygenation of the Earth's surface.**



Great Oxygenation Event (2.4-2.0 Ga)	Neoproterozoic Oxygenation Event (0.8-0.5 Ga)
<b>Tectonics:</b>	
<p>Break-up of a possible Neoproterozoic supercontinent (Heaman, 1997; Aspler and Chiarenzelli, 1998; Buchan et al., 1998; Bleeker, 2003; Reddy and Evans, 2009) and the formation of the supercontinent Nuna (1.9-1.8 Ga; Hoffman, 1997; Rogers and Santosh, 2002; Zhao et al., 2002, 2004; Campbell and Allen, 2008; Reddy and Evans, 2009).</p>	<p>Break-up of the supercontinent Rodinia (&gt;825 Ma) and the subsequent amalgamation of the supercontinent Gondwana (Dalziel, 1991; 1997; Moores, 1991; Hoffman, 1991; Meert and Torsvik, 2003; Meert, 2003; Boger and Miller, 2004; Veevers, 2004; Collins and Pisarevsky, 2005; Li et al., 2008b; Pisarevsky et al., 2008).</p>
<b>Climate:</b>	
<p>Low latitude glaciations, commonly referred to as the Makganyene and/or Huronian glaciation, and possibly the development of a Snowball Earth in the Early Paleoproterozoic (2.5 – 2.2 Ga; Evans et al., 1997; Kirschvink et al., 2000; Evans, 2003a; Tajika, 2003; Kopp et al., 2005; Kasting and Ono, 2006).</p>	<p>Widespread low-latitude glaciations whereby the Sturtian (&lt;740-647 Ma) and the Marinoan glaciation (&lt;660-635 Ma) might have reached the extent of a Snowball Earth (Coleman, 1926; Hambrey and Harland, 1981; Kennedy et al., 1998; Hoffman et al., 1998; Hoffman and Schrag, 2002; McCay et al., 2006; Fairchild and Kennedy, 2007).</p>
<b>Biology:</b>	
<p>Increase in taxonomic diversity and expansion of stromatolite reefs (Melezhik et al., 1997, 1999b; Grotzinger and Knoll, 1999; Papineau et al., 2009).</p> <p>Emergence of eukaryotes prior to 1.8 Ga (Doolittle et al., 1996; Brocks et al., 1999; Cavalier-Smith, 2002; Douzery et al., 2004; Yoon et al., 2004; Hedges et al., 2004; Knoll et al., 2006)</p>	<p>Increase in diversity of acritarchs and other protistan morphotypes by 750-800 Ma (Butterfield et al., 1994; Butterfield and Rainbird, 1998; Knoll et al., 2006, and references therein).</p> <p>Major biological innovations including the evolution of large architecturally complex organisms exemplified by the Ediacara biota and the Cambrian Explosion (Darwin, 1859; Sprigg, 1947; Raff and Raff, 1970; Runnegar, 1982; McMenamin and McMenamin, 1990; Valentine, 1992; Bowring and Erwin, 1998; Knoll, 2000; Zhuravlev, 2001; Narbonne and Gehling, 2003; Conway Morris, 2006).</p>

**Table 1.2: Lines of evidence for the oxygenation of the Earth’s surface during the Paleoproterozoic and the Precambrian-Cambrian transition. Major steps in biological evolution, especially during the Precambrian-Cambrian transition have been considered as evidence for a rise in atmospheric oxygen levels but due to major disagreements amongst the scientific community they are listed in Table 1.1.**

Great Oxygenation Event (2.4-2.0 Ga)	Neoproterozoic Oxygenation Event (0.8-0.5 Ga)
<b>Redox-sensitive elements:</b>	
<p>Preservation of uraninite (UO<sub>2</sub>), pyrite (FeS<sub>2</sub>) and siderite (FeCO<sub>3</sub>) as detrital placers in river deposits older than about 2.3 Ga (e.g. Holland, 1984, 1994; Clemmey and Badham, 1982; Cloud, 1972; Rasmussen and Buick, 1999).</p> <p>No Fe oxidation and Fe remobilization in paleosols older than about 2.2-2.3 Ga (Rye and Holland, 1998; Yang and Holland, 2003) and the appearance of red bed deposits around 2.2 Ga (Cloud, 1968; Holland, 1984, 1994).</p> <p>Banded Iron Formations (BIFs) are common before 2.4 Ga, absent between 2.4 and 2.0 Ga and re-emerge between 2.0 and 1.8 Ga (Cloud, 1972; Canfield, 1998; Isley and Abbott, 1999).</p> <p>Low content of redox-sensitive trace metals (e.g. Mo, U, V) in black shales before 2.2 Ga (Davy, 1983; Scott et al., 2008)</p>	<p>Increasing Ce anomaly towards the Neoproterozoic – Cambrian boundary (Yang et al., 1999; Ling et al., in review).</p> <p>Enrichment of Mo in black shales between 663 and 551 Ma (Scott et al., 2008)</p>
<b>Sulphur isotopes:</b>	
<p>Large mass-independent fractionation of sulphur (MIF-S) prior to 2.41 Ga and no significant MIF-S signal after 2.32 Ga (Farquhar et al., 2000, 2010b; Farquhar and Wing, 2003; Bekker et al., 2004).</p> <p>Increase of mass-dependent S fractionation with <math>\Delta^{34}\text{S}</math> values between 20 and 40‰ after about 2.3 Ga (Cameron, 1982; Cameron and Hattori, 1987; Canfield, 1998, 2001a; Canfield and Raiswell, 1999; Habicht et al., 2002; Strauss, 2004).</p>	<p>Increasing <math>\Delta^{34}\text{S}</math> values (45 - 70‰), exceeding the range achieved by sulphate reduction, between 800 and 700 Ma (e.g. Canfield and Teske, 1996; Lyons et al., 2004).</p>
<b>Carbon isotopes:</b>	

<p>Positive <math>\delta^{13}\text{C}_{\text{carb}}</math> values (<math>\sim+10\%</math>) between about 2.3 and 2.1 Ga (Des Marais et al., 1992; Karhu, 1993; Karhu and Holland, 1996; Schidlowski, 2001).</p>	<p>Long lived positive <math>\delta^{13}\text{C}_{\text{carb}}</math> excursion after 800 Ma accompanied by increasing <math>^{87}\text{Sr}/^{86}\text{Sr}</math> ratios (Asmerom et al., 1991; Derry et al., 1992; Kaufman and Knoll, 1995; Shields, 1999, 2007; Calver, 2000; Halverson et al., 2005, 2007).</p> <p>Prolonged negative <math>\delta^{13}\text{C}_{\text{carb}}</math> excursion between ca. 600 and 550 Ma (Condon et al., 2005; Melezhik et al., 2005a; Le Guerroué et al., 2006a,b; Fike et al., 2006; Jiang et al., 2007a; Kaufman et al., 2007).</p>
<p><b>Other approaches:</b></p>	
<p><math>\delta^{15}\text{N}</math> values rose by about 2‰ before about 2.67 Ga. It has been interpreted to indicate the onset of coupled nitrification and denitrification or anammox reactions in the surface ocean, which requires the presence of <math>\text{O}_2</math> (Godfrey and Falkowski, 2009).</p> <p>Increasing Cr isotope fractionation (<math>\delta^{53}\text{Cr}</math>) recorded in BIF's between 2.8 and 2.45 Ga indicate rise in oxidative weathering (Frei et al., 2009).</p>	<p>Positive <math>\delta^{53}\text{Cr}</math> values of up to 4.9‰ indicate significantly rising atmospheric <math>\text{O}_2</math> levels (Frei et al., 2009).</p>

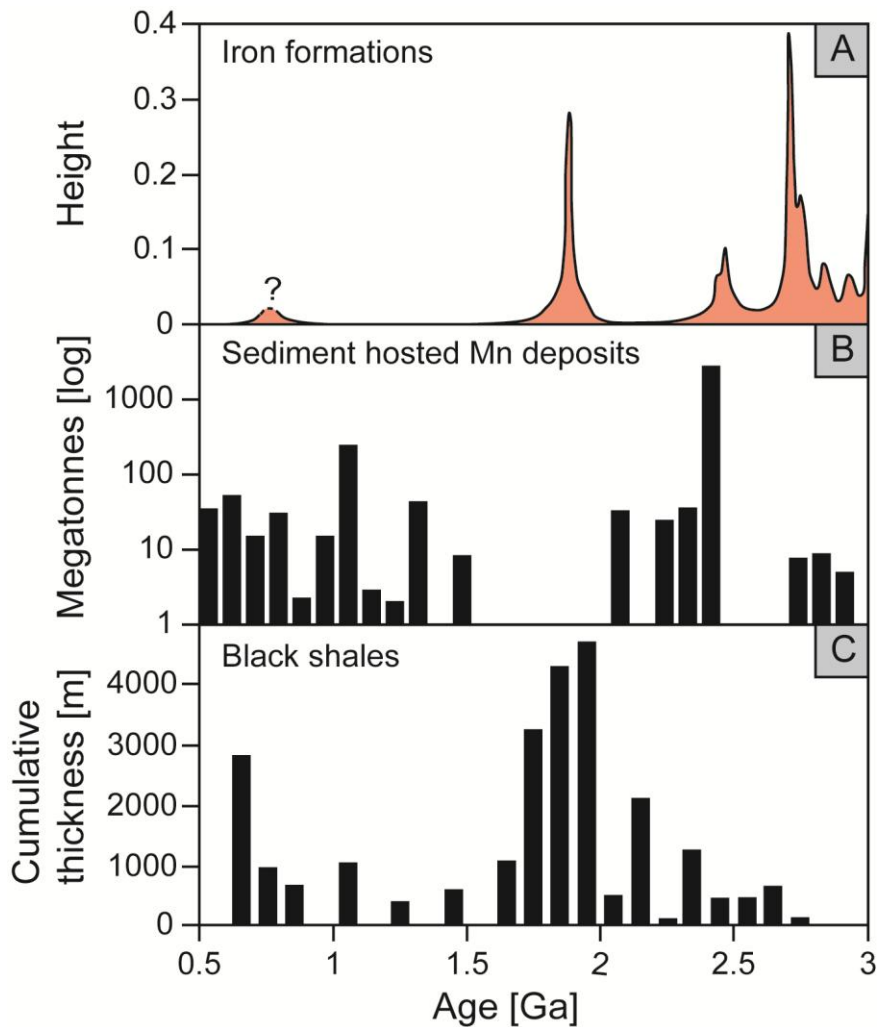


**Figure 1.2: A) Time series of the occurrence of iron formations throughout Earth’s history (see Isley and Abbott, 1999, for further details). B) Mass-age distribution of sediment-hosted manganese ores (modified from Maynard, 2010). C) Frequency distribution of total thickness of black shale (Condie et al., 2001).**

During the third stage, the Earth experienced a long period of apparent environmental stability, the so called ‘boring billion’, lasting from 1.85 – 0.85 Ga (Buick et al., 1995; Holland, 2006), with little or no record of continental ice-sheets and probably greatly reduced rates of biological innovations. Whereas the oxygen levels are poorly constrained during this long interval, possibly in the range of 5% to 18% PAL (Canfield and Teske, 1996), discussion is rife concerning the redox conditions and chemical composition of the deep ocean at this time. The

disappearance of banded iron formations after 1.8 Ga led to the earlier conclusion that levels of atmospheric O<sub>2</sub> increased high enough to ventilate the deep ocean so that dissolved Fe could not persist (Cloud, 1972, Holland, 1984, 2004). Further evidence in favour of an at least mildly oxygenated deep ocean are the absence of both manganese and phosphorite deposits during the 'boring billion', although the latter might have been the result of a very small delivery rate of organic matter to the deep ocean due to the absence of significant ballasting, i.e. the absence of organisms producing faecal pellets, and therefore inhibiting the transport of O<sub>2</sub> to the deep ocean (Logan et al., 1995). Furthermore, oxidation of Fe<sup>2+</sup> would have led to Fe(OH)<sub>3</sub> precipitation and would not have been available to transport PO<sub>4</sub><sup>3-</sup> to the bottom waters (e.g. Holland, 2006; Algeo and Ingall, 2007).

However, a relatively new model of the Proterozoic ocean has emerged since Canfield (1998) pointed out that the deep ocean remained anoxic after the great Oxidation Event in the Paleoproterozoic and even redox stratified with widespread euxinia in the deep ocean after about 1.84 Ga (Poulton et al., 2004a, 2010; Johnston et al., 2006), with sulphidic conditions possibly even affecting the photic zone (Brocks et al., 2005) from the Mesoproterozoic until at the mid-Neoproterozoic. The first appearance of large sediment-hosted massive sulphide deposits about 1.8 Ga might provide further evidence for a shift to sulphidic conditions (Lyons et al., 2006). However, Slack et al. (2007) considered that modest Ce anomalies and the presence of ferric iron in volcanogenic massive sulphide deposits (VSM) indicate the presence of low amounts of oxygen rather than sulphidic conditions in the deep marine environment at 1.7 Ga. Spatial variability in the Proterozoic ocean redox structure prevailed at least during the transitional periods after the GOE and prior to the Neoproterozoic – Cambrian boundary, where sulphidic conditions might have been restricted to near-shore environments, similar to the oxygen minimum zone in the modern ocean (Poulton et al., 2010; Li et al., 2010), and anoxic-ferruginous conditions might have been the dominant feature of the Precambrian ocean (Poulton and Canfield, 2011).

The concept of a 'Canfield ocean', similar to an earlier idea of 'progressive ventilation' by Berry and Wilde (1978), is mainly based on  $\Delta^{34}\text{S}$  values, i.e. the isotopic fractionation of sulphur between sulphide and sulphate, but has since been supported by molybdenum isotope

studies and iron speciation analysis of Proterozoic marine sediments (Canfield and Raiswell, 1999; Shen et al., 2002, 2003; Arnold et al., 2004; Poulton et al., 2004a; Brocks et al., 2005; Canfield et al., 2008; Lyons et al., 2009; Poulton et al., 2010). In other words, substantial deep ocean ventilation was delayed until the Late Neoproterozoic. Such a scenario would have had important implications for the biosphere due to the reduced availability of redox-sensitive, bio-essential trace metals (e.g. Anbar and Knoll, 2002) and for climate, because the flux of biogenic methane from oceans to atmosphere is sensitive to ocean oxygenation (Pavlov et al., 2003; Kaufman and Xiao, 2003; Arnold et al., 2004). According to Canfield (1998), BIFs ceased being deposited because dissolved iron would have been bound to relatively insoluble sulphides in the Proterozoic 'Canfield' ocean. Therefore, BIF precipitation depended on Fe delivery to the ocean and sulphate reduction rates, the latter being significantly enhanced since the onset of widespread oxidative weathering and therefore increased sulphate delivery rates to the ocean after the GOE. The postulated period of widespread euxinia is bracketed by peaks in the abundance of black shale from 2.0-1.8 Ga and from 0.8-0.6 Ga (see Fig. 1.2c; Condie et al., 2001), which has also been used as an argument against Canfield's hypothesis, stating that euxinic environments are supposed to preserve high concentrations of organic matter (e.g. Meyer and Kump, 2008). But the lack of significant organic rich successions during that time actually supports the idea of widespread oxygen deficiency as organic matter would have been more equally distributed globally.

After the 'boring billion', the Earth's surface environment blundered into roaring times during the fourth stage, lasting from 0.85 to 0.54 Ga. Besides tectonic reorganization, climatic shifts from icehouse to greenhouse conditions, and major biologic innovations, several lines of evidence point to a second 'Great Oxygenation Event' during the Precambrian – Cambrian transition, which is here referred to as the Neoproterozoic Oxygenation Event (see table 1.1 and 1.2). As with the GOE, major changes in biogeochemical cycling during the Neoproterozoic - Cambrian transition likely took place as a result of a steep increase in oxygen concentration in the atmosphere and the oceans. The biogeochemical parameters leading to this assumption are shortly outlined in the following and more thoroughly discussed in the subsequent chapters. A second long-lived positive  $\delta^{13}\text{C}$  excursion occurred during this period, indicating major

perturbations to the carbon cycle possibly due to the global increase in organic burial, and therefore signalling increasing primary productivity and the generation of excess O<sub>2</sub> (Knoll et al., 1986; Derry et al., 1992). The significant Neoproterozoic increase in the seawater <sup>87</sup>Sr/<sup>86</sup>Sr ratio (Shields and Veizer, 2002; Shields, 2007), which reflects the relative contribution of strontium to the ocean from continental weathering and from hydrothermal activity (Veizer, 1989), might represent further, although indirect, evidence for increased oxygen content in the atmosphere due to intensified primary productivity fuelled by increased nutrient supply to the oceans. Additional support for increasing nutrient supply has recently been forwarded by Planavsky et al. (2010), who demonstrated peaking phosphorus concentrations in the ocean in the aftermath of widespread, low-latitude glaciations. Furthermore, a prolonged, extremely negative δ<sup>13</sup>C excursion after ca. 580 Ma might indicate the oxidation (or remineralization) of a large pool of organic carbon represented by the deep ocean (Rothman et al., 2003; Le Guerroué et al., 2006a,b; Fike et al., 2006; McFadden et al., 2008). As already mentioned with regard to the GOE, the sulphur isotopic record of sulphides and sulphates is a powerful tool for tracing the oxidation state of the Earth's surface. But, unlike during the GOE, where the dominant S fractionation process shifts from mass-independent fractionation to sulphate reduction, the sulphur cycle during the Neoproterozoic - Cambrian transition might have been strongly influenced by the development of non-photosynthetic sulphide-oxidizing organisms and the disproportionation of intermediate sulphur compounds due to the further oxygenation of the atmosphere and the persistent ventilation of the deep ocean (e.g. Canfield and Teske, 1996; Canfield, 1998).

Finally, the fifth stage is characterized by significantly varying but persistently high atmospheric oxygen levels (Berner et al., 2003; Berner, 2004, 2006) and occasional oceanic anoxic events (OAE's; e.g. Meyer and Kump, 2008).

## **1.2. Tectonics and climate during the Neoproterozoic - Cambrian transition**

### **1.2.1. Tectonic reorganization from the mid-Neoproterozoic to Early Cambrian (825 - 530 Ma)**

Valentine and Moores (1970) were the first to propose that a supercontinent, comprising all existing continents on Earth, existed towards the end of the Precambrian (see also Dewey and Burke, 1973). They named this supercontinent Pangea I, which later was changed to Rodinia (McMenamin and McMenamin, 1990, see also Meert and Powell, 2001), from the Russian word '*rodit*' meaning 'to give birth', following the idea that the supercontinent spawned all subsequent continents.

Based on geological and paleomagnetic evidence (Piper et al., 1976; Bond et al., 1984; Eisbacher, 1985; Bell and Jefferson, 1987; Dalziel, 1997; Piper, 2000; Meert and Torsvik, 2003) and extensive studies on the assembly and break-up of Rodinia (Dalziel, 1991; 1997; Moores, 1991; Hoffman, 1991; Meert and Torsvik, 2003; Meert, 2003; Collins and Pisarevsky, 2005; Li et al., 2008b; Pisarevsky et al., 2008), the history of the Late Precambrian supercontinent is better understood today, as well as the subsequent reassembly into Gondwanaland.

The formation of Rodinia took place between 1100 and 900 Ma during which all other continents converged towards Laurentia, the biggest continent at that time which gave rise to the Grenville orogeny (see reviews by Li et al., 2008b; Meert and Torsvik, 2003). The break-up of Rodinia started around 825 Ma, or possibly some 50 million years earlier (e.g. Paulsson and Andreasson, 2002), caused by superplume activity and subsequent continental rifting with another magmatic peak around 800 Ma (e.g. Li et al., 2003a, b; Ernst et al., 2008) together with a possible true polar wander event and movement of Rodinia from high latitudes to an equatorial position (Evans, 2003b; Li et al., 2004; Maloof et al., 2006). A further equatorial superplume event may have broken apart the western half of Rodinia around 750 Ma (see Fig. 4). Australia-East Antarctica and South China were separated from each other at 720 Ma and Kalahari and Siberia may have started to break away from Laurentia by this time. The interval from 750 – 700 Ma corresponds also to the time when the first global Neoproterozoic glaciation occurred (<720 Ma: Macdonald et al., 2010), when most continents were located at low- to



moderate latitudes (e.g. Hoffman et al., 1998). The further alignment of the continents along the paleo-equator between 650 – 630 Ma (see Fig. 1.3), in addition to the generally low-latitude arrangement of continents in the late Neoproterozoic, may have led to the later end-Cryogenian or ‘Marinoan’ glaciation at ca. 650 Ma (Kirschvink, 1992; Hoffman and Schrag, 2002; Li et al., 2008b).

Around 600 Ma, West Gondwana was largely united, Amazonia, West Africa and Congo-San Francisco having converged, whereas Amazonia and Rio de la Plata were still attached to Laurentia, Baltica, Siberia and North China remained isolated (e.g. Trompette, 1997; Pease et al., 2006; Cawood and Pisarevsky, 2006; Zhang et al., 2006). It is unclear whether Laurentia was located at high- or low-latitudes at this time, but the former is more probable when it comes to explain the ca. 580 Ma Gaskiers glaciation (Cawood and Pisarevsky, 2006; Meert and van der Voo, 1994), contemporaneous with the opening of the Iapetus Ocean. The convergence of East and West Gondwana, closing the Mozambique Ocean from ca. 650 to 515 Ma, led to the rise of an enormous mountain chain, the East African-Antarctic orogen sometimes referred to as the Transgondwanan Supermountain, which possibly represents the biggest continent-continent collision in Earth history (Stern, 1994; Abdelsalam et al., 2003; Boger and Miller, 2004; Jacobs and Thomas, 2004; Squire et al., 2006). It has been argued that this putative, very large orogen consequently gave rise to high weathering rates which were enhanced due to the emergence of primitive soil biota (possibly as early as 700 Ma: Kennedy et al., 2006), the lack of protective plants, and the vicinity to the equator, leading to a major increase in nutrient delivery to the ocean (Squire et al., 2006; see also chapter 1.4.2.). By the early Cambrian (540 – 530 Ma, see Fig. 1.3), the long-lived supercontinent of Gondwanaland had finally amalgamated by closing the ‘Mozambique Ocean’ and involved the final docking of India to Australia-East Antarctica (e.g. Meert, 2003; Meert and Torsvik, 2003; Collins and Pisarevsky, 2005; Boger and Miller, 2004, Veevers, 2004).

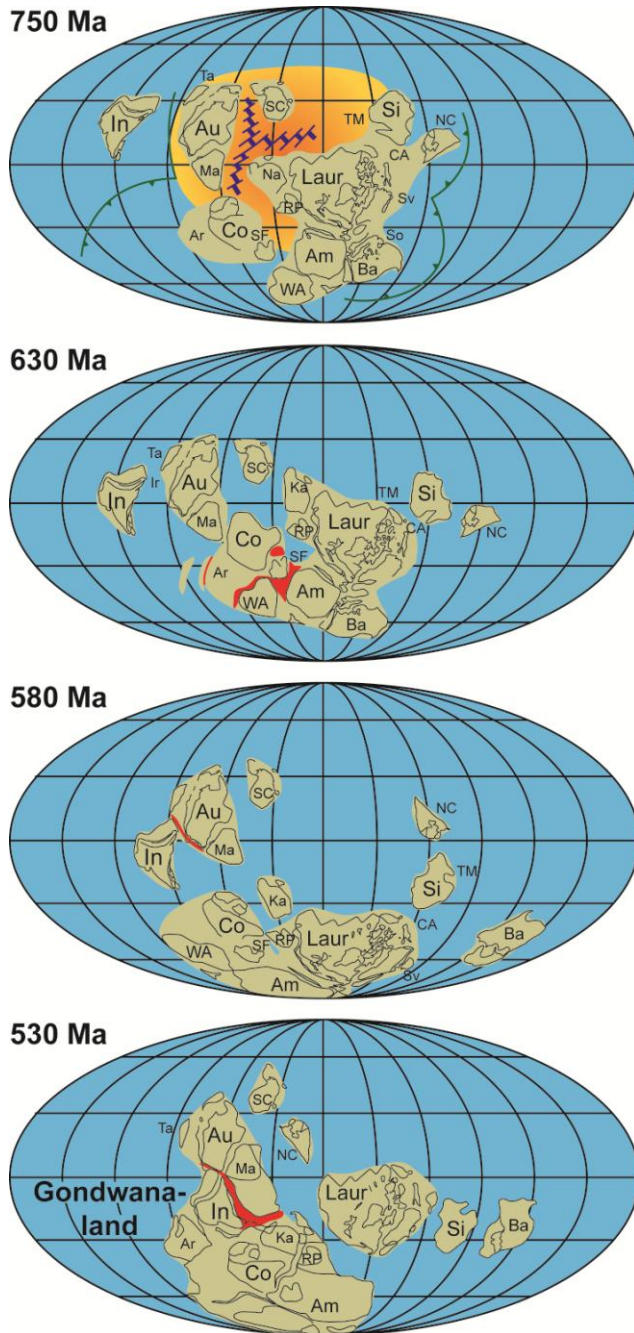


Figure 1.3: The paleogeographic situation 750 million years ago. The western part of Rodinia drifted away due to an equatorial superplume. Between 750 and 700 Ma most continents were located at low- to moderate latitudes. By 630 Ma, a further alignment along the paleo-equator had taken place. Most continents moved to higher latitudes by 580 Ma. The formation of the long-lived supercontinent of Gondwanaland was completed by ca. 530 Ma. See Li et al. (2008b) for the more extensive paleogeographic reconstruction between 1100 and 530 Ma.

However, a healthy scepticism must be applied regarding ancient continental configuration. As Scotese (2004) pointed out, uncertainties of paleomagnetically determined positions increase steeply with age. The position and motion of the continents in Precambrian reconstructions are only poorly constrained which naturally leads to disagreement amongst the scientific community (e.g. Piper, 2000; Meert, 2003; Squire et al., 2006; Meert and Lieberman, 2008).

Stern (2005) formulated the hypothesis that the modern style of 'subduction tectonics', whereby the Earth's mantle convection is driven by the sinking of cold, dense lithosphere at subduction zones, originated as late as the Neoproterozoic. Prior to 1 Ga, the Earth might not have been cool enough to establish the density inversion required for subduction (see also Davies, 1992) because the mantle lithosphere would have been thinner and oceanic crust would be much thicker as it has been shown that the thickness of the oceanic crust scales to the temperature in the source region (McKenzie and Bickle, 1988; Pollack, 1997; Sleep, 2000; Moores, 2002). The evidence compiled and put forward by Stern (2005) rely on the geological record : 1) the oldest unequivocal ophiolites, which require subduction to be formed, have an age of ca. 1.04 Ga (Khain et al., 2002), slightly predating Neoproterozoic times, 2) blueschists and amphibole-bearing, metamorphosed rocks that are stable under high pressure and low temperatures and characterize Pacific-type orogenic belts (Ernst, 2003), appear 800 – 700 Ma (Maruyama et al., 1996) and possibly ca. 940 Ma (Shu and Charvet, 1996), and 3) the oldest reliably dated ultrahigh-pressure (UHP) metamorphic terranes, which bear coesite and/or diamond and are typical for alpine-type orogenic belts (Ernst, 2003), forming under temperatures of 700 – 900°C and pressures as high as 3-4 GPa (Ernst and Peacock, 1996), was metamorphosed ca. 620 Ma (Jahn et al., 2001) . These require subduction of continental crust to depths of 100 – 125 km, as a result of continent-continent collision, and subsequent exhumation (Liou et al., 2004). The temporal succession of these events is consistent with our understanding of the subduction-driven Wilson-supercontinent tectonic style (Wilson, 1966; Stern, 2005) and might represent a final step according to the progressive cooling of the Earth (Ernst, 2007). However, the concept of a rather late appearance of modern-style plate tectonics is controversial and the discovery of Archean eclogites, late Archean subduction related

Kuroko-type volcanogenic massive sulphide deposits, mid-Archean island arc volcanics, isotopic data from the oldest zircons and ophiolites from the Paleoproterozoic argue for modern-style subduction processes possibly back to the Hadean (Cawood et al., 2006 and references therein; see also Sleep, 1992; Windley, 1995; Smithies et al., 2003).

Beside the raised idea of a close relationship between tectonic reorganization and Earth's climate, several researchers, amongst others Valentine and Moores (1970) and McMenamin and McMenamin (1990), recognised also a close link between biological diversification and the divergence of environments (shallow, nutrient-rich shelves and coastal areas) due to the break-up of Rodinia, the period of maximum dispersal between 750 to 700 Ma (Stern et al., 2008) and the subsequent maximum in the abundance of passive margins (see Fig. 1.4; Bradley, 2008). Passive margins can also be the site of increased organic matter burial and thus enhance the accumulation of O<sub>2</sub> in the atmosphere (e.g. Knoll, 1986). On the other hand, the formation of supercontinents could as well be related to and trigger increases in atmospheric oxygen (Lindsay and Brasier, 2002; Squire et al., 2006; Campbell and Allen, 2008; Campbell and Squire, 2010): enhanced orogeny due to continent – continent collision during the assembly of supercontinents lead to increased erosion and therefore to a large release of nutrients to the ocean which then favour explosive production of algae and cyanobacteria and thus a marked increase in photosynthetic production of O<sub>2</sub>. Additionally, enhanced productivity might be a result of glacial melting, e.g. after the Gaskiers glaciations, leading to an increase in nutrient supply to the ocean (Canfield et al., 2007) and, probably more important, of enhanced circulation in the deep oceans due to redistribution of landmasses and opening or closing of 'oceans', e.g. the Mozambique and Iapetus between 650 – 530 Ma (Meert and Lieberman, 2008).

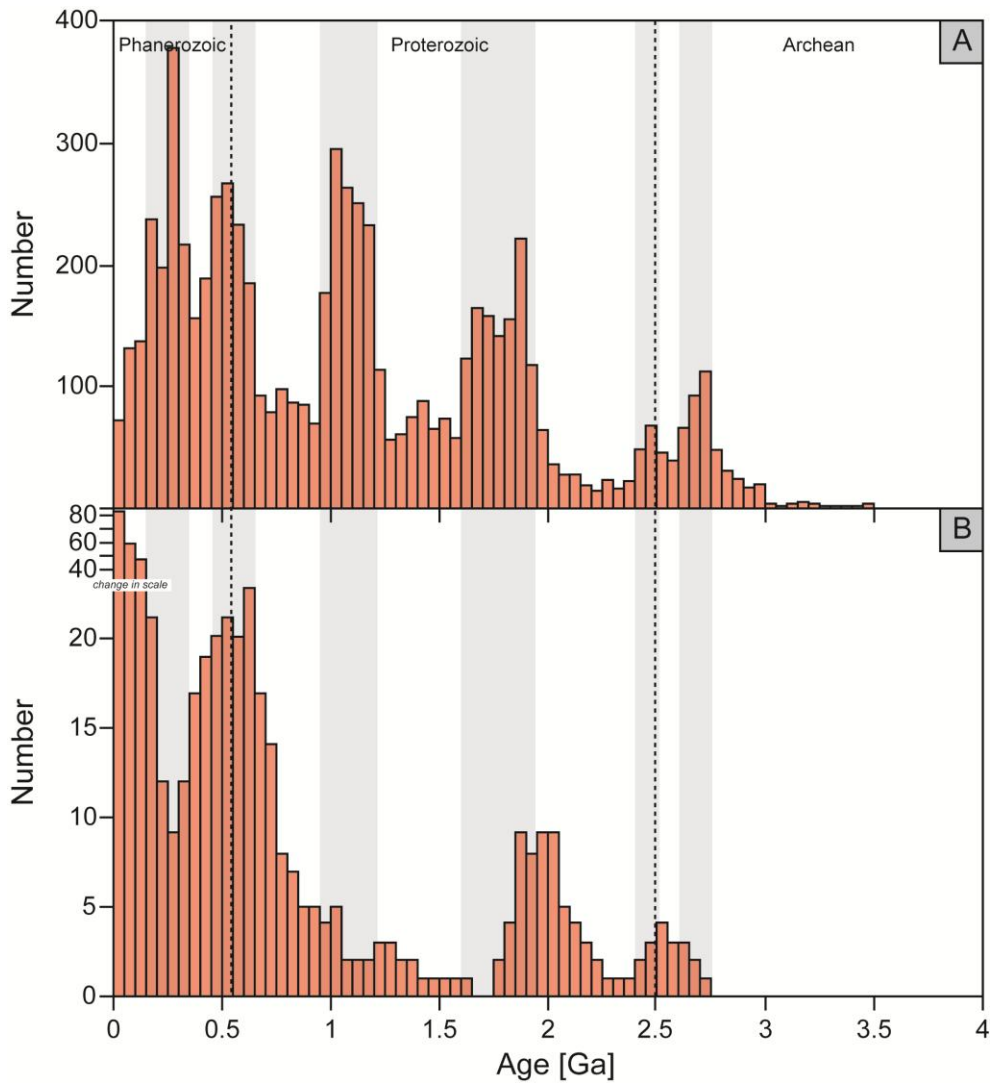


**Figure 1.4: A) Histogram showing U/Pb ages of 5,246 concordant detrital zircons from 40 major rivers supplemented by 1,136 Australian dune zircons and 583 from Antarctic Palaeozoic sediments; periods of supercontinent formation are shaded grey (Campbell and Allen, 2008). B) Histogram showing age distributions of the ancient passive margins (Bradley, 2008).**

### 1.2.2. Climatic shifts in the Neoproterozoic 750 – 580 Ma

Since James Thomson recorded Precambrian glacial deposits for the first time in 1871 (Spencer, 1971), the worldwide distribution of Neoproterozoic glacigenic deposits became gradually apparent during the last century (Coleman, 1926; Hambrey and Harland, 1981; Kennedy et al., 1998; McCay et al., 2006; Fairchild and Kennedy, 2007). Notably, faceted and striated clasts indicative of subglacial transport and dropstones, clast clusters and till pellets derived from floating ice are important indicators for ancient glaciations alongside detailed facies analysis (Hambrey and Harland, 1981). Based on radiometric data and other studies (e.g. Kennedy et al., 1998; Hurtgen et al., 2005; Halverson, 2006), the current view is that there were three or four episodes of glaciation in the Neoproterozoic (see Fig. 1.5), none of them before 750 Ma. The two end-Cryogenian glaciations both show evidence for low-latitude glaciers and are commonly referred to as the ‘Sturtian’ glaciation (ca. 720 – ca. 660 Ma) which has been recorded in Australia (type location: South Australia), Laurentia, China and elsewhere (e.g. Brasier et al., 2000; Fanning and Link, 2004; Macdonald et al., 2010), and the ‘Marinoan’ glaciation (ca. 650 – 635 Ma) with records in Australia (type location: South Australia), Laurentia, N and S Africa and China (e.g. Hoffmann et al., 2004; Condon et al., 2005). A possible glaciation at ca. 750 Ma and the mid-Ediacaran Gaskiers glaciations (ca. 580 Ma) evidenced in Avalonia (type location), Australia, SW-Gondwana and N China (Thompson and Bowring, 2000; Bowring et al., 2003; Calver et al., 2004; Frimmel, 2008; Hoffman and Li, 2009) were possibly of only regional significance (Fairchild and Kennedy, 2007).

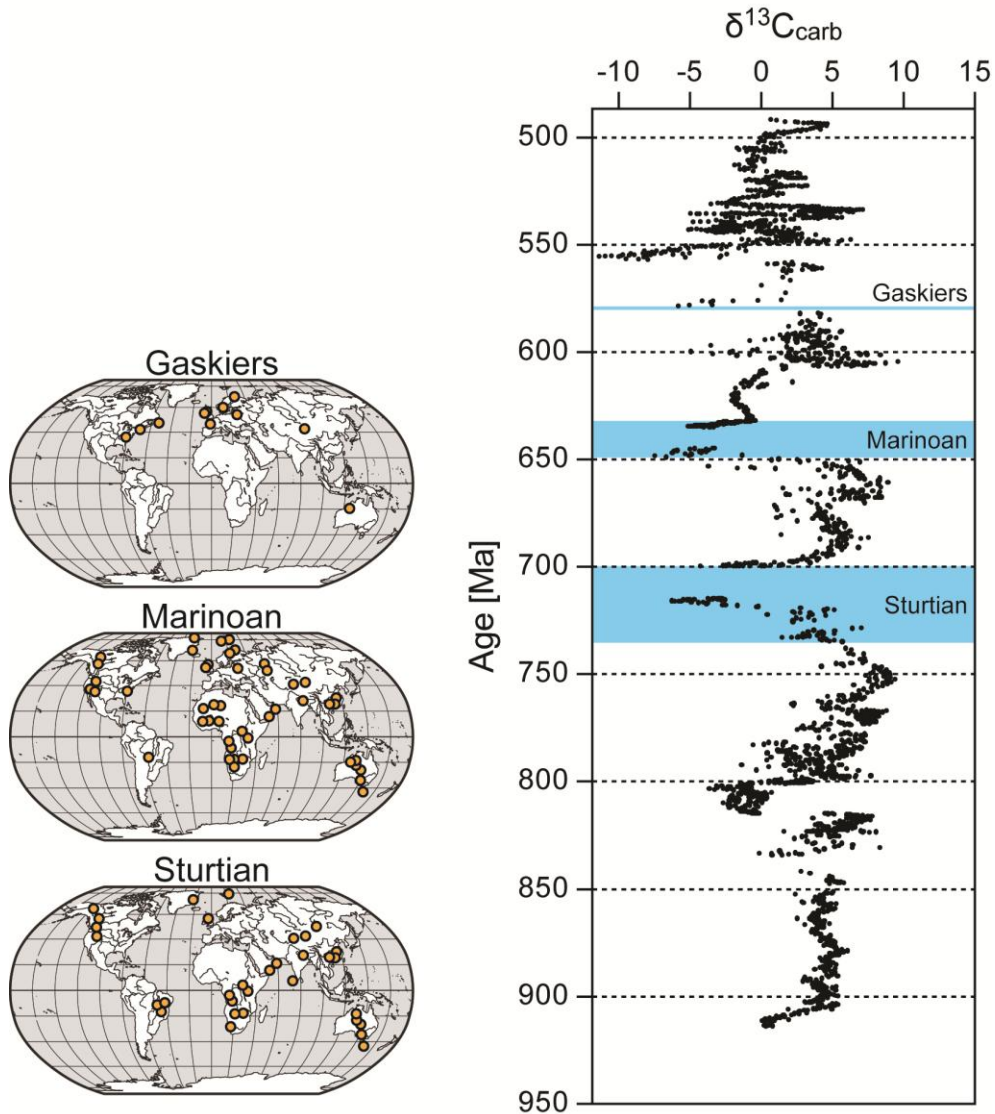


Figure 1.5: Present global distribution of Sturtian, Marinoan and Ediacaran glacial and glacial-marine deposits (left, after Fairchild and Kennedy, 2007), and secular variation in the carbon isotopic composition ( $\delta^{13}\text{C}$ ) of marine carbonates from 910 to 490 Ma (right, modified after Halverson et al., 2005, 2006). The negative  $\delta^{13}\text{C}$  anomalies characterizing the Sturtian and Marinoan glacial intervals suggest that they were globally synchronous.

These glacial stratigraphic units, sometimes referred to as tillites, are sometimes overlain by a cap carbonate with a very negative  $\delta^{13}\text{C}$  signature, but only the Marinoan glacial deposits display overlying cap carbonates on a global scale (Shields, 2005). There is little

agreement concerning the causes of the widespread occurrence of these carbonates. Several models have been proposed including an overturn of an anoxic deep ocean, melting of large-scale methane clathrate reservoirs, or algal blooms in a low salinity meltwater plume that separated the surface from deep ocean waters (Shields, 2005). In particular, cap carbonates may have been a result of extreme chemical weathering triggered by a hothouse condition following the Snowball Earth and they could provide a physical record of the resulting perturbations in the global carbon cycle (Kennedy, 1996; Hoffman et al., 1998).

The Snowball Earth hypothesis (Hoffman et al., 1998; Hoffman and Schrag, 2002) being widely contested, other models have to be considered (see Fig. 1.6). There is still some debate whether the Sturtian and/or the Marinoan glaciation were global events but, a pragmatic synthesis of more extreme models such as the Snowball Earth (Kirschvink, 1992; Hoffman et al., 1998), the High-tilt Earth (Williams, 1975, 1993; Williams et al., 1998) or the Zipper-Rift Earth (Eyles and Januszczak, 2004) a Slushball Earth seems more likely (see Fig. 6; Hyde et al., 2000; Fairchild and Kennedy, 2007). According to Fairchild and Kennedy (2007), the icehouse period from 750 – 580 Ma, was superseded by a super-greenhouse event (Hoffman et al., 1998; Kaseman et al., 2005; Bao et al., 2008), represents an event which stands rather isolated within greenhouse conditions characterizing the Earth in most of its history and is most likely associated with low atmospheric pCO<sub>2</sub> levels. Therefore, the Neoproterozoic glaciations are likely to be linked to global geochemical cycles of oxygen and carbon. They propel biological innovations and deep Earth processes as most plausible causes for these atmospheric changes. But, as highlighted above, the break-up of Rodinia and the assembly of Gondwanaland might well have been an additional cause leading to widespread glaciations, as the physical and chemical face of the Earth changed during the course of tectonic reorganization, in particular the predominantly low-latitude alignment of continental landmass. This has mainly two reasons: (1) as silicate weathering rates are temperature dependant, the drawdown of CO<sub>2</sub> would have been accentuated when the largest part of the continental surface was situated in 'tropical' latitudes (Marshall et al., 1988; Worsley and Kidder, 1991), and (2) as continents are more reflective than the open ocean, their low-latitude position would have led to an increased global albedo (Walker et al., 1981; Kirschvink, 1992). These effects would have been amplified



by glaciations resulting in a positive feedback as more reflective continental shelves would have been exposed to weathering (Hoffman and Schrag, 2002) and elevated erosion rates and organic productivity would have enhanced organic burial and hence, further reduced atmospheric pCO<sub>2</sub> (Maloof et al., 2006).

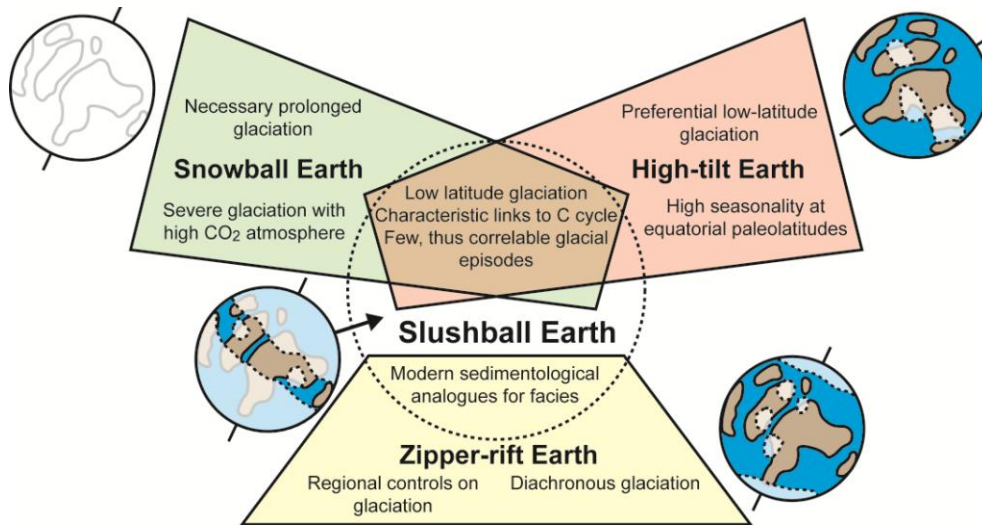


**Figure 1.6: Venn diagram illustrating the essential differences in interpretation used to supportive contrasting views of Neoproterozoic glaciation. For example, the Snowball and High-tilt models are distinct, although they accept some evidence in common, as illustrated. Distribution of ice in sketch maps is shown by cross-hatched ornament (after Fairchild and Kennedy, 2007).**

Furthermore, the oxygen and carbon cycle are also coupled to climate via methane. As already mentioned, Canfield (1998) developed a model for the Proterozoic ocean where the ocean would have been pervasively anoxic below its surface and therefore predisposed to elevated rates of methanogenesis. The methane being oxidized through increasing oxygen content in the Neoproterozoic atmosphere would have led to a switch from greenhouse to icehouse conditions, acting as an important stimulus for the initiation of glaciation (Schrag et al., 2002). On the other hand, destabilization of methane clathrates during deglaciation may have acted as a positive feedback towards a (super-) greenhouse world (Ridgwell et al., 2003). Although high pCO<sub>2</sub> conditions probably persisted for several millions of years after the end-

Cryogenian snowball glaciations (Le Hir et al., 2009), the recovery to more temperate greenhouse conditions on Earth would have been driven by unusually high silicate weathering rates, leading to increased nutrient delivery to the oceans and consequently high organic carbon burial and sustained deep-ocean anoxia (Kirschvink et al., 2000; Elie et al., 2007). Another consequence of a rapidly melting snowball Earth is that the ocean would have been covered by low-density meltwater creating a stable density stratification which would have decoupled photosynthesis from respiration (Hoffman, 2009). Higher temperatures would have lowered the O<sub>2</sub> concentration in surface waters and resisted downwelling while low ambient sulphate concentrations would limit anaerobic respiration. Despite a lower primary productivity due to suppressed nutrient-rich upwelling, organic carbon burial rates could have increased. Indications for this organic carbon burial lie in widespread black shale deposition in basal Ediacaran cap carbonate sequences on a global scale (Grantham et al., 1988; Halverson and Hurtgen, 2007).

The lack of convincing globally correlative glacial deposits and low paleoinclinations, means that the short lived Gaskiers glaciation during the Ediacaran Period more likely resembled typical Phanerozoic glaciations (Evans, 2003a; Halverson, 2006) but was nevertheless associated with by a large decline in  $\delta^{13}\text{C}$  (see Fig. 1.5). No undisputed evidence (e.g. Bertrand-Sarfati et al., 1995), such as glacial deposits, indicates periods of cold climate in the Early Cambrian (Hambrey and Harland, 1981; Evans, 2003a; Porter et al., 2004) and it has been demonstrated that very high pCO<sub>2</sub> levels, although declining, were characteristic of the Cambrian Period as a whole (Riding, 2006; Berner, 2006; Bao et al., 2008). Nevertheless, glaciations have been much more common since 720 Ma (see Fig. 1.1), suggesting an overall cooling of the Earth's long-term climate, superimposed by developing regulatory feedbacks involving an increasingly complex biosphere (Evans, 2003a). Moreover, the distribution of glacial deposits throughout Earth's history indicate a switch from mainly low-latitude glaciations in the Neoproterozoic to high-latitude glaciations in the Phanerozoic, notably occurring within a 100 My interval coinciding with major biological innovations during the Neoproterozoic - Cambrian transition (Evans, 2003a; see also Tajika, 2003).

### **1.3. Biological innovations during the Neoproterozoic – Cambrian interval**

#### **1.3.1. The origin of life on Earth, the advent of photosynthesis and the animal revolution**

Biological processes and life on Earth in general are the most direct and probably the strongest link to the history of oxygen on Earth's surface, first through photosynthesis and second as beneficiary of increasing oxygen levels on Earth in the case of respiring organisms.

Although there are some, controversial, indications for the oldest putative microfossils being of an age of 3.5 billion years, geochemical evidence indicates that life probably originated 3.8 billion years ago (Schopf and Packer, 1987; Mojzsis et al., 1996; Tice and Lowe, 2004) but certainly before 2.7 Ga (Brocks et al., 1999, 2003; Archer and Vance, 2006). Photosynthesizing cyanobacteria, with two combined photosystems ultimately producing free oxygen: PSI, which strips electrons from chlorophyll to generate energy, and PSII, which replenishes the electron-pool by oxidizing H<sub>2</sub>O to O<sub>2</sub> (e.g. Ort et al., 1996; Blankenship and Hartman, 1998; Ferreira et al., 2004; Blankenship et al., 2007), represents the most significant source of oxygen on Earth, and likely emerged at least in the Neoproterozoic by 2.7 Ga (Buick, 1992; Beukes and Lowe, 1989; Brocks et al., 1999; Brasier et al., 2006; see also Blankenship and Hartman, 1998; Godfrey and Falkowski, 2009), perhaps 3.5 Ga (Schopf and Packer, 1987; Awramik et al., 1983, 1988; Schopf, 1993, 2006) and possibly even before 3.8 Ga (Schidlowski, 1988, 2001; Mojzsis et al., 1996; Ohmoto, 1997; Rosing, 1999; Rosing and Frei, 2004).

It has been suggested that cyanobacterial oxygenic photosynthesis evolved from pre-existing anoxygenic phototrophs by lateral transfer of a photosystem gene cassette (Blankenship, 1992; see also Knoll, 2003a for a review) which might have happened relatively late considering the history of prokaryotes (Woese, 1987; Pace, 1997), and possibly postdated the emergence of aerobic respiration (Castresana and Saraste, 1995; Vargas et al., 1998) as oxygen was probably produced in trace amounts through photodissociation of H<sub>2</sub>O vapour in an atmosphere dominated by CO<sub>2</sub>, N<sub>2</sub> and H<sub>2</sub>O with lesser amounts of CO and H<sub>2</sub> prior to the emergence of photosynthesis (e.g. Canuto et al., 1983; Holland, 1984).

Beside putative microfossils and carbon isotope studies, a promising approach to demonstrate the presence of cyanobacteria in ancient ocean uses molecular biomarkers, notably 2 $\alpha$ -methylhopanes (Summons et al., 1999; Brocks et al., 1999, 2003), although the possibility that such biomarkers can have more diverse origins and not necessarily reflect the emergence of cyanobacteria has been expressed by several studies (Fischer et al., 2005; Kopp et al., 2005; Rashby et al., 2007; Rasmussen et al., 2008). A recent study by Godfrey and Falkowski (2009) demonstrated that an increasing trend towards higher  $\delta^{15}\text{N}$  values in kerogen in the Paleoproterozoic might reflect a change in nitrogen cycling due to the emergence of a source of  $\text{O}_2$ , most likely photosynthesising organisms prior to 2.7 Ga. However, Kopp et al. (2005) raised scepticism concerning the antiquity of oxygen producing organisms and advocated a later emergence of oxygenic photosynthesis perhaps even after the Archean-Proterozoic transition, which would have directly and rapidly triggered a planetary-scale glaciation known as the Makganyene or Huronian glaciations (~2.3-2.2 Ga: e.g. Hambrey and Harland, 1981; Kopp et al., 2005; Kasting and Ono, 2006).

After about 1.9 Ga, the first eukaryotes seem to have made their appearance on Earth, but remained highly conservative throughout much of the Proterozoic (Knoll, 2003a, b; Knoll et al., 2006). However, opinions as to the antiquity of eukaryotes and the history of their diversification range widely (see review by Knoll, 2006, and references therein). Paradoxically, as Johnston et al. (2009) recently pointed out, it may well be that the surprisingly long Mesoproterozoic 'boring billion', where seemingly stable low oxygen levels in the atmosphere and surface waters and anoxia in the deep ocean perpetuated, might have been sustained by anoxygenic photoautotrophs such as green and purple sulphur bacteria as well as physiologically versatile cyanobacteria, which in the presence of sulphide down-regulate PSII and obtain fewer (or no) electrons from water, instead oxidizing  $\text{S}^{2-}$  to  $\text{S}^0$ .

The time span that stretches from the late Neoproterozoic through to the mid-Cambrian (~800-501 Ma) witnessed increases in the diversity of acritarchs and other protistan morphotypes in fossil assemblages (Knoll et al., 2006 and references therein; Moczydlowska, 2008), heralding the evolution of architecturally complex bauplans and metazoans (Darwin, 1959; Walcott, 1899; Sprigg, 1947; McMenamin, 1990; Signor and Lipps, 1992; Valentine, 1992;

Bowring and Erwin, 1998; Knoll, 2000; Zhuravlev, 2001; Narbonne and Gehling, 2003; Narbonne, 2005; Peterson et al., 2005; Conway Morris, 2006; Marshall, 2006; McCall, 2006; Erwin, 2006; Meert and Lieberman, 2008; Budd, 2008; Payne et al., 2009). We can therefore adopt the view that the two major steps in the oxygenation of the Earth's surface broadly correlate with the most important biological upgrades; first from prokaryotes to eukaryotes around the GOE and then from single-celled to multicellular organisms in the Neoproterozoic. Crown-group members of red, yellow-brown and green algae, heterokonts (a major line of eukaryotes, today mostly consisting of diatom species) and testate amoebae had appeared by 750 Ma (Butterfield, 2004), but the evolution of animals happened later in the Proterozoic, exemplified by the appearance of the Ediacara Biota (e.g. Glaessner, 1959; Narbonne and Gehling, 2003). In a recent study of sterane biomarkers from the Huqf Group, Oman, Love et al. (2009) presented evidence for the presence of metazoans (*Demospongiae*) prior to the end of the Cryogenian glaciations (ca. 635 Ma), representing the oldest indication for animals in the fossil record (see also Valentine, 2002). Molecular clock estimates point to an age of >600 Ma for bilaterian phyla (Peterson et al., 2004, Douzery et al., 2004), but simpler, radial organisms must have predated this development (Valentine, 2002). More compelling evidence, such as Twitya discs, which possibly represent metazoans predating the 'Marinoan' glaciation (e.g. Hofmann et al., 1990; Knoll and Walter, 1992), fossilized cnidarians, possible bilaterian eggs and embryos preceding the Ediacaran radiation (Xiao et al., 1998; Xiao and Knoll, 2000; Yin et al., 2007) make it clear that the classic Ediacaran biota does not represent the first appearance of either crown-group eukaryotes or the oldest animals but merely the emergence of large and architecturally more complex organisms (Narbonne, 2005). And, enhancing the biomarker and molecular clock evidence for an early appearance of sponges, Maloof et al. (2010) have recently presented fossils older than 635 Ma which might well represent the oldest animal remains.

The Ediacaran type-biota, first recognized and described by Billings (1872), are difficult to interpret (see review by Narbonne, 2005). Studies over the last decade indicate that the Ediacaran organisms were composed of soft, flexible tissue and were most likely immobile animals or animal grade organisms (Gehling, 1999; Narbonne, 2005) and although stem-group bilaterian animals, 'failed experiments' and perhaps representatives of other eukaryotic

kingdoms are found in the Ediacaran fossil record, it seems likely that the Ediacara biota was dominated by stem and crown groups of the radial phyla (Sprigg, 1947, 1949; Narbonne, 2005). Even the earliest Ediacaran communities (ca. 575 Ma, Narbonne and Gehling, 2003; see Fig. 1.7) exhibited vertical and lateral niche subdivision, similar to Phanerozoic and modern communities. Later ecological and biological innovations include mobility (>555 Ma, Martin et al., 2000; Droser et al., 2002; Grazhdankin, 2004), calcification (550 Ma, Grotzinger et al., 2000; Hofmann and Mountjoy, 2001; Brennan et al., 2004), and predation (<549, Bengtson and Zhao, 1992; Hua et al., 2003).

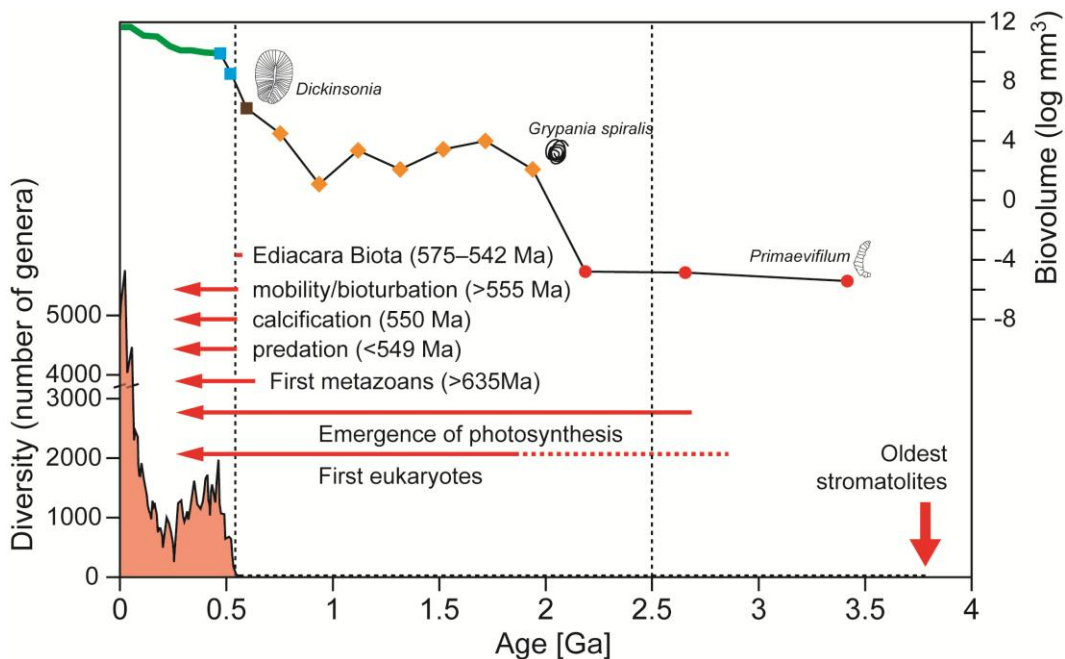


**Figure 1.7: The Neoproterozoic Oxygenation Event possibly unleashed major biological innovations including the appearance of new biological and ecological strategies: the first metazoans (e.g. Hofmann et al., 1990; Love et al., 2009), the appearance of the first large and architecturally complex organisms during the Ediacaran (Narbonne, 2005), the Cambrian Explosion with subsequent rapid increase in diversity (red shaded area; Peters, 2005; Marshall, 2006), the emergence of mobility (Martin et al., 2000), biological calcification (Grotzinger et al., 2000) and predation (Bengtson and Zhao, 1992). The upper curve shows the (logarithmic) increase of the maximum size of organisms throughout Earth history: red dots: prokaryotes, orange diamonds: protists, brown square:**

**vendobiont (probable multicellular eukaryote, e.g. *Dickinsonia*), blue squares: animals, green line: vascular plants (modified after Payne et al., 2009).**

Following the disappearance of the Ediacaran macrofauna after the Neoproterozoic - Cambrian boundary, which is defined by the first appearance of the trace fossil *Treptichnus pedum* 542±1 million years ago (Brasier et al., 1994; Landing, 1994; Droser et al., 1999; Valentine, 2002), a most significant evolutionary step took place known as the Cambrian 'Explosion', accordingly a subject of much debate (Gould, 1989; Conway Morris, 1992; Knoll and Carroll, 1999; Budd and Jensen, 2000; Conway Morris, 2006; Knoll, 2003b; Marshall, 2006; Budd, 2008). The causes leading to at least the near-extinction (and/or the disappearance from the fossil record) of the Ediacaran biota, which may have created an ecospace in which the Cambrian biota radiated (Seilacher, 1984), remain elusive but three hypotheses attempt to explain this phenomenon (Narbonne, 2005): (1) A short-lived interval of global ocean anoxia and/or widespread methane release (Kimura and Watanabe, 2001), which is supported by a sharp negative  $\delta^{13}\text{C}$  excursion that marks the global extinction of two major Ediacaran species (Amthor et al., 2003): *Cloudina*, a millimetre-sized, tubular fossil of one of the earliest biomineralizing animals, commonly used as a latest Ediacaran index fossil (Grant, 1990; Hofmann and Mountjoy, 2001), and *Namacalathus*, millimetre- to centimetre-sized globular and goblet-shaped calcified shells from the Neoproterozoic Nama Group in Namibia (Grotzinger et al., 2000), (2) because microbial mats, critical for the preservation of the Ediacaran type-biota (Gehling, 1999), massively decreased in abundance due to the rapid evolution of grazing and burrowing organisms during the Cambrian explosion, the scarcity of Ediacaran survivors in the Cambrian could be due to taphonomic conditions rather than evolutionary disappearance (Jensen et al., 1998) and, (3) the incoming of widespread predation at the Ediacaran – Cambrian boundary could have had a lethal effect on the soft-bodied, immobile Ediacaran biota (e.g. Bengtson, 2002).

Concerning the overall causes explicitly leading to the Ediacaran radiation and the subsequent 'Cambrian explosion', a rainbow of plausible triggers have been put forward: (1) environmental explanations, notably rising atmospheric oxygen levels (Nursall, 1959; Berkner

and Marshall, 1965; Cloud, 1968; Knoll and Carroll, 1999; Payne et al., 2009), the extreme greenhouse conditions following 'snowball Earth' (Hoffman et al., 1998), the Acraman meteorite impact (Grey et al., 2003; Williams and Wallace, 2003), a rapid decrease in orbital obliquity of ca. 30° (Williams, 1993, 2008), a period of unusually fast plate-motions (Kirschvink et al., 1997), repeated methane-release thermal cycling events (Kirschvink and Raub, 2003), a dramatic shift in terrestrial weathering processes (Kennedy et al., 2006) and changes in continental sediment accumulation during supercontinent amalgamation (Brasier and Lindsay, 2001), (2) developmental innovations, such as the evolution of Hox genes (Peterson and Davidson, 2000; Erwin and Davidson, 2002), and (3) ecological explanations, concerning new trophic capacities, like (anti-)predation ('arms race') and cropping, (e.g. Stanley, 1976; Butterfield, 2001; Bengtson, 2002), or new ecological niches (Valentine, 1980; Valentine and Walker, 1986).

Some evidence is present that the initial colonization of the land surface through fungi and photosynthetic microbes and algae also took place during the Neoproterozoic, and possibly already in the Mesoproterozoic. That step, which would have altered the physical, chemical and climatic conditions in the Precambrian world, is sustained by studies on paleokarstic surfaces (Horodyski and Knauth, 1994), karstic profiles depleted in  $^{13}\text{C}$  (Kenny and Knauth, 2001), microbial mat textures in fluvial environments (Prave, 2002), and molecular clock evidence (Heckman et al., 2001). In particular, an increasing colonization of the land surface would have had important consequences as continental (silicate) weathering would have been enhanced, leading to a decrease of  $\text{pCO}_2$  in the atmosphere and accounting for a rising  $^{87}\text{Sr}/^{86}\text{Sr}$  ratio during the Neoproterozoic, among other, less direct effects (Lenton and Watson, 2004; Kennedy et al., 2006; Fairchild and Kennedy, 2007).

It has already been mentioned that the break-up of Rodinia probably led to new environments for life (see Chapter 1.2.1.). On the other hand, the Neoproterozoic glaciations may well have represented evolutionary bottlenecks (James et al., 2005; Narbonne, 2005; Knoll et al., 2006) although several recent studies support a generally undisturbed biodiversity during the glaciations (Corsetti et al., 2003, 2006; Olcott et al., 2005; Moczydlowska, 2008; Nagy et al., 2009). Perhaps, as Hoffman (2009) recently pointed out, crack systems, consisting of fresh



cracks which would immediately freeze over with new sea-ice being full of brine channels which are known to be inhabited by eukaryotes, protists and prokaryotes, could have represented extensive and reliable refugia. However, after the Gaskiers glaciation, the eukaryotes underwent an explosive diversification in the postglacial world exemplified by the seemingly abrupt appearance of large spiny acritarchs (Grey et al., 2003) and large Ediacara-type fronds (Narbonne and Gehling, 2003). To what extent the Neoproterozoic glaciations impacted on the evolution of the biosphere is unclear but it is clear that bacterial and eukaryotic life persisted throughout the icehouse period from 750 – 580 Ma.

The putative oxygenation of the Neoproterozoic atmosphere to near present levels could on the one hand have been triggered by biological evolution and on the other hand may have represented a threshold factor that permitted the emergence of large animals seen in the fossil record of the Ediacara biota and the subsequent Cambrian explosion (e.g. Runnegar, 1991; Knoll, 2003a, b; Narbonne, 2005).

### **1.3.2. The oxygen requirements of early metazoans**

Photochemical models show that in order to establish an ozone layer capable of absorbing UV radiation potentially harmful to life, the partial pressure of oxygen in the atmosphere should be at least 0.002 bar (Berkner and Marshall, 1965; Kasting and Donahue, 1980; Kasting, 1987), which was presumably attained during the GOE. Paleontological evidence is consistent with predictable evolutionary steps occurring after the GOE, e.g. leading to the first fossils that are visible to the naked eye, *Grypania spiralis*, by 1.89 Ga (Han and Runnegar, 1992; Samuelsson and Butterfield, 2001; Schneider et al., 2002). Beside these extrinsic requirements for biological development, most living organisms and all living eukaryotes need a certain amount of molecular oxygen at some stage during their life cycle (e.g. Bloch, 1962; Mason, 1965; Brunet, 1967; Runnegar, 1991; Burmester and Burmester, 2002; Catling et al, 2005; Budd, 2008). Presumably, there is an absolute requirement for molecular oxygen to form the 4-ring cholestane structure found in all sterols, which are abundant membrane components responsible for rigidity in most eukaryotes and in a few bacteria (e.g. Brocks et al., 2003; Catling

and Claire, 2005; Di Giulio, 2003), of between about  $1 \cdot 10^{-3}$  and  $6 \cdot 10^{-3}$  PAL (Rogers and Stewart, 1974; Jahnke and Klein, 1979, 1983; Runnegar, 1991). Modified sterols (steranes) have been found in Late Archean shales (2.78 to 2.45 Ga; Brocks et al., 2003), indicating that trace amounts of oxygen were present at that time, possibly marking the onset of the GOE. But more recently, some workers have presented evidence showing that  $O_2$  is not necessarily a prerequisite in order to form steranes (Kopp et al., 2005; Kirschvink and Kopp, 2008). Collagen, proteins found exclusively in metazoans, have also an absolute requirement for molecular oxygen which might partly explain the emergence of animals in the Neoproterozoic (Towe, 1981; Saul and Schwartz, 2007; Saul, 2009).

It has also been argued that in order to prevent the biologically harmful influence of certain oxygen species, notably the superoxide radical ( $O_2^{\cdot-}$ ), singlet oxygen ( $^1O_2$ ), hydrogen peroxide ( $H_2O_2$ ) and the hydroxyl radical ( $\cdot OH$ ), antioxidants, such as the enzyme superoxide dismutase, have evolved relatively early in the history of life (Runnegar, 1991; see also Fee, 1982). But closer constraints regarding the timing of antioxidant evolution in organisms and what oxygen concentration would have triggered it, remain elusive.

Depending on an organism's size, shape and physiology, minimum requirements for oxygen can be inferred for aerobic organisms (see table 1.3; Raff and Raff, 1970; Runnegar, 1982, 1991; Catling et al., 2005; Budd, 2008; Fenchel and Finlay, 2008). Hence, maintaining the flux of oxygen to the mitochondria, the cell organelle carrying out aerobic respiration, limits the size of an organism according to the ambient oxygen availability, whereby the body mass of a given organism is proportional to its metabolic rate (Robinson et al., 1983; Runnegar, 1991). Further constraints are given by the shape of the organism: for organisms relying solely on epithelial diffusion of  $O_2$ , the most efficient shape would be a disk, such as Ediacaran *Aspidella* (Billings, 1872; Gehling et al., 2000) and the reasonably large *Dickinsonia* (Runnegar, 1982, 1991; Retallack, 2007). Nevertheless, Runnegar (1991) argued that *Dickinsonia* was probably too large to rely on epithelial diffusion alone but would have been able to exist in dysoxic conditions if it had blood to transport oxygen within its body (see also Catling et al., 2005). However, Danovaro et al. (2010) recently reported the discovery of metazoans (Phylum *Loricifera*) that thrive in permanently anoxic sediments through an anaerobic metabolism that is similar to that

demonstrated so far only for unicellular eukaryotes. This finding could further complicate the search for absolute constraints for a minimum level of oxygen necessary for life (see also Shields-Zhou and Och, 2011).

Nevertheless, Payne et al. (2009) recently compiled the largest organisms per period of Earth history and found that the maximum size increased by 16 orders of magnitude since the origin of life. Most of the size increase happening during two broad steps coinciding with the end of the GOE ~1.9 Ga and the inferred Neoproterozoic Oxygenation Event (see Fig. 1.1 and 1.7).

Besides the major biological innovations comprising the emergence of the Ediacara biota and the Cambrian Explosion (see chapter 1.3.1.), the fossil assemblages dating from the earlier Neoproterozoic, compiled by Knoll et al. (2006), contain an increased diversity of acritarchs (e.g. Butterfield and Rainbird, 1998), notably followed by an explosive diversification of acanthomorph (spiny) acritarchs after ca. 600 Ma (Grey et al., 2003), small branched structures interpreted as siphonocladalean green algae (Butterfield et al., 1994), vase-shaped microfossils (VSM; Porter and Knoll, 2000; Li et al., 2008a), possible fungi (Butterfield, 2005a) and a modest diversity of other colonial to multicellular eukaryotes (Butterfield et al., 1994; Butterfield, 2005b). In summary, the time span from the Late Mesoproterozoic to the Cambrian witnessed major clade divergence within the eucarya and an overall increase in organism size and complexity. How these events precisely relate to the Neoproterozoic Oxygenation Event is currently still under debate and is most probably a result of combined feedback mechanisms and direct and indirect environmental triggers involving climate and tectonics.

**Table 1.3: Size limitation of diffusion-based aerobic life (Catling et al., 2005).** The first three columns are for organisms relying solely on diffusion of O<sub>2</sub> to all internal cells. The other columns are for creatures with blood circulation that rely on diffusion only through an epidermal layer. Here,  $M$  is the metabolic rate of O<sub>2</sub> consumption (in cm<sup>3</sup> of O<sub>2</sub> h<sup>-1</sup> cm<sup>-3</sup> of tissue),  $K$  is a permeability constant for O<sub>2</sub> through tissue (in cm<sup>2</sup> of O<sub>2</sub> atm<sup>-1</sup> h<sup>-1</sup>),  $P_{ex}$  is the external P<sub>O2</sub> (in atm), and  $P_b$  is the average P<sub>O2</sub> in the blood (in atm). We assume that  $M = 0.03$  cm<sup>3</sup> of O<sub>2</sub> h<sup>-1</sup> cm<sup>-3</sup> of tissue for the first three organisms and  $M = 0.03$  and  $M = 0.01$  cm<sup>3</sup> of O<sub>2</sub> h<sup>-1</sup> cm<sup>-3</sup> of tissue for organisms with circulation. The latter represents the empirical range of metabolic rate for the organism size. Maximum size is calculated assuming  $P_b$  is an average of arteries  $\sim P_{ex}/2$  and veins  $\sim 0$  atm, and  $K = 8 * 10^{-4}$  cm<sup>2</sup> of O<sub>2</sub> atm<sup>-1</sup> h<sup>-1</sup> (Weisfogh, 1964; Brown, 1984). Epidermal layers vary from about 10 to 30  $\mu$ m. For the animals with circulation, an epidermal layer of thickness  $d = 30$   $\mu$ m is assumed. PAL of O<sub>2</sub> = 0.21 atm.

Parameter	Organism shape and physiology					
	Organisms with diffusion only			Organisms with blood circulation		
	Cylinder of radius $a$	Sphere of radius $a$	Disk of thickness $a$	Cylinder of radius $a$	Sphere of radius $a$	Disk of thickness $a$
Minimum $P_{ex}$ for given size, $a$	$\frac{Ma^2}{4K}$	$\frac{M}{6K}^2$	$\frac{Ma^2}{8K}$	$\frac{aMd}{2K} + P_b$	$\frac{aMd}{3K} + P_b$	$\frac{aMd}{2K} + P_b$
Theoretical maximum size	$\sqrt{\frac{4K}{M} P_{ex}}$	$\sqrt{\frac{6K}{M} P_{ex}}$	$\sqrt{\frac{8K}{M} P_{ex}}$	$\frac{2K}{Md} (P_{ex} - P_b)$	$\frac{3K}{Md} (P_{ex} - P_b)$	$\frac{2K}{Md} (P_{ex} - P_b)$
Maximum size at $P_{ex}$ of 0.21 atm	~1.5mm	~1.8mm	~2.1mm	9-28mm	13-43mm	~9-28
0.021 atm (10% PAL)	~0.5mm	~0.6mm	~0.7mm	0.8-3mm	1.2-4mm	0.8-3mm
0.002 atm (1% PAL)	~150 $\mu$ m	~180 $\mu$ m	~200 $\mu$ m	-	-	-

## **1.4. Isotopic evidence in support of the Neoproterozoic Oxygenation Event**

### **1.4.1. Carbon isotopes**

#### **1.4.1.1. The biogeochemical carbon cycle**

Following the review by Des Marais (2001), the biogeochemical carbon cycle can be divided into four subcycles that differ in their pathways with respect to reservoir sizes, processes, time frames and isotopic range whereas all pathways ultimately pass through the atmosphere and the hydrosphere, which allows even its remotest constituents to influence the ancient and modern Earth surface environment (see Fig. 1.8). The fastest subcycle, working on timescales from hours to thousands of years and consisting of the smallest reservoirs, includes only the hydro-, the atmo-, and the biosphere (HAB), whereas the latter dominates the exchange of carbon between CO<sub>2</sub> and organic matter through photosynthesis, the key mechanism in oxygen generation, and respiration. The sedimentary subcycle (SED), operating on timeframes of thousands to hundreds of millions of years (the average half life of sedimentary rocks is about 200 million years: Derry et al., 1992), includes the reservoirs of sedimentary organic matter and carbonates. The sedimentary subcycle strongly influences the HAB subcycle; for example by limiting global productivity through sedimentation and therefore removal of nutrients (e.g. Holland, 1984). Crucially, the balance between sedimentation of oxidized (carbonate, sulphate and ferric iron) and of reduced (organic carbon, sulphide and ferrous iron) species determines the abundance of oxygen and sulphate in the hydro- and atmosphere (Garrels and Perry, 1974; Holland, 1984; Hayes and Waldbauer, 2006). The slower subcycles involving the metamorphism of more deeply buried sedimentary and igneous rocks (MET) and the mantle-crust subcycle (MAN), including the mantle carbon reservoir and the processes of subduction and volcanism, proceed on timeframes of millions to billions of years. Especially processes at subduction zones are critical with respect to redox balances in the carbon cycle: organic carbon carries reduced species into subduction zones whereas sulphate

and ferric iron carry the oxidizing power. The carbon involved is being transferred either to the mantle or the crust (Hayes and Waldbauer, 2006).

Carbon cycling was probably more vigorous on the ancient Earth, notably in the Archean, than today, due to higher crustal production and therefore higher rates of mantle carbon outgassing (Des Marais, 1985). However, this does not preclude significant fluctuations in response to tectonic cycles of orogenesis, MOR spreading and metamorphism. There is no consensus whether the crustal carbon inventory exceeded the modern inventory because of the lower penetration depth of subducting slabs (Des Marais, 1985; McCulloch, 1993) and greater difficulties in retaining carbon by the slabs, or, alternatively, whether greater rates of mantle-crust exchange might have buffered Archean crustal and surface inventories of carbon similar to modern inventories (Sleep and Zahnle, 2001).

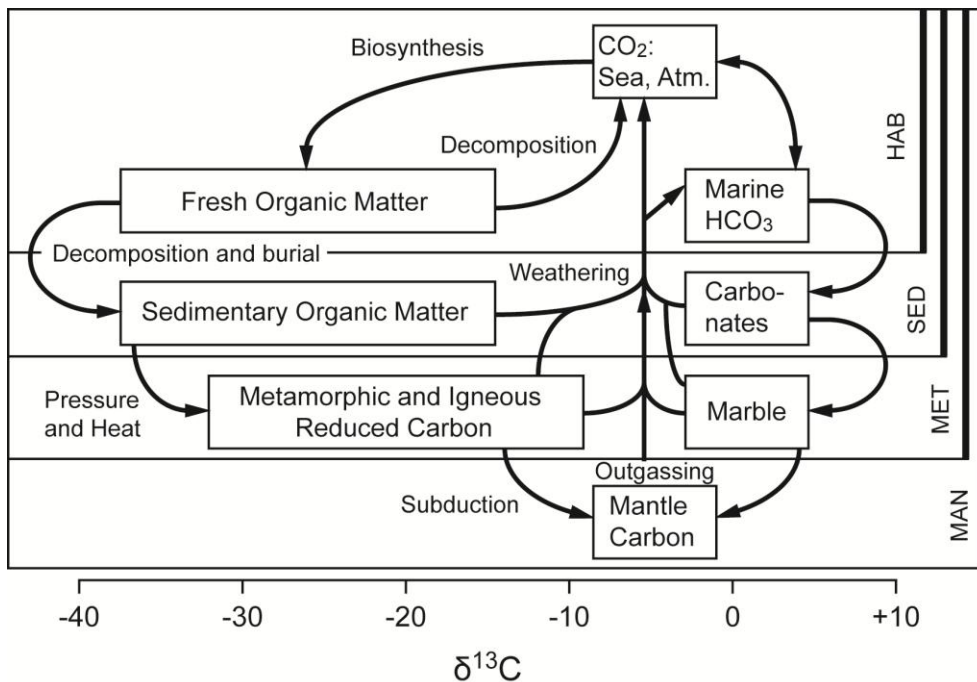


**Figure 1.8: The biogeochemical carbon cycle with principal reservoirs in the mantle, crust, oceans and atmosphere and how they are linked together (Des Marais, 2001). The horizontal dimension of the boxes indicates the typical range of the  $\delta^{13}\text{C}$  values of each reservoir. The axis on the right denotes the duration of the path of carbon through each of the four subcycles.**

#### 1.4.1.2. The carbon isotopic record

The carbon isotopic record is the basic metric of biogeochemical change over geological time (Schidlowski, 1988; Hayes et al., 1999). The isotopic fractionation of carbon occurs in the exogenic part, or the 'reaction chamber', of the carbon cycle, where the  $\delta^{13}\text{C}$  values of freshly deposited sedimentary carbon are established, comprising the atmosphere, hydrosphere and carbon exchanging sediments and soil and the interactions between them consisting of erosion, outgassing, transport, chemical transformations, sedimentation and burial of carbon. The most important process fractionating carbon isotopes is the biological fixation of  $\text{CO}_2$ , where  $^{12}\text{CO}_2$  is preferentially incorporated into photosynthesizing organisms relative to  $^{13}\text{CO}_2$ , catalysed by the enzyme ribulose-bisphosphate-carboxylase-oxygenase (RuBisCo) (O'Leary, 1981; Schidlowski, 2001; Sharp, 2007). RuBisCo is deemed the most abundant protein on Earth (Ellis, 1979) and interestingly, its function as  $\text{CO}_2$  fixator is competitively inhibited by oxygen (Warburg, 1920; Björkman 1966).

The amount of carbon within Earth's exogenic reaction chamber is controlled by the input from the mantle and by recycling of carbon within the crust, whereas the output is given by sedimentary burial and the weathering of seafloor basalts (Staudigel et al., 1989; Des Marais 2001; Hayes and Waldbauer, 2006). The carbon isotopic composition of carbonates, denoted by  $\delta^{13}\text{C}_{\text{carb}}$ , generally provides information about the global average  $\delta^{13}\text{C}_{\text{carb}}$  composition of deposited inorganic carbon from solution in open marine environments. Values of  $\delta^{13}\text{C}_{\text{org}}$  in marine settings are principally determined by biologically fixed  $\text{CO}_2$  (Des Marais, 2001).

Hayes and Waldbauer (2006) concluded that the  $\delta^{13}\text{C}$  value of carbonate rocks of around zero, rather than -5‰ which is the value of mantle carbon (Pearson et al., 2004; Sharp, 2007), indicates a continuous and substantial release of oxidizing power into the carbon cycle. Following that idea, the oxidation of the crust would have been more continuous than episodic and the increases in steady-state levels derive either from a combination of geological and biological changes or from biological changes alone.

During the past 800 My, the isotopic difference between  $\delta^{13}\text{C}_{\text{carb}}$  and  $\delta^{13}\text{C}_{\text{org}}$  was 30‰ on average (Hayes et al., 1999). To quantify relative fluxes of  $\text{C}_{\text{carb}}$  and  $\text{C}_{\text{org}}$ , the respective

isotopic values need to be incorporated into the isotopic mass balance where  $\delta^{13}\text{C}_{\text{in}}$  represents the isotopic composition of carbon entering the exogenic part of the carbon cycle and  $f_{\text{carb}}$  and  $f_{\text{org}}$  the fraction of carbon buried in carbonates or in organic form, respectively (Des Marais, 2001):

$$f_{\text{org}} = (\delta^{13}\text{C}_{\text{carb}} - \delta^{13}\text{C}_{\text{in}}) / (\delta^{13}\text{C}_{\text{carb}} - \delta^{13}\text{C}_{\text{org}})$$

The value of  $f_{\text{org}}$  acts as an indicator of biological productivity, organic decomposition and the processes involved in sedimentation and burial of carbon. A high value of  $f_{\text{org}}$ , i.e. increased organic burial, can indicate changes in the oxidation state of the environment provided that the fractionation between inorganic and organic carbon is constant as well as the  $\text{CO}_2$  flux and  $\delta^{13}\text{C}_{\text{in}}$ , because reduced carbon is withdrawn from the exogenic part of the carbon cycle (e.g. Des Marais, 2001; Hayes and Waldbauer, 2006).

However, the carbon isotopic record in carbonates and buried organic carbon can to a certain extent reflect the properties of the biogeochemical carbon cycle, i.e. the size of the individual reservoirs, in particular within the biosphere and geosphere, the nature of the interaction between them, and the changes which occurred in the carbon cycle throughout Earth history (e.g. Rothman et al., 2003; Sharp, 2007). Furthermore, secular trends in the carbon isotope composition of carbonates ( $\delta^{13}\text{C}_{\text{carb}}$ ) can act as a proxy for global biological productivity and burial of organic carbon and hence, provide important clues regarding the oxygenation of the Earth's surface through time (Kump and Arthur, 1999; Anbar and Knoll, 2002).

#### **1.4.1.3. The carbon isotopic record during the Neoproterozoic**

Corresponding to the crucial role of the carbon cycle in the redox state of the hydrosphere and the atmosphere, both major oxygenation events, in the Paleoproterozoic and in the Neoproterozoic, are characterized by large global excursions in  $\delta^{13}\text{C}_{\text{carb}}$  (see Fig. 1.5 and 1.9, Des Marais, 2001; Shields and Veizer, 2002; Halverson et al., 2005, 2007). After major



fluctuations during the Great Oxidation Event, which were accompanied by extensive oxidation of paleosols, a severe decline in the abundance of banded iron formations and the oxidation of heavy metals, such as U and Ce (see reviews by Canfield, 2005; Holland, 2006), the Mesoproterozoic experienced relative stability in crustal dynamics, climate and oxidation state of the surface environment during a remarkably long interval (Buick et al., 1995; Brasier and Lindsay, 1998) with  $\delta^{13}\text{C}_{\text{carb}}$  values between ca. -1 and +4‰ (Kah et al., 1999; Shields and Veizer, 2002).

The carbon isotopic record during the Neoproterozoic is reminiscent of the one during the Paleoproterozoic but has been studied in much greater detail due to the greater quantity and quality of preserved successions, and accordingly, has been considered to reflect the major climatic, tectonic and biological events which accompanied the Neoproterozoic Oxygenation Event. Between 800 and 540 Ma, two globally concordant patterns are particularly indicative of an increasingly oxygenated Earth surface:

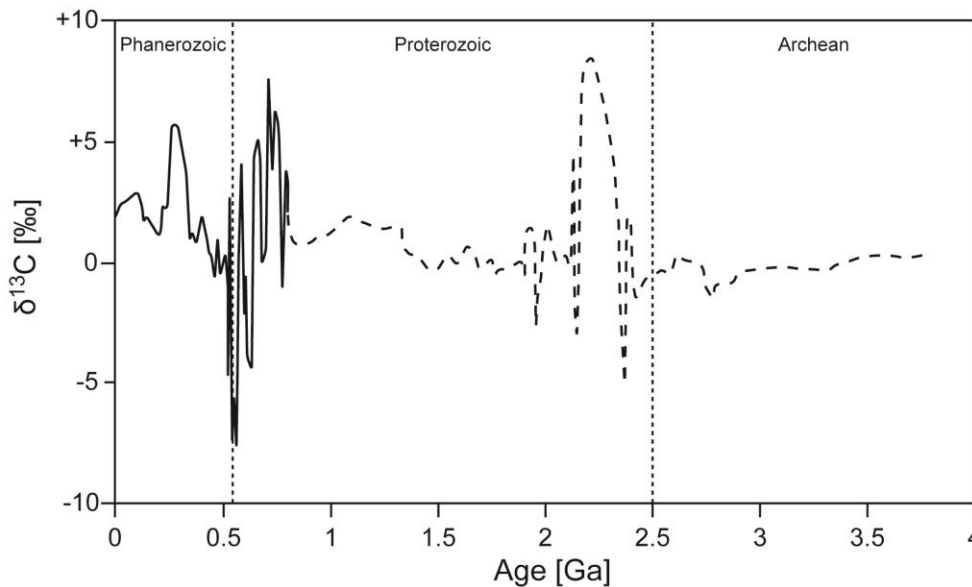


**Figure 1.9: The  $\delta^{13}\text{C}$  record throughout Earth history whereby the dashed interval is based on limited data. Compiled by Campbell and Allen (2008) using data from Brasier and Lindsay (1998), Lindsay and Brasier (2002), Shields and Veizer (2002), Bergman et al. (2004) and Halverson et al. (2005).**

1) Exceptionally long-lived positive  $\delta^{13}\text{C}_{\text{carb}}$  excursions occurred after about 800 Ma, which are punctuated by pronounced negative  $\delta^{13}\text{C}_{\text{carb}}$  excursions associated with but not uniquely correlated to global ice ages (see Fig. 1.5; Kaufman and Knoll, 1995; Shields and Veizer, 2002; Halverson et al., 2005). The strongly positive  $\delta^{13}\text{C}_{\text{carb}}$  values of  $\geq 5\text{‰}$  imply enhanced burial of organic carbon on a global scale (Derry et al., 1992; Des Marais et al., 1992) and therefore an enhanced flux of oxidizing power to the surface environment. Higher burial of organic matter, i.e. higher degree of preservation of organic matter within clastic sediments mainly depends on 1) high sedimentation rates (Bernier and Canfield, 1989), 2) high productivity, stimulated by nutrient supply (Froelich et al., 1982) and 3) an anoxic water column, retarding the oxidation of settling organic matter (Derry et al., 1992). As indicated by strontium isotope data from prior to 600 Ma, when seawater  $^{87}\text{Sr}/^{86}\text{Sr}$  increased steeply (Veizer, 1989; Asmerom et al., 1991; Jacobsen and Kaufman, 1999; Halverson et al., 2007; Shields, 2007), erosion rates, and therefore sedimentation rates were low and therefore also the nutrient supply to the oceans (Asmerom et al., 1991; Derry et al., 1992). Hence, high proportional rates of organic burial,  $f_{\text{org}}$ , do not necessarily imply high absolute rates of burial (Stein, 1990; Kaufman and Knoll, 1995; Hayes et al., 1999) and high  $f_{\text{org}}$  during the Cryogenian most probably indicate an anoxic water column (Canfield, 1998; Canfield et al., 2008; Nagy et al., 2009). In addition, Logan et al. (1995) also suggested that the widespread development of faecal pellets, an important mechanism transporting organic matter to the deep water in the modern ocean, could have prevented organic matter from being oxidized early in the water column.

Furthermore, a study by Kennedy et al. (2006) showed an increase in clay mineral deposition, in particular the appearance of smectite (Weaver, 1967, 1989), from the Late Precambrian until the Early Cambrian (850-530 Ma) in response to a fundamental change in the dominant weathering mechanism from mechanical weathering to more efficient biota-assisted chemical weathering. As clay minerals represent the major cause of carbon preservation and burial in the modern system due to the affinity of organic matter to disperse among or bind to clay minerals (Keil et al., 1994; Ransom et al., 1998; Kennedy et al., 2002; Mayer et al., 2004), the initiation of a 'Clay Mineral Factory' (Kennedy et al., 2006) in the Late Neoproterozoic would support the proposed increase in organic carbon burial. But this concept has recently

been challenged by Tosca et al. (2010) who demonstrated that chemical weathering indices actually decrease in the late Neoproterozoic together with a switch to micaceous clays. This indicates that, while there is no absolute increase in clay mineral content in the organic rich shales they analysed, physical erosion dominates the clay composition across the Neoproterozoic – Cambrian boundary.

Squire et al. (2006) also suggested a close relationship between the  $\delta^{13}\text{C}_{\text{carb}}$  record and the continental configuration. Between 900 and 650 Ma, while the continental fragments of Rodinia drifted apart, continentally derived detritus accumulated mainly at the rifted margins along which the continents separated. Hence, the burial of organic matter might have been slow but relatively undisturbed with a high preservation factor (see also Kirschvink and Raub, 2003). During the subsequent Transgondwanan orogenesis, the former stable shelves of the continental fragments were uplifted and eroded, and their organic carbon oxidized.

However, it is difficult to quantify to which extent oxidizing power would have been released as the rates of volcanic outgassing over time are poorly known as well as the isotopic fractionation between DIC and carbonate removed from seawater during seafloor weathering (Bjerrum and Canfield, 2004; Hayes and Waldbauer, 2006).

2) Extremely negative  $\delta^{13}\text{C}_{\text{carb}}$  excursions, initially identified by Pell et al. (1993) and Burns and Matter (1993) in mid-Ediacaran rocks of Australia and Oman respectively, a prolonged negative  $\delta^{13}\text{C}_{\text{carb}}$  excursion between ca. 600 and 550Ma, representing the largest decrease of  $\delta^{13}\text{C}_{\text{carb}}$  in marine carbonates in Earth history with values from +5‰ down to -12‰, followed by a sub-linear recovery to positive  $\delta_{\text{carb}}$  values has been recognized in the Shuram Formation of the Nafun Group in Oman (Le Guerroué et al., 2006a,b; Fike et al., 2006) with potential correlatives in Ediacaran strata elsewhere (the Johnny Formation of Death Valley: Corsetti and Kaufman, 2003, 2005; Kaufman et al., 2007; the Wononoka Formation of the Adelaide rift complex: Calver, 2000; Walter et al., 2000; the Doushantuo Formation of the Yangtze Platform: Yang et al., 1999; Jiang et al., 2003b, 2007a; Condon et al., 2005; McFadden et al., 2008; the post-Marinoan Windermere Supergroup: Narbonne et al., 1994; James et al., 2001; the Nama and Tsumeb groups of Namibia: Kaufman et al., 1993; Grotzinger et al., 1995; Saylor et al., 1998;

and in SE Siberia: Pokrovsky and Gertsev, 1993; Melezhik et al., 2005a, 2009; Pokrovsky et al., 2006). In contrast to the other Neoproterozoic negative  $\delta^{13}\text{C}_{\text{carb}}$  excursions (see Fig. 1.5), there is no evidence for a major glaciation which could be linked to the event except for the Gaskiers ca. 580 Ma which is considered to be a non-global event with no recognizable imprint in the Nafun stratigraphic record (Halverson et al., 2005; Le Guerroué et al., 2006b).

The proposed explanations for the negative shifts in  $\delta^{13}\text{C}_{\text{carb}}$  values, which include prior build-up of mantle-derived carbon in the atmosphere–ocean reservoir during a Snowball period of prolonged hydrological shutdown (Hoffman et al., 1998), the overturn of a stratified ocean with a strongly functioning biological pump (Grotzinger and Knoll, 1995; Knoll et al., 1996; Kaufman et al., 1997) and seepage from a light carbon reservoir of methane clathrates (Dickens et al., 1995; Kennedy et al. 2001; Schrag et al., 2002; Jiang et al., 2003a), cannot be applied to the much longer lasting (7 - 50 My) more pronounced event during the mid/late Ediacaran (Bowring et al., 2007; Jiang et al., 2007a; Fike et al., 2006; Le Guerroué et al., 2006a,b; Melezhik et al., 2009). A model proposed by Rothman et al. (2003), which involves remineralization of a large dissolved organic carbon (DOC) pool in the ocean of between 100 and 1000 times the modern inventory of DOC and a dissolved inorganic carbon (DIC) reservoir 10 times smaller than DOC reservoir, may theoretically explain such a long-lived phenomena and would imply an at least mildly oxygenated deep ocean which would have been established during the Neoproterozoic Oxygenation Event (see also Fike et al., 2006; Jiang et al., 2007a; McFadden et al., 2008). Several studies reported a  $\delta^{13}\text{C}$  depth gradient in the Neoproterozoic (James et al., 2001; Zhou et al., 2004a; Shen et al., 2005; Jiang et al., 2007a; Giddings and Wallace, 2009), whereby shallow water carbonates mostly exhibit higher  $\delta^{13}\text{C}$  values (up to 11‰: Giddings and Wallace, 2009) than deep water facies, indicating a stratified Neoproterozoic Ocean and the establishment of a large deep water DOC pool according to Rothman et al. (2003). Nevertheless, an opposite trend has been demonstrated by Melezhik et al. (2009) in the very extensive Neoproterozoic carbonate succession developed on the western slope of the Aldan Shield in Southeast Siberia, where deep-water facies are less depleted in  $^{13}\text{C}$  than the shallow-water facies indicating that a large DOC pool in the deep ocean might not have been a global phenomena or it might have varied in time and extent throughout the Neoproterozoic.

However, Bristow and Kennedy (2008) have challenged the idea that the final oxidation and removal of the excess DOC resulted in the Shuram excursion using a numerical method to quantify the demand for oxidants needed to drive a negative  $\delta^{13}\text{C}_{\text{carb}}$  excursion of the recorded magnitude and duration. The results showed that for a duration of 30 Myr, a pool of DOC between ca. 6000 and 12000 times the modern inventory would have been necessary and the combined Ediacaran oxidant inventory of oxygen (100% PAL) and sulphate (5mM) would have been exhausted within ca. 800 Kyr, although several other biogeochemical proxies indicate that oxygen and sulphate levels have risen or were at least maintained during the Shuram excursion.

It has also been argued that the negative  $\delta^{13}\text{C}_{\text{carb}}$  values in the Neoproterozoic were the result of meteoric diagenesis (Knauth and Kennedy, 2009) and/or the product of burial diagenesis (Derry et al., 2010). Both are based on covariation patterns of  $\delta^{13}\text{C}$  with  $\delta^{18}\text{O}$  (see also Fike et al., 2006), which is usually a good indicator for diagenetic alteration (e.g. Marshall, 1992). If this is the case, other, new intriguing questions remain: why did this massive alteration of carbonate rocks occur globally in the Neoproterozoic at supposedly similar times and rather isolated in Earth history? However, others have argued that positive covariation of carbon and oxygen isotopes could also result from processes occurring in silled, salinity stratified basin with limited marine connection (Talbot, 1990; Bristow and Kennedy, 2008).

The debate concerning the most negative shift in recorded  $\delta^{13}\text{C}_{\text{carb}}$  values in Earth history, notwithstanding its primary origin, is far from over and will more likely be the result of multiple causes (e.g. Melezhik et al., 2009). Nevertheless, it's probable that the oxygenation of the deep ocean played an important role in causing these major perturbations in the global carbon cycle.

#### **1.4.1.4. Total organic carbon content in sedimentary rocks throughout Earth's history**

It has been shown that organic carbon burial is the main mechanism controlling the carbon isotope record in carbonates and that black shale deposition peaked in the Early Paleoproterozoic and the Late Neoproterozoic (see Fig. 1.2 and 1.10). It appears that the extremely positive  $\delta^{13}\text{C}$  excursion during the Great Oxygenation Event, with the highest values

characterizing the Lomagundi-Jatuli Event, predates the massive accumulation of black shales after 2 Ga, whereby sediments with anomalously high organic carbon (up to 98%) deposited during the so called Shunga Event ~2 Ga have been described (Melezhik et al., 1999a,b; Melezhik, 2005b). A similar pattern is observed in the Neoproterozoic, where the long-lived positive  $\delta^{13}\text{C}$  excursion predates an increase in black shale deposition. However, a compilation of TOC content in organic rich sediments (see Fig. 1.10) shows that times of elevated black shale deposition are not contemporary with occurrences of maximum TOC concentrations and high TOC contents of over 15% are found in sedimentary successions deposited prior to both, the Great Oxygenation and the Lomagundi-Jatuli Event. This suggests that organic carbon burial is on one hand controlled by widespread, disseminated sequestration and more localized, highly concentrating depositional settings and that buried organic matter might be less straightforward to find when it comes to explain major positive  $\delta^{13}\text{C}$  excursions. But this fails to explain the tendency of  $^{13}\text{C}$  enriched carbonates to occur before massive black shale deposition. A tentative explanation would be that in the absence of significant  $\text{C}_{\text{org}}$  oxidation due to the absence of free  $\text{O}_2$  and inhibited bacterial sulphate-reduction, and the lack of efficient ballasting mechanisms (Logan, 1995), a dissolved organic carbon pool might have been accumulating for tens of millions of years prior to both Oxygenation Events, the accumulation itself creating oxidative power.

Much less black shale was deposited during the Mesoproterozoic together with lower TOC contents which might be explained by suppressed biological productivity or, due to dominantly anoxic and even euxinic conditions in the oceans, highly disseminated organic carbon sedimentation although low and relatively invariant  $\delta^{13}\text{C}$  values during that time do not support the latter. Therefore, a scarcity of life during the 'Boring Billion' might be indicated leading to overall low organic production and consistently high TOC concentrations in black shales deposited from the Late Neoproterozoic on, highly profitable for the petroleum industry, might intuitively be attributed to enhanced primary productivity in concert with the diversification of organisms.

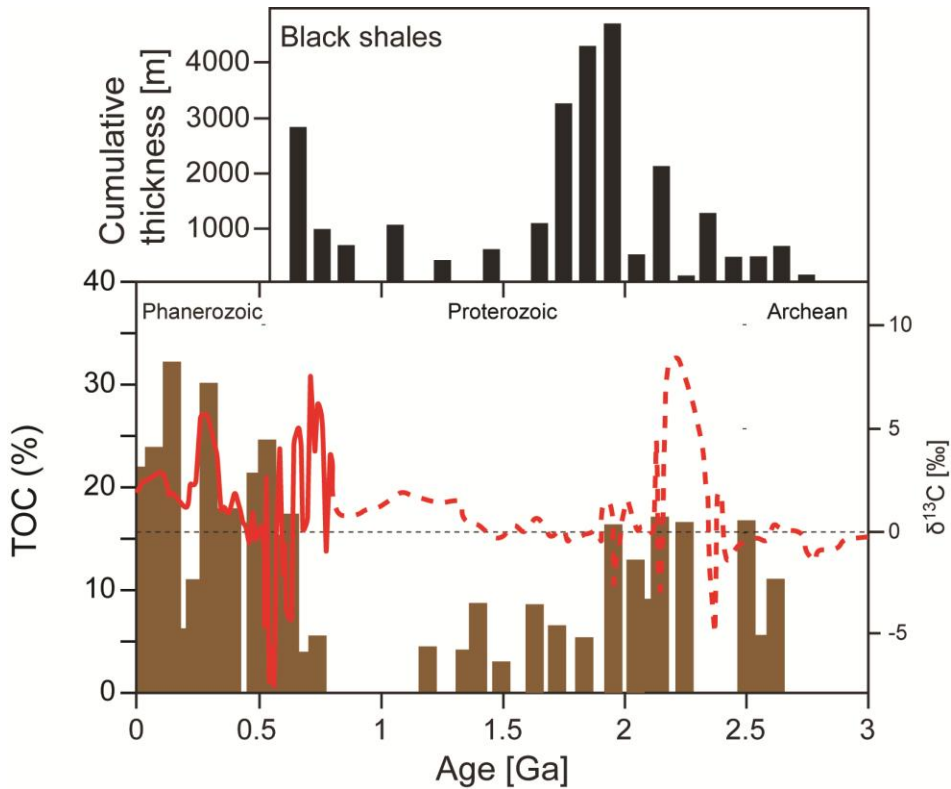


**Figure 1.10: Compilation of TOC contents in black shales compared to black shale abundances (top) and  $\delta^{13}\text{C}_{\text{carb}}$  curve throughout the last 3 billion years. Note that positive  $\delta^{13}\text{C}_{\text{carb}}$  excursions tend to precede peaks in black shale deposition. TOC concentrations have been binned into their respective periods in Earth history and references are in the appendix.**

## 1.4.2. Strontium isotopes

### 1.4.2.1. The $^{87}\text{Sr}/^{86}\text{Sr}$ ratio of the ocean

Strontium has four stable isotopes,  $^{84}\text{Sr}$ ,  $^{86}\text{Sr}$ ,  $^{87}\text{Sr}$  and  $^{88}\text{Sr}$ , whereby the isotope  $^{87}\text{Sr}$  is radiogenic.  $^{87}\text{Sr}$  is generated by the  $\beta$ -decay of  $^{87}\text{Rb}$  with a half life of 48.8Gyr (see review by Veizer, 1989) making  $^{87}\text{Sr}$  an important isotopic tracer of age and sources in cosmochemical and geochemical materials (Faure, 1986) and it is particularly useful for Sr chemostratigraphy, reconstructing global tectonics and tracing diagenetic processes (Veizer, 1989; Banner, 2004). One of the most interesting properties of  $^{87}\text{Sr}$  in the ocean is that it can reflect changes in the

relative contribution of the continental and the mantle chemical reservoirs when normalized to the stable isotope  $^{86}\text{Sr}$  (e.g. Faure, 1986; Veizer, 1989; Veizer et al., 1999).

The primordial strontium isotopic ratio at the time of the Earth formation, some 4.6 Gyr ago, is approximately 0.699 (Wetherill et al., 1973). The further Sr isotopic evolution of distinct geological reservoirs has been a function of their Rb/Sr ratio and is mainly controlled by the fact that the differentiation of the Earth has been accomplished by the process of fractional crystallization, leading to granitic melts and, subsequently, continents. The point is that Sr, and in particular Rb, preferentially accumulates in the melt, resulting in high Rb/Sr ratios in the continental crust and its progressive decrease in the residual mantle. Hence, today's continents are enriched in radiogenic  $^{87}\text{Sr}$ , with a higher enrichment in older continental segments having a  $^{87}\text{Sr}/^{86}\text{Sr}$  ratio of more than 0.710, whereas the mantle and oceanic crust have a depleted  $^{87}\text{Sr}/^{86}\text{Sr}$  ratio of about  $0.703\pm 1$ . This difference between the isotopic values of the continents and the mantle is crucial in understanding the Sr isotopic evolution of seawater.

The Sr budget in the modern ocean is controlled by the following inputs: river runoff, for which the  $^{87}\text{Sr}/^{86}\text{Sr}$  signature can be seen as a function of the ratio between carbonate and silicate weathering (Shields, 2007), groundwater runoff, oceanic crust-seawater interactions and, diagenetic reflux of Sr into the oceans. At steady state, the inputs are counteracted by: sedimentary removal of Sr and exchange of radiogenic Sr during submarine hydrothermal alteration of ocean basalts. The sources of Sr can be summarized by the two isotopic end-members: the submarine, chemical alteration of oceanic crust ( $^{87}\text{Sr}/^{86}\text{Sr} \sim 0.703$ : Hofmann, 1997) and the subaerial, chemical weathering of the continental crust and its sedimentary cover ( $^{87}\text{Sr}/^{86}\text{Sr} \sim 0.712$ : Palmer and Edmond, 1989; Peucker-Ehrenbrink and Miller, 2006). In the modern ocean, these fluxes with their respective Sr concentration and isotopic composition lead to a seawater  $^{87}\text{Sr}/^{86}\text{Sr}$  ratio of  $0.709241\pm 32$  (Elderfield, 1986), with a homogenous distribution in seawater as the residence time of Sr (3-5 My) is long compared to the mixing time of the ocean ( $\sim 1$  Ky) (Halverson et al., 2007). These numbers indicate that about twice as much Sr in the ocean derives from river runoff than from hydrothermal exchange (Shields, 2007; Richter et al., 1992). The Sr delivered to the ocean is mostly derived from weathered carbonates ( $\sim 55\%$ : Bickle, 1994), due to the high Sr content and high solubility of those minerals.



However, the Sr isotopic content in carbonate rocks, which reflects to a close approximation the Sr signature of the seawater at their time of formation, can provide information about the extent of chemical weathering in the past and give clues about probable constraints on primary productivity and photosynthetic surface activity, and therefore the oxygen content in the atmosphere and oceans throughout the Earth history.

Similar to Sr isotopes, the ratio  $^{143}\text{Nd}/^{144}\text{Nd}$  can be used to measure the relative contribution of continental weathering to their seawater budget, whereby the radiogenic isotope  $^{143}\text{Nd}$  is generated by the decay of  $^{147}\text{Sm}$ . However, beside a much lower residence time in the ocean and being much more reactive while remaining relatively immobile during postdepositional alteration, the crucial difference compared with Sr is that the continental crust has depleted  $^{143}\text{Nd}/^{144}\text{Nd}$  values, thus leading to a mirrored pattern compared to the  $^{87}\text{Sr}/^{86}\text{Sr}$  curve (Jacobsen, 1988; Asmerom et al., 1991; Kaufman et al., 1993; Banner, 2004). However, the more complicated geochemical cycling of Nd makes its use as a paleoenvironmental proxy less straightforward than for Sr (Banner, 2004, and references therein).

#### **1.4.2.2. Changes in the seawater $^{87}\text{Sr}/^{86}\text{Sr}$ ratio during the Neoproterozoic**

Because seafloor spreading rates have changed only little over the past 150 Myr, the hydrothermal input of Sr can be considered to be constant for this time interval and it is possible to relate the  $^{87}\text{Sr}/^{86}\text{Sr}$  curve to riverine input from continental weathering (François and Walker, 1992; Kennedy et al., 2006). Because the spreading rates are not constrained for the time before 180 Ma, caution is appropriate when applying this approach to older sediments. Furthermore, variations in the isotopic composition of the upper mantle and particularly river runoff also affect the  $^{87}\text{Sr}/^{86}\text{Sr}$  ratio (Veizer et al., 2003; Shields, 2007). Nevertheless, the rise in the  $^{87}\text{Sr}/^{86}\text{Sr}$  ratio during the Neoproterozoic is impressive as it begins at very low ratios (<0.7060; e.g. Asmerom et al., 1991) early in the Neoproterozoic, eventually rising to values higher than >0.7090 (e.g. Shields, 1999, 2007; Calver, 2000) during the Cambrian Period. A recent compilation by Halverson et al. (2007) of high-quality  $^{87}\text{Sr}/^{86}\text{Sr}$  data across several Neoproterozoic sections around the world confirms this rise in seawater  $^{87}\text{Sr}/^{86}\text{Sr}$ .

However, Shields (2007) has proposed plausible evolutionary trends for the major Sr sources accounting for the increasing  $^{87}\text{Sr}/^{86}\text{Sr}$  ratio in Neoproterozoic seawater, which are carbonate/silicate weathering and oceanic crust-seawater interactions, in order to normalize the seawater  $^{87}\text{Sr}/^{86}\text{Sr}$  curve against the isotopic evolution of Sr sources to the ocean (see Fig. 1.11). He puts forward three possible explanations for the Neoproterozoic to Cambrian rise: (1) an increased  $^{87}\text{Sr}/^{86}\text{Sr}$  ratio of the rocks undergoing weathering, (2) a decrease in the mantle Sr input and/or seafloor spreading rates and (3), an increase in overall continental (or merely silicate) weathering rates. While (1) is plausible, neither Nd isotope data (e.g. Jacobsen, 1988; Felitsyn and Morad, 2002) nor the Sr isotopic composition of detrital silicates (e.g. Goldstein, 1988) supports a more radiogenic continental runoff during the late Neoproterozoic and Cambrian relative to today (Shields, 2007). The approach (2) may have exerted second order variations, but the excellent correlation of the seawater  $^{87}\text{Sr}/^{86}\text{Sr}$  curve and seawater  $\delta^{34}\text{S}$  implies that absolute fluxes and not the isotopic evolution of those fluxes lead to first-order  $^{87}\text{Sr}/^{86}\text{Sr}$  trends (see Fig. 10). Moreover, a sustained decrease in seafloor spreading rates seems to be improbable during a time of such rapid continental reconfiguration, generally high sea-levels and widespread arc collision and rifting (Kirschvink et al., 1997).

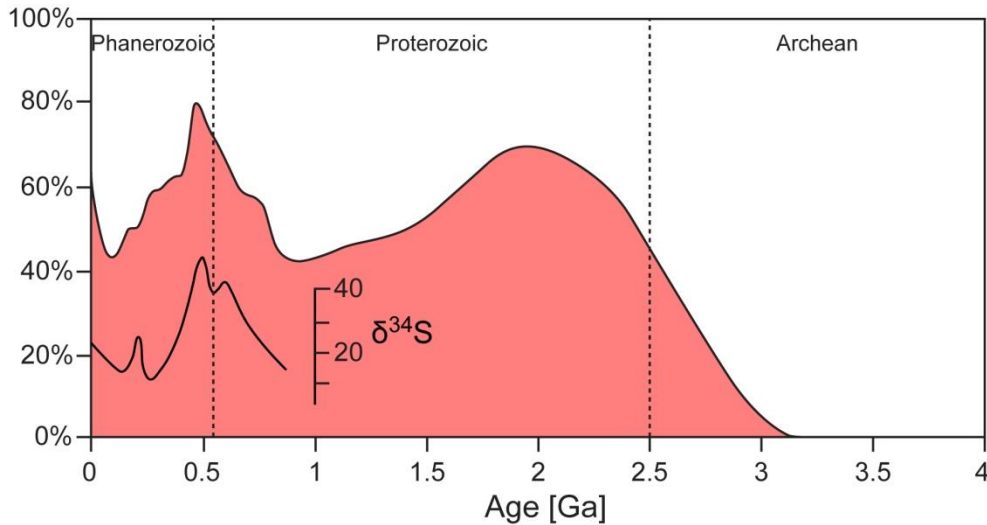


**Figure 1.11: The normalized seawater  $^{87}\text{Sr}/^{86}\text{Sr}$  curve. Note that the excellent correlation of the seawater  $^{87}\text{Sr}/^{86}\text{Sr}$  curve and seawater  $\delta^{34}\text{S}$  implies that absolute fluxes and not the isotopic evolution of those fluxes lead to first-order  $^{87}\text{Sr}/^{86}\text{Sr}$  trends (Shields, 2007).**

Hence, a sustained increase in overall continental and/or silicate weathering rates represents the most plausible explanation for the Neoproterozoic-Cambrian rise in the seawater  $^{87}\text{Sr}/^{86}\text{Sr}$  ratio. This is consistent with the period of continental break-up of Rodinia (see chapter 1.2.1.) and is possibly a consequence of increased rates of physical weathering which lead to higher chemical weathering rates (Gaillardet et al., 1999), also supported by increasing clay content in marine sediments (Kennedy et al., 2006), during times of supercontinent break-up and microcontinent collision (Jacobsen and Kaufman, 1999; Squire et al., 2006). This interpretation is supported by sediment flux rates which seem to correlate well with the normalized  $^{87}\text{Sr}/^{86}\text{Sr}$  curve (Hay et al., 2001). Furthermore, the rise to peak  $^{87}\text{Sr}/^{86}\text{Sr}$  values corresponds to the formation of huge mountain chains (Jacobsen, 1988; Squire et al., 2006) which would have promoted physical weathering. Enhanced silicate weathering has also been predicted by modelling climate and runoff (e.g. Donnadieu et al., 2006). Increased chemical weathering of rocks would have led to an increased flux of nutrients to the ocean whereby phosphorus plays a particularly crucial role as biolimiting element over geological timescales (Lenton and Watson, 2000).

The rise in the  $^{87}\text{Sr}/^{86}\text{Sr}$  ratio also begins at the onset of the long-lived positive  $\delta^{13}\text{C}_{\text{carb}}$  excursion characteristic for the later Neoproterozoic and it has been argued that weathering-driven increases in productivity might have led to higher rates of organic carbon burial in the newly formed passive margins of the rifting supercontinent. This process could have supported and enhanced the oxygenation of the Earth's surface during the Neoproterozoic –Cambrian transition (Derry et al., 1992).

However, the direct coupling of the two proxies, the  $^{87}\text{Sr}/^{86}\text{Sr}$  ratio and  $\delta^{13}\text{C}_{\text{carb}}$  values has been disputed by Halverson et al. (2007), notably because of their contradictory behaviour during the 'Bitter Springs Stage' ca. 850 Ma. Furthermore, it has to be considered that the  $^{87}\text{Sr}/^{86}\text{Sr}$  ratio does not necessarily reflect the extent of continental weathering as the erosion of platform carbonates and evaporites buffer the ocean against changes in  $^{87}\text{Sr}/^{86}\text{Sr}$  (Edmond, 1992). In addition, supercontinent assembly has the effect of shifting away rainfall from radiogenic continental interiors to non-radiogenic juvenile crust on the edges of the continents whereas continental break-up should cause the  $^{87}\text{Sr}/^{86}\text{Sr}$  ratio to rise by shifting the source of rainfall to older, more radiogenic and recently extended and uplifted continental interiors (Donnadieu et al., 2004; Halverson et al., 2007). However, as mentioned above, the excellent correlation between the normalized  $^{87}\text{Sr}/^{86}\text{Sr}$  and seawater  $\delta^{34}\text{S}$  curves implies that absolute fluxes and not the isotopic evolution of those fluxes led to first-order  $^{87}\text{Sr}/^{86}\text{Sr}$  trends, as the  $\delta^{34}\text{S}$  record is thought to reflect changes in the biogeochemical cycling of sulphur (e.g. Strauss, 1999; see also next chapter), and so ought to be independent of changes in the  $^{87}\text{Sr}/^{86}\text{Sr}$  isotopic composition or age of rocks exposed to weathering (Shields, 2007).

### **1.4.3. Sulphur isotopes**

#### **1.4.3.1. The sedimentary sulphur cycle**

The sulphur cycle is in some ways similar to the carbon cycle; in both cases the elements form solids in oxidized and reduced states, sulphate and sulphide for sulphur and carbonates and organic matter for carbon, respectively. And pyrite burial, such as the burial of organic

carbon, accounts for an important amount of O<sub>2</sub> released to the atmosphere. The near surface reduction of sulphur and carbon from dissolved carbonate and sulphate species is a biologically mediated process which in both cases is a kinetically controlled process whereby the reduced phases are depleted in the heavier isotopes (<sup>34</sup>S and <sup>13</sup>C) compared to seawater values (Sharp, 2007). Furthermore, the S and C cycles are closely linked together through sulphate reduction, which most commonly proceeds via reoxidation of organic substrates. The exospheric sulphur cycles includes the following reservoirs: the ocean, with a present sulphate concentration of about 28 mM and modern  $\delta^{34}\text{S}_{\text{sulphate}}$  values of about 21.0‰, which due to its long residence time of 10 to 20 My is both homogenous throughout the ocean and buffered against short term (<1My) variations (Rees et al., 1978; Claypool et al., 1980; Hurtgen et al., 2006), rivers and lakes, with variable  $\delta^{34}\text{S}$  values and a total amount of  $1.3 \times 10^{18}$  g sulphur, shales, with modern  $\delta^{34}\text{S}$  values of about -17‰ and a budget of  $4.74 \times 10^{21}$  g sulphur, and evaporites with modern  $\delta^{34}\text{S}$  values of about 16‰ and a budget of  $4.86 \times 10^{21}$  g sulphur (e.g. Sharp, 2007).

The  $\delta^{34}\text{S}$  composition of seawater sulphate in steady state is a function of the mass and isotopic composition of the sulphur fluxes into and out of the ocean. The source of sulphate into the ocean is mainly supplied by the oxidative weathering of <sup>34</sup>S-depleted sulphides and the dissolution of evaporite minerals. The removal of sulphur from the ocean is maintained by microbially mediated pyrite formation, accompanied by a large isotopic fractionation, and the precipitation of evaporites, accompanied by negligible fractionations (e.g. Canfield, 2001a, b).

#### **1.4.3.2. Sulphur isotope fractionation**

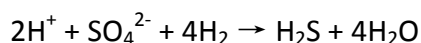
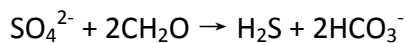
Sulphur has four stable isotopes, <sup>32</sup>S accounting for 95% of the total sulphur on Earth, <sup>34</sup>S, <sup>33</sup>S and <sup>36</sup>S, in order of decreasing abundance. The minor isotopes <sup>33</sup>S and <sup>36</sup>S will not be discussed in this review due to their relatively poor coverage in sulphur isotope studies of the past 2.5 billion years. Nevertheless, they play an important role in mass-independent-fractionation (MIF's) which constrain the GOE during the Paleoproterozoic (Hulston and Thode, 1965; Farquhar et al., 2000, 2010b; Bekker et al., 2004) and Johnston et al. (2005a) provided some evidence that different types of sulphur metabolic processes impart different multiple

sulphur signatures (including  $^{33}\text{S}$  and  $^{36}\text{S}$ ) which could be used to interpret and identify different types of biological sulphur fractionations in the geologic record.

Today, the most important catalyst for sulphur isotope fractionation is the sulphur metabolism of microbes, especially during, but not restricted to, the process of sulphate reduction (Jones and Starkey, 1957; Harrison and Thode, 1958; Kaplan and Rittenberg, 1964) which has been active since the Archean (Shen et al., 2001; Shen and Buick, 2004; Archer and Vance, 2006). In a nutshell, there are three microbial processes which lead to fractionation through microbial sulphur metabolism: (1) Assimilatory sulphate reduction, (2) Dissimilatory sulphate reduction and, (3) sulphide oxidation:

1. Fractionations associated with assimilatory sulphate reduction are generally small, with  $\Delta$  values ( $\delta^{34}\text{S}_{\text{sulphate}} - \delta^{34}\text{S}_{\text{organic}}$ ) mostly below 5‰ (Kaplan and Rittenberg, 1964; Trust and Fry, 1992). The small fractionations are a result of the unidirectional transport of sulphate into the cell, which means that even if internal cellular processes impart fractionation, no net fractionation will be observed as there is no exchange between internal and external sulphate pools (e.g. Rees, 1973). Most organic sulphur in living organisms is ultimately derived from assimilatory sulphate reduction (Canfield, 2001a).

2. Dissimilatory sulphate reduction: A process conducted by several major lineages within the bacterial domain, in particular among the  $\delta$ -subdivision of the Proteobacteria and to lesser extent gram-positive bacteria (Stackebrandt et al., 1995; Castro et al., 2000). These sulphate reducers gain energy for their growth by catalyzing exergonic chemical reactions in which organic carbon or  $\text{H}_2$  (gas) is oxidized while sulphate is reduced (Canfield, 2001a, b), without incorporating sulphur into any organic compound, following the equations:



Sulphate reducing bacteria (SRB) are widely distributed in anoxic environments containing sulphate and have a broad ecological tolerance, including thermophile and halotolerant bacteria (e.g. Sagemann et al., 1998; Brandt et al., 2001). Based on extensive studies of SRB, in particular of the species *Desulfovibrio desulphuricans*, the following major controls on isotope fractionation during sulphate reduction can be formulated (Canfield, 2001a): (1) when organic electron donors are used, lower specific rates of sulphate reduction ( $\text{mol cell}^{-1} \text{time}^{-1}$ ) lead to higher fractionations, (2) lower fractionations (3-16‰; Kaplan and Rittenberg, 1964; Kemp and Thode, 1968) are achieved when  $\text{H}_2$  is used as electron donor, particularly at low specific rates of sulphate reduction, (3) small fractionations (<4‰; Harrison and Thode, 1958) occur under sulphate-limiting conditions ( $\sim <1\text{mM}$ , Harrison and Thode, 1958), and (4) when sulphur is abundant ( $>1\text{mM}$ ), high fractionations ranging from 3 to 46‰ with an average of 18‰ are provided (Canfield and Teske, 1996).

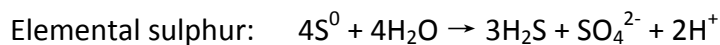
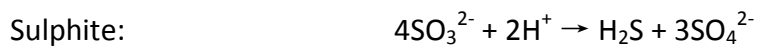
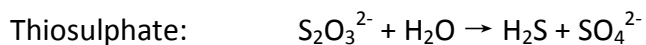
Dissimilatory sulphate reduction begins with the transport of sulphate across the cell membrane together with cations,  $\text{H}^+$  for freshwater species and  $\text{Na}^+$  for marine species (Cypionka, 1995), to balance the charge of  $\text{SO}_4^{2-}$ . The reversible process of sulphate transport into the cell is accompanied by a small isotope effect ( $\delta^{34}\text{S}_{\text{sulphate-out}} - \delta^{34}\text{S}_{\text{sulphate-in}}$ ) of about 3‰ (Harrison and Thode, 1958; Rees, 1973) but possibly lower. Within the cell cytoplasm, sulphate is activated with ATP to form the intermediate compound APS, with no isotope effect, which is then reduced to sulphite ( $\text{SO}_3^{2-}$ ), fractionating ( $\delta^{34}\text{S}_{\text{sulphate}} - \delta^{34}\text{S}_{\text{sulfite}}$ ) in the range of 22 to 24‰ (Harrison and Thode, 1957, 1958). The last step consists of further reducing sulphite to sulphide whereby indirect reduction pathways involving thiosulphate ( $\text{S}_2\text{O}_3^{2-}$ ) and trithionate ( $\text{S}_3\text{O}_6^{2-}$ ) may also occur (Brunner and Bernasconi, 2005 and references therein). A large range of fractionation averaging 18‰ has been observed during sulphite reduction ( $\delta^{34}\text{S}_{\text{sulfite}} - \delta^{34}\text{S}_{\text{sulphide}}$ ; Kemp and Thode, 1968; see review by Canfield, 2001a). Thus, when adding up the amount of fractionation for each individual step, a maximum value for  $\Delta^{34}\text{S}$  ( $\delta^{34}\text{S}_{\text{sulphate}} - \delta^{34}\text{S}_{\text{sulphide}}$ ) of 45-50‰ is obtained, which corresponds to the maximum of 46‰ measured during sulphate reduction by pure cultures (Canfield, 2001a). Nevertheless, the total amount of sulphur isotope fractionation strongly depends on the environmental conditions outlined above and the species involved. Detmers et al. (2001) for example have measured isotope fractionation by 32

different sulphate-reducing organisms and found a range in fractionation from only 2‰ to 42‰, whereby the SRB which are able to completely oxidize the organic substrate (complete oxidizers) provided higher fractionations than incomplete oxidizers. Furthermore, it seems that temperature also affects the extent of fractionation as individual species of sulphate reducers generally only metabolize within the temperature range of 20-40°C (e.g. Knoblauch et al., 1999; see also Canfield et al., 2000). In nature, however, no such low fractionations as in pure cultures have been measured, probably related to generally lower specific rates of sulphate reduction observed under *in situ* conditions due to substrate limitation (Canfield, 2001b). However, more recent observations from natural environments report fractionations of up to 77‰ due to sulphate reduction alone (Rudnicki et al., 2001; Wortmann et al., 2001; Werne et al., 2003; Canfield et al., 2010) which would confirm modelling experiments challenging the long held conception of intercell sulphur cycling during bacterial sulphate reduction (Rees, 1973), suggesting values exceeding 48‰ and possibly even 70‰ (Goldhaber and Kaplan, 1980; Brunner and Bernasconi, 2005).

3. Sulphide oxidation: The third mainly biologically mediated process, but also including inorganic pathways, is pervasive in marine and lacustrine environments supporting sulphate reduction. For example, in marine coastal sediments typically 90% or more of the sulphide produced through sulphate reduction is reoxidized (Jørgensen, 1982; Canfield and Teske, 1996). The varied but poorly known pathways of sulphide oxidation in nature include (Canfield, 2001a): (1) the inorganic oxidation of sulphide to sulphate, elemental sulphur and other intermediate sulphur compounds, (2) the non-phototrophic, biologically mediated oxidation of sulphide and elemental sulphur, (3) the oxidation of reduced sulphur compounds by different anoxygenic phototrophic bacteria, and (4) the disproportionation of sulphur compounds with intermediate oxidation states. Whereas the first three of these follow the mechanism of true sulphide-oxidation, requiring either the introduction of an electron acceptor or the fixation of organic carbon from CO<sub>2</sub> to balance the sulphide oxidation, the disproportionation of sulphur intermediate compounds requires no external electron donor or acceptor and balances the production of sulphate by the production of sulphide (Canfield, 2001a).



Only small or negligible fractionations accompany the process of phototrophic oxidation of sulphide and elemental sulphur, the non-phototrophic oxidation of elemental sulphur, thiosulphate ( $S_2O_3^{2-}$ ) and sulphite as well as sulphide to elemental sulphur and, the inorganic oxidation pathways of sulphur compounds. An exception is made for the non-phototrophic oxidation of sulphide to polythionates ( $S_xO_6^{2-}$ ) or sulphate when these oxidized species are minor reaction products (Kaplan and Rittenberg, 1964; Canfield, 2001a). The fourth possible pathway, the disproportionation of sulphur compounds, introduced by Bak and Pfennig (1987) represent another process transforming intermediate sulphur species beside reduction and oxidation. Sulphate reducing bacteria have been found to disproportionate the intermediate sulphur compounds thiosulphate, sulphite and elemental sulphur to sulphide and sulphate (Bak and Pfennig, 1987; Thamdrup et al., 1993; Janssen et al., 1996; Finster et al., 1998):



Thiosulphate ( $S_2O_3^{2-}$ ) is composed of an inner sulphonate sulphur ( $-SO_3^-$ ) and an outer sulphane sulphur ( $-S$ ) whereby sulphate produced during disproportionation should be derived from the sulphonate sulphur and accordingly, sulphide from the sulphane sulphur. In pure culture experiments (Habicht et al., 1998; Cypionka et al., 1998), fractionation associated with the disproportionation of intermediate sulphur compounds showed that the sulphide produced is depleted in  $^{34}S$  compared to sulphane sulphur, although the magnitude of depletion varies considerably and is greatest when sulphide is purged from the system. Sulphate is depleted in  $^{34}S$  compared to the sulphonate sulphur when sulphide is actively purged from the system but enriched when sulphide accumulates.

Sulphite disproportionation leads to large depletions of  $^{34}S$  in sulphide within the range of 21 to 37‰ depending on the organism analyzed and sulphate enriched in  $^{34}S$  within the

range of 7 to 12‰ (Habicht et al., 1998). While studies analyzing the fractionation during the disproportionation of elemental sulphur yielded less pronounced values: sulphate was more enriched in  $^{34}\text{S}$  by  $18.3 \pm 1.3\%$  and sulphide depleted by only  $6.1 \pm 0.4\%$  (Canfield et al., 1998).

In summary, high S fractionations can be achieved when sulphides depleted in  $^{34}\text{S}$  through sulphate reduction are involved in a cyclical process in which they are reoxidized to elemental sulphur which subsequently undergoes bacterial disproportionation to form extremely  $^{34}\text{S}$  depleted sulphide ( $\Delta^{34}\text{S} = 45$  to  $70\%$ ) or by sulphate reduction alone under circumstances not yet fully understood ( $\Delta^{34}\text{S} > 77\%$ ).

#### **1.4.3.3. The sedimentary sulphur isotope record**

As sulphate reduction is the major process leading to sulphide formation, we can expect that the isotopic composition of sulphides preserved in sediments to reflect that of the sulphide produced during sulphate reduction (Canfield, 2001a, b). However, Phanerozoic sulphides are far more depleted in  $^{34}\text{S}$ . No particular control on sulphate reducing organisms in nature, such as particularly low rates of sulphate reduction, nor the fractionation associated with pyrite formation from dissolved sulphide (<1‰), could be identified to account for such high fractionation (Price and Shieh, 1979; Habicht and Canfield, 2001). Therefore it seems that sulphur is further fractionated during sulphide oxidation and, due to low fractionation imparted during the direct oxidation of sulphide to sulphate, the disproportionation of intermediate sulphur compounds probably account for the high depletion in  $^{34}\text{S}$  in sulphides found in marine sediments (Jørgensen, 1990; Canfield and Thamdrup, 1994; Canfield and Teske, 1996). In addition, Habicht and Canfield (2001) could show that at low rates of sulphate reduction, sulphides are even more depleted in  $^{34}\text{S}$  as a higher proportion of the sulphide produced is channelled through sulphur intermediate compounds by subsequent disproportionation reactions whereas sulphide is readily oxidized to sulphate when higher specific rates of sulphate reduction prevail.

To measure the extent of fractionation occurred during sulphide formation, the sulphur isotopic signature of coeval sulphate has to be analyzed. Reliable data for the Phanerozoic, for example compiled by Claypool et al. (1980), have been achieved relying on sulphate isotope studies on evaporites (gypsum/anhydrite). Due to the poor preservation potential of gypsum under surficial weathering conditions and the difficulty of achieving gypsum saturation in sulphate-poor Precambrian seawater (Kah et al., 2001; Lyons et al., 2004), sulphate remains scarce in the Precambrian (Grotzinger and Kasting, 1993; Canfield and Farquhar, 2009). The lack of gypsum data in the Precambrian has partly been compensated by sulphur isotope measurements of bedded barite (e.g. Canfield, 1998) but the patchiness of the barite data and its limited capacity to record primary seawater chemistry makes it less applicable. Carbonate-associated sulphate (CAS) has emerged as a valuable alternative since Burdett et al. (1989) showed that CAS can record the isotopic signature of contemporaneous seawater and ancient evaporite deposits (e.g. Strauss, 1999; Gellatly and Lyons, 2005; Ries et al., 2009). However, the mere process of extracting CAS from carbonates reveals significant difficulties and makes some previously published studies at least questionable (Shields, 2010, personal communication).

#### **1.4.3.4. The sulphur isotopic record during the Precambrian**

During the Archean the isotope record of sedimentary sulphides (see Fig. 1.12) typically shows values within 10‰ of the mantle value of 0‰ with fractionations of <15‰, although based on sparse data concerning seawater sulphate (Shen et al., 2001). Low fractionations throughout the Archean probably represent sulphide formation by sulphate reduction in a sulphate-poor ocean with sulphate concentrations below 1mM (Canfield, 2001a). According to Canfield and Raiswell (1999), the first S isotope evidence for sulphate-reducing bacteria (SRB) in sedimentary rocks can be dated at ca. 2.7 Ga. In the absence of sulphate, SRB's may have evolved much later, in concert with increasing concentration of sulphate in seawater. Oxygenic photosynthesis, which probably appeared around 2.7 Ga (see Chapter 1.3), is critical in driving sulphate delivery to the ocean through oxidative continental weathering (Lyons et al., 2004). Nevertheless, in the possible absence of oxygenic photosynthesis, photochemical oxidation of

volcanic SO<sub>2</sub> and anoxygenic photosynthesis may have been the dominant sources of sulphate for early SRB (e.g. Farquhar et al., 2000). And, under low oxygen concentration in the atmosphere, mass-independent sulphur fractionation prevail and complicate the Archean sulphur isotope record (e.g. Pavlov and Kasting, 2002; Farquhar and Wing, 2003; Ohmoto et al., 2006).

A substantial rise in sulphur isotope fractionation between coeval sulphate and sulphide occurred after 2.3 Ga and probably represents an increasing concentration of sulphate in seawater as a result of increasing oxidative weathering after the GOE (Cameron, 1982; Cameron and Hattori, 1987; Canfield, 1998, 2001a; Canfield and Raiswell, 1999; Habicht et al., 2002; Strauss, 2004).

The isotopic composition of sedimentary sulphides between 2.3 and 1 Ga varies greatly but the maximum fractionations generally remain of the same magnitude observed for modern sulphate reducers with non-limiting sulphate concentrations. Extensive deposition of banded iron formations (BIF's) occurred before and after the Great Oxygenation Event until about 1.8 Ga (Isley and Abbott, 1999). As introduced earlier, Canfield (1998) argued that the cessation of BIF deposition after 1.8 Ga resulted from sulphide titrating the iron from the deep ocean as soon as H<sub>2</sub>S production exceeded Fe delivery to the ocean. This was due to a major increase in continental chemical weathering, which enhanced the flux of sulphate to the ocean which was then readily reduced to sulphide by SRB, leading to a sulphate-poor (5-15% of the modern ocean reservoir; Kah et al., 2004), but sulphide-rich ocean. Hence, inducing the transition from an anoxic, Fe(II) rich ocean to a redox stratified ocean with widespread sulphidic conditions ca. 1.8 Ga which possibly persisted until the Neoproterozoic (Canfield, 1998; Poulton et al., 2004a; Canfield et al., 2008; Li et al., 2010).

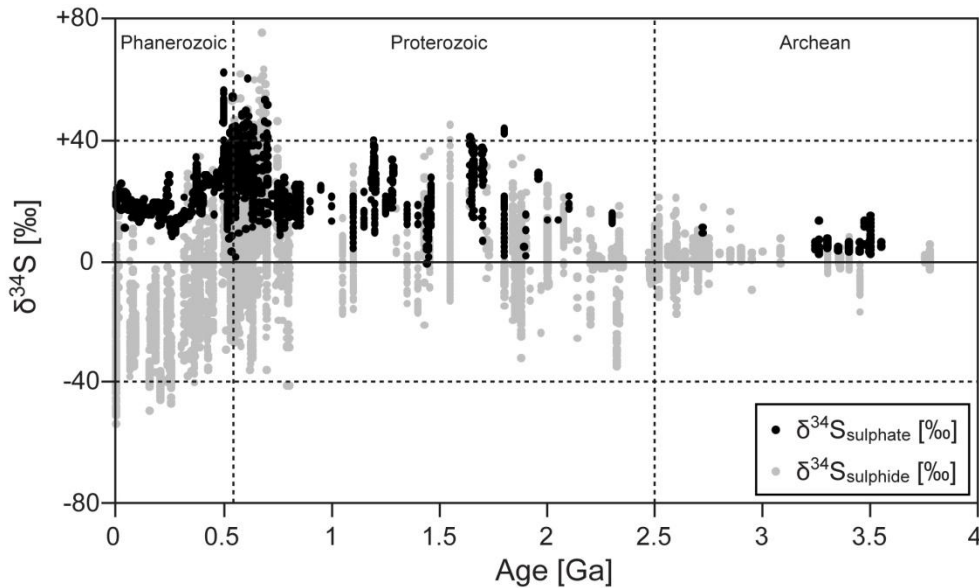


**Figure 1.12: A compilation of sulphur isotopes measured in sulphide and sulphate minerals. Note that the sulphide and sulphate isotopic values are not necessarily from coeval marine sulphides and sulphates. Nevertheless,  $\Delta^{34}\text{S}$  values in the Archean do not exceed 20‰ and the maximal Paleo- and Mesoproterozoic  $\Delta^{34}\text{S}$  values are around 45‰. It is only from the Neoproterozoic on that sulphur fractionation attains values between 40 and 70%.  $\delta^{34}\text{S}_{\text{sulphide}}$  values are compiled by Canfield and Farquhar, 2009;  $\delta^{34}\text{S}_{\text{sulphate}}$  values are from Holser and Kaplan, 1966; Claypool et al., 1980; Strauss, 1993, 1999; Fox and Videtich, 1997; Misi and Veizer, 1998; Shields et al., 1999, 2004; Shen et al., 2000; Walter et al., 2000; Strauss et al., 2001; Hurtgen et al., 2002, 2004, 2005; Gorjan et al., 2003; Kah et al., 2004; Goldberg et al., 2005; Peryt et al., 2005; Gellatly and Lyons, 2005; Hough et al., 2006; Gill et al., 2007; Prokoph et al., 2008; Canfield and Farquhar, 2009 and Ries et al., 2009.**

Towards the Neoproterozoic-Cambrian transition, the next major increase in fractionation occurs, exceeding the range in which sulphate reducers commonly fractionate. Thus, it has been suggested that the disproportionation of intermediate sulphur compounds exerted a significant influence on sulphide isotope fractionation for the first time in the Neoproterozoic (Canfield and Teske, 1996; Canfield, 1998; Canfield, 2001a), but probably not before 580 Ma (Hurtgen et al., 2005) although this metabolism was probably already active by 1.3 Ga (Johnston et al., 2005b). Persistently low sulphate concentrations throughout the Proterozoic compared to modern values could also have prevented  $\Delta^{34}\text{S}$  values to exceed 46‰

(Hurtgen et al., 2005) and it has been argued that the advent of bioturbation 10-15 My before the Neoproterozoic – Cambrian boundary had a profound impact on seawater sulphate concentrations by increasing the oxygen penetration depth and enhancing the oxidation of pyrite in the sediment (Turchyn and Schrag, 2004; Canfield and Farquhar, 2009). Nevertheless, although major uncertainties still remain due to the difficulties in the acquisition of reliable  $\delta^{34}\text{S}_{\text{sulphate}}$  data, the sulphur isotope signature in late Neoproterozoic marine sediments has been interpreted to express a further increase in the oxygen availability, accompanied by the ultimate oxygenation of the deep ocean (Canfield, 1998), and thus enhance the oxidative portion of the sulphur cycle and promoting the development of non-photosynthetic sulphide-oxidizing bacteria (Canfield and Thamdrup, 1994; Canfield and Teske, 1996). The associated biotic and abiotic production of intermediate sulphur compounds would have supported disproportionation reactions (Canfield and Teske, 1996; Lyons et al., 2004).

Paradoxically, several studies investigating sulphur isotopes in terminal Proterozoic sedimentary formations in Canada (Strauss et al., 1992), Poland (Bottomley et al., 1992), Namibia (Ries et al., 2009) and China (Liu et al., 2006) found superheavy pyrite which at least in Ries et al. (2009) exceeded S isotope values in coeval CAS and thus even exhibit negative  $\Delta^{34}\text{S}_{\text{sulphate-sulphide}}$ . The occurrence of superheavy pyrite after about 750 Ma would be consistent with low sulphate concentrations and the reappearance of ferruginous conditions in the Late Neoproterozoic ocean (Canfield et al., 2008) and where  $\delta^{34}\text{S}_{\text{sulphide}}$  even exceeds  $\delta^{34}\text{S}_{\text{sulphate}}$ , intense aerobic reoxidation of sedimentary pyrite could play a role as the oxidation of  $\text{H}_2\text{S}$  yields  $\text{SO}_4^{2-}$  and other oxidized species depleted in  $^{34}\text{S}$  by 4‰-5‰ under abiotic processes (Fry et al., 1988) and up to 18‰ when bacterially mediated (Kaplan and Rittenberg, 1964).

And, last but not least, positive averages in pyrite  $\delta^{34}\text{S}$  values in the Precambrian could, analogous to the carbon cycle, result from significant pyrite burial which is missing from the known sedimentary pyrite record (e.g. Farquhar et al., 2010a). Canfield (2004) suggested that the deep water sulphide pool could have been lost to subsequent subduction. The Neoproterozoic Oxygenation Event and the advent of bioturbation would not only have increased sulphate concentrations in the ocean but also changed the fraction of sulphur lost to

pyrite burial (Canfield and Farquhar, 2009; Farquhar et al., 2010a) and led to generally negative pyrite  $\delta^{34}\text{S}$  values in the Phanerozoic.

#### **1.4.3.5. Total sulphur and pyrite content in sedimentary rocks throughout Earth's history**

Similar to the sedimentary organic carbon record (see Fig. 1.13a), compiled sulphur concentrations in organic-rich shales throughout the last 3 billion years reveal peaks exceeding 20% total sulphur in the Paleoproterozoic around 2 Ga and during the Precambrian-Cambrian transition. However, a pitfall in supporting extreme sulphur concentrations around 2 Ga might be given by considering the data obtained by Loukola-Ruskeeniemi (1991) from metamorphosed black shale successions as diagenetic or hydrothermal remobilisation of sulphur-rich fluids might well enhance this signal. However, both increases and subsequent peaks at the beginning and end of the Proterozoic fit well into the paradigm of increasing sulphate concentrations in the ocean during these intervals (e.g. Canfield and Farquhar, 2009) which would have enhanced sulphate-reduction rates and can be reconciled with the isotopic record. The enhanced burial of reduced carbon and sulphur both advocate rising oxygen levels on the Earth's surface. Again, the question whether the absence of sulphur enriched black shales during the Mesoproterozoic results from widespread precipitation over large euxinic portions of the seafloor or because sulphate delivery to the ocean decreased after the initial increase during the Great Oxygenation Event remains difficult to answer.

Average  $\text{S}/\text{C}_{\text{org}}$  ratios reveal that relative to TOC contents, sulphur concentrations increased to a much greater extent during the Oxygenation Events whereby low  $\text{S}/\text{C}_{\text{org}}$  ratios prevail in the Mesoproterozoic and decreased significantly during the Phanerozoic (see Fig. 1.13b; Raiswell and Berner, 1986). Sediments enriched in S often indicate euxinia whereby S and  $\text{C}_{\text{org}}$  contents are decoupled, contrary to oxic depositional environments where S concentration usually tracks  $\text{C}_{\text{org}}$  (Berner and Raiswell, 1983, 1984; Raiswell and Berner, 1985). Pyrite precipitation is controlled by Fe availability and low S concentrations and  $\text{S}/\text{C}_{\text{org}}$  ratios in black shales prior to the Neoproterozoic might be a result of Fe-limited, widespread euxinia.

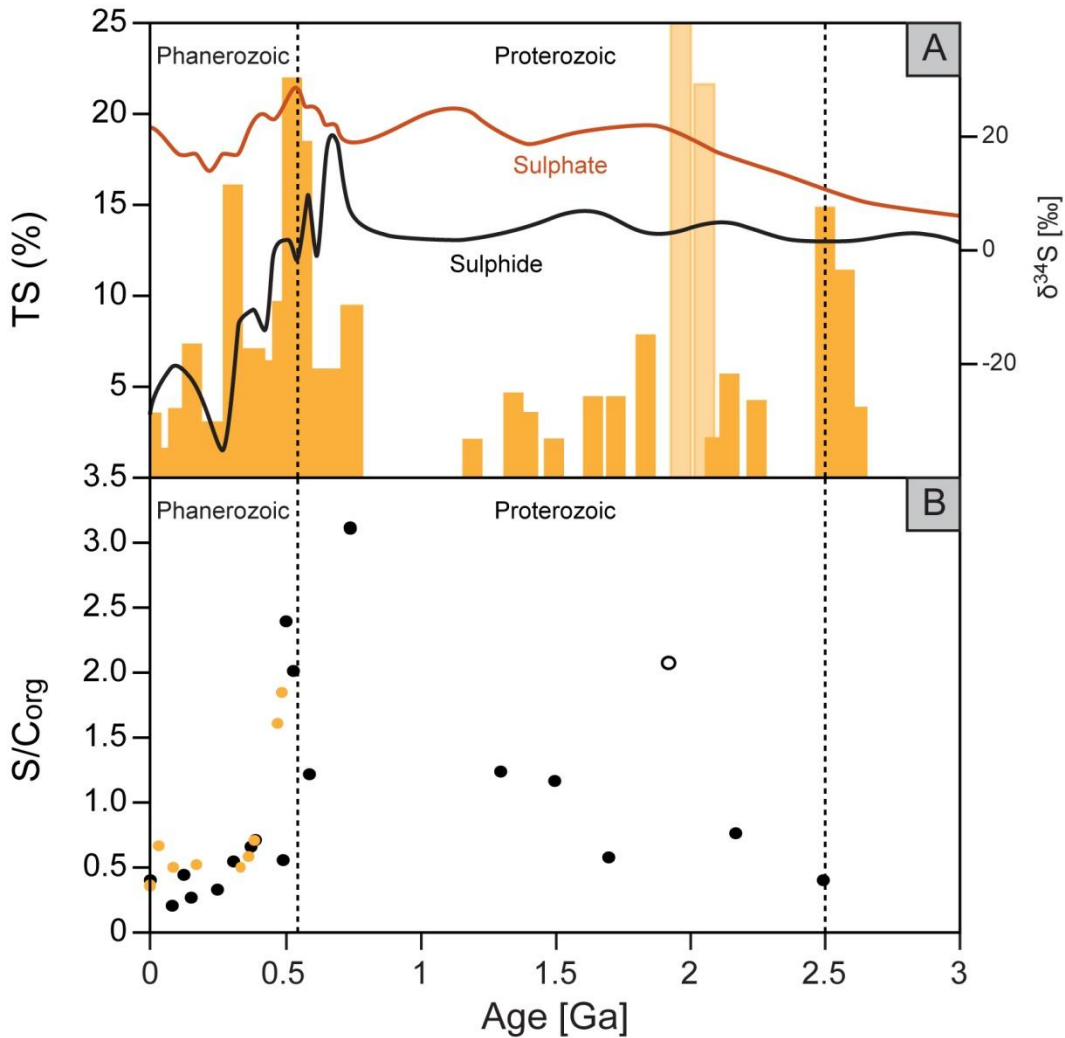


Figure 1.13: A) histogram showing total sulphur and/or pyrite contents in black shale binned into their respective time periods (see appendix for references). Shaded columns represent extremely high values found in metamorphosed black shales and might be of hydrothermal origin (Loukola-Ruskenieemi, 1991). The  $\delta^{34}\text{S}$  curves represent averages per time period compiled by Canfield and Farquhar, 2009. B) Average S/C ratios per period exhibit a peak after the GOE (empty circle shows average mostly based on data from Loukola-Ruskenieemi, 1991) and in particular a well supported maximum during the Precambrian – Cambrian transition. Orange dots represent data from Raiswell and Berner (1986) and confirm globally high S/C ratios during that interval.



#### 1.4.4. Chromium isotopes

Under modern atmospheric conditions, the mobile Cr(VI) anion ( $\text{HCrO}_4^-$ ) is the most thermodynamically stable form of chromium. Oxidation of Cr(III) to Cr(VI) in soils depends upon the co-occurrence of Cr(III) (bound most commonly as  $\text{FeCr}_2\text{O}_4$ ) and manganese oxides, the latter catalyzing Cr(III) oxidation. The most important source of chromium to the ocean is riverine influx whereby Cr(VI), mobilized through oxidative weathering, is delivered as either chromate ( $\text{CrO}_4^{2-}$ ; alkaline pH) or bichromate ( $\text{HCrO}_4^-$ ; acidic pH) ions (Oze et al., 2007). The total dissolved Cr concentration in the modern ocean is in the range of 2 to 10 nM with a relatively short residence time of  $\sim 2.5$  to  $4 \times 10^4$  years (Campbell and Yeats, 1981). Cr(VI) can be reduced microbially (Sikora et al., 2008) and in presence of aqueous Fe(II) or Fe(II)-containing minerals (Ellis et al., 2002).



Cr(VI) is efficiently reduced to Cr(III) in presence of Fe(II) and is subsequently scavenged into Fe(III) – Cr(III) oxyhydroxides (Fendorf, 1995; Sass and Rai, 1987). At equilibrium, the  $\text{Cr(VI)O}_4^{2-}$  anion is enriched by up to 7% at room temperature in  $^{53}\text{Cr}$  compared to coexisting compounds containing Cr(III) (Frei et al., 2009 and references therein). Hence, subsurface aqueous environments will have positive  $\delta^{53}\text{Cr}$  values (Izbicki et al., 2008) and because of the effective sequestration of Cr(VI) during Cr reduction and subsequent precipitation of Cr(III) with Fe-oxyhydroxides, the stable Cr isotope signatures of chemically precipitated Fe(III)-rich sediments should mirror sea water from which the Fe oxides precipitated (Frei et al., 2009). Oxidation and solubilization of Cr from soils is strongly dependent on the presence of  $\text{MnO}_2$ , which is stable under elevated oxygen fugacities. Hence, the delivery of Cr to the ocean is limited by the absence of Mn(IV) under low atmospheric oxygen levels.

A recent study by Frei et al. (2009) on numerous Precambrian iron formations identified six stages of Cr cycling (see Fig. 1.14), identifying a rise in  $\delta^{53}\text{Cr}$  values between 2.8 and 2.45 Ga, as further supporting evidence for the GOE. An apparent return to lower  $\delta^{53}\text{Cr}$  values between

2.45 and 1.9 Ga possibly indicates fluctuating atmospheric oxygen concentrations and would explain why it took several hundred million years for the sulphide flux to overwhelm the hydrothermal Fe(II) flux, thus allowing sulphidic conditions to develop eventually at ~1.84 Ga (Poulton et al., 2004a; Frei et al., 2009).

An increase to strongly positive  $\delta^{53}\text{Cr}$  values in the late Neoproterozoic between ~750 Ma and the Precambrian – Cambrian boundary represent promising new evidence for atmospheric oxygen concentrations attaining possibly modern levels during the Precambrian – Cambrian transition. The recent research on stable chromium isotopes with regard to the oxygenation history of the Earth’s surface is enticing but further studies and an enhancement of the available dataset needs to be carried out.

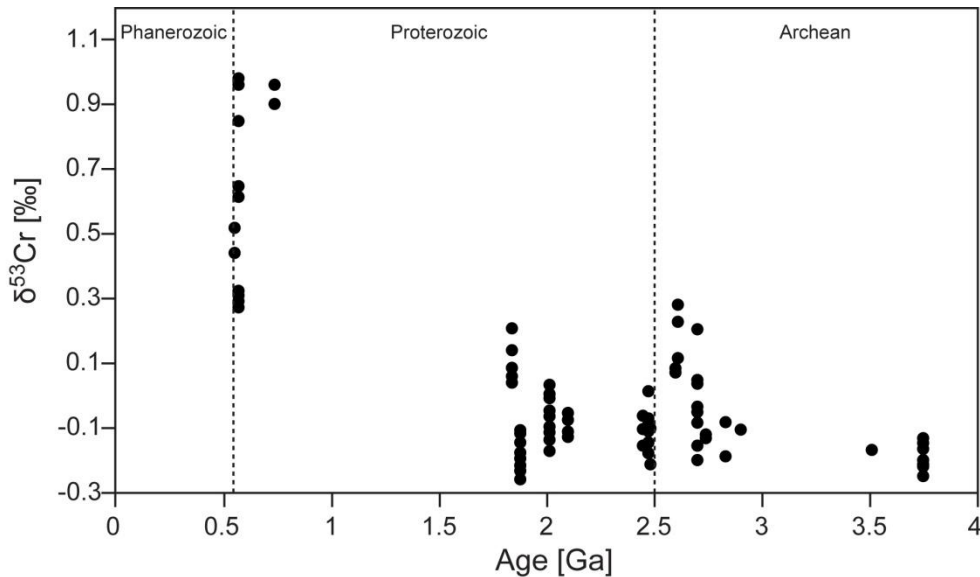


**Figure 1.14:** Graph showing the key aspects of the Precambrian history of hexavalent chromium in sea water. Increasing Cr isotope fractionation ( $\delta^{53}\text{Cr}$ ) recorded in BIF’s between 2.8 and 2.45 Ga indicate an increase in oxidative weathering with a possible return to reduced atmospheric oxygen levels between 2.45 and 1.9Ga. BIF’s deposited during the late Neoproterozoic between ~750 Ma and the Precambrian – Cambrian boundary record strongly positive  $\delta^{53}\text{Cr}$  values ranging from 0.9‰ to 4.9‰ which may provide further evidence for the NOE (Frei et al., 2009).

#### 1.4.5. Molybdenum isotopes

Molybdenum has seven naturally occurring stable isotopes of 10-25% abundance covering a mass range of ~8% (see Fig. 1.15; Anbar, 2004). These unusual isotope characteristics combined with the pronounced redox-sensitivity and covalent-type bonding, both of which tend to drive isotope fractionation, make the Mo isotope system a promising target for stable isotope investigations of ancient ocean redox conditions (Barling et al., 2001; Siebert et al., 2003; Anbar, 2004; Arnold et al., 2004). The reporting conventions of Mo isotopic signatures vary, but are typically reported as

$$\delta^{97/95}\text{Mo} = [({}^{97}\text{Mo}/{}^{95}\text{Mo})_{\text{sample}}/({}^{97}\text{Mo}/{}^{95}\text{Mo})_{\text{standard}} - 1] * 1000$$

because  ${}^{97}\text{Mo}$  and  ${}^{95}\text{Mo}$  are the only Mo isotopes completely free of isobaric interferences from other elements when measuring them in ICP-MS (Anbar et al., 2001; Barling et al., 2001; Anbar, 2004).

Mo isotope fractionation within the ocean system is mostly a result of Mo removal, preferentially lighter Mo isotopes, to ferromanganese oxides (Barling et al., 2001; Barling and Anbar, 2004; Wasylenki et al., 2006), suboxic sediments and euxinic sediments (McManus et al., 2002, 2006; Siebert et al., 2003, 2006; Nägler et al., 2005; Poulson et al., 2006), while weathering imparts a relatively minor isotopic effect (Siebert et al., 2003). In suboxic and euxinic settings, Mo isotope fractionation most likely occurs during ligand-exchange steps or during Mo reduction (Anbar and Rouxel, 2007) whereby there is a broad correlation between the Mo concentration and  $\delta^{97/95}\text{Mo}$  in sediments deposited under suboxic conditions (Siebert et al., 2003) and  $\delta^{97/95}\text{Mo}$  values approaching seawater values in euxinic depositional settings (Anbar, 2004).

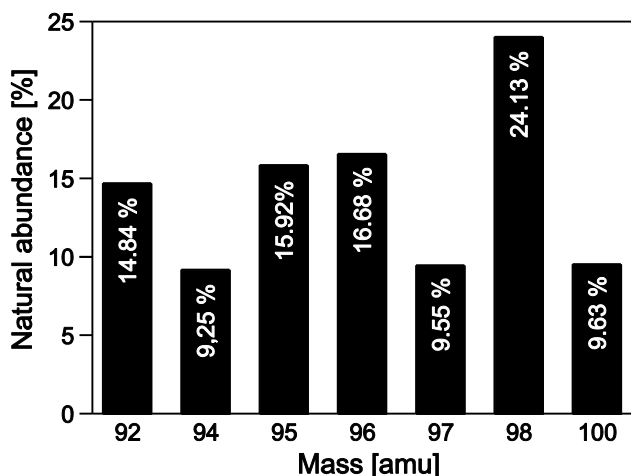


**Figure 1.15: The average natural abundances of the stable isotopes of Mo as recommended by IUPAC. The Figure is from Anbar (2004), based on Moore et al. (1974).**

Neglecting the relatively minor influence of suboxic sediments on the isotope budget and assuming that ferromanganese oxides and euxinic sediments have complementary isotopic compositions relative to the input, one light and the other heavy, a simplified mass balance equation (Barling et al., 2001; Siebert et al., 2003; Anbar, 2004) can be expressed as:

$$\delta^{97/95}\text{Mo}_{\text{input}} = f_{\text{ox}} * \delta^{97/95}\text{Mo}_{\text{ox}} + f_{\text{eux}} * \delta^{97/95}\text{Mo}_{\text{eux}}$$

where the subscript *input*, *ox* and *eux* denote the riverine input, and oxic and euxinic sediments respectively, and  $f_{\text{ox}}$  and  $f_{\text{eux}}$  denote the fraction of total Mo removed to each sediment type ( $f_{\text{ox}} + f_{\text{eux}} = 1$ ). In present seawater with a  $\delta^{97/95}\text{Mo}$  value of 1.5‰, Mo isotope signatures of source and sinks can be approximated as follows: (riverine) source: ~0‰, oxic sink: ~-0.5‰ and euxinic sink: ~1.3‰ (Anbar, 2004). Hence, an expansion of euxinic environments should lead to a decrease in the extent of Mo isotope fractionation in the ocean and should be reflected in sedimentary Mo.

This could make molybdenum isotopes to a powerful global paleoredox proxy although only a few attempts have been carried out to elucidate paleoredox conditions in ancient oceans using Mo isotopes (Arnold et al., 2004; Siebert et al., 2005; Wille et al., 2007; Lehmann et al.,

2007; Kendall et al., 2009), most notably Arnold et al. (2004), who have analyzed mid-Proterozoic euxinic black shales from the McArthur and the Tawallah Basins of Northern Australia and provided further evidence for widespread anoxia during the mid-Proterozoic (Canfield, 1998; Canfield and Raiswell, 1999; Poulton et al., 2004a; Canfield et al., 2008), which agree with the more recent study by Kendall et al. (2009) on the same black shale formations.

### **1.5. Rare Earth Element (REE) patterns as paleoredox proxies: the cerium anomaly**

Under normal surface conditions, Ce is the only REE that can be easily oxidized from Ce(III) to its relatively insoluble form Ce(IV). Hence, shale-normalized (Post Archean Australian Shale: PAAS) seawater-type REE patterns typically show a relative depletion of Ce with respect to its neighbours lanthanum (La) and praeodymium (Pr), or neodymium (Nd), from which the Ce anomaly ( $Ce_{anom.}$ ,  $Ce/Ce^*$ ) can be calculated (Bau and Dulski, 1996; PAAS from McLennan, 1989):

$$Ce_{anom} = Ce_{PAAS} / (0.5La_{PAAS} + 0.5Pr_{PAAS})$$

Elderfield and Greaves (1982) first proposed to use the Ce anomaly in order to decipher redox conditions as a consequence of the change in the ionic state of Ce as a function of oxidation state. Under normal surface conditions, Ce is the only REE that can be easily oxidized from Ce(III) to its relatively insoluble form Ce(IV) and can therefore be scavenged from an oxic water column (Wright et al., 1987; Liu et al., 1988). Under oxidizing conditions, Ce(IV) remains immobile within sediments but would tend to be lost under more reducing conditions (Wilde et al., 1996), e.g. in black shales deposited under anoxic or even sulphidic conditions, leading to a negative Ce anomaly. A similar redox sensitivity is recognized for Mn enrichment in shales deposited under oxic conditions (Calvert and Pedersen, 1993).

Modern marine authigenic carbonates, phosphates and cherts incorporate the REE distribution patterns of the seawater in which they precipitated (Wright et al., 1987; Elderfield

and Pagett, 1986; Palmer and Elderfield, 1986; Grandjean et al., 1987; Sholkovitz and Shen, 1995; Shields and Stille, 2001). However, subsequent post-depositional, diagenetic exchange (Elderfield and Pagett, 1986; German and Elderfield, 1990) or surface weathering (McArthur and Walsh, 1984; Bonnoit-Courtois and Flicoteaux, 1989) can alter the original REE patterns. Furthermore, caution must be applied when using the Ce anomaly for paleoredox reconstructions as Ce depletion does not solely depend on the oxidation potential (German and Elderfield, 1990; Shields and Stille, 2001) but also on microbial activity that catalyses the oxidation of Ce(III) (Moffett, 1990), as well as the pH (Brookins, 1989; Tricca et al., 1999; Stille et al., 2003), depth (Piepgras and Jacobsen, 1992) and age of seawater body (German and Elderfield, 1990). Guo et al. (2007) have also hypothesized that REE patterns could also mirror mineral phases which have been precipitated within the water column above the redox boundary and not within the sediment, where other geochemical proxies such as Th/U ratios indicate reducing conditions. Negative Ce anomalies have also been observed in association with ocean regression which were also characterized by a rise in  $\delta^{13}\text{C}_{\text{carb}}$  values (Wang et al., 1993; Shields et al., 1997; Shields and Stille, 2001); such periods of 'ventilation' and/or redox stratification have been proposed to explain these trends (Wang et al., 1993; Marshall, 1992).

Nevertheless, the conservative nature of the REE as a group and the anomalous behaviour of Ce within this group could still provide limited potential in distinguish anoxic and oxic water bodies in the geological past (Wright et al., 1987; Holser, 1997; Shields et al., 1997; Shields and Stille, 2001) or for pinpointing major changes in oxygen availability such as during the GOE (Bau et al., 1998) or during the Neoproterozoic - Cambrian transition (Yang et al., 1999, Guo et al., 2007; Ling et al., 2009).

Only little work has been done using the Ce anomaly in order to constrain the putative Neoproterozoic - Cambrian oxygenation due to its ambiguous behaviour. But previous studies, all effectuated on the Yangtze Platform, South China, indicate a trend to increasingly negative Ce anomaly throughout the Precambrian- Cambrian transition (Yang et al., 1999; Guo et al., 2007; Komiya et al., 2008; Ishikawa et al., 2008; Ling et al., 2009). In addition, Komiya et al. (2008) have compiled Ce anomaly data (see Fig. 1.16) which shows perturbations in their

geochemical cycling during the GOE and again during the Neoproterozoic - Cambrian transition which might suggest a shift to more oxidizing conditions on Earth's surface.

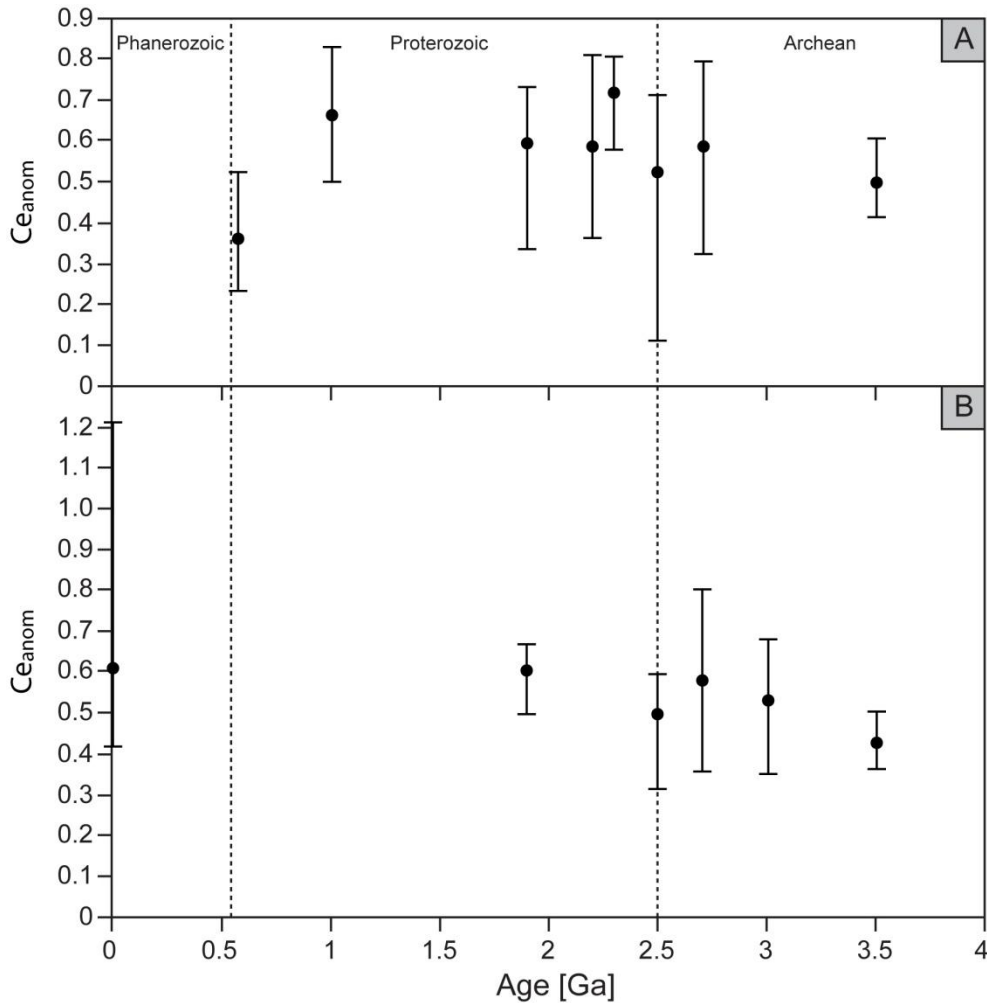


**Figure 1.16: A) Compiled average cerium anomalies in shallow-marine carbonates throughout Earth's history and B) compiled average Cerium anomalies in deep-sea carbonates (Komiya et al., 2008). Note that the overall high variability of the Ce anomaly makes a meaningful interpretation difficult.**

## **2. Redox-sensitive trace-metals and iron speciation**

### **2.1. Redox-sensitive trace metals**

Many trace elements are present in the water column either in soluble form or adsorbed onto particles. This removal of dissolved trace metals from seawater to the sediments results from either biotic or abiotic processes, the latter being controlled by redox conditions prevailing in the water column and underlying sediments. Expressed in general terms, abiotic processes are relatively limited in oxic environments but some trace element enrichment can occur under suboxic conditions through diffusion across the sediment-water interface or through remobilization and repartitioning along redox gradients within the sediments. Furthermore, the redox cycling of manganese and iron can play an important role in trace metal concentrations in marine sediments. A particularly efficient enrichment of trace elements is achieved under reducing conditions, including adsorption of metallic ions or ionic species onto organic or mineral substrates, formation of organometallic complexes and, precipitation of (iron-) sulphides and/or insoluble oxyhydroxides.

As the present study focuses on the oxygenation of the Earth's surface during the Neoproterozoic-Cambrian transition, attention will be directed towards the significance of studies on redox conditions in marine settings, which track the relative distribution of oxidizing agents across depositional and diagenetic gradients and biogeochemical processes that control their distribution. In order to describe paleoredox conditions, the following gradations are commonly used: oxic, suboxic and anoxic (see table 2.1; Tyson and Pearson, 1991). Anoxic conditions can be non-sulphidic (ferruginous) or sulphidic when H<sub>2</sub>S occurs in the water column, also being referred to as euxinic.



**Table 2.1: Redox classification of the depositional environment, after Tyson and Pearson, 1991, reproduced from Tribovillard et al., 2006.**

<b>Redox classes</b>	Oxic	Suboxic	Anoxic (no free H <sub>2</sub> S in the water column)	Euxinic (free H <sub>2</sub> S present in the water column)
<b>O<sub>2</sub> concentration in bottom waters (ml O<sub>2</sub>/H<sub>2</sub>O)</b>	[O <sub>2</sub> ] > 2	2 > [O <sub>2</sub> ] > 0.2	[O <sub>2</sub> ] < 0.2	[O <sub>2</sub> ] = 0

The redox state of marine sediments basically results from the balance between the flux of organic matter to the seafloor and the flux of dissolved oxidants to the sedimentary porewaters from the overlying seawater. Hence, oxic conditions allow aerobic organisms to use O<sub>2</sub> from the overlying water column or from porewaters for their metabolism (i.e. organic matter decomposition). When O<sub>2</sub> becomes depleted, the process of organic matter decomposition continues via organisms using secondary oxidant sources in the following order dictated by the relative free energy gain stemming from each microbial process (e.g. Froelich et al., 1979): nitrate, manganese and iron oxides and oxyhydroxides, and sulphate. As secondary oxidants become exhausted, methanogenic bacteria begin to break down organic matter through oxidative-reductive disproportionation of carbon.

To ascertain whether trace elements are enriched or depleted in a particular marine sediment, several factors must be considered which may exert undesirable influence on trace element concentration in order to make assumptions with regard to paleoenvironmental conditions: (1) Detrital sources, which can be accounted for by crossplotting trace element versus aluminium or titanium, as both elements are commonly overwhelmingly of detrital origin and which are usually immobile during diagenesis (see chapter 4.4; Calvert and Pedersen, 1993; Tribovillard et al., 1994; Hild and Brumsack, 1998; Böning et al., 2004). If a good correlation is observed and if the trace element concentration is close to average shale values, the detrital influence might be too great and the trace element is unsuitable for paleoenvironmental analysis. This is often the case for Cr, occasionally for U and Ba but only

rarely for Mo and V (Jones and Manning, 1994; Caplan and Bustin, 1999). (2) Hydrothermal sources, especially cold seeps, which mainly affects the accumulation of Ba, Sr, Zn and Mn (Pujol et al., 2006) as paleoenvironmental indicators. Furthermore, hydrothermal activity can also release large quantities of manganese and iron, which can influence the trace element concentration through their redox cycling in oxygen deficient environments (Morford et al., 2005).

The degree of trace element enrichment or depletion is commonly expressed relative to average crust or average shale (Wedepohl, 1971; Taylor and McLennan, 1985; McLennan, 2001) and, to prevent the effect of trace element dilution due to variable amounts of mineral phases of biogenic origin, such as carbonate and opal, trace element concentration can be normalized against aluminium, titanium, scandium etc. content which are relatively immobile during diagenesis (see chapter 4.4; Calvert and Pedersen, 1993; Van der Weijden, 2002).

## **2.2. The redox-sensitive trace metals Mo, V and U as paleoredox proxies for the Neoproterozoic - Cambrian transition**

Redox proxies with minimal detrital influence are uranium, vanadium and molybdenum (see table 2.2; Tribouillard et al., 2006), which is another reason why they constitute a particularly tempting way of reconstructing paleoenvironmental conditions besides their pronounced redox sensitivity. The investigation of redox-sensitive trace-metal enrichment in marine sediments throughout Earth's history has the potential to reflect the evolution of oxygen in the atmosphere and ocean (e.g. Emerson and Huested, 1991; Algeo, 2004; Scott et al., 2008). The formation of their reduced species can be arranged amongst denitrification and sulphate-reduction reactions (see table 2.3) and their relative enrichment in the sediment can indicate the prevailing redox conditions within the depositional environment, e.g. U and V accumulate from denitrifying conditions on whereas authigenic enrichment of Mo sets in only when sulphate-reducing conditions are met (see Fig. 2.1).

**Table 2.2: Characteristics of U, V and Mo (in present day seawater where applicable; Morford and Emerson, 1999; Tribovillard et al., 2006; Algeo and Tribovillard, 2009).**

	Uranium	Vanadium	Molybdenum
Biological essential element	No	Yes	Yes
Ocean distribution	Conservative	Quasi conservative	Conservative
Concentration	14 nM	39.3 nM	105 nM
Residence time	0.45 My	0.05 My	0.78 My
Main species in oxic water	$\text{UO}_2(\text{CO}_3)_3^{4-}$	$\text{HVO}_4^{2-}$ and $\text{H}_2\text{VO}_4^-$	$\text{MoO}_4^{2-}$
Speciation in reducing conditions	$\text{UO}_2$ , $\text{U}_3\text{O}_7$ or $\text{U}_3\text{O}_8$	$\text{VO}^{2-}$ , $\text{VO}(\text{OH})_3^-$ , $\text{VO}(\text{OH})_2$ , $\text{V}_2\text{O}_3$ or $\text{V}(\text{OH})_3$	Thiomolybdates $\text{MoO}_x\text{S}_{4-x}^{2-}$

**Table 2.3: Half-cell reaction assuming standard state conditions (modified from Piper, 1994, and references therein).**

Eh (V)	Half-cell reaction	Pathway
-0.698	$2\text{NO}_3^- (\text{aq}) + 10\text{e}^- + 12\text{H}^+ (\text{aq}) \rightarrow \text{N}_{2(\text{g})} + 6\text{H}_2\text{O}(\text{l})$	Denitrification
-0.296	$\text{Fe}(\text{OH})_{3(\text{s})} + 1\text{e}^- + 3\text{H}^+ (\text{aq}) \rightarrow \text{Fe}^{2+} (\text{aq}) + 3\text{H}_2\text{O}(\text{l})$	
-0.013	$\text{UO}_2(\text{CO}_3)_2^{2-} (\text{aq}) + 2\text{e}^- + 2\text{H}^+ (\text{aq}) \rightarrow \text{UO}_{2(\text{s})} + 2\text{HCO}_3^- (\text{aq})$	
0.018	$\text{Fe}_2\text{O}_{3(\text{s})} + 2\text{e}^- + 6\text{H}^+ (\text{aq}) \rightarrow 2\text{Fe}^{2+} (\text{aq}) + 3\text{H}_2\text{O}(\text{l})$	
0.040	$2\text{H}_2\text{VO}_4^- (\text{aq}) + 2\text{e}^- + 4\text{H}^+ (\text{aq}) \rightarrow \text{V}_2\text{O}_{4(\text{s})} + 4\text{H}_2\text{O}(\text{l})$	
0.055	$\text{SO}_4^{2-} + 8\text{e}^- + 9\text{H}^+ (\text{aq}) \rightarrow \text{HS}^- (\text{aq}) + 4\text{H}_2\text{O}(\text{l})$	Sulphate-reduction
0.170	$\text{MoO}_4^{2-} (\text{aq}) + 2\text{e}^- + 4\text{H}^+ (\text{aq}) \rightarrow \text{MoO}_{2(\text{s})} + 2\text{H}_2\text{O}(\text{l})$	
0.175	$\text{MoO}_4^{2-} (\text{aq}) + 18\text{e}^- + 2\text{SO}_4^{2-} (\text{aq}) + 24\text{H}^+ (\text{aq}) \rightarrow \text{MoS}_{2(\text{s})} + 12\text{H}_2\text{O}(\text{l})$	

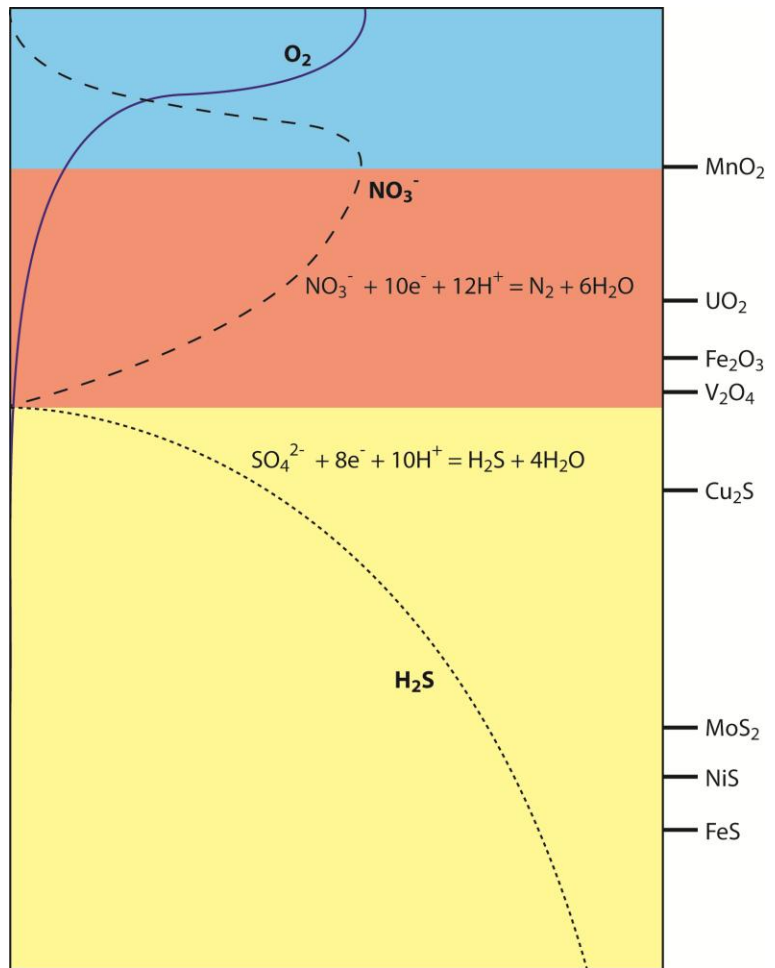


**Figure 2.1: Schematic profile across a redox stratified water column. Stabilities of trace-element species are shown on the right. Modified after Piper and Calvert (2009).**

### 2.2.1. Uranium

Uranium behaves conservatively in oxygenated seawater being mainly present as U(VI) in the stable and highly soluble form of uranyl carbonate complex  $(UO_2(CO_3)_3)^{4-}$ . U is primarily sequestered from the water column by diffusion across the water-sediment interface of reducing sediments, and is enriched by reduction reactions and adsorption or precipitation as uraninite ( $UO_2$ ),  $U_3O_7$  or  $U_3O_8$  (Tribovillard et al., 2006 and references therein). The reduction of U(VI) to U(IV) occurs under conditions similar to Fe(III) to Fe(II) reduction (Klinkhammer and Palmer, 1991; Crusius et al., 1996; Zheng et al., 2000; Morford et al., 2001; Chaillou et al., 2002; McManus et al., 2005). Authigenic U enrichment is considered to take place primarily within the sediments as the reduction of U(VI) uranyl carbonate to the immobile U(IV) fluoride complex is decoupled from the amount of free  $H_2S$  and not directly linked to the redox cycling of Fe and

Mn in the water column (Algeo and Maynard, 2004; McManus et al., 2005). Hence, oxygen penetration depth and sedimentation rate may play a role (Crusius and Thomson, 2000). In the reduced state, U sequestration might be accelerated by the formation of organometallic ligands in humic acids (see Tribovillard et al., 2006 and reference therein). The reoxidation of sediments can cause accumulated U to be remobilized and erase the primary U signal (e.g. Morford et al., 2001; see also McManus et al., 2005). Despite being otherwise geochemically similar to uranium, thorium is relatively unaffected by redox conditions, therefore remaining insoluble in seawater and mostly delivered through detrital input. Hence, the ratio Th/U can be used in order to reconstruct the redox condition which prevailed at the time of deposition (e.g. Adams and Weaver, 1958; Jones and Manning, 1994). Furthermore, the assumption that the flux of scavenged Th reaching the sediment is known and equal to the rate of  $^{230}\text{Th}$  production from the decay of  $^{234}\text{U}$  in the overlying water (Bacon, 1984) means that conclusions can be made regarding the sedimentation rate, i.e. when the accumulation rate of scavenged Th is higher/ lower than its computed production rate, the deposited sediment has probably undergone focusing/winning (see also Henderson and Anderson, 2003). It appears that a Th/U ratio of 0 to 2 indicates anoxic bottom waters whereas a ratio equal or higher than the value of the upper continental crust of 3.8 would signify oxic conditions (Adams and Weaver, 1958; Wignall and Twitchett, 1996; Kimura and Watanabe, 2001). And because detrital material has an average Th/U ratio of 3.8, the amount of authigenically enriched U can be approximated using the calculation:  $U_{\text{aut}} = U_{\text{total}} - \text{Th}/3$  (e.g. Jones and Manning, 1994) although Th/U ratios tend to increase with age (see below) and a value of 4 might be a better choice for Precambrian marine sediments. However, a tentative compilation of total uranium enrichment in black shales throughout Earth's history shows a marked increase during the Neoproterozoic - Cambrian transition (see Fig. 2.2), which can be interpreted as both, a result of an increasingly oxygenated Earth's surface leading to a significant retreat of anoxic environments in the deep ocean and a rise in dissolved U being delivered to the ocean. Nevertheless, a critical appraisal of U enrichment in ancient black shales is strongly advised as Th/U ratios in Precambrian sediments show values which are mostly above 3.8. Previous studies have shown that the detrital Th/U ratio is increasing with age, falling from around 4 in the Archean to values of 3

during the Paleozoic and 2.55 in the late Phanerozoic (McLennan and Taylor, 1980; Taylor and McLennan, 1985). This is consistent with a decrease of mantle Th/U ratios after the GOE, attributed to the preferential recycling of continent-derived U back to the mantle relative to Th, the so called Post-Archean Uranium Recycling (Zartman and Richardson, 2005; Cuney, 2010). However, that means that reductive sequestration and authigenic precipitation of U were important enrichment mechanisms during the GOE, the NOE and throughout the subsequent Phanerozoic. The exclusively high Th/U ratios (>2) between the later Paleoproterozoic and the Neoproterozoic, with minima gradually decreasing towards the Precambrian-Cambrian boundary, could be explained by widespread anoxic environments leading to the depletion of the U inventory in seawater together with an inhibited replenishment from the continents.

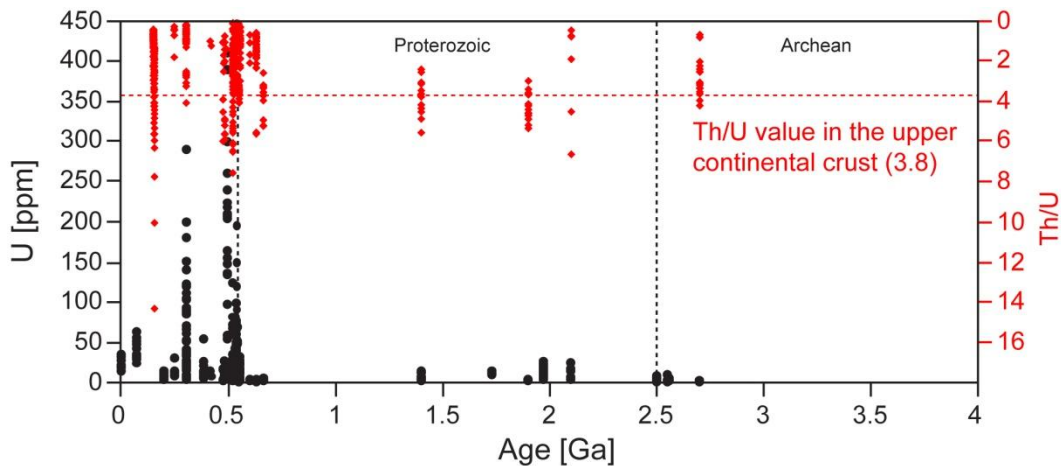


**Figure 2.2:** A tentative compilation of Uranium enrichment and Th/U ratios in black shales throughout Earth’s history (references can be found in the appendix).

### 2.2.2. Molybdenum

Molybdenum in oxic water is mainly present as molybdate ( $\text{MoO}_4^{2-}$ ; Broecker and Peng, 1982), and primarily delivered to the oceans through riverine influx. In the modern ocean, molybdate has a long residence time ( $\sim 780$  Ky), making Mo the most abundant transition metal in modern seawater (Collier, 1985), and is well-mixed (Morford and Emerson, 1999; Siebert et

al., 2003). Furthermore, Mo environmental chemistry in oxygenated system is loosely similar to sulphur, for which the dominant species is  $\text{SO}_4^{2-}$  (Anbar, 2004), and it has been suggested that the role of Mo as bioessential trace metal might be hampered by  $\text{SO}_4^{2-}$  (Marino et al., 2003).

Under oxic conditions, Mo is easily captured by Mn-oxyhydroxides, generally at the sediment surface, but no significant enrichment is achieved under suboxic conditions (Bertine and Turekian, 1973; Berrang and Grill, 1974; Calvert and Pedersen, 1993; Crusius et al., 1996). Under anoxic conditions however, Mo is removed from the aqueous phase and its precipitation is controlled by the concentration of dissolved sulphide in the water column or in the sediment pore water (Helz et al., 1996). A possible way of scavenging Mo from the aqueous environment and its fixation in the sediment is through a geochemical switch in which  $\text{H}_2\text{S}/\text{HS}^-$  transforms Mo from a conservative element to a particle-reactive species in marine environments through the inorganic pathway  $\text{MoO}_4^{2-} \rightarrow$  thiomolybdates ( $\text{MoO}_x\text{S}_{4-x}$ ,  $x=0-3$ ) achieved via successive sulphidation reactions in settings with free hydrogen sulphide beyond threshold concentration in the 100  $\mu\text{M}$  range where Mo removal is nearly quantitative (Helz et al., 1996; Erickson and Helz, 2000; Zheng et al., 2000; Vorlicek and Helz, 2002). Persistently sulphidic conditions seem to be required for this reaction which in the sediment is catalyzed by proton donors or in the presence of some active-surface minerals such as kaolinite (Vorlicek and Helz, 2002). Once thiomolybdate has formed, Mo is scavenged by forming bonds with metal-rich (notably Fe) particles, sulphur-rich organic molecules (Helz et al., 1996; Tribovillard et al., 2004b) and Fe sulphide (Huerta-Diaz and Morse, 1992; Helz et al., 1996; Bostick et al., 2003; Vorlicek et al., 2004). Helz et al. (1996) also suggested the formation of Fe-Mo-S cluster compounds which are able to survive on geological timescales.

Today, molybdate is removed from the water column (1) by co-precipitation and burial with Mn-oxyhydroxides (Bertine and Turekian, 1973), a slowly occurring process which accounts for only 35% of the annual riverine flux and (2) in presence of sulphide-rich pore and bottom waters which accounts for 65% of the total Mo removal even though they only represent less than 2% of the modern seafloor (Scott et al., 2008).

Due to its unique bimodal geochemical characteristics, molybdenum is considered particularly useful in reconstructing paleoredox conditions, whereby high and variable Mo

concentrations (in the range of tens to hundreds of ppm on a total sediment basis), typically occurring in black shales, saprolites, and other organic rich sediments, are considered to be diagnostic of deposition under euxinic conditions.

Recently, Scott et al. (2008) analyzed Mo concentrations and TOC and generated Mo/TOC ratios from Precambrian black shales and assembled them with published data from Precambrian and Phanerozoic black shales. The Mo content and the Mo/TOC ratio measured from euxinic black shales can reflect the size of the oceanic Mo reservoir as determined by the weathering flux and the relative influence of the sulfidic and oxic sinks (Algeo and Lyons, 2006). In modern euxinic environments, although Mo generally covaries positively with TOC, the extent of enrichment is strongly dependent on the Mo reservoir (Algeo and Lyons, 2006). In addition to hydrographic properties, such as the extent of basin restriction and timescales of deep water renewal, the Mo/TOC ratio can also reflect the different degrees of selective organic carbon loss through thermal processes during burial of ancient shales (Wilde et al., 2004). However, Mo enrichment in euxinic marine sediments can also indicate drawdown of the Mo inventory on an oceanic scale during times of widespread oxygen deficiency (Emerson and Husteded, 1991; Algeo, 2004, Pearce et al., 2008; Scott et al., 2008).

The study by Scott et al. (2008), limited to euxinic black shales, could decipher three stages of Mo cycling based on marked shifts in the magnitude of Mo enrichment and Mo/TOC and broadly delineated by both great oxygenation events at the beginning and the end of the Proterozoic Eon. Stage 1 is characterized by typically low values except for the Mo content recorded in the ~2.5 Ga Mount McRae shale (Anbar et al., 2007) and Wille et al. (2007) deciphered increasing Mo enrichment in the sediments of the Ghaap Group, Transvaal Supergroup, between 2.64 and 2.5 Ga (see also Kendall et al., 2010). But, the low Mo/TOC during this interval still suggests dissolved Mo concentrations well below those of the Black Sea. This so called Mount McRae 'whiff' interval might reflect mild oxidative weathering of continental material during the Archean, including transient events of slightly elevated O<sub>2</sub> in the surface ocean and atmosphere, consistent with the emergence of photosynthesizing cyanobacteria by about 2.7 Ga (Brocks et al., 1999, 2003). Anbar et al. (2007) proposed that pyrite and molybdenite could have been oxidized even at very low pO<sub>2</sub> prevailing at this time



(see chapter 1), therefore representing a large enough source to enrich euxinic marine sediments. Figure 2.3a shows an extended compilation of molybdenum concentrations in organic rich shales deposited under anoxic or even euxinic conditions throughout the last 4 billion years confirming Scott's (2008) study. An exponential increase in Mo concentrations can be observed from the Cryogenian on which culminates in the Early Cambrian. Further peaks can be seen during the Pennsylvanian (318 – 299 Ma) and the Albian (112 – 100 Ma). Mo/TOC ratios increase accordingly (see Fig. 2.3b) while a massive peak is observed during the Neoproterozoic – Cambrian transition which could indicate a exponential increase in the oceanic Mo reservoir or represent the result of a bias towards black shale successions from South China (Wallis, 2006; Guo et al., 2007) where a prominent stratiform Ni-Mo-PGE ore horizon of disputed origin occurs within Early Cambrian black shales (see chapter 5.3.2; Coveney and Chen, 1991; Steiner et al., 2001; Lehmann et al., 2007).

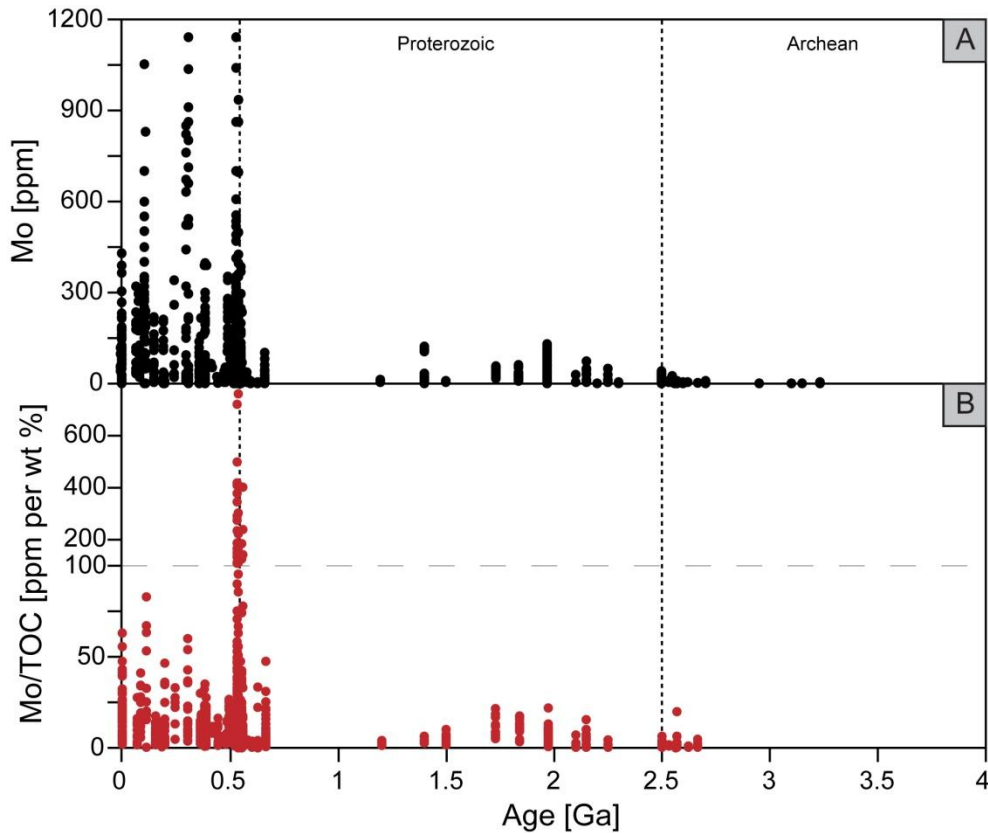


**Figure 2.3: A) Temporal trends in Mo concentrations in anoxic organic rich black shales** Concentrations from the Neoproterozoic – Cambrian transition (~660-520 Ma) are predominantly data from South China from this study and Wallis (2006). **B) Temporal trends in Mo/TOC ratios in anoxic black shales.** Note that ratios higher than 100 are plotted on a different scale and are exclusively from black shale samples from South China (this study; Wallis, 2006). The other references can be found in the appendix.

### 2.2.3. Vanadium

Vanadium is present as V(V) in the quasi-conservative form of vanadate oxyanions ( $\text{HVO}_4^{2-}$  and  $\text{H}_2\text{VO}_4^-$ ) under oxic conditions. Vanadate readily adsorbs onto both Mn- and Fe-oxyhydroxides (Wehrly and Stumm, 1989) and possibly kaolinite (Breit and Wanty, 1991). When mildly reducing conditions are encountered, V(V) is reduced to V(IV) and forms vanadyl ions ( $\text{VO}^{2+}$ ), related hydroxyl species  $\text{VO}(\text{OH})_3^-$  and insoluble hydroxides  $\text{VO}(\text{OH})_2$ , the reaction being

favoured by humic and fulvic acids (Tribovillard et al., 2006). In the marine environment, V(IV) ionic species may be removed by surface adsorption processes or by formation of organometallic ligands (Emerson and Husted, 1991; Morford and Emerson, 1999). Under euxinic conditions, V is further reduced to V(III) due to the presence of H<sub>2</sub>S and can be taken up by geoporphyrins or is precipitated as solid oxide V<sub>2</sub>O<sub>3</sub> or hydroxide V(OH)<sub>3</sub> phase (Wanty and Goldhaber, 1992). A result of the two-step reduction process of V may be the formation of separate V carrier phases of contrasting solubilities under anoxic non-sulfidic versus euxinic conditions (Calvert and Pedersen, 1993; Algeo and Maynard, 2004). Thus, V is not trapped in solid solution by Fe-sulphides (Algeo and Maynard, 2004) and may be removed from pore waters below the level of Mn-Fe-reduction (Morford and Emerson, 1999). The ratio V/(V+Ni) has been used as indicator for the redox condition during the deposition of marine sediments during the Phanerozoic (Hatch and Leventhal, 1992; Jones and Manning, 1994; Rimmer, 2004) and the late Precambrian (Guo et al., 2007). It has been demonstrated that, while chemical alteration of the sediments can change the absolute concentration of V and Ni, their proportionality is likely to remain constant and is, at least partly, controlled by the redox potential during deposition (Lewan, 1984). While V/(V+Ni) ratios are likely to be low in sediments deposited under oxic conditions amounting to 0.71 in average shale (McLennan, 2001), Hatch and Leventhal (1992) found in a study of Upper Pennsylvanian black shales that ratios above 0.84 are characteristic for euxinic depositional environments. However, such a strict application of V/(V+Ni) ratios has to be appreciated with much caution and might strongly differ depending on geological age and geographic setting (Rimmer, 2004).

A compilation of V concentrations in black shales shows a pattern similar to the Mo compilation (see Fig. 2.3), i.e. an overall strong enrichment after the Precambrian – Cambrian transition (see Fig. 2.4a, b), further supporting an increase in the oxygenation of the Earth surface during the late-Ediacaran.

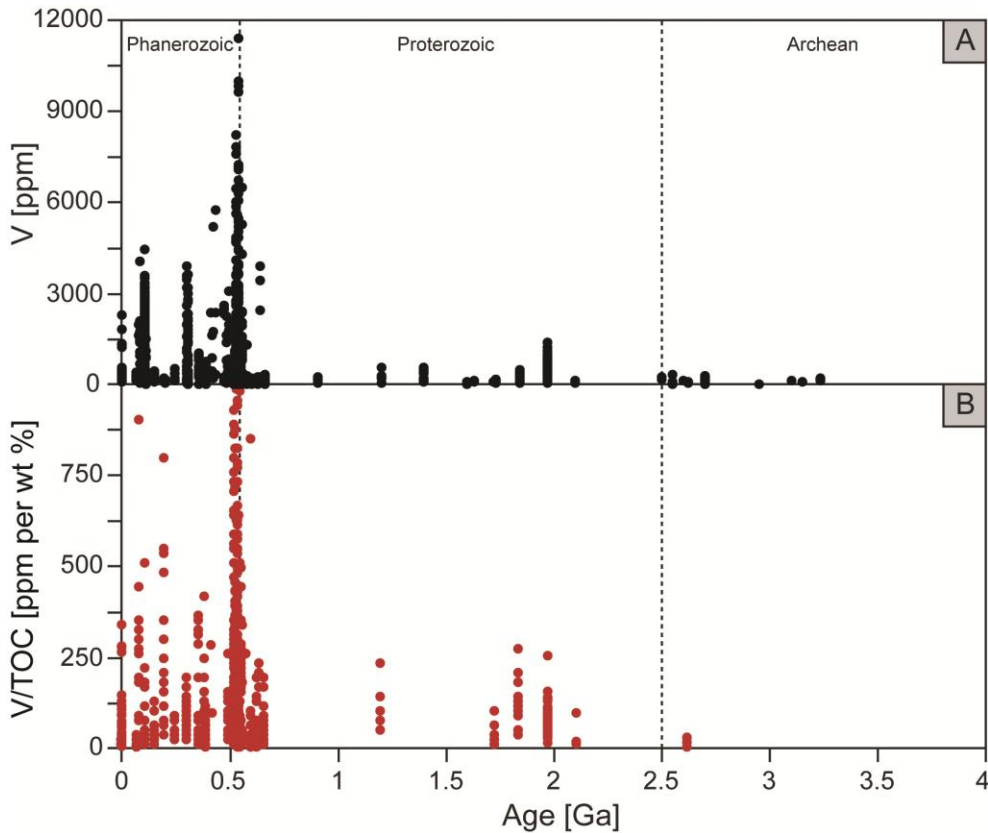


**Figure 2.4: A) A compilation of vanadium concentrations in black shales (see appendix for references). B) Similar to Mo/TOC ratios, V/TOC ratios greatly increase across the Precambrian-Cambrian boundary whereby the highest values (exceeding 1000) are exclusively from black shales sampled in South China (this study; Wallis, 2006).**

#### 2.2.4. Other trace-elements and biological productivity

According to Redfield's (1934) early studies, marine organic matter is mainly composed of carbon, nitrogen and phosphorus in the proportion of 106:16:1. However, C:N:P ratios can vary considerably and are more likely to average 117:16:1 (Anderson and Sarmiento, 1994; see also Lenton and Watson, 2000; Algeo and Ingall, 2007). It has emerged that most trace-metals are also largely involved in biogeochemical cycling processes, some of them represent key bio-nutrients and required for organisms to live and thrive (e.g. Bruland, 1983). Accordingly, the Redfield ratio could for instance be approximately extended to



based on the stoichiometry of model species analysed by Ho et al. (2003) which also varies considerably between individual species (see also Collier and Edmond, 1984; Brumsack, 1986; Piper, 1994). Furthermore, barium has also been associated with biological productivity whereby barite in settling oceanic particles is more a consequence of decomposition and uptake in microenvironments rather than the secretion of barite by specific organisms (e.g. Dymond et al., 1992; McManus et al., 1998). However, in marine sediments, Ba occurs in detrital plagioclase crystals and barite ( $BaSO_4$ ; Bishop, 1988) whereby biogenic barium and barite have been proposed as paleoproductivity proxy because of its relationship with organic matter and refractory nature in sediments where no intense sulphate-reduction has taken place (Tribovillard et al., 2006 and references therein). The dissolution of barite by sulphate-reduction can cause Ba migration through pore waters and re-precipitation where oxic conditions are met, a behaviour similar to Mn, which limits its use as a paleoproductivity proxy (Dymond et al., 1992; Torres et al., 1996; see also McManus et al., 1998). Another trace-nutrient is nickel, whose complexation with organic matter accelerates scavenging in the water column and enrichment in the sediment, where it can be released during organic matter degradation (Tribovillard et al., 2006 and references therein). When sulphides and Mn are absent, such as under moderately reducing conditions, Ni is released to the porewaters or diffuses into the overlying waters whereby sulphate-reducing environments can cause Ni to be incorporated as insoluble NiS into pyrite (Huerta-Diaz and Morse, 1992; Morse and Luther, 1999). Although copper only partly behaves as a trace-nutrient, it is also scavenged from the water column accelerated by complexation with organic matter and adsorption onto Fe-Mn-oxyhydroxides (Tribovillard et al., 2006 and references therein). After organic matter decay and/or reductive dissolution of Fe-Mn-oxyhydroxide phases, Cu is released to pore waters and sulphate-reducing conditions lead to incorporation into pyrite or precipitation as CuS and  $CuS_2$  (Huerta-Diaz and Morse, 1992; Morse and Luther, 1999). Zinc behaves similarly, forming organic complexes and adsorbing onto Fe-Mn-oxyhydroxides and being incorporated into pyrite as ZnS or forming its

own sulphides, notably sphalerite [(Zn, Fe)S], under sulphate-reducing conditions (Huerta-Diaz and Morse, 1992; Morse and Luther, 1999). Other than Ni, Cu and Zn, cadmium is only present in one coordination state. It is mainly delivered to the sediments with organic matter, released during organic matter decay and enriched as sulphide under reducing conditions, whereby it is more likely to form CdS than to co-precipitate with FeS (Huerta-Diaz and Morse, 1992).

The above mentioned trace elements are dominantly delivered to the sediment as organometallic complexes, reflecting the bio-accumulation by marine plankton (e.g. Brumsack, 2006), and fixed when strongly reducing conditions are met, whereas the accumulation of Mo, V and U is more tightly controlled by redox conditions. It is unlikely that Mo and V are significantly pre-concentrated in plankton and dissolved Mo shows no and V only a weak nutrient-like distribution in the water column (Piper, 1994, and references therein; Brumsack, 2006; Piper and Calvert, 2009). Concurrent enrichment of, for instance Ni and Cu, together with V, U and Mo in case of euxinic conditions, can therefore give insight into whether high productivity and organic matter delivery to the deep sea triggered reducing conditions or if watermass restriction and/or stagnation are the controlling parameters (e.g. Tribovillard et al., 2006). A tentative compilation of Ni and Cu concentrations in anoxic black shales (see Fig. 2.5) shows that, contrary to Mo, V, and U, their concentrations did not increase to the same extent during the Precambrian-Cambrian boundary, especially not if generally lower TOC contents are considered during the 'Boring Billion' (see Fig. 1.10). This further supports that the very low concentrations of redox-sensitive trace-metals (Mo, V, U) prior to the Neoproterozoic Oxygenation Event indeed result from a switch in the overall redox potential on the Earth's surface and are only secondarily, if at all controlled by changes in the amount of primary productivity over time.

However, the role of Mo as trace-nutrient is crucial for organisms performing nitrogen fixation, the capability of reducing N<sub>2</sub> to biologically useful ammonia limited to some bacteria and archaea, where it is present in one kind of nitrogenase metalloenzymes, as part of a Fe<sub>7</sub>MoS<sub>9</sub> cluster (Howard and Rees, 1996). Alternative nitrogenase enzymes include Fe alone or V and Fe, which are both less efficient (Eady, 1996; Anbar and Knoll, 2002). Mo and V are also included in a suite of other enzymes and low potential oxygen atom transfers in organisms, the latter being

particularly important under very low oxygen levels (Stiefel, 1997; Williams and Fraústo da Silva, 2002). It has therefore been hypothesized that low availability of these redox-sensitive trace-metals before the NOE (see Fig. 2.2 and 2.3) might have effectively impeded nitrogen fixation by prokaryotes, leading to biologically available nitrogen limitation, as opposed to phosphorus in the Phanerozoic (Anbar and Knoll, 2002; Saltzman, 2005; Zerkle et al., 2006; Glass et al., 2009; Planavsky et al., 2010).

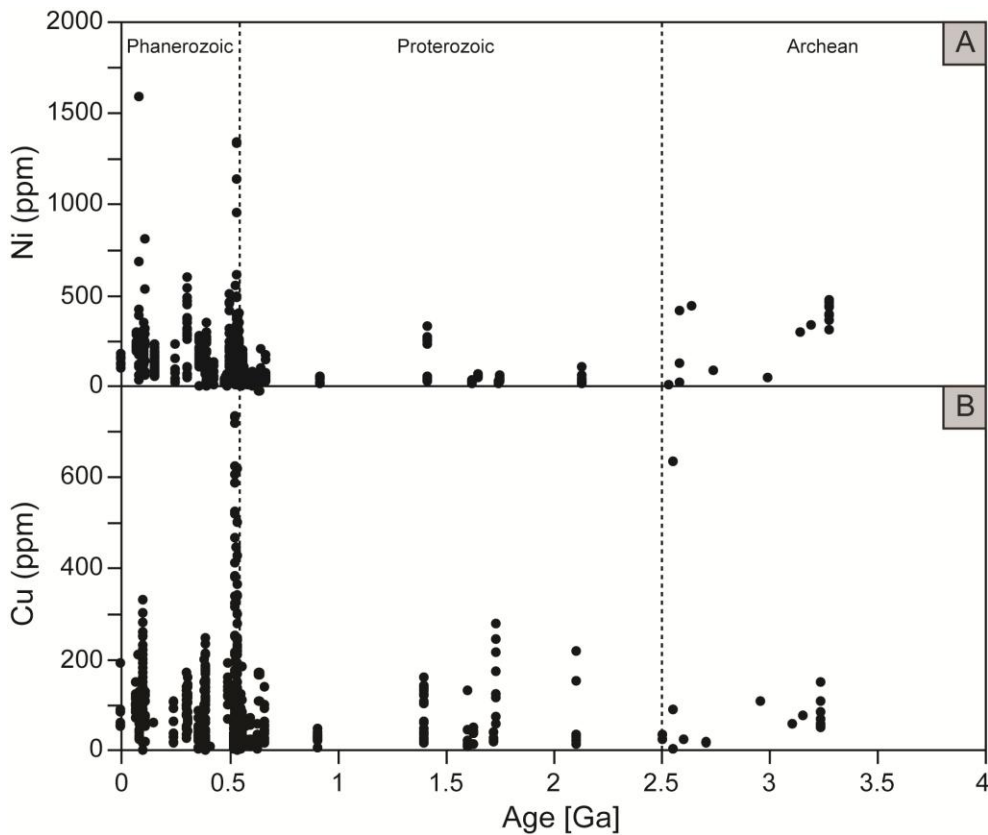


**Figure 2.5: A) Nickel concentrations in black shales across the last 4 billion years remain essentially within the same magnitude except for in sediments deposited during the Precambrian-Cambrian transition on the Yangtze Platform, where extremely high concentrations likely to be associated with hydrothermal enrichment have been omitted for better visibility (see appendix). B) Peaks in copper concentrations, similar to Ni, basically remain stable but with some fluctuations showing a slight increase after the GOE before decreasing again until the Neoproterozoic. Extreme enrichments from the Yangtze Platform have also been omitted for better visibility (see appendix).**

### 2.3. Iron speciation: A proxy for the oxygenation of the deep ocean

The use of iron speciation, or the sequential extraction procedure for iron, as an indicator of the redox conditions under which ancient and modern sediments have been deposited, is basically a further development of the degree of pyritisation (DOP; Berner, 1970; Raiswell et al., 1988). The DOP determines the extent to which iron minerals potentially reactive towards dissolved sulphide have been transformed into pyrite

$$\text{DOP} = \text{Fe}_{\text{py}} / [\text{Fe}_{\text{py}} + \text{Fe}_{\text{HCl-extractable}}]; \text{Fe}_{\text{HCl-extractable}} = \text{Fe extracted by boiling with 12N HCl}$$

and can therefore indicate deposition beneath oxic or anoxic bottom waters (e.g. Raiswell and Al-Biatty, 1989; Gagnon et al., 1995; Raiswell and Canfield, 1998; Poulton et al., 1998; Müller, 2002; Schenau et al., 2002; Lyons et al., 2003). However, although high DOP values (>0.55; Raiswell et al., 1988) almost invariably record euxinia, such environments can also yield values spanning from high to intermediate due to an overestimation of the reactive iron extracted by boiling, concentrated HCl, i.e. the dissolution of silicate-bound iron which is not reactive to H<sub>2</sub>S (Canfield et al., 1992; Lyons and Severmann, 2006). Therefore, methods to define and quantify reactive iron more precisely have been developed (see review by Lyons and Severmann, 2006), notably iron speciation.

The iron speciation scheme identifies seven operationally derived iron pools (Poulton and Canfield, 2005): (1) carbonate associated Fe (Fe<sub>carb</sub>), including siderite and ankerite; (2) easily reducible oxides (Fe<sub>ox1</sub>), including ferrihydrite and lepidocrite; (3) reducible oxides (Fe<sub>ox2</sub>), including goethite, hematite and akaganéite; (4) magnetite (Fe<sub>mag</sub>); (5) poorly reactive sheet silicate Fe (Fe<sub>PRS</sub>); (6) pyrite Fe (Fe<sub>py</sub>); and (7) unreactive silicate Fe (Fe<sub>U</sub>). Iron species which are highly reactive towards dissolved sulphide (Fe<sub>HR</sub>) include Fe<sub>py</sub>, Fe<sub>mag</sub>, Fe<sub>ox</sub> and Fe<sub>carb</sub> and in contrast to the DOP, excludes poorly reactive iron. The ratio Fe<sub>HR</sub>/Fe<sub>T</sub> has been applied to modern (Canfield et al., 1996; Raiswell and Canfield, 1996, 1998), Phanerozoic (Raiswell et al., 2001; Poulton and Raiswell, 2002), Proterozoic (Shen et al., 2002, 2003; Poulton et al., 2004a; Canfield et al., 2007, 2008) and even Archean (Reinhard et al., 2009) marine sediments in order



to demonstrate or infer deposition beneath an anoxic water column. The separate identification of minerals containing ferrous iron such as magnetite ( $\text{Fe}_{\text{mag}}$ ), siderite and ankerite (as part of  $\text{Fe}_{\text{carb}}$ ), because they are likely to be 'highly reactive' towards dissolved sulphide (Poulton et al., 2004b) and may occur in elevated concentrations in marine sediments deposited beneath an Fe(II)-containing water column, the iron speciation scheme could distinguish between anoxic Fe(II) containing depositional conditions and sulphidic conditions (Poulton et al., 2004b; Poulton and Canfield, 2005). However, although high  $\text{Fe}_{\text{HR}}$  enrichment is considered to be diagnostic for deposition beneath a sulphidic water column (Raiswell and Canfield, 1996; Wijsman et al., 2001; Lyons et al., 2003), the ratio  $\text{Fe}_{\text{HR}}/\text{Fe}_{\text{T}}$  alone cannot distinguish between a non-sulphidic, ferruginous water column and a sulphidic water column (Poulton and Canfield, 2011), which ultimately depends on the possibility of sulphate-reduction potentially inhibited by low sulphate concentrations. Hence, the  $\text{Fe}_{\text{Py}}/\text{Fe}_{\text{HR}}$  ratio must be applied in combination with the  $\text{Fe}_{\text{HR}}/\text{Fe}_{\text{T}}$  ratio in order to determine whether the deposition of a given marine sediment occurred under oxic, anoxic-ferruginous or sulphidic conditions. In modern marine sediments deposited under an oxic water column, the  $\text{Fe}_{\text{HR}}/\text{Fe}_{\text{T}}$  ratio does not exceed 0.38 (Raiswell and Canfield, 1998; Canfield et al., 2008). A higher proportion of highly reactive iron would indicate an anoxic water column whereby a  $\text{Fe}_{\text{Py}}/\text{Fe}_{\text{HR}}$  ratio exceeding 0.8 characterizes sulphidic bottom waters (Canfield et al., 2008). However, the Phanerozoic average in  $\text{Fe}_{\text{HR}}/\text{Fe}_{\text{T}}$  for oxic deposition is  $0.14 \pm 0.08$  (Poulton and Raiswell, 2002), hence, ancient marine sediments such as of Neoproterozoic age may as well display lower  $\text{Fe}_{\text{HR}}/\text{Fe}_{\text{T}}$  ratios although bottom waters were anoxic (Canfield et al., 2007). Also, while  $\text{Fe}_{\text{Py}}/\text{Fe}_{\text{HR}}$  ratios above 0.8 clearly indicate sulphidic conditions, values around 0.7 are more equivocal but do not exclude sulphidic conditions as some Fe oxide minerals might escape sulphidization during settling through the water column (März et al., 2008; Poulton and Canfield, 2011).

The highly reactive iron cycle is composed of several sources including riverine, glacial and hydrothermal fluxes, coastal erosion, atmospheric dust and diagenetic recycling whereby the largest fraction remains in estuaries, much of it gets deposited into shelf sediments and finally deep sea sediments (Fig. 2.6; Poulton and Raiswell, 2002; Raiswell, 2006, and references therein). The shelf-to-basin iron shuttle, whereby Fe is remobilized during diagenesis, and the

transport of hydrothermal Fe under anoxic conditions are the main mechanisms leading to iron sequestration and fixation under an anoxic or euxinic water column, the latter being characterized by syngenetic pyrite formation (Canfield et al., 1996; Wijsman et al., 2001; Lyons et al., 2003; Raiswell and Anderson, 2005), whereby enhanced reactivity of the detrital iron pool has also been suggested (Anderson and Raiswell, 2004).

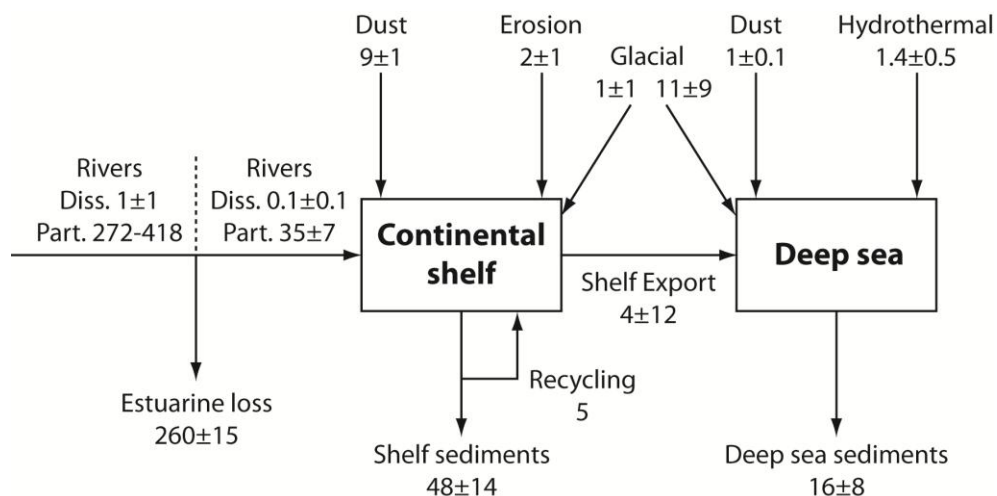


**Figure 2.6: The global highly reactive iron cycle with modern fluxes in Tg year<sup>-1</sup>(Raiswell, 2006).**

The oxygenation of the deep ocean inferred by iron speciation analysis carried out in the past decade unveils an increasingly complex history. Whereas Holland (2006) essentially postulated a transition from anoxic ferruginous conditions after the GOE, the concept of Canfield (1998), who advocated a stratified ocean after the GOE with widespread sulphidic conditions, has unleashed several studies arguing for more variable conditions (see Fig. 2.7). According to Reinhard et al. (2009), episodic accumulation of oxygen in the atmosphere could have led to localized euxinic conditions in the late Archean in an ocean otherwise characterized by ferruginous conditions. After about 1.8 Ga, the transition to a possibly widely sulphidic ocean occurred concomitant with the cessation of BIF's (Poulton et al., 2004a, 2010) and Canfield et al. (2007, 2008) presented evidence from the deep marine succession in Newfoundland that the proportion of highly reactive iron versus total iron ( $Fe_{HR}/Fe_T$ ) decreased to modern, oxic values after the Gaskiers glaciations ca. 582 Ma. However, the oxygenation of

the deep ocean was not universal and bottom water chemistry might have only changed locally. And perhaps surprisingly, sulphidic conditions seem to have been rare during the late Neoproterozoic, occurring before the Sturtian glaciations and around the Precambrian – Cambrian boundary (see Fig. 2.7; Canfield et al., 2008).

And last but not least, recent studies from supposedly transitional intervals in the late Archean (Reinhard et al., 2009), the Paleoproterozoic (Poulton et al., 2010) and the late Neoproterozoic (Li et al., 2010), showed that sulphidic conditions might have prevailed along continental margins above an otherwise ferruginous deep ocean, roughly analogous to modern oxygen minimum zones (see also reviews by Lyons and Gill, 2010; Poulton and Canfield, 2011).

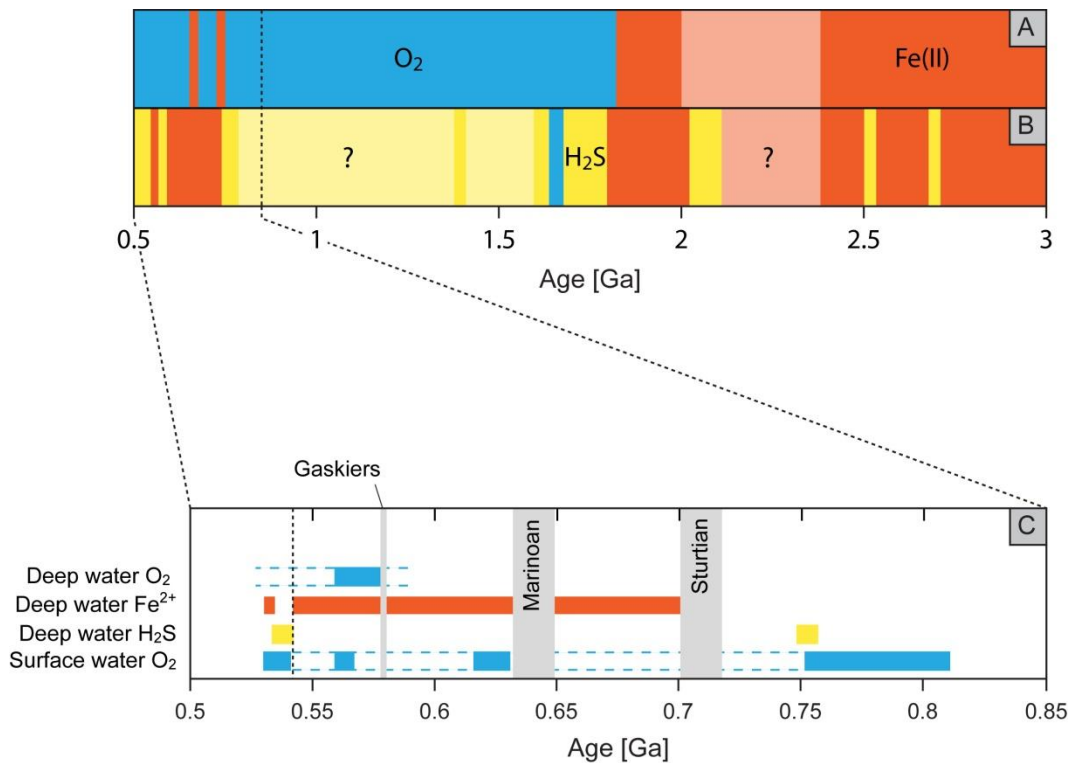


**Figure 2.7:** A) shows the conception of an essentially anoxic ferruginous deep sea until after the GOE when BIF's disappear from the geological record ~1.8 Ga and the onset of oxic conditions interrupted by a return of ferruginous conditions during the 'Snowball Earth' glaciations as outlined by Holland (2006). B) A more complex of oceanic redox states which became apparent after the concept of Canfield's ocean (Canfield, 1998) showing intermittent euxinia before the last appearance of BIF's (Reinhard et al., 2009) and the onset of widespread euxinia around 1.8 (e.g. Poulton et al., 2004), with

possibly oxic intervals (Slack et al., 2007), and the return of ferruginous deep ocean waters towards the Neoproterozoic – Cambrian transition with the development of euxinia in the Cambrian (Canfield et al., 2008; Gill et al., 2011) before the deep sea got pervasively ventilated in the Phanerozoic (A + B modified after Lyons and Gill, 2010). C) Summary of the results from Canfield et al. (2008) based on iron speciation analysis of Neoproterozoic – Cambrian marine sediments.

#### **2.4. Redox-sensitive trace-metals and iron speciation in black shales on the Yangtze Platform**

Until today, most studies investigating the Neoproterozoic Oxygenation Event from an elemental perspective, notably redox-sensitive trace-metals in black shales, have been carried out on samples collected on the Yangtze Platform. And as I pointed out earlier, the steep increase in Mo, V and U concentrations in black shales within a relatively narrow time span around the Precambrian – Cambrian boundary is exclusively reported from the Yangtze Platform and regardless of whether the environmental conditions were unique from a global point of view, the Yangtze Platform, from the shelf to the deeper basin, represents an exceptionally interesting geological archive of the changes in the biogeochemical cycling that occurred during these eventful times. Previous studies have either focussed on a few more or less isolated sections (Guo et al., 2007; Li et al., 2010) or simply included geochemical data from the Yangtze Platform into temporally and spatially very extensive geochemical studies (Scott et al., 2008; Canfield et al., 2008). The scope of the following study lies therefore on comparing several successions of mostly organic-rich marine sediments all over the Yangtze Platform deposited between ca. 663 Ma and the Early Cambrian ca. 520 Ma under different environmental conditions.

The reliability of redox-sensitive trace-metals as paleoredox proxies can be expected to be particularly complicated during the Precambrian – Cambrian transition while iron speciation can be expected to better reflect prevailing redox conditions when applied with appropriate care. Coincidentally, available iron speciation studies from the Precambrian – Cambrian transition have so far failed to demonstrate sulphidic conditions elsewhere than on the Yangtze

Platform (Canfield et al., 2008; Li et al., 2010), which adds to the special interest in conducting a geographically extensive investigation on the geochemical characteristics of marine sedimentation across the platform.

### **3. Geological setting**

#### **3.1. The geological evolution of the Yangtze Platform during the Neoproterozoic and Early Cambrian**

The Neoproterozoic sedimentary successions of the Yangtze platform were greatly influenced by the tectonic history of the South China craton, one of three major tectonic cratons in China (see Fig. 3.1). The South China craton consists of the Yangtze and the Cathaysia block which have previously been thought to have amalgamated during the formation of the Jiangnan fold belt (or Sibao-Jinning orogeny) at around 900 Ma as part of the Grenvillian orogenic belt (Li et al., 1995, 2002, 2003b; 2005). However, others have advocated a younger age (ca. 800 Ma: Zhou et al., 2002a, b, 2004b) and Zhao et al. (2011) have recently demonstrated that the Jiangnan fold belt is not a Grenvillian feature and that the Yangtze and Cathaysia blocks amalgamated not earlier than ca. 830 Ma. Within a similar time span, during the break-up of Rodinia, a plume-centre was located under South China inducing widespread granite intrusions around the Yangtze block (Li et al., 1999b, 2003a), such as the 819±7 Ma Huangling Granite in the Three Gorges Area (Ma et al., 1984), and major rifting basins were formed along the southeastern and western margins of the South China craton (Li et al., 2003b; Wang and Li, 2003). The subsequent thermal subsidence created the necessary accommodation space for the Neoproterozoic sediments which unconformably overlie Mesoproterozoic metamorphic rocks or early Neoproterozoic rift-related bimodal magmatic rocks and reflect the different rifting phases (Wang and Li, 2003). The Ediacaran Yangtze platform (see Fig. 3.1) developed over a Neoproterozoic rifted continental margin presumably initiated along the southeastern side of the Yangtze block ~ 800 Ma (Li et al., 1999b; Wang and Li, 2003; Jiang et al.,

2003b, 2006a). Whereas the Cryogenian successions were deposited during this rifting-drifting event, the post-glacial Ediacaran carbonate rocks were presumably deposited in a passive margin setting, although the timing of the rift to post-rift transition is still unclear (Wang and Mo, 1995; Jiang et al., 2003b; Wang and Li, 2003; Zheng et al., 2004).

However, the Neoproterozoic sedimentary successions of the Yangtze platform, which despite the complex tectonic history of China remained relatively undeformed, can be subdivided into three main intervals: pre-glacial predominantly volcano-siliciclastic rocks (e.g. the ~750 Ma Liantuo Formation in the platform and the Banxi Group in the basin), two Cryogenian glacial diamictite intervals (the Gucheng/Tiesiao/Chang'an formations and the Nantuo Formation) separated by an interglacial unit (the Datangpo/Xiangmeng formations) and post-glacial Ediacaran marine carbonates and shales (the Doushantuo Formation and the Dengying/Liuchapo formations).

The present study focuses on black shale successions from the interglacial Datangpo Formation to Early Cambrian (ca. 520 Ma) which are abundant on the Yangtze Platform (see Fig. 3.1). The term black shale herewith refers to homogenous or laminated dark to black siliciclastic marine sediments with grain sizes from clay to silt fraction and elevated organic content of predominantly above 1%. The stratigraphic positions and the correlation of the analyzed sections are summarized in digital form and can be found in the supplementary CD-ROM at the back of the thesis.

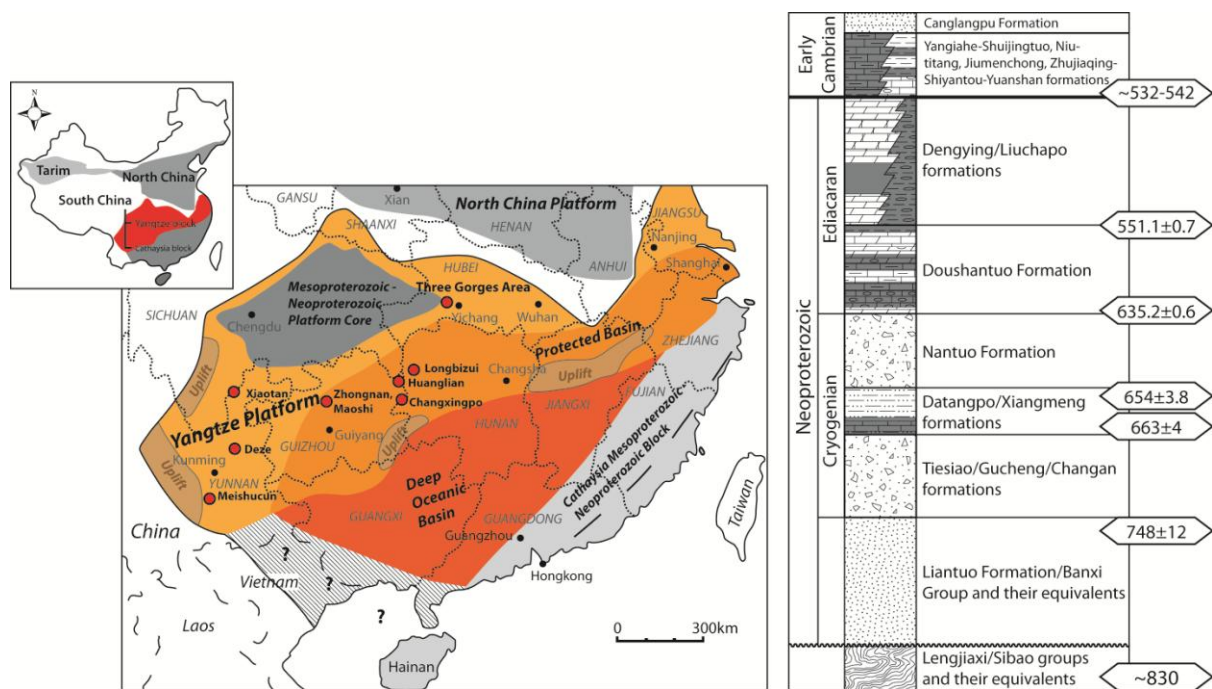


Figure 3.1: Simplified geological map of South China with the locations of the studied sections in both, the Yangtze platform and the basin (modified after Steiner et al., 2001a; Ling et al., 2007) and a simplified stratigraphic overview of the Yangtze platform (modified after Jiang et al., 2007a). The term ‘Protected Basin’ refers to the seafloor from the platform margin to the deepest parts of the basin. Ages between 830 and 820 Ma have been established from numerous granitoids and ultra-mafic intrusive rocks found in the metamorphosed, Early Neoproterozoic strata (Lengjiaxi/Sibao Groups) which are unconformably overlain by the Liantuo Fm./Banxi Group constrained with ages of 748±12 Ma from the upper Liantuo Fm. (Ma et al., 1984) and 758±23 Ma (Yin et al., 2003) and 809±8.4Ma (Zhang et al., 2008a) from the upper Banxi Group. An ash bed within the lower interglacial Datangpo Fm. yielded an age of 663±4 Ma (Zhou et al., 2004a) while an age of 654±3.8 Ma has been determined for the upper (Datangpo equivalent) Xiangmeng Fm. (Zhang et al., 2008b). The deposition of the Doushantuo Fm. is well constrained by ages of 635.2±0.6Ma and 632.5±0.5 Ma from ash beds within and on top of the cap carbonates at the base of the Doushantuo Fm. (Condon et al., 2005) and 551.1±0.7Ma near the Doushantuo/Dengying boundary (Condon et al., 2005; Zhang et al., 2005). Several ages between ca. 532 and 542 have been determined in various sections covering the earliest Cambrian (see chapter 3.1.3. and review by Jiang et al., 2011).

## 3.2. The Cryogenian

### 3.2.1. The Datangpo Formation

The Datangpo Formation represents the interglacial sedimentary succession between the two end-Cryogenian glacial diamictites, the Tiesiao Formation and the Nantuo Formation, probably equivalent to the Sturtian and Marinoan glaciations respectively which is supported by a U-Pb age taken from a tuffaceous bed at the base of the Datangpo Fm. pointing to an age of  $663\pm 4$  Ma (Zhou et al., 2004a). The maximum thickness of the Datangpo Fm. is about 200 m, measured at Zhailangou, Guizhou Province (Zhou et al., 2004a), which is near our studied section in the Changxingpo mine (see Fig. 3.2). The transition from the underlying Tiesiao diamictite is relatively sharp, although the uppermost Tiesiao Fm. consists of more fine grained material. The boundary between the Tiesiao and the Datangpo formations is indicated by a dm-thick finely laminated brownish mudstone. The base of the Datangpo Fm. consists of a succession of dark coloured manganese carbonate with varying thickness which was around 2 m in the area around Changxingpo Mine, where the sampling has been carried out, and about 6 m at Zhailangou (Chen et al., 2008), Xiangtan (Liu, 1990, Liu et al., 2006), and Minle (Tang and Liu, 1999; Feng et al., 2010), all in Hunan Province. At the Shitang mine, about 80 km north west of Changxingpo, the Mn carbonates occur in lenses with a maximum thickness of 1.3 m above a ca. 2 m thick pyrite-rich succession of black shales overlying cross-bedded sandstone which possibly belong to the Tiesiao Fm. The base of the Datangpo Fm. at the Yuxin mine, close to Shitang, is again different: sandstones are followed by black shales (similar in Shitang) but the 1.5 m thick Mn carbonate succession is halfway interrupted by a 20 cm thick bed of friable, organic rich black shale. Black shales also overlie the Mn carbonates here.



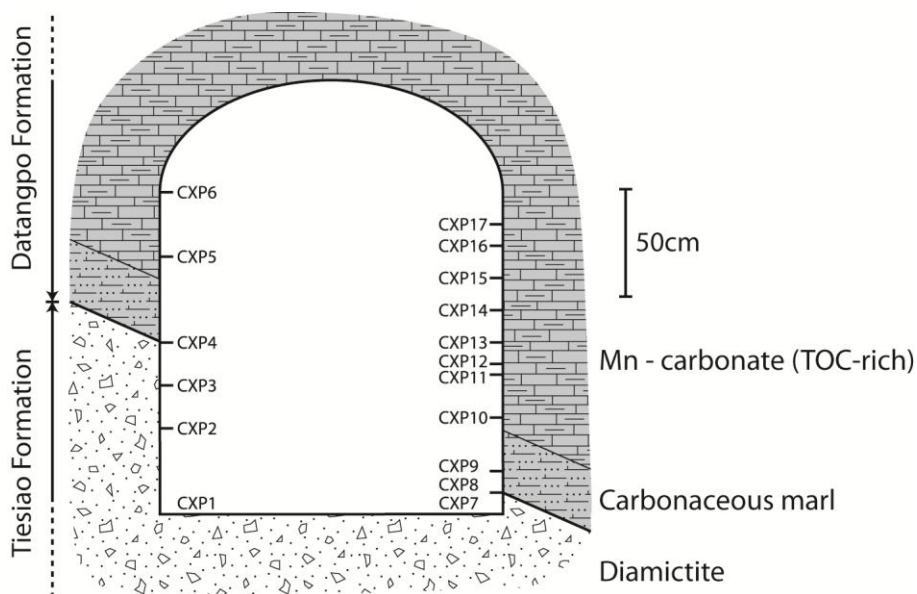


**Figure 3.2: A transect across the Changxingpo Mine at the sampling site with organic rich Mn-carbonates of the interglacial Datangpo Fm. overlying the glacial deposits of the Tiesiao Fm.**

### 3.3. The Ediacaran

#### 3.3.1. The Doushantuo Formation (ca. 635 – 551 Ma)

The Doushantuo Fm. is probably amongst the most extensively studied Neoproterozoic formations worldwide, notably because it has yielded the richest fossil record of this crucial time period, including acritarchs, algae, macroscopic bilaterians and fossil embryos (Xiao et al., 1998; Zhang et al., 1998; Xiao and Knoll, 2000; Chen et al., 2000, 2003; Condon et al., 2005; Jiang et al., 2006a, 2007a; Ling et al., 2007; McFadden et al., 2008; Ohno et al., 2008; Bristow et al., 2009). Overlying the glacial diamictites of the Nantuo Fm., the cap carbonate of the Doushantuo Fm. records the end of the Marinoan ‘Snowball Earth’ glaciation (Hoffman et al., 1998). Based on U-Pb age constraints and, most importantly, an extremely negative  $\delta^{13}\text{C}$  excursion of arguable duration between 580 and 550 Ma, the Doushantuo Fm. has been correlated with the Johnnie Formation of the Death Valley (USA), the Krol Formation in the Lesser Himalayas (India), the Wonoka Formation of the Adelaide rift complex (AUS), the Shuram

Formation in Oman, the post-Marinoan Windermere Supergroup (USA), the Nama and Tsumeb groups of Namibia and in the Neoproterozoic of SE Siberia (Le Guerroué et al., 2006a; Zhou and Xiao, 2007; Jiang et al., 2008).

Although the Doushantuo Formation was deposited between 635 and 551 Ma (Condon et al., 2005), covering about 90% of the Ediacaran Period, it does not exceed a thickness of about 320 m (Vernhet, 2007, and references therein). Whether it reflects a very condensed succession or contains large undetected hiatuses is presently unclear, the former being more likely (Zhou et al., 2007). Vernhet (2007) identified three different depositional environments in a study of several sections in the Chinese provinces Hunan, Guizhou and Hubei spanning shallow-water subtidal shelf environment over intertidal or shoals environment to deep-water basins, illustrating the wide bathymetric range under which the sedimentation of the Doushantuo Fm. took place on the Yangtze platform (see Fig. 3.4; see also Jiang et al., 2003b; Vernhet and Reijmer, 2010; Jiang et al., 2011).

In the Yangtze Gorges area, the type locality of the Ediacaran (Sinian) system in China (Lee and Chao, 1924), the Doushantuo Fm. can be broadly subdivided into four lithological members (Wang et al., 1998). Member I consists of cap carbonates which extend throughout the central and southern Yangtze platform. They are characterized by tepee-like structures, sheet cracks, macropeloids, barite crystal fans, and negative  $\delta^{13}\text{C}$  values (Jiang et al., 2003a, 2006a; Zhou et al., 2004a). A U-Pb age of  $635.2 \pm 0.6$  Ma has been determined from an ash layer within the cap carbonate (Condon et al., 2005). In the Three Gorges area, the cap carbonates have a thickness of about 5 m and are thus relatively thin compared to other basal Ediacaran cap carbonates around the world (Hoffman et al., 2007). The overlying second member is between 80 and 140 m thick and is composed of organic-rich calcareous mudstone, thin bedded dolomicrite and interbedded black shales. An ash layer dating from  $632.5 \pm 0.5$  Ma is situated a few meters above the cap carbonate (Condon et al., 2005; cp. Zhang et al., 2005:  $621 \pm 7$  Ma). Abundant centimetre-sized chert nodules, although decreasing up-section, occur in the lower-middle part of member II and contain numerous acanthomorphic acritarchs and multicellular algae (Zhang et al., 1998; Yin et al., 2007; Zhou et al., 2007). The sparse sedimentary structures include parallel laminations, crinkle laminations and rare

intraformational breccias indicate that wave and current activity were probably absent during the sedimentation of member II (Zhou et al., 2007).

Member III is between 30 and 60 m thick and composed of medium to thick-bedded dolomite with thin chert horizons and irregular chert nodules that grade up section into thin-bedded limestone and dolomite interbeds (i.e. ribbon rocks). Although most chert layers are late diagenetic in origin, some of them contain very well preserved microfossils (Zhang et al., 1998; Xiao, 2004). Sedimentary structures include scour marks, crinkle laminations, low angle cross-bedding, and sandy layers capping limestone and dolomite bedding surfaces are common, indicating that deposition occurred under water depths shallower than the underlying Member II, possibly in shallow subtidal environments (Zhou et al., 2007). Member IV, commonly referred to as the Miaohe Member, is again a succession of black shales and organic-rich mudstone. Sedimentary structures are absent apart from the fine lamination and abundant, sometimes huge ( $\phi > 1\text{m}$ ), carbonate concretions. Pyrite and barite are also common features of this member. An ash bed on the top of the Miaohe Member has been dated and yields a U-Pb age of  $551.1 \pm 0.7$  Ma (Condon et al., 2005).

We studied the Doushantuo Fm., or parts of it, at several locations on the Yangtze platform: Jiulongwan and Jijiawan in the Yangtze Gorges area, Hubei Province (see Fig. 3.5), and Maoshi (see Fig. 3.6; northwest of Zunyi, Guizhou Province)

At the section visited at Jiulongwan a substantial part of Member II has been sampled from right above the cap carbonate throughout a discontinuously exposed succession of massive grey dolomite beds with interbedded black shales (see Fig. 3.5a). Further outcrops sampled around Jiulongwan comprise the more than 10 m thick Miaohe Member (see Fig. 2.2b), consisting of laminated black shales, barite and abundant huge carbonate nodules which lie between Member III and the wavy, shaly horizon with a pyrite rich layer which constitutes the contact to the overlying Dengying Fm. Below the Miaohe Member, the top of Member III consists of dark grey dolomite which grade downwards into paler banded carbonates (ribbon rocks) followed by a sequence of yellow-brownish sandy siltstones and then again dolomite beds with some intercalated chert beds. No boundary between the Doushantuo Member II and III could be located in this region.

At the Jijiawan section, the lower black shales of the Doushantuo Member II and the black shales of the Miaohe have been investigated. Member III was heavily tectonized and the top consisted of massive dolomites without apparent bedding while the lower part of the black shales of the Miaohe Mb. were slightly weathered and rather brittle (see Fig. 3.5c).

The outcrop of the Doushantuo Fm. including the transition to the overlying Dengying Fm. we visited at the Maoshi section, Guizhou Province, was presumably deposited in an intra-shelf basin and consisted of carbonate-rich black shales which correlate with the Miaohe Member (see Fig. 3.5 and 3.6) and an about 1 m-thick succession of organic-poor sandy shales on top underneath the dark carbonates of the Dengying Fm. This black shale member at the top of the Doushantuo Fm. occurs in almost all paleoenvironments of the Yangtze platform and marks the base of a new sequence and marine transgression (Zhu et al., 2003). And, like the cap carbonates, can be used as a stratigraphic marker. However, due the high lithostratigraphic variability of the Doushantuo Fm. throughout South China, it is unclear to what extent the subdivision into four members can be applied away from the southern limb of the Huangling anticline in the Yangtze Gorges area (Vernhet, 2007; McFadden et al., 2008). The more widely accessible Songlin section nearby Maoshi in Guizhou Province has been described to start with a 5 m-thick cap carbonate followed by 50 m of dark-grey to black shale and siltstone with some very fine-grained sandstone layers within the shales and siltstones and lenticular and nodular carbonates present within the lower half of this interval. The uppermost 30 m are composed of black shale, siltstone, very fine-grained sandstone, muddy silty dolomite and an increasing abundance of chert and phosphatic nodules towards the top (Jiang et al., 2008).

However, in a few sections in the Hubei Province and in numerous sections in the Hunan and Guizhou Provinces, limestone units represent large scale olistoliths interbedded with thick intervals of para- to autochthonous black shales with common gravity-related sedimentary structures (Vernhet et al., 2006; Vernhet, 2007). Furthermore, phosphorite horizons occur within the Doushantuo Fm. in certain limited areas containing the Weng'an and the Miaohe biota (Li, 1986; Steiner, 1994; Ding et al., 1996; Xiao and Knoll, 2000). Although the phosphorite facies can record paleoceanographic and paleoenvironmental changes, a detailed correlation of these phosphorite horizons are questionable and therefore cause problems in determining

exact ages for the Weng'an biota and other phosphorites of the Doushantuo Fm. (Li et al., 1998; Xiao et al., 1998; Zhang et al., 1998; Zhu et al., 2003).

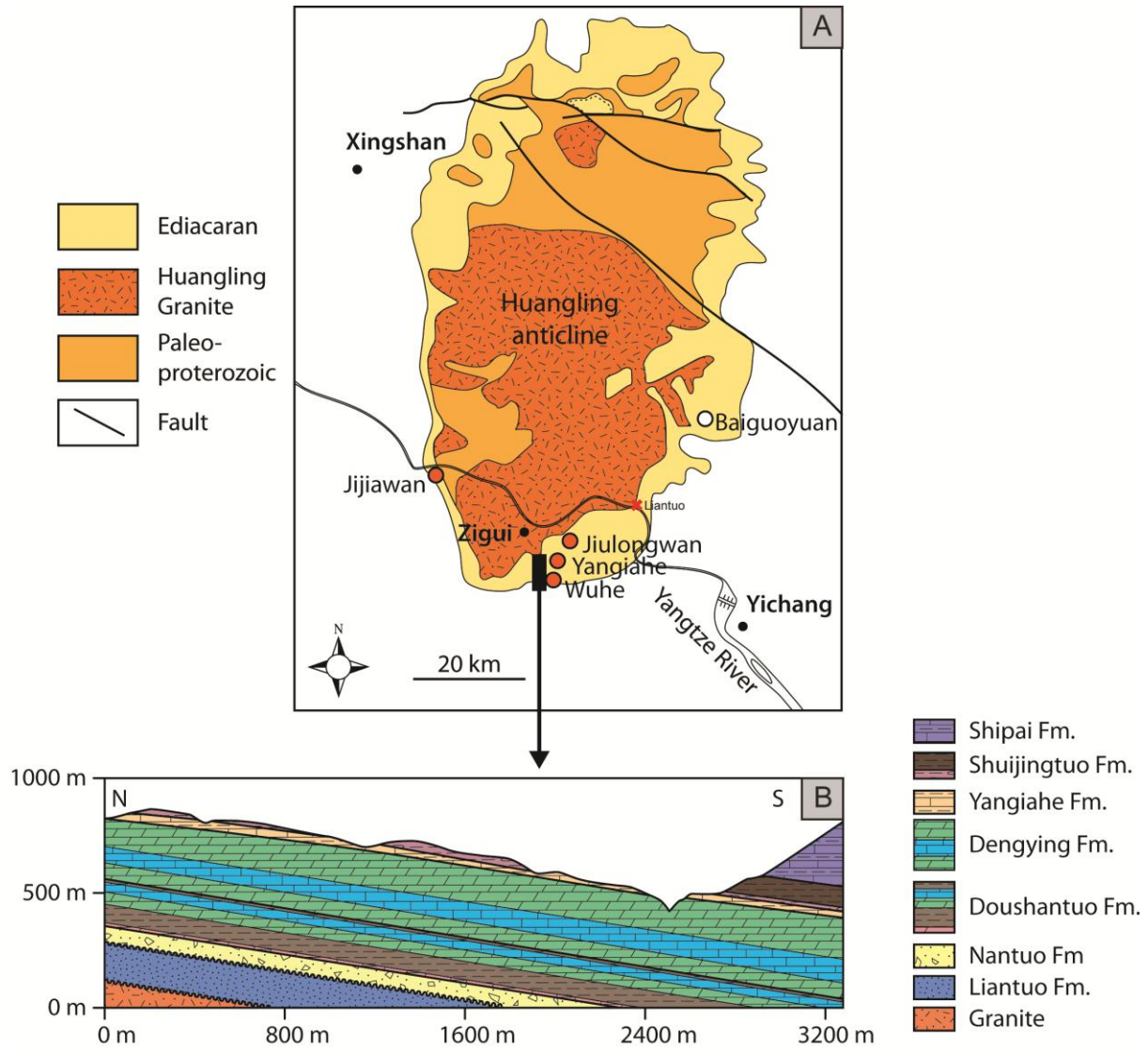


**Figure 3.3: A) A simplified geological map of the Three Gorges Area (modified after McFadden et al., 2008). B) Approximate transsection through the sedimentary succession South of the Huangling Granite (modified after Ishikawa et al., 2008).**

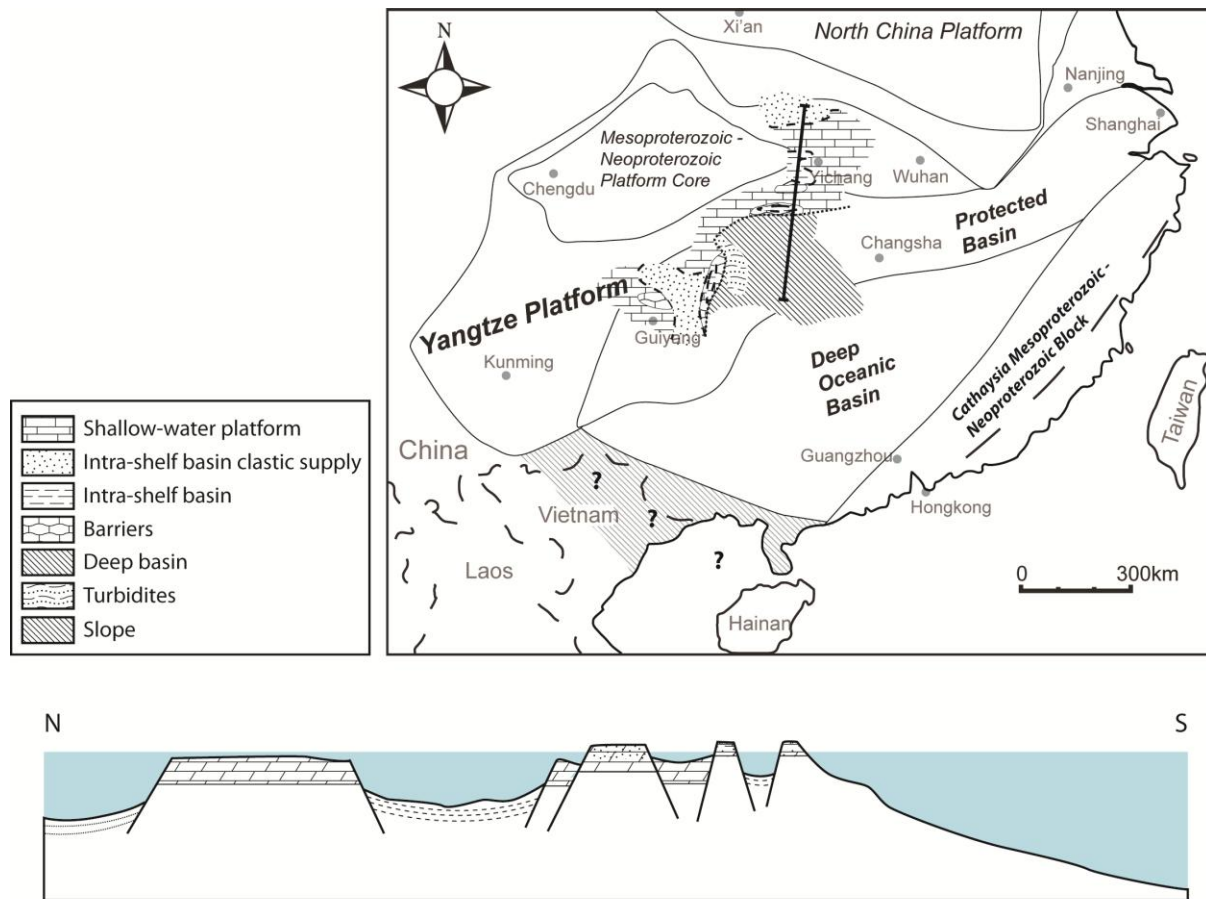


Figure 3.4: The Paleoenvironmental reconstruction of the late Ediacaran platform from Vernhet (2007) is shown on the map with a possible transect across a rimmed carbonate platform as suggested by Jiang et al. (2003b).

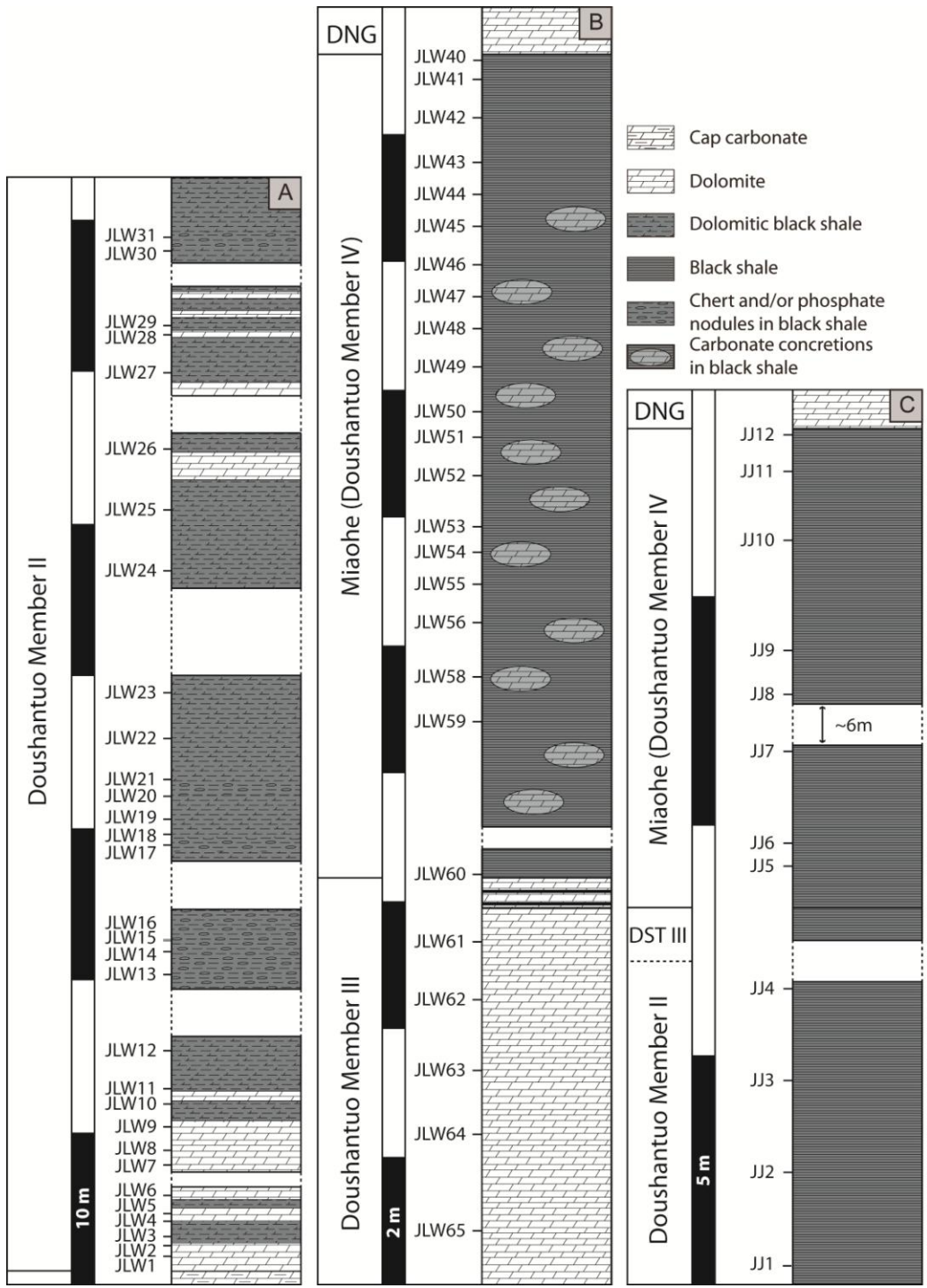
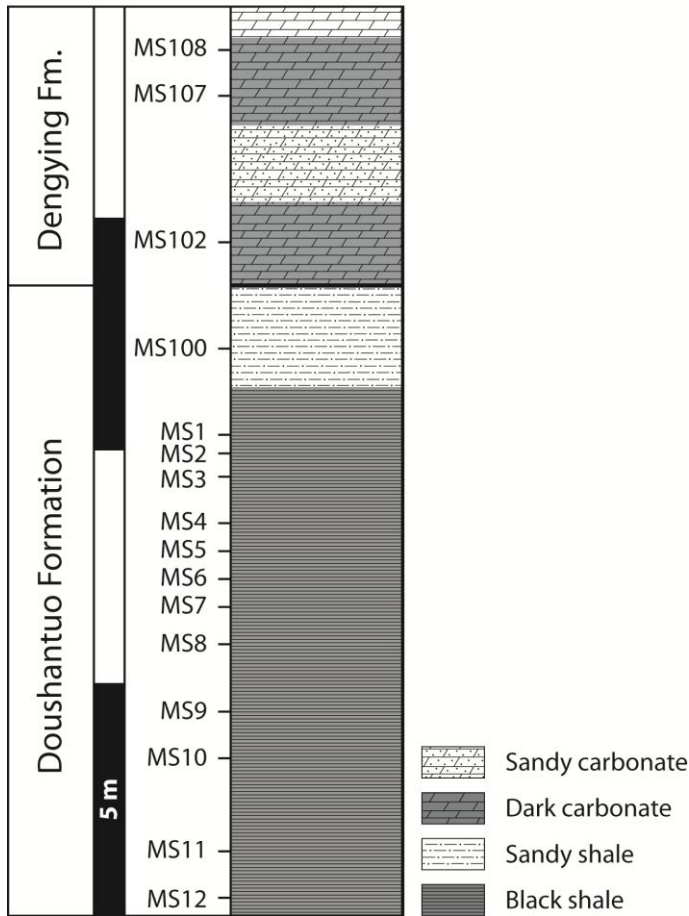


Figure 3.5: A) The Doushantuo member II sampled along a road at Jiulongwan with several parts weathered away from the outcrop. B) The upper Member III and the whole Miaohe Member of the Doushantuo Fm. C) Parts of Member II and the Miaohe Member at the Jijiawan section, the boundary between Member II and III so far not been reported from Three Gorges Area.



**Figure 3.6: The sampled Maoshi section, Guizhou Province, where the boundary between the Doushantuo and Dengying formations are exposed.**

### **3.3.2. The Dengying and Liuchapo formation (ca. 551 – 542 Ma)**

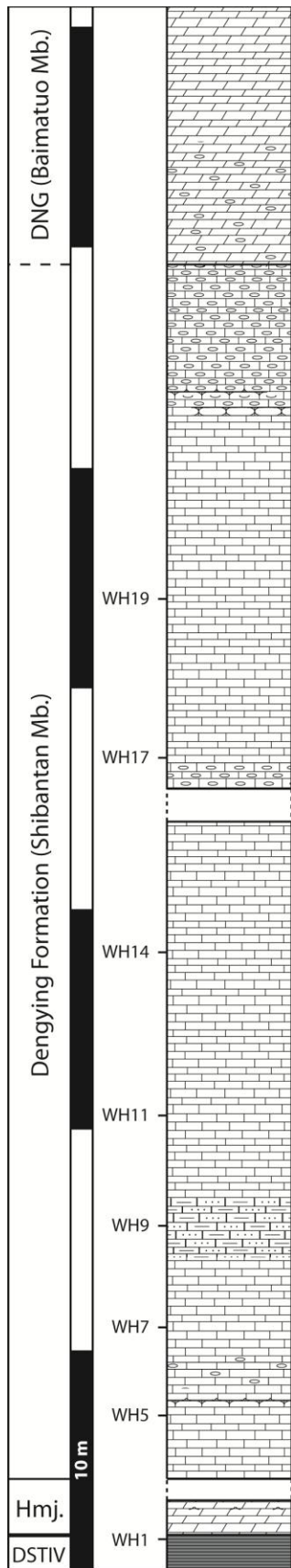
In contrast to the underlying Doushantuo Fm., a relatively short time interval, from 551 to 542 Ma, is represented by the much thicker (ca. 240-850m) Dengying Fm. which can be subdivided into three members based on their respective lithology (Zhao et al., 1988). In the Three Gorges area these are: The Hamajing Member at the base (20-190 m thick) which consists of light-grey, medium- to thick-bedded dolomite with intercalated thin chert layers, the overlying Shibantan Member (100-160m), characterized by dark grey, thin-bedded limestone and on top, the Baimatuo Member (60-570m) which is composed of light-grey, thick-bedded



dolomite. The algal fossil *Vendotaenia antiqua*, the macrofossils *Paracharnia dengyingensis* and *Yangtziramulus zhangji*, possible sponge spicules and *Planolites*-like trace fossils can be found in the Shibantan Member (Sun, 1986; Zhao et al., 1988; Steiner et al., 1993; Shen et al., 2009) while characteristic fossils in the Baimatuo Mb. include the *Cloudina*-like tubular fossil *Sinotubulites baimatuoensis* and several ichnogenera in its lower part (Chen et al., 1981; Zhao et al., 1988). The tripartite subdivision of the Dengying Fm. can be recognized across the platform although a different terminology is sometimes used (Ding et al., 1992; Zhu et al., 2003; Steiner et al., 2007). The following outcrops including the Dengying Fm. have been visited during this study but only little analysis has been carried out due to a general low content of sedimentary organic matter: Zhongnan (see Niutitang Fm.), Maoshi, Xiaotan (see Zhujiaping Fm.), Jiulongwan (see Doushantuo Fm.) and Wuhe. At the Maoshi section, Guizhou Province, the base of the Dengying Fm. is a succession of alternating black carbonates, which get paler up-section, and sandy carbonates (see Fig. 3.6). At the Wuhe section (see Fig. 3.7) in the Three Gorges Area, the base of the Hamajing Mb. consists of wavy beds of massive dolomite with some tee-pee like structures which are probably slump-structures and not genuine tee-pees. The base of the Shibantan Mb. is characterized by thinly bedded limestone followed by a succession of dark, pyrite-rich, macrocrystalline limestone beds, a few intercalated chert layers and chert nodules. The top of the Shibantan Mb. is rich in chert nodules and grades into what is possibly the Baimatuo Mb. with low amplitude wavy bedding of the carbonates.

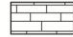



The depositional environment of the Dengying Formation is interpreted as a widespread prograding platform. Oolitic textures and oncolites in the dolomitic Hamajing Member are characteristic of a high-energy environment following the black shale deposition at the top of the Doushantuo Fm., indicating a sea-level drop during the transition from the Doushantuo to the Dengying Fm. Towards the southeast, the carbonate successions becomes gradually condensed, ultimately changing into the slope and basinal facies of the corresponding Liuchapo Formation (see Fig. 5 in Steiner et al., 2007). The Liuchapo Fm. is mainly composed of black silicified shales of which the upper part has been sampled at Huanglian, Guizhou Province, and Longbizui, Hunan Province, both close to the provincial border at about 70 km distance from each other (see Chapter 3.1.3.). Sequence analysis of the Liuchapo Fm. suggests that the lower

and middle part correlate with the Hamajing and Shibantan members of the Dengying Fm., the lower part being deposited during a sea level high stand following the transgressive facies of the Miaohe Mb. of the Doushantuo Fm. and followed by a deepening upwards transgressive succession equivalent to the Shibantan Mb. (Wang et al., 1998). The trace fossils *Planolites* and *Skolithus* and the small shelly fossils *Anabarites trisulcatus*, *Protohertzina*, *Hyolithellus* together with monoplacophorans, gastropods and chancellorides found within the upper part of the Liuchapo Fm. suggests equivalence with the lowermost Cambrian in Yunnan Province (Wang et al., 1998, and references therein) and hence, the possibility that the uppermost Liuchapo Fm. was deposited across the Precambrian – Cambrian boundary.



**Figure 3.7: The sampled succession of the Dengying Formation at Wuhe, Three Gorges Area (left). An impression of the massive cliffs representing the Dengying Fm. in the Three Gorges Area (below).**



-  Limestone
-  Cherty/silty limestone
-  Tee-Pee structure in dolomite
-  Black shale

### **3.4. The Early Cambrian**

The Global Standard Stratotype-section and Point (GSSP) for the base of the Cambrian system is the first appearance datum (FAD) of the trace fossil *Trichophycus pedum* in the Fortune Head section, Newfoundland, Canada (Brasier et al., 1994; Landing, 1994; Babcock and Peng, 2007). However, due to a lack of convincing evidence for the occurrence of the trace fossil *Trichophycus pedum* in Cambrian sediments in South China and convincing absolute age constraints (Compston et al., 1992, 2008; Yang et al., 1996; Jenkins et al., 2002), the Precambrian-Cambrian boundary definition focuses on the biostratigraphy of small shelly fossils (Steiner et al., 2007) and the Meishucun section (Kunyang Mine, near Kunming, Yunnan Province) has been considered as a possible Precambrian-Cambrian boundary stratotype (Cowie, 1985; Luo et al., 1992; Shields et al., 1999) although small shelly fossils (SSF's) may occur stratigraphically below Cambrian-type trace fossils (Lindsay et al., 1996), as is the case in South China.

#### **3.4.1. The Zhujiqing Formation (ca. 542 – 526 Ma)**

The Ediacaran-Cambrian boundary interval in eastern Yunnan, which has traditionally been regarded as a good candidate for the Early Cambrian stratotype (Luo et al., 1982, 1984), can be divided into five intervals (Zhu et al., 2001; Zhu et al., 2003) spanning over three Formations, in ascending order the Zhujiqing Fm., the Shiyantou Fm. and the Yuanshan Fm. The first interval, the Daibu Member at the base of the Zhujiqing Fm., is composed of laminated chert with intercalations of laminated dolomite and black shales and lies between the thick-bedded dolomites of the Dengying Fm. and the first occurrence of SSF's within the overlying phosphorites. No SSF's have so far been recovered from the Daibu Mb. and it is therefore disputed whether it constitutes the base of the Cambrian although this assumption has been made when drawing the following stratigraphic columns. The overlying Zhongyicun Member mainly consists of phosphorite and phosphatised dolomite with abundant SSF's. The dating of an altered bentonite layer within the Zhongyicun Mb. yielded a SHRIMP U-Pb age of

539.4±2.9 Ma (Compston et al., 2008). The Dahai Member is built up by dolomite and limestone and represents the uppermost part of the Zhujiqing Fm. The fourth interval lies between the base of the Shiyantou Fm. and the horizon indicated by the first occurrence of trilobites in the Yuanshan Fm. and the fifth interval (Qiongzhusian) comprises the two earliest trilobite zones as well as the sediments containing the Chengjiang biota (Hou et al., 1991; Babcock et al., 2001).

The outlined successions above can be recognized in several sections in Yunnan and Sichuan Province and represent shallow water platform facies. Despite being devoid of significant successions of black shales, parts of the Zhujiqing Fm. have been sampled in the Deze section (Dahai Mb., see Fig. 3.8), North of Kunming, Yunnan Province.

The mining of phosphorites from the Zhongyicun Mb. around Deze, Yunnan Province, offer an excellent insight into Early Cambrian sediments and especially the Zhujiqing Fm. The uppermost 15m of the Daibu Mb. exhibit chert beds alternating with bedded siltstone. The abundance of bedded chert increases towards the top of the Daibu Mb. before the onset of massive phosphorites of in the Zhongyicun Mb., which have mostly been excavated, leading to a well recognisable marker across the landscape. The sampled base of the Dahai Mb. (ca. 7m), overlying the massive phosphorite beds of the Zhongyicun Mb., is characterized by dolomite beds with abundant phosphate nodules, some thin phosphorite layers and a 30 cm thick shale horizon (see Fig. 3.8).

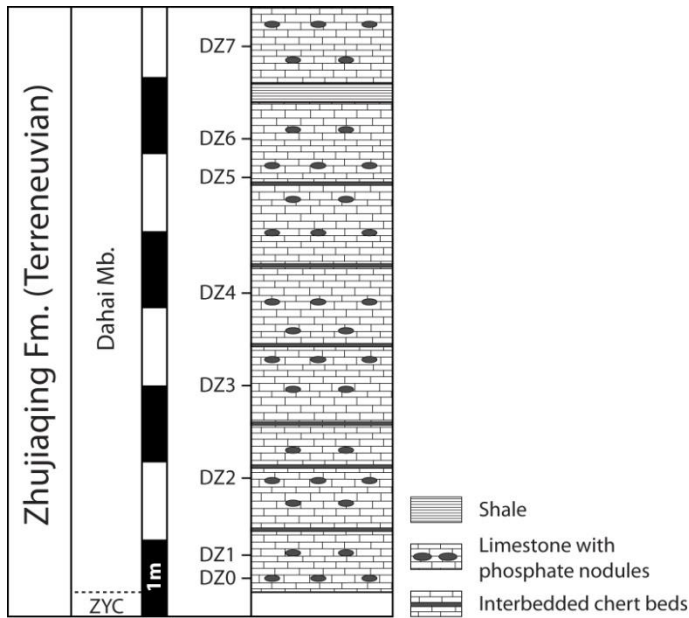


**Figure 3.8: The sampled part from the Dahai Mb. at the Deze section. The boundary between the Zhongyicun and the Dahai members lies within and uncertainty of 1-2 m.**

### 3.4.2. The Niutitang Formation (ca. 542 – 520? Ma)

The Early Cambrian Niutitang Fm. unconformably overlies the Dengying Fm. and its base contains stratiform chert, nodular and bedded phosphates and black shales with a very high organic content of up to 15% (Steiner et al., 2001a) representing a typical transgressive facies. A conspicuous Ni-Mo-sulphide ore horizon is intercalated with black shales in this basal part of the Niutitang Fm. and represents a characteristic feature of many Early Cambrian sections deposited in the transitional zone between the platform and basin (Coveney and Chen, 1991; Lott et al., 1999; Steiner et al., 2001a; Lehmann et al., 2007; Jiang et al., 2006b, 2007b; Wille et al., 2008; Pašava et al., 2008; Chen et al., 2009; Wen and Carignan, 2011). The upper part mainly consists of shales and black shales. The whole Niutitang formation is about 60 m thick and recognized in several sections in Guizhou and Hunan Province. We sampled the base of the Niutitang Fm. at the Zhongnan section, Guizhou Province, where a ca. 1 m-thick phosphorite layer with possibly glauconite in the lower part, represents a typical transgressional facies and sets on right above the Dengying/Niutitang unconformity (see Fig. 3.9)

and is followed by a ca. 20 cm-thick pyrite-rich black shale horizon which indicates the sulphide ore horizon. The overlying strata consist of black shales with very high organic carbon content.

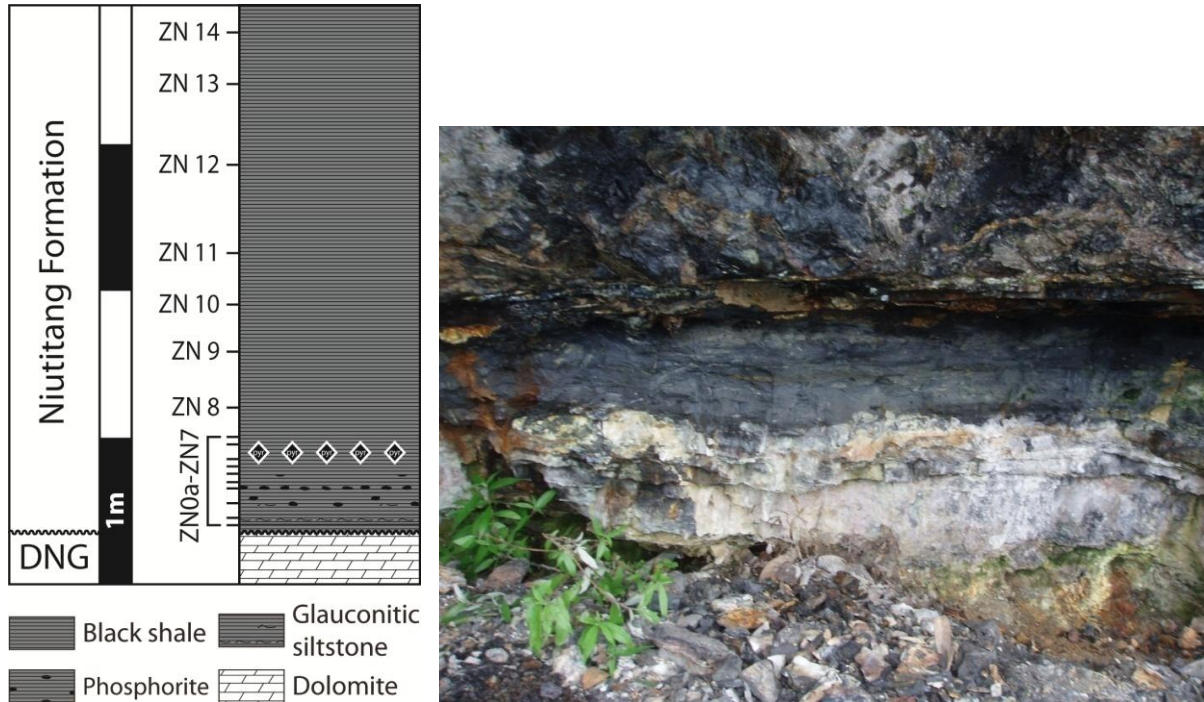


**Figure 3.9: The stratigraphy at Zhongnan where the Niutitang Fm. unconformably overlies the Late Ediacaran Dengying Fm. (left). The photo shows how the Ni-Mo-sulphide ore layer has been mined below the hanging wall of black shales (right).**

### 3.4.3. The Jiumenchong Formation (ca. 542 – 520? Ma)

The Early Cambrian Jiumenchong Formation is about 200m thick and represents slope to basinal sediments overlying the cherty shales and chert beds of the Late Ediacaran Liuchapo Fm. It is composed of black-greyish carbonaceous shale, mudstone and limestone. Bivalved arthropods (*Sunella*) and tubular fossils (*Sphenothallus*) have been reported from within the black shale at the lower part of the Jiumenchong Fm. while trilobites are found within the upper limestone part, including *Hupeidiscus orientalis*, *Sinodiscus changyangensis* and *Metaredlichia* sp. (Yang et al., 2003). The region around Huanglian is rich in outcrops but

stratigraphic control is complicated by tectonic deformation and heavy weathering in some parts. The uppermost 10m of the cherty shales of the Liuchapo Fm. and the first 2m of the overlying, very black shales of the Jiumenchong Fm. have been sampled at Huanglian where, in addition, two samples have been recovered from the Miaohe Mb. of the Doushantuo Fm. (see chapter 3.1.2.). The situation at Longbizui is more straightforward where the stratigraphy from the Sturtian equivalent diamictites up to the Cambrian Jiumenchong Fm. is well exposed. Sampling has been conducted across the Precambrian – Cambrian transition whereby a 1m thick, organic-rich horizon is observed within the cherty shales about 40m below the Liuchapo/Jiumenchong boundary. A succession of more massive, bedded cherts occurs just below the boundary to the Jiumenchong black shales, which continue for at least 40m upwards and include a few horizons rich in macroscopic pyrite crystals (see Fig. 3.10).



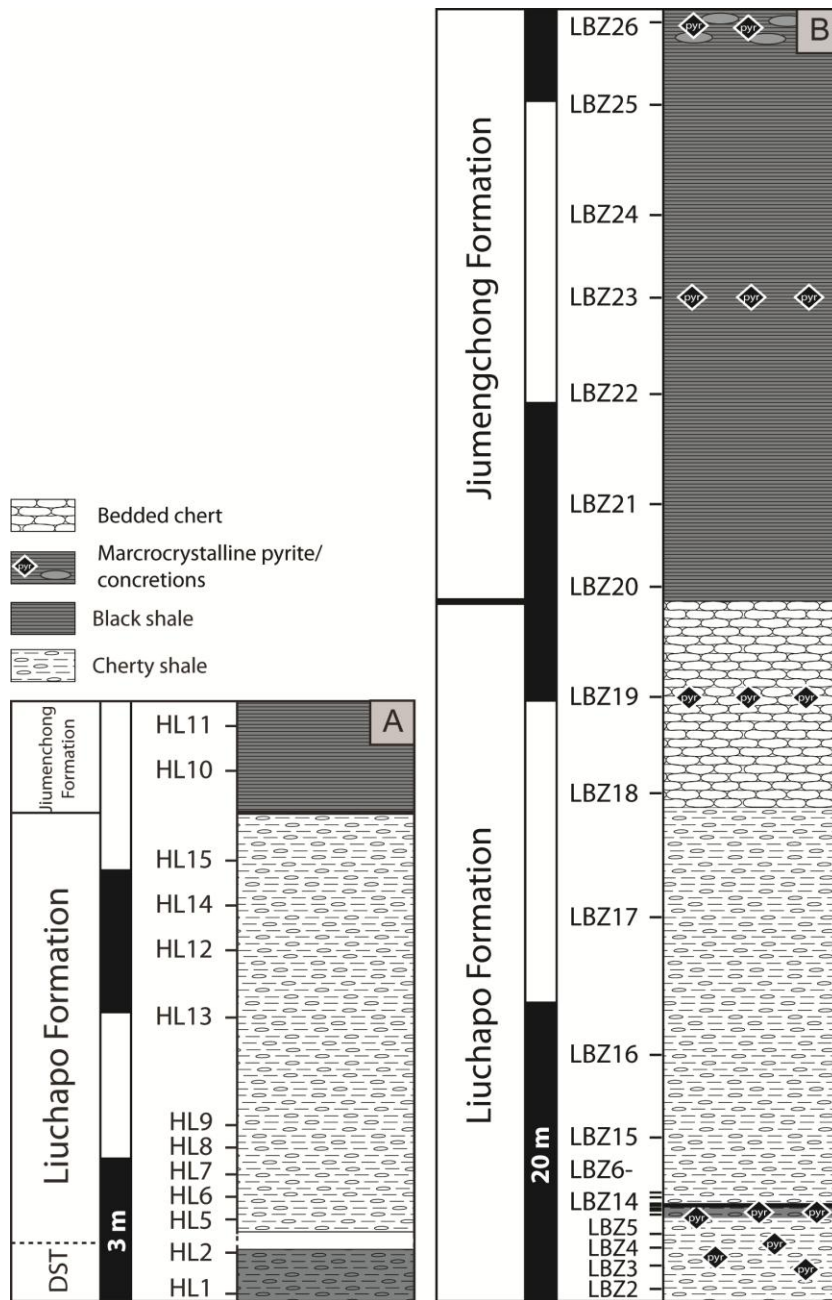


Figure 3.10: The Liuchapo/Jiumengchong boundary sections, equivalent to the Precambrian – Cambrian transition, at Huanglian and Longbizui, Hunan Province.

#### **3.4.4. The Yanjiahe and Shuijingtuo formations (ca. 542 – 521 Ma)**

The Yanjiahe Fm. which covers the base of the Cambrian south of the Huangling anticline in the Three Gorges Area (see Fig. 3.2) overlies pale, massive dolomites of the Dengying Fm. (Baimatuo Mb.) above a sharp, wavy boundary. The Yanjiahe Fm. is about 35 m thick and consists of dolomitic muddy limestone, calcareous black shale and some sandstone and chert (Ishikawa et al., 2008). The above Shuijingtuo Fm. is about 100 m thick and mainly consists of black shale with many prominent carbonate nodules (Ishikawa et al., 2008). Mainly based on carbon isotope stratigraphy it is likely that the upper part of the Yanjiahe Fm. is equivalent to the Dahai Mb. of the Zhujiqing Fm. (Zhou et al., 1997; Ishikawa et al., 2008).

The sampling of the Yanjiahe and Shuijingtuo formations has been conducted at the Wuhe section (see Fig. 3.11a), where the base of the Yanjiahe Fm. is characterized by grey carbonate beds with thin chert intercalations. Abundant phosphatic cherts are observed in the middle part of the Yanjiahe Fm. whereas massive dolomite beds followed by organic-rich black dolomite interbedded with siltstone including regular shaped certified carbonate nodules occur in the upper part before the boundary to the Shuijingtuo Fm. The boundary zone is characterized by a thin (ca. 10 cm) phosphorite bed followed by a conglomeratic layer with ripped-up clasts and framboidal pyrite crystals. The basal Shuijingtuo Fm. consists of black shales with abundant huge dolomite concretions and some intercalated grey massive dolomite beds. At the Jijiawan section (see Fig. 3.11b), sampling began within sandy dolomites of what possibly represents the lower part of the Shuijingtuo Fm. followed by dark-grey carbonates with soft, silty intercalations and then thin-bedded black shales with huge nodules and a few carbonate beds a break in the exposure of the outcrop occurs. About 10m further up in the stratigraphy, brittle black shales with abundant carbonate concretions reappear and characteristic white crystals, presumably barite, occur in between the relatively thin layers. The succession becomes sandier upwards and sandy carbonates appear at the upper tens of meters of the Shuijingtuo Fm. (inaccessible cliffs) before the onset of the greenish-brownish mudstones of the Shipai Fm.

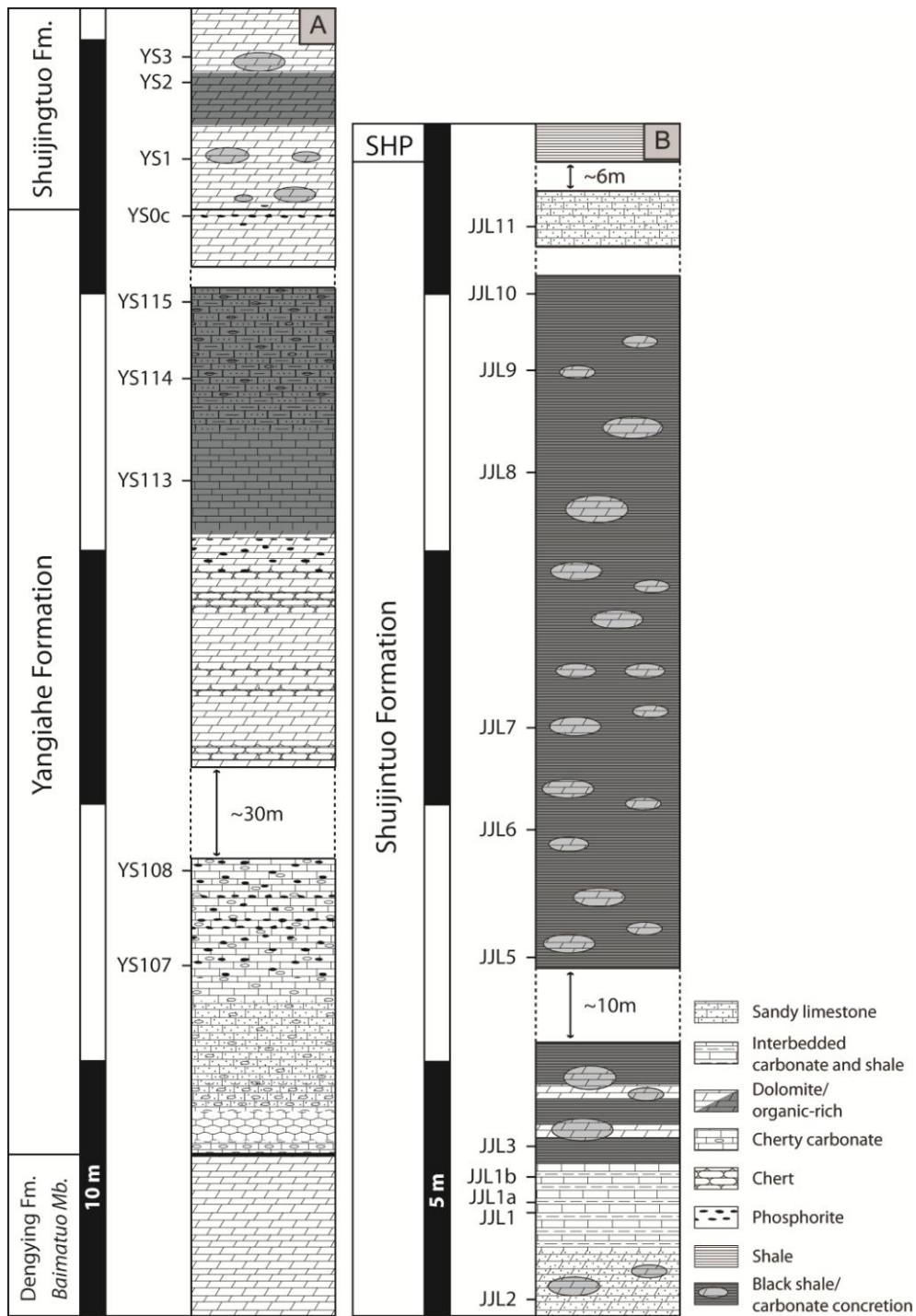


Figure 3.11: A) The Precambrian – Cambrian transition at Wuhe, Hubei Province. B) The Early Cambrian sedimentary successions at Jijiwan, Hubei Province. Not that the Yanjiahe – Shuijingtuo formation boundary is unclear and the sampled succession might be from the Shuijingtuo Fm. only.

### **3.4.5. The Xiaotan section: probably the best Precambrian – Cambrian succession in the world!**

The Xiaotan section, Yunnan Province, is situated along the Jingsha River, one of the major headwater streams of the Yangtze River, and exhibits an unusually complete and expanded stratigraphic column spanning the upper part of the end-Neoproterozoic Dengying Fm. to at least the mid-Cambrian Canglangpu Fm. (see Fig. 3.12). An erosional surface separates the massive grey dolomites of the upper Dengying Fm. from the > 90m thick Daibu Mb., which is characterized by dark siliceous micritic dolomites (at the base), and chert layers and nodules, sandy dolomites and dolomite nodules (at the top). The onset of the ca. 80m thick Zhongyicun Mb. is easily recognizable by dark phosphorite beds which are less pronounced in the middle part of the member, where a U-Pb SHRIMP age of  $539.4 \pm 2.9$  has been reported from Meishucun section (Compston et al., 2008), but reappear in massive beds in the upper part. Furthermore, siliceous dolomites, dolomites, sandy dolomites and shales are common within the Zhongyicun Mb. The overlying Dahai Mb. consists of a lower dolomite and a thicker upper limestone part and is about 70m thick. The base is characterized by a few chert nodules and abundant dolomite nodules before a disturbed, perhaps tectonically induced, zone sets in. The undisturbed upper part is composed of massive carbonate beds reaching individual thicknesses of up to 1m. A characteristic positive  $\delta^{13}\text{C}$  excursion has been observed during the Dahai interval which can additionally be used for correlation across the platform (Zhou et al., 1997; Shen and Schidlowski, 2000; Ishikawa et al., 2008; Li et al., 2009). The contact between the Dahai Mb. and the Shiyantou Fm. is again very sharp, changing from massive carbonates, which are slightly sandy towards the boundary, to the black shales of the Shiyantou Fm. The Shiyantou Fm. overlies the Dahai Mb. after a sharp lithological change from phosphatic carbonates to siliciclastic rocks representing a clearly recognizable boundary throughout the Yangtze platform and probably represents a major tectonic event (Zhu et al., 2003).

Iridium enrichment has been reported from within a metal-enriched layer close to the Dahai/Shiyantou boundary that can be interpreted to represent a maximum flooding surface with minimal sedimentation (Hsü et al., 1985; Wallis, 2006). The base of the Shiyantou Fm.,

recognized in sections in the southwestern part of the Yangtze platform, is characterized by a thin phosphatic conglomerate followed by a thicker clay member indicating a rapid deepening event (Zhu, 1997). The overlying 100-190 m consists of a black shale succession overlain by paler siltstones which possibly represent a shoaling up sequence from suboxic into more oxic conditions (Zhu, 1997). Geochronological analysis of single zircons from a bentonite layer within tuffaceous marl at the base of the Shiyantou Fm. in the Meishucun section, Yunnan Province, yielded a U-Pb SHRIMP age of  $526.5 \pm 1.1$  (Compston et al., 2008). At the Xiaotan section, the base of the Shiyantou Fm. is recognised through a thin, conglomeratic, phosphate-rich layer overlying the sandy carbonates of the Dahai Mb. The following 32m consist of black shales with a few beds of laminated dolomite and dolomite concretions; some of them being septarian concretions, for which the formation mechanism is still unclear (Pratt, 2001). This black shale succession ends with a 0.5m thick layer of sandy siltstone before an 80m thick succession of paler siltstones with diverse coloration from yellowish, brownish, greenish, light grey to grey that transition into a 50m thick succession of fine-grained laminated greenish sandstone with a few visible cross stratifications. The following ca. 20m are characterized by grey calcareous sandstones with abundant siliceous nodules. The overlying 40m of black shale contains some dolomite concretions, a 2.5m thick intercalation of massive dolomite beds in the middle and more abundant dolomite concretions in the upper part. The lower part of this second black shale member contains numerous white 'chips' oriented parallel to the fine lamination. The overlying 40m of alternating greenish-greyish siltstones and dolomite beds with abundant elongated dolomite concretions constitutes the top of the Shiyantou Fm. This similarity to the boundary succession between the Zhujiaying and the Shiyantou Fm. could again indicate a rapid deepening event. A profile of ca. 15m within the lower Shiyantou black shale succession has also been sampled at Meishucun near the Kunyang Mine, Yunnan Province, starting about 5m above a thin, only locally occurring, bentonite layer between the Dahai Mb. and the Shiyantou Fm.

The base of the Yuanshan Fm. consists of a third succession of thin beds of black and dark shales after a thin layer with large, rounded crystalline calcite components in finely laminated black siltstone which represents the Shiyantou/Yuanshan formation boundary ( see

Fig. 3.12). After 27m of these black shales, follows a ca. 50m succession of more massive dark grey calcareous siltstone beds and then a 36m thick member of more massive greenish siltstones. The top 3m of the Yuanshan Fm. are characterized by irregularly laminated brownish-yellowish siltstone with some grey nodules and sandstone lenses just beneath the massive, colourful, cross-stratified sandstones of the Canglangpu Fm.

It has been shown that global sea-levels rose generally throughout the Cambrian in a series of transgression-regression cycles of shorter duration (Miller et al., 2005; Haq and Schutter, 2008) which might correspond to the changes in lithology observed at Xiaotan: notably the three black shale successions interpreted as deepening events.

To our knowledge, no large fossils have been discovered at Xiaotan and the known fossil record is limited to small shelly fossils (SSF's; Li and Xiao, 2004; Steiner et al., 2007). They can be divided into up to four distinct assemblages in the Zhongyicun Member, the Dahai Member and in the upper Shiyantou/lower Yuanshan formations (see also Qian and Bengtson, 1989) where they are succeeded by the earliest record of Chinese trilobites (e.g. Steiner, 2001). Burgess shale-type fossiliferous strata occur within the Yuanshan Fm. near Kunming on the southern Yangtze Platform, and include the extraordinarily well preserved Chengjiang Biota (e.g. Babcock et al., 2001; Hagadorn, 2002), which represent the oldest fossil Lagerstätte of that type (Gaines and Droser, 2010).

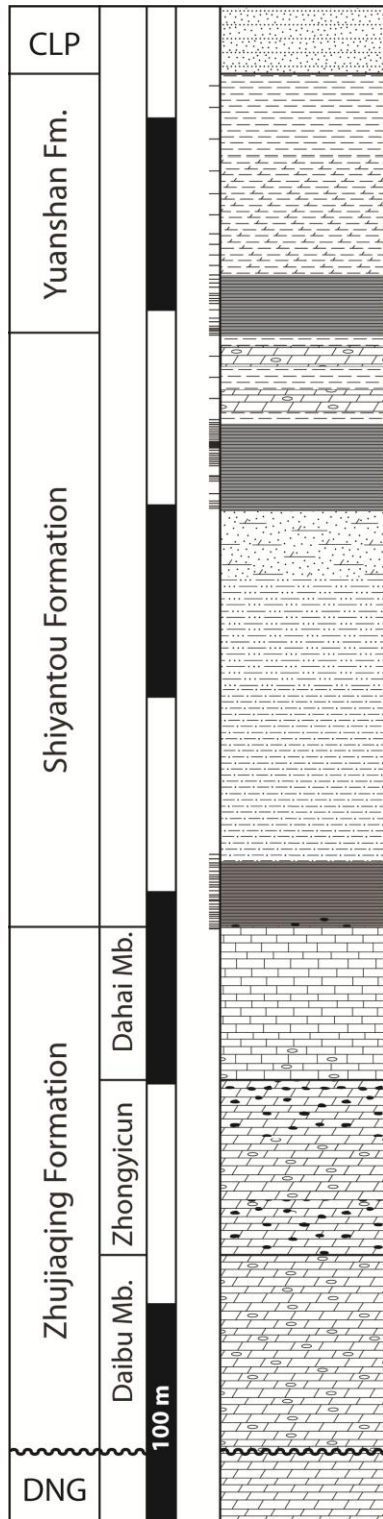


Figure 3.12: A schematic stratigraphic profile as seen at Xiaotan, Sichuan Province (left), reaching from the upper Dengying Fm. (DNG) to the Middle Cambrian Canglangpu Fm. (CLP). The sampled intervals are indicated and more details regarding sampling can be found in chapter 5.3.3. The photo below shows the boundary between the Shiyantou and Yuanshan formations at the Xiaotan section.



## **4. Materials and Methods**

### **4.1. Instrumental analysis**

#### **4.1.1. X-ray fluorescence spectrometry (XRF)**

The basic principle of an XRF spectrometer is to use primary radiation from an X-ray tube to excite secondary (fluorescent) X-ray emission from a particular sample which includes characteristic X-ray peaks related to the corresponding major and trace elements in the sample (see Fig. 4.1; e.g. Fitton, 1997). Because characteristic X-ray peaks are superimposed on a background of radiation from the X-ray tube, the intensity of the background radiation is subtracted from the characteristic peak whereby the net intensity at each of the peak positions is calibrated against known synthetic standards and reference materials. The lower limits of detection for the elements measurable by XRF are given in Fig. 4.2.

The insensitivity of X-rays to chemical bonding and valence effects allows the direct analysis of solid samples avoiding the need for dissolution or other chemical pre-treatment. However, the quantitative analysis and correction of absorption and enhancement effects of a given sample assumes that the sample is homogenous. This means that a sample has to be finely grinded in a way to minimize particle-size effects and was carried out in the present study by milling the bulk rock samples with a tungsten-carbide mill.

For the analysis of trace elements, around 10 mg of sample powder has been pressed into a disc-shaped pellet using ~1 ml of a 20% araldite solution as binding agent. The only way to eliminate particle size effects completely is to homogenize the sample by fusion. However, as the added flux dilutes the sample, enhancing X-ray background levels and reducing the net intensity of the fluorescent radiation, this procedure is only applied for major elements.

The procedure starts with drying about 3 g of sample powder overnight at 110°C in a glass bottle. 0.7 g of the powder is then accurately weighed into platinum crucibles and ignited at 1100°C for about 20 min covered by lids. The remaining sample is then weighed again to calculate the volatile-free sample weight. 6 times the sample weight of flux is then added (Alfa-



Aesar Spectroflux 105: Li-tetraborate, Li-carbonate and La-oxide), plus about 0.02 g extra to account for volatiles in the flux, and fused at 1100°C. Usually the flux loss on ignition exceeds the extra weight added and the weight has to be made up by adding more flux in order to approach the weight of the sample and 6 times its weight during flux fusion as closely as possible. Following that, the mixture is again fused with Meker burners and the liquid is casted into round, flat beads, labelled and introduced into the XRF.

Major and trace element concentrations in the black shale samples from the Zhongnan, Xiaotan (XT1-29), Meishucun, Huanglian, Changxingpo and Maoshi sections have been measured using a Philips PW2400 X-ray fluorescence spectrometer at the Royal Holloway University of London. Based on multiple measurements of 6 black shale samples, the precision lies within 4% for major elements and 10% for minor elements whereby the inaccuracy is highest in samples with small trace-element contents.

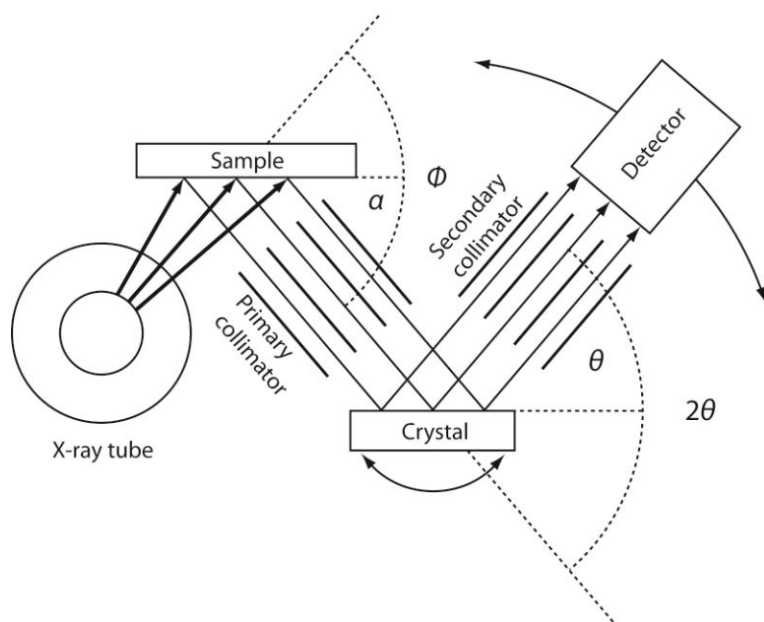


**Figure 4.1: Schematic depiction of a typical XRF spectrometer. Thick lines with arrows indicate primary X-ray radiation from an X-ray tube which ionizes the sample by displacing electrons from its component atoms which in turns causes an electron from an outer shell to fill the vacancy ultimately leading to the emission of secondary (fluorescent) X-ray photons with characteristic energy and wavelength parameters of the atom. This photon will either be absorbed within the atom (especially**

when this atom is small) or escape and form part of the characteristic spectrum. The resulting small proportion of the generated secondary X-rays is then collimated to form a parallel beam which is diffracted by a synthetic analyzing crystal and then collimated again before passing to an X-ray detector. The crystal can rotate around an axis on its surface while the secondary collimator and the detector are coupled to the crystal so that they move in an arc around the rotation axis of the crystal by twice its angular rate of rotation to keep the angle of incidence equal to the angle of reflection ( $\theta$ ). The Bragg equation relates the angle  $\theta$  to wavelength  $\lambda$ :  $n\lambda = 2d \sin\theta$ , whereby  $n$  is an integer and  $d$  the lattice spacing of the crystal. After Fitton (1997).

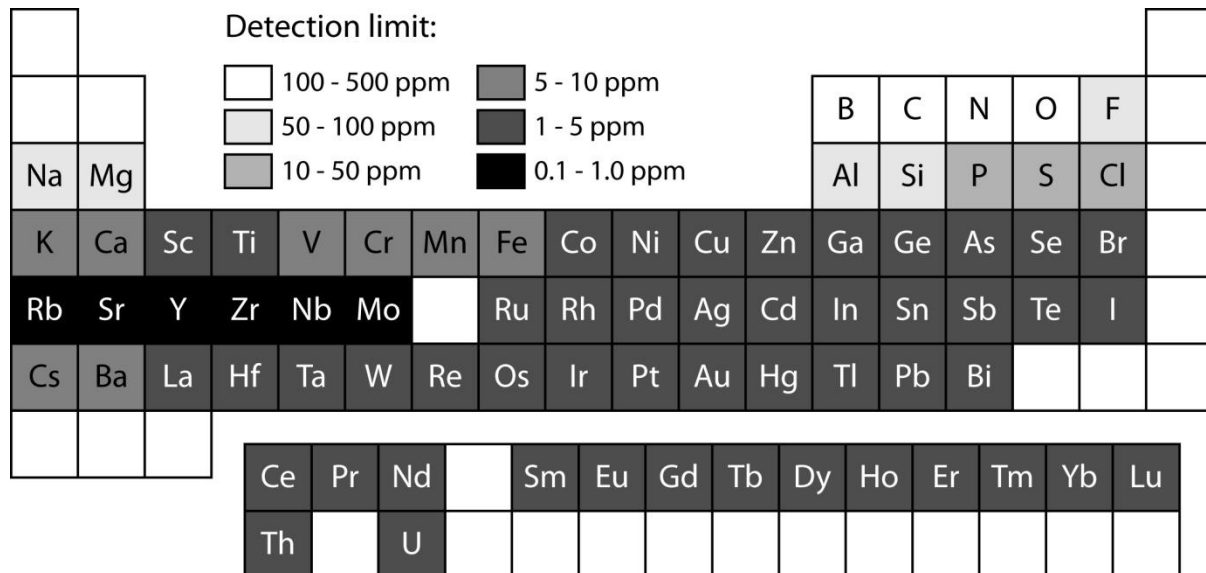


Figure 4.2: Periodic table illustrating the elements which can be determined in geological material using X-ray fluorescence spectrometry and approximate detection limits (Fitton, 1997).

#### 4.1.2. Inductively coupled plasma mass spectrometry (ICP-MS)

This multi-element technique consists of positive ions generated in inductively coupled plasma which are extracted, via a differentially pumped air-vacuum interface, to a low-resolution mass spectrometer (Jarvis, 1997). The sample is usually dissolved and diluted before being introduced and converted by a nebulizer into an aerosol which is then converted into

large droplets by a nebulizer before attaining the plasma torch. The sample aerosol is then rapidly volatilized, dissociated and ionised. The ions are extracted by a decrease in pressure and focussed using a set of lenses before entering the mass spectrometer, usually a quadrupole. The ions are then separated on the basis of their mass to charge ratio and a detector receives an ion signal proportional to their concentration. While the relatively low mass resolution of a quadrupole mass analyser is sufficient to separate adjacent elemental mass numbers, interferences from polyatomic ions might cause a problem. This particularly applies to vanadium and arsenic in the presence of chloride. Further problems might arise through refractory oxide ions where the elements with the highest oxide bond strength, including Al, Ba, Mo, P, REE, Si, Ti and Zr, yield the most oxide ions although rarely develop oxide abundances exceeding 1.5% (see Jarvis (1997) for a more detailed description of possible interferences).

Trace element concentrations of samples from the Xiaotan (XTY1-61 and XTS1-14), Deze, Jiulongwan, Jijiawan and Wuhe sections have been measured using the solutions obtained by the total iron dissolutions (1000× dilution) carried out at Newcastle University (see chapter 4.2). These have been evaporated in order to remove the HCl and then redissolved using nitric acid. The final solution, containing 0.15ml HNO<sub>3</sub>, 0.1ml 500 ppb Rh for instrument calibration and 3.75ml H<sub>2</sub>O, was analysed by Heizhen Wei from the State Key Laboratory for Mineral Deposits Research, Nanjing University, using a Finnigan Element II ICP-MS. The precisions are generally better than 5% for the analysed elements based on long-term uncertainty of the lab measurement on standard carbonate.

However, the major source of inaccuracies is sample preparation which has to be carried out with great care to avoid contamination and incomplete dissolution of the sample. Apart from that, the precision of the ICP-MS is high for most of the elements measurable (see Fig. 4.3).

		Detection limit:																
		Li	Be															
		Na	Mg									B						
												Al	Si	P	S	Cl		
		K	Ca	Sc	Ti	V	Cr	Mn	Fe	Co	Ni	Cu	Zn	Ga	Ge	As	Se	Br
		Rb	Sr	Y	Zr	Nb	Mo		Ru	Rh	Pd	Ag	Cd	In	Sn	Sb	Te	I
		Cs	Ba	La	Hf	Ta	W	Re	Os	Ir	Pt	Au	Hg	Tl	Pb	Bi		

**Figure 4.3: Elemental limits of detection when using an ICP-MS (after Jarvis, 1997).**

#### 4.1.3. Laser Ablation ICP-MS (LA-ICP-MS)

A continuous piece rock of about a meter length has been recovered from the top of the Doushantuo Member IV (Miaohe) at the Jiulongwan section for high resolution Laser Ablation ICP-MS analysis in order to record fine changes in the geochemistry of this laminated black shale. After transport, the brittle black shales fell apart but the original position could still be identified and seven blocks with a surface width of 2.5cm and a height of 5cm have been sawn out (see Fig. 4.4a) and scanned perpendicular to the lamination by laser ablation (Resonetics RESOLUTION M-50). A custom-build excimer (193 nm) laser-ablation system with two-volume laser-ablation cell coupled to a quadrupole ICP-MS (see Fig. 4.4b; Müller et al., 2008) has been used at the Royal Holloway University of London under the guidance of Christina Manning and Wolfgang Müller. The spot size of the laser has been set to a diameter of 96 μm which ablated the rock material at a speed of 50 μm/s. The sample aerosol is then flushed out by He and led into the ICP-MS (Agilent 4500 Series) for which the procedure has been broadly outlined in chapter 4.1.2. Together with the sample, an industry standard (NIST 610) is fixed to the sample holder for reference. The output looks like in figure 4.5, where background radiation is

measured before and after the measurement of the standard, followed by the sample analysis and again before and after the second standard measurement.

The raw data can be divided in baseline, standard and sample measurement and processed by hand or by using imaging software (Woodhead et al., 2007). For the current study, the dataset has been processed by first subtracting the average background signal (baseline) from the standard and sample values of each element analysed (see appendix). The corrected standard and sample values are then normalized to previously defined silicon concentrations. In the case of the present study, SiO<sub>2</sub> concentrations of about 70% have been assumed based on XRF measurements of similar lithologies from equivalent stratigraphic levels but elsewhere on the Yangtze Platform. Because element concentrations in our standard are known, the whole dataset can be adjusted to semi-quantitative element concentrations in each of our black shale samples. But because it is very unlikely that Si concentrations are constant throughout the sample especially not at such high resolution, the results must be treated with caution. In order to estimate possible miscalculations due to inhomogeneous distribution of Si within the sample, element mapping has been carried out on a Jeol JXA-8100 electron probe microanalyzer at the UCL under the guidance of Andy Beard. Prior to analysis, thin sections of the same sample surface have been produced, finally polished and coated with pure carbon. The analysed surface measured 900\*900µm with a resolution of 1µm (see Fig. 4.6).

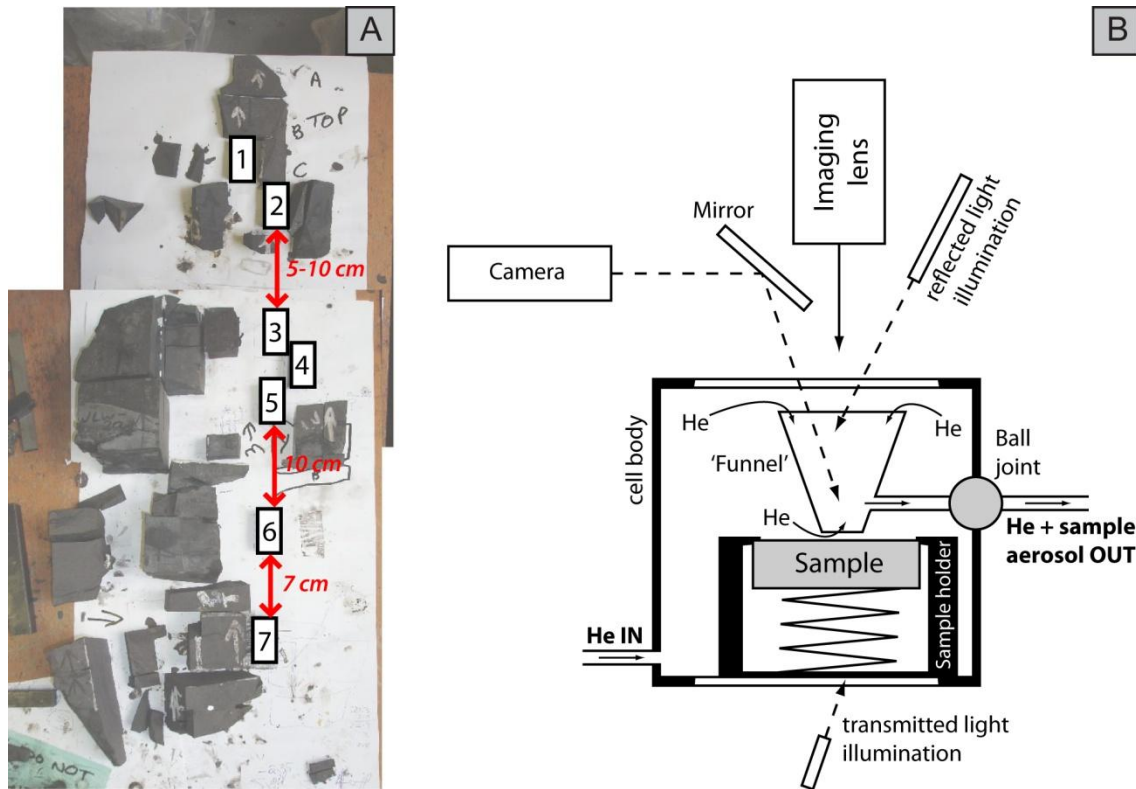


**Figure 4.4: A) The continuous but scattered black shale interval from the top of the Miaohé Mb. (see chapter 3.1.2.) with the indicated positions of the 7 sample blocks. B) Highly schematic cross section of the Laurin two-volume laser-ablation cell (not to scale). Helium (He) enters the cell body at its bottom, and flows from both bottom and top through the funnel, where the He flow entrains the aerosol that condensed out from the laser-induced plasma. The funnel-shaped upper cell and the tilted reflected light illumination improve the off-axis viewing system. Sample aerosol and He leave the LA cell for the ICP-MS via an exit tube connected to the cell body via a ball joint (Müller et al., 2008).**

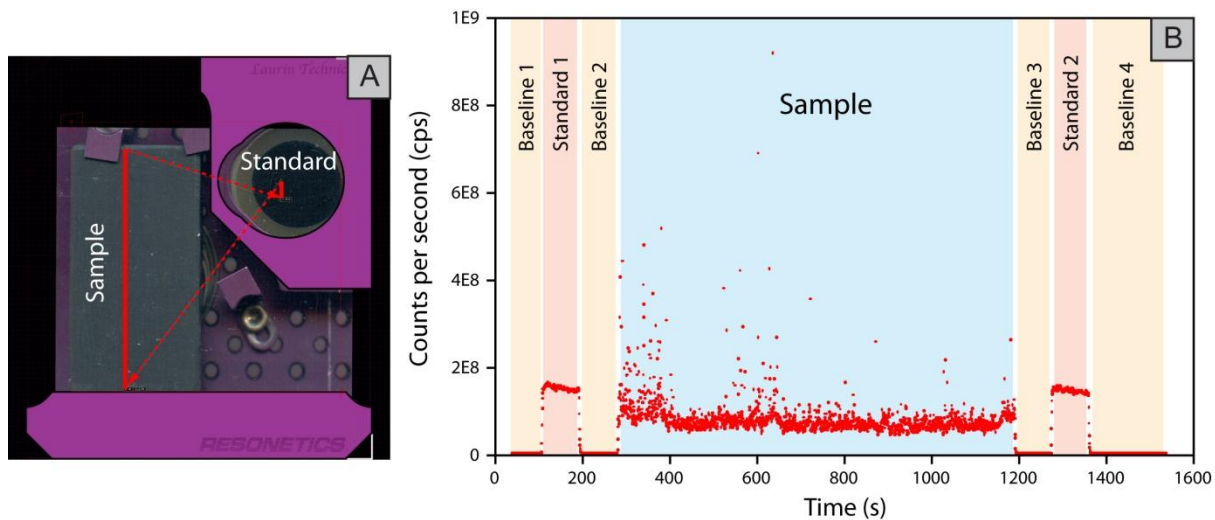


Figure 4.5: A) Shows the sample holder with the sample block and standard from above. The solid red lines indicate the laser ablation tracks. B) Output of the unprocessed data showing the total signal intensity (CPS) as the laser moves through the procedure.

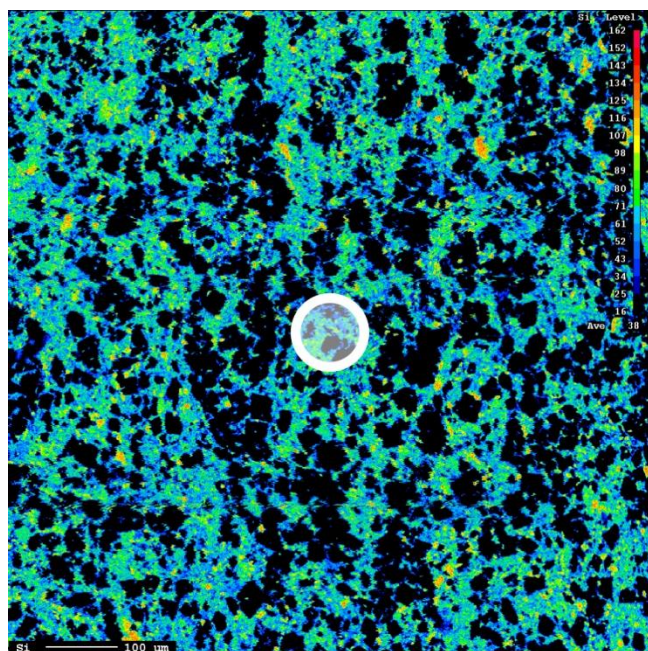


Figure 4.6: A 900x900µm element map for Si carried out by an electron probe microanalyser (Jeol JXA-8100) on a black shale sample. The size of the laser beam is projected in the middle of the map and illustrates the inhomogeneities possibly leading to inconsistencies when normalizing the LA-ICP-MS signal to a single element concentration for sedimentary rocks.

## 4.2. A comparison between XRF and ICP-MS analytical results

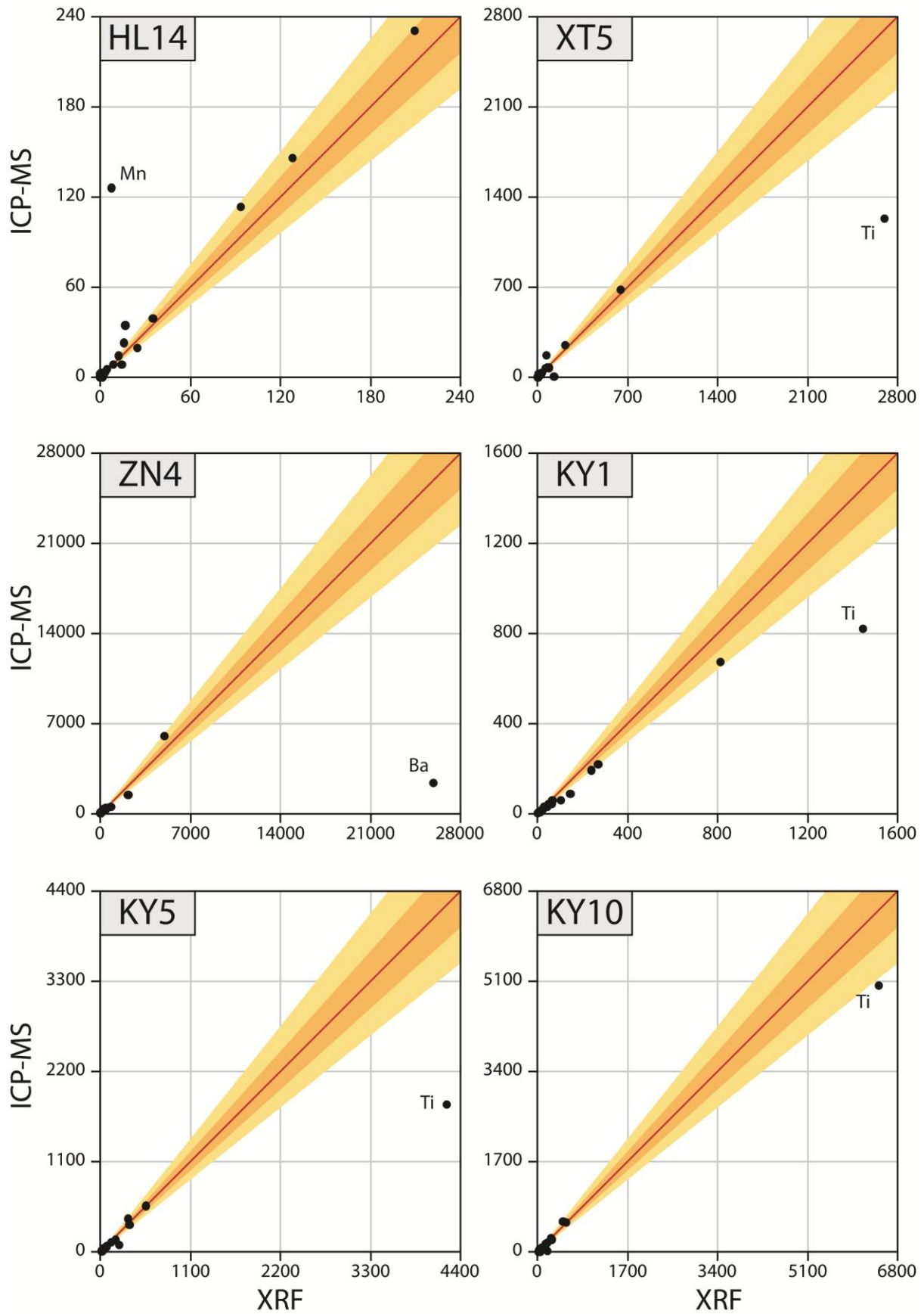
10 samples from different sections and geochemical compositions have been measured with both the XRF and ICP-MS techniques and although the same powders have been used, some disparity can be expected due to the different sample preparation. This particularly applies for a couple of elements which are present in barely soluble mineral phases and hence difficult to measure using ICP-MS analysis, such as barium in barite and titanium in certain silicate minerals. The samples measured by both methods and the respective results can be found in the appendix while correlation patterns are shown in figures 4.7 and 4.8.

We see that there is no clear trend showing that either method over- or underestimates element concentrations in a consistent way. Sc varies significantly between XRF and ICP-MS measurements whereby the relatively low concentrations in HL14 are more than 95% higher when measured with ICP-MS. Higher concentrations exhibit less disparity but show higher XRF values in all CXP samples and KY1 of up to 38.6%. Low Ti values in HL14 are slightly overestimated by the ICP-MS but apart from that are consistently higher, up to over 57% for KY5, when measured with the XRF, indicating Ti concentrations in HL14 below detection limit and barely soluble Ti phases when abundant. V and Cr concentrations generally agree well between both methods, remaining within 20% difference except for KY1 and CXP10 (see Fig. 4.7). Mn shows huge discrepancies where the concentration is low in HL14 and XT5 but generally remains within  $\pm 20\%$  difference in the other samples with higher Mn content. Ni varies similarly, except for CXP13 where the XRF method yields an almost 35% higher concentration. Cu is mostly underestimated by the ICP-MS, mostly in ZN4 (41% less) and CXP 13 (51% less) with respect to XRF analysis. Element concentrations in ZN samples show more than double the concentration when measured with the ICP-MS in the case of XRF values less than 20 ppm but are generally underestimated with regard to XRF measurements when higher concentrations are found (up to 39.3% in ZN4). Ga, Rb, Sr and Y generally vary significantly within  $\pm 50\%$  while Zr is consistently grossly underestimated by 40 to 100% when measured by ICP-MS due to highly insoluble Zr phases. Nb as well varies a lot being mostly underestimated by the ICP-MS. Mo is often only present in trace amounts and therefore particularly prone to



varying outcomes depending on the measurement method applied but except for KY1 and CXP10 remains within 30% difference (see Fig. Fig. 4.7). Ba concentrations mostly agree well within 20 to 30% except for the very high concentration in ZN4 where the ICP-MS measurement is ten times lower than the XRF value. The Rare Earth Elements La, Ce and Nd generally agree well and discrepancies of over 30% are only found where concentrations are low, such as in HL14 and XT5. Pb and Th exhibit significant variations as well and Th in particular is extremely underestimated in the CXP samples analysed by ICP-MS.

However, although we often found different results for elements concentrations depending on the method used, a good correlation between XRF and ICP-MS for each sample can generally be expected as demonstrated in figure 4.7. Mo concentrations do exhibit significantly different results when both analytical methods are compared, exceeding 50% in some samples but V concentrations agree reasonably well with each other (see Fig. 4.8), which might be due to the usually much lower Mo contents compared to V and hence, a greater affinity to inaccuracies due to sample preparation and contamination.



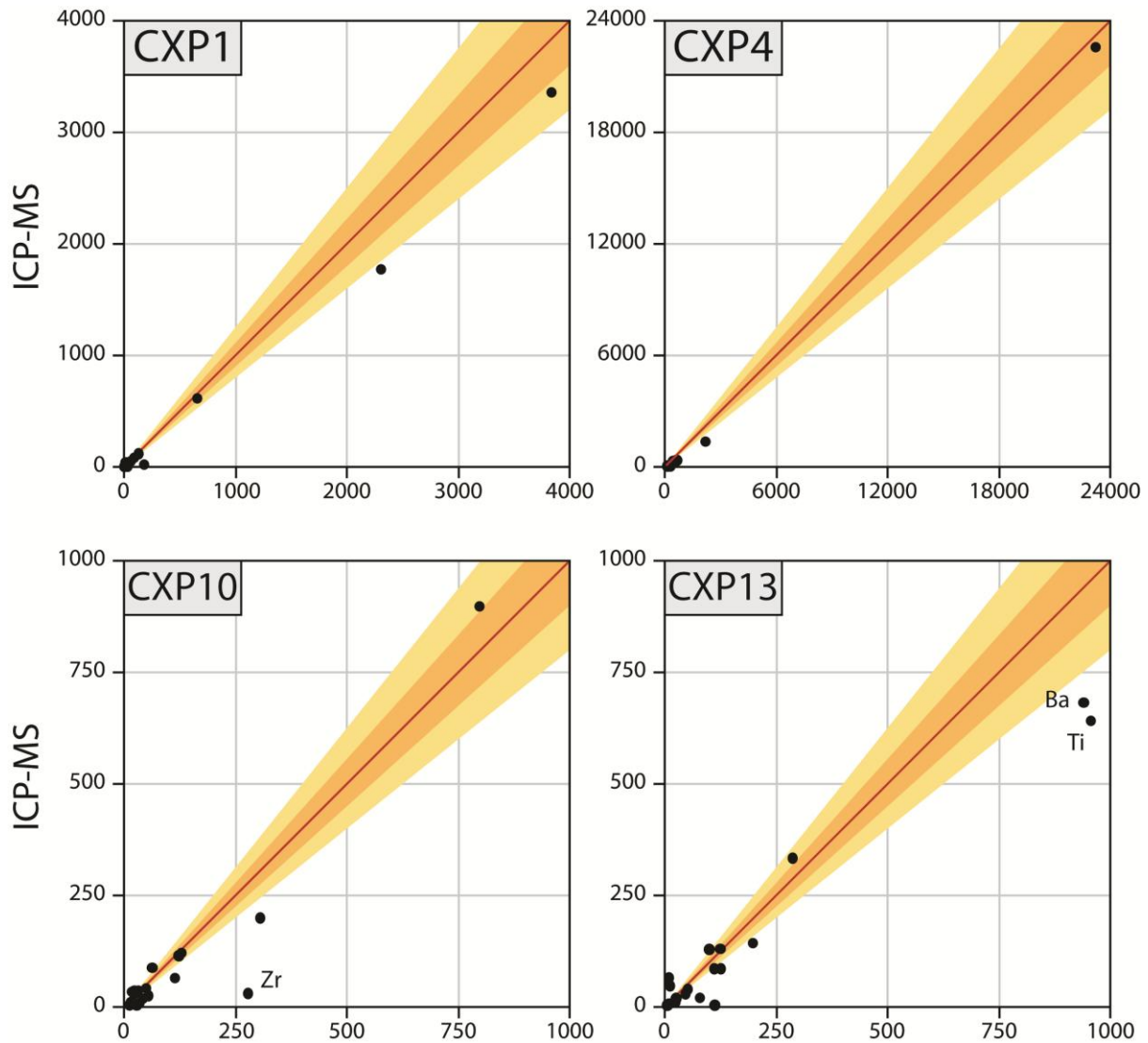
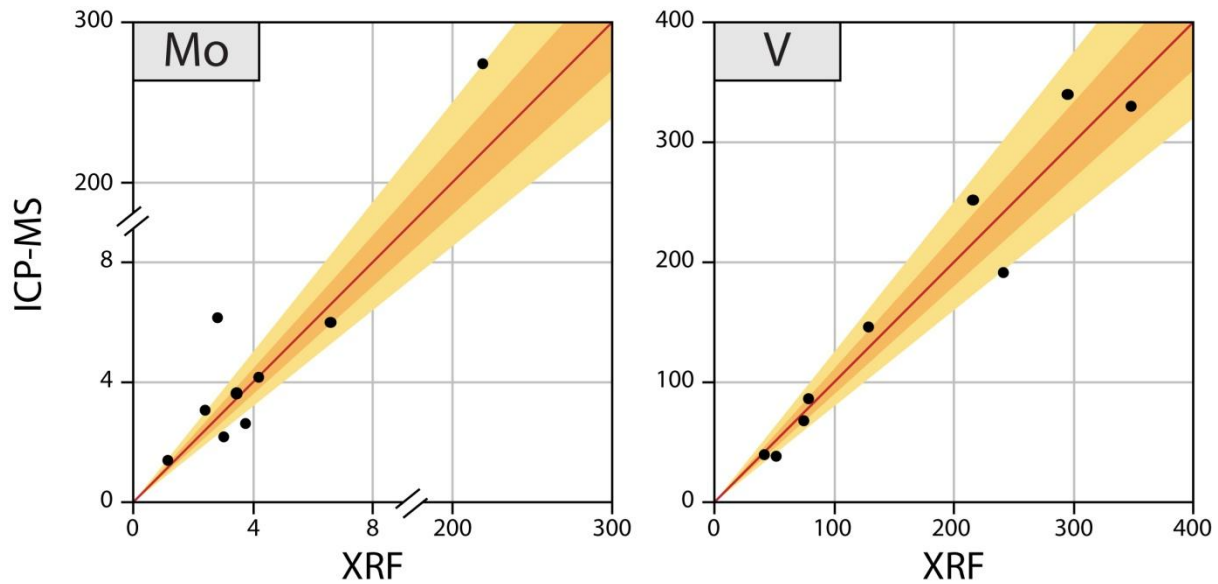


Figure 4.7: Covariation patterns of element concentrations obtained by both, XRF and ICP-MS measurements. The orange beam represents 10% and the yellow beam 20% deviation. Note that the fundamentally different sample preparation method for the respective analytical technique may lead to significant differences for some elements in some samples largely depending on the lithology in particular for Ti which is often strongly underestimated by ICP-MS analysis due to its incorporation into insoluble siliciclastic components, and Ba due to difficultly soluble barite crystals.



**Figure 4.8: Covariation patterns for Mo and V analysed by XRF and ICP-MS. The orange beam represents 10% and the yellow beam 20% deviation. Note that low Mo concentrations might be prone to inaccuracies of up to 50% and more. Obtained V concentrations agree reasonably well and differences remain mostly within 20% without a consistent trend.**

### 4.3. Iron speciation analysis

#### 4.3.1. The procedure

The sequential extraction procedure for iron recognizes seven operationally derived iron pools (see chapter 2.3; Poulton and Canfield, 2005): (1) carbonate associated Fe ( $Fe_{carb}$ ), including siderite and ankerite; (2) easily reducible oxides ( $Fe_{ox1}$ ), including ferrihydrite and lepidocrocite; (3) reducible oxides ( $Fe_{ox2}$ ), including goethite, hematite and akaganéite; (4) magnetite ( $Fe_{mag}$ ); (5) poorly reactive sheet silicate Fe ( $Fe_{PRS}$ ); (6) pyrite Fe ( $Fe_{py}$ ); and (7) unreactive silicate Fe ( $Fe_U$ ). The highly reactive portion of the iron pool includes  $Fe_{carb}$ ,  $Fe_{ox}$ ,  $Fe_{mag}$  and  $Fe_{py}$  which, except for  $Fe_{py}$ , were sequentially extracted according to the methods outlined by Poulton and Canfield, 2005 whereby  $Fe_{ox1}$  and  $Fe_{ox2}$  ( $\rightarrow Fe_{ox}$ ) were extracted together, as a differentiation of these two iron pools is not necessary for our purpose. The

sequential extraction was carried out using one unit of each powdered sample ranging from 50 to 100mg.  $Fe_{carb}$  was extracted from the sediment by adding 10ml of 1M sodium acetate adjusted to pH 4.5 by using acetic acid into the test tube which is then shaken for 48h at 50°C. The resulting solution was carefully removed from the test tube and diluted 20 times in water. For extracting  $Fe_{ox}$ , a sodium dithionite solution ( $50g\ l^{-1}$ ) buffered to pH 4.8 with 0.35M acetic acid and 0.2M sodium citrate (Mehra and Jackson, 1960; Lord III, 1980) has been prepared and used immediately after preparation in order to prevent the solution from oxidizing. 10ml of the solution was then poured into the test tube and then shaken for two hours at room temperature before being diluted 20 times.  $Fe_{mag}$  in the remaining sediment was extracted by adding 10ml of a 0.2M ammonium oxalate and 0.17M oxalic acid solution (pH 3.2; McKeague and Day, 1966; Phillips and Lovley, 1987), the resulting solution being diluted in the same way as for the  $Fe_{carb}$  and  $Fe_{ox2}$  extraction.

The extraction of pyrite Fe ( $Fe_{py}$ ) has been done separately by weighting about 4g of sample powder (depending on the broadly estimated pyrite content). The equipment for the sulphide extraction consisted of an array of six round glass flasks on hot plates whereby the flasks have three apertures one for introducing the sample powder, one for the influx of an inert gas ( $N_2$ ) and one leading into a condensating unit which ends into a plastic tube with a pipette in a test tube. During the procedure, two Fe sulphide phases have to be taken into consideration: acid volatile sulphide (AVS) and chromium reducible sulphide (CRS). AVS is rare in ancient sediments and basically corresponds to the FeS content, a precursor of  $FeS_2$ . The eventual occurrence of AVS was detected by heating up the sample after adding a 50% HCl solution (Cornwell and Morse, 1987), the resulting  $H_2S$  gas is then led, supported by a flow of  $N_2$  gas, into a water filled test tube with added silver nitrate (usually 0.25ml of  $170g\ l^{-1}$  silver nitrate) which results in the precipitation of  $Ag_2S$  which is then collected. The extraction of AVS lasts about 1 hour but is usually aborted if nothing is present after 15 minutes. The subsequent extraction of CRS is attained by adding chromous chloride ( $CrCl_2$ ,  $533g\ l^{-1}$ , Canfield et al., 1986) to the sediment and boiling it for one hour. The escaping  $H_2S$  gas resulting from the dissolution of  $FeS_2$  was then again precipitated as  $Ag_2S$  in the test tube with silver nitrate which would have been replaced if the previous extraction with HCl yielded a significant amount of AVS. The

collected  $\text{Ag}_2\text{S}$  precipitates were then carefully filtered and dried before being weighted and the corresponding concentration of  $\text{FeS}_2$  originally contained in the samples can be calculated. It must be considered that a slight loss of sulphide can occur using this method, especially in sulphide poor samples. Repeated pyrite extraction of 6 black shale samples showed a precision of about 30% whereby the inaccuracy inversely scaled to the pyrite content.

In order to evaluate the total iron concentration ( $\text{Fe}_T$ ), the sample powder has to be completely dissolved. At first, a sample amount ranging between 100 and 200mg has been weighed into porcelain beakers and ashed overnight at  $550^\circ\text{C}$  in order to oxidize organic matter and sulphides. 5ml of nitric acid was then added to the ashed powder followed by 2ml hydrofluoric acid (HF) and a few drops of  $\text{HClO}_4$ . The mixture was dried (normally overnight) on a hot plate at  $130^\circ\text{C}$ . Then, 2.5ml boric acid ( $50\text{g l}^{-1}$ ) were added and dried up again. The remains of each sample were then again dissolved in 5ml of 50% HCl and heated on a hotplate until total dissolution occurred. The resulting solution was diluted by first filling it up to 100ml with water and second by taking 0.1ml of this solution and diluting it into 4.9ml of water, resulting in a volume of 5l for every powdered sample.

The concentrations of  $\text{Fe}_{\text{carb}}$ ,  $\text{Fe}_{\text{ox}}$ ,  $\text{Fe}_{\text{mag}}$  and  $\text{Fe}_T$  in the prepared solutions were measured using an atomic absorption spectrometer (AAS) and calculated back to the original concentration in the respective samples. The analytical precision after the sequential extraction is high with 2% for  $\text{Fe}_{\text{carb}}$  and 10% for  $\text{Fe}_{\text{ox}}$ . The accuracy of  $\text{Fe}_{\text{mag}}$  measurements could not be determined due to concentrations close to zero in the repeatedly analysed samples.  $\text{Fe}_T$  is accurate within 20% uncertainty based on the repeated dissolution of 40 samples.

#### **4.3.2. Comparing total iron measurements (XRF and AAS)**

One can imagine that precise concentrations of total iron are crucial for reliable iron speciation analysis. As already mentioned, in certain cases total dissolution of a given sample can barely be attained and this might also affect  $\text{Fe}_T$  concentrations measured with the AAS. It is therefore not surprising that  $\text{Fe}_T$  concentrations measured by XRF generally yield slightly higher  $\text{Fe}_T$  contents although with a few exceptions (see appendix). However, AAS results agree very

well with the presumably more precise XRF values, rarely showing more than 20% difference (see Fig. 4.9).

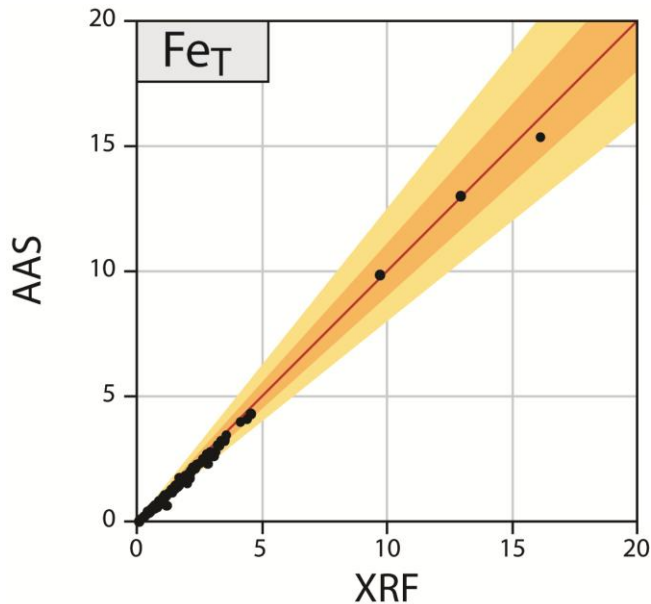


**Figure 4.9: Plot showing the almost perfect correlation of Fe<sub>T</sub> concentrations obtained by AAS and XRF. The orange beam represents 10% and the yellow beam 20% deviation.**

#### **4.4. Carbon and sulphur analysis**

##### **4.4.1. C/S analyser**

The measurement of carbon and sulphur concentrations has been carried out with a Leco C/S analyser at the Wolfson Laboratory, University College London. The C/S analyzer works as an induction furnace whereby carbon is oxidised to CO<sub>2</sub> and sulphur to SO<sub>2</sub> which is then measured by infrared detectors. The sample powders have been analysed for total carbon and total sulphur after weighing around 200mg into ceramic crucibles and the addition of iron chips to accelerate the burning process. For total organic carbon (TOC) measurement, the sample was treated with a 10% hydrochloric acid (HCl) solution in porous crucibles to dissolve carbonate whereby under some circumstances where high dolomite contents could be expected, a few drops of concentrated HCl have been added. After the subsequent filtering, a thorough rinse and drying the sample overnight, TOC contents have been measured following

the above procedure. The accuracy of the results has regularly been checked by introducing a reference material after every 10 samples and a few samples have been measured twice and agree within 10% uncertainty.

#### 4.4.2. Sulphide isotopes

For samples which yielded enough Ag<sub>2</sub>S residue (>0.03g) after the sulphide extraction procedure (see chapter 4.3.1.) have been analysed for sulphide isotopes using a Finnigan MAT DeltaPlus plumbed to a Carlo Erba elemental analyser through a Conflo II interface. All analytical work has been carried out by the group of Prof. Harald Strauss at the Institute for Geology and Paleontology, University of Münster, Germany.

#### 4.5. Trace-metal normalisation

The trace-metal content in organic-rich sediments is composed of three sources which are 1) terrestrial input through rivers or as aerosols, 2) plankton and 3) early diagenetic enrichment (e.g. Brumsack, 2006). To better reflect authigenic trace-element accumulation and rule out possible terrestrial contamination, trace-metal concentrations are often normalized to an element of predominantly, if not exclusively, detrital origin which is not affected by biological or diagenetic processes. Al is commonly used for that purpose but as it is often not included in the dataset, other elements such as K, Li, Sc, Ga, Zr and Ti can as well be used (e.g. Van der Weijden, 2002). Instead of simply normalizing a given trace-element to Al, enrichment factors are often used. This consists of dividing normalized trace-elements in the sample by the respective normalized trace-element in average shale:

$$EF = \left( \frac{\text{element}}{Al} \right)_{\text{sample}} / \left( \frac{\text{element}}{Al} \right)_{\text{Av.shale}}$$



Any possible enrichment is then indicated by EF values exceeding 1 and depletion of the element in EF values less than 1. Average shale composition and the roughly similar upper continental crust (UCC) composition has been evaluated ever since people have investigated shales (Wedepohl, 1971, 1995; Taylor and McLennan, 1985; Drever et al., 1988; McLennan, 2001) even for black shale specifically (Yudovich and Ketris, 1994). A further advantage of normalizing trace-metal contents is that it corrects for dilution by carbonates and other mineral phases devoid of Al (or another normalizing factor), which on the other hand can lead to unrealistically high enrichment factors or to other misleading results such as spurious correlations between trace-elements (Van der Weijden, 2002; Brumsack, 2006). Another approach is to evaluate the non-detrital or excess fraction of a given trace-metal (Brumsack, 2006):

$$element_{XS} = element_{sample} - Al_{sample} \left( \frac{element}{Al} \right)_{Av.shale}$$

However, the analysis of trace-metal concentrations and their eventual normalization to average shale or exclusively detrital elements has to take into account numerous factors which can affect the mineral composition of the sediment, such as diagenetic alteration and atypical mineral provenances.

For the present study, trace-metal concentrations have preferentially been normalized to Sc as it is part of the dataset acquired by both, XRF and ICP-MS analysis. The error margins in measuring Sc content by ICP-MS are also significantly smaller than for Ti for instance although Sc is generally present at much lower concentrations (see chapter 4.1.4.). In addition, Kimura and Watanabe (2001) found that V varies in proportion to Sc rather than other insoluble elements such as Al and Ti (see also Guo et al., 2007).

## **5. Results and discussion of the investigated sections**

In the following chapter several elements are mentioned as part of the analytical results but the discussion and interpretation mostly focuses on Mo, V and U, iron speciation analysis and Fe-S-C systematics. In some cases P, Ba Mn and Ni constitute an important characteristic of a sedimentary succession and deserve special attention. The traditionally used paleoredox proxies Th/U and V/(V+Ni) are mentioned for comparison but are of limited use in marine sediments deposited before and during the Precambrian – Cambrian transition where the biogeochemical cycling of redox-sensitive trace-elements experienced major perturbations. Two carbonate successions have been included and the results are outlined for the middle Dengying Fm. (Shibantan Mb.) and uppermost Zhujiqing Fm. (Dahai Mb.) without much discussion as, although respectable TOC contents are sometimes attained, no significant enrichment in redox-sensitive elements took place.

### **5.1. The Cryogenian**

#### **5.1.1. The Datangpo Formation: a geochemical profile from the manganese mine at Changxingpo, Guizhou Province**

A short interval of 2.25m has been sampled at the Changxingpo Mine including the black shale succession, which is more appropriately described as carbonaceous marl, at the base of the Datangpo Fm. They overlie the glacial deposits of the Tiesiao Fm. and are rather thin, based on the analysed TOC contents, and do not exceed 50cm. Although the sediments yield higher organic content further up, this increase in TOC content is accompanied by increasing Mn concentrations up to over 17% in the manganese-carbonates whereby a good correlation between TOC and Mn is observed throughout the sampled section ( $R^2 = 0.65$ ). Total sulphur concentrations are rather high at the top of the Tiesiao Fm. near the boundary (5.6%) but remain around 2% prior to the deposition of the Mn-carbonate. Pyrite and TS contents correlate well but there is a significant amount of non-pyrite sulphur of about 70%. Total Fe

content varies between 1.2 and 4.3% whereby the lowest values are found within the Mn-carbonate and the highest at the top of the Tiesiao Fm. P concentrations are all below 0.3% and negatively correlated with Fe contents. Ba concentrations increase from the carbonaceous marl on and reach a maximum of 1252.6 ppm about 25cm below the Mn-peak. Mo and V concentrations are relatively low and moderately enriched with Mo within the carbonaceous marl (up to 28.6 ppm) with Mo/TOC ratio of up to  $47.3 \times 10^{-4}$ . The same applies to other redox-sensitive trace-metals such as U but also Ni, Cu, Zn etc.  $Fe_{HR}/Fe_T$  ratios remain above 0.38 except for the region around the Tiesiao/Datangpo boundary where they decrease to around 0.32. Th/U ratios are greatly elevated with two digit values and a maximum of 93.8 and  $V/(V+Ni)$  decrease upwards to values below 0.6 within the Mn-carbonates. Pyrite sulphur isotopic values are greatly elevated, varying between 20 and 60‰ which broadly track Mn concentrations.

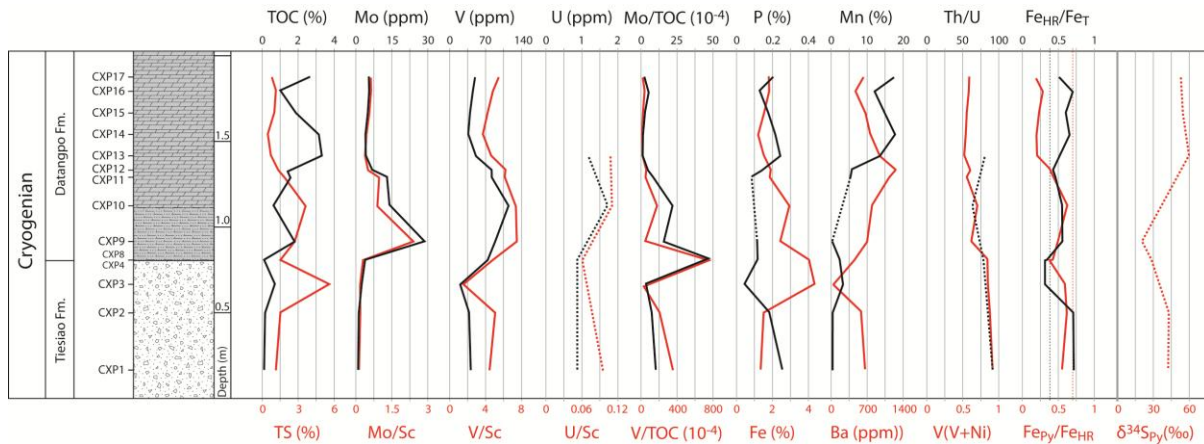
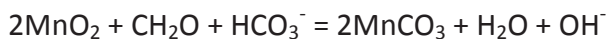


**Figure 5.1: The geochemical profile across the Tiesiao/Datangpo boundary in the Changxingpo Mine. Note that the carbonaceous marl at the base of the Datangpo Fm. has been qualified as black shale in several other basal Datangpo successions (e.g. Chen et al., 2008; Feng et al., 2010). Dashed curves indicate lower resolution. The  $Fe_{HR}/Fe_T$  threshold for anoxic deposition of 0.38 is indicated by a dashed black line and the threshold of 0.7 above which  $Fe_{Py}/Fe_{HR}$  ratios indicate deposition under euxinic conditions is indicated by a dashed red line.**

### 5.1.2. Discussion

Manganese is usually delivered to the sediment as Mn-oxyhydroxide (mainly MnO<sub>2</sub> and MnOOH) in the form of oxide coatings on detrital particles where it can be released when reducing conditions are met (see review by Tribovillard et al., 2006). Mn-oxyhydroxides can also dissolve while settling through the water column and in an anoxic water column, Mn accumulates as Mn<sup>2+</sup>. When clastic sedimentation is low, this causes Mn-oxyhydroxides to accumulate along the margin of an anoxic deep water body where the reaction with organic matter leads to the formation of secondary Mn-carbonates, which represents the only sink for Mn because the redoxcline acts as an efficient barrier against Mn loss (Brumsack, 2006), due to a shift towards more alkaline conditions (e.g. Liu et al., 2006):



Because about one half of the carbon in Mn-carbonates derives from organic carbon,  $\delta^{13}\text{C}$  values are usually relatively low (Liu et al., 2006). Furthermore, the oxidation of organic matter by Mn-oxyhydroxides can also remove some pyrite from the sediment (Aller and Rude, 1988). Both the correlation between Mn and TOC contents and the decreasing total sulphur and pyrite content as Mn contents increase support that Mn accumulated together with decomposing organic matter and thus suggest at least moderately oxic conditions (e.g. Calvert and Pedersen, 1996; see also Feng et al., 2010). But that also means that eventual diagenetic pyrite formation takes place relatively late, after Mn-oxyhydroxides converted to Mn-carbonates from a limited amount of sulphate within the sediment. Together with restricted access to sulphate in the overlying waters this results in very heavy  $\delta^{34}\text{S}_{\text{Pyrite}}$  values (Okita, 1992). Heavy S-isotopes are common in sediment-hosted Mn deposits and has been demonstrated in several Chinese Neoproterozoic deposits and elsewhere (Tang and Liu, 1999; Li et al., 1999a; Liu et al., 2006 and references therein).

Manganese ores are often found in close association with glacial deposits and therefore occur more abundantly in the Paleo- and the Neoproterozoic with a well-defined gap between

1800 and 1120 Ma (see Fig. 1.2b, Maynard, 1991; Roy, 2006; Maynard, 2010). A model by Gorjan (2000, 2003) suggested ocean turnover after the melting of 'Snowball Earth' whereby Mn (and Fe) rich upwelling waters which would have caused the widespread deposition of Mn (and Fe) deposits. But Liu et al. (2006), who studied the manganese ore on several sections on the Yangtze Platform, pointed out that sedimentary manganese ores are often interbedded with glacial deposits and are more likely found in narrow rifts than open shelves which is better explained by a 'Slushball' or 'Zipper-Rift Earth and partially retreating ice sheets (see review by Fairchild and Kennedy, 2007). An enhanced source for Mn and Fe would have been rapid deposition of lateritic soil residues introduced by low latitude glaciers into a suboxic or anoxic basin (Liu et al., 2006).

Low trace-metal concentrations can be expected due to non-sulphidic conditions in the water column and do not suggest a depleted trace-metal inventory prior to the Neoproterozoic Oxygenation Event. Moreover, elevated Mo/TOC ratios at the base of the Datangpo Fm. exceed values observed for the preceding Precambrian (see Fig. 2.3). The low Mo and V concentrations with maxima below the Mn-carbonate indicate an anoxic to suboxic environment during the deposition of the carbonaceous marl and the very low U content possibly even diagenetic remobilisation probably due to a redoxcline below the sediment-water interface and further support an environment prone to extensive Mn deposition. The higher Fe enrichment and pyrite sedimentation at the top of the Tiesiao Fm. and in the black shale prior to the Mn-carbonate further illustrate the greater insolubility of iron sulphide compared to Mn sulphide (alabandite; e.g. Liu et al., 2006). Similar to Fe, the lack of significant redox-sensitive trace-metals enrichment reflects their characteristic to form insoluble sulphide minerals which are therefore likely to be scavenged in deeper, anoxic portions of the water column (Maynard, 2010).

## 5.2. The Ediacaran and Precambrian – Cambrian boundary sections

### 5.2.1. The Maoshi section, Guizhou Province: A Doushantuo/Dengying boundary succession

The Doushantuo/Dengying boundary section, with a total length of about 19m (see Fig. 5.2), shows elevated TOC contents within the upper Doushantuo Fm. of between 1 and 3.6% which roughly correlate with high total sulphur contents of up to 3.25%. Almost all sulphur is present in pyrite except in one sample (MS10) about 9m below the boundary to the overlying Dengying Fm., where significant non-pyrite sulphur is indicated. There is no significant trace-metal enrichment and concentrations vary slightly around upper continental crust (UCC) values. Accordingly, we find very low Mo/TOC below  $4 \times 10^{-4}$  and V/TOC ratios with a maximum of  $144.5 \times 10^{-4}$ . Fe and P contents are broadly correlated within the upper Doushantuo Fm. with maxima of 3.5% and 0.8% respectively. The upper Doushantuo Fm. is overall depleted in Mn and slightly enriched in Ba, the latter showing gently decreasing concentrations across the Doushantuo/Dengying boundary and correlating very well with V concentrations ( $R^2 = 0.84$ ). Iron speciation data indicates anoxic conditions throughout with a possibly euxinic interval around 5m below the formation boundary where  $Fe_{Py}/Fe_{HR}$  ratios reach values above 0.7 over a length of about 2.5m. This interval is followed by a drop in S, Fe, Mn and Mo but not V while TOC even increases.  $V/(V+Ni)$  ratios are between 0.6 and 0.95 with overall lower values within the basal Dengying Fm. The  $Fe_{HR}/Fe_T$  ratio drops to 0.17 in the uppermost sample from the Dengying Fm. concomitant with a  $Fe_T$  content of only 0.04%.

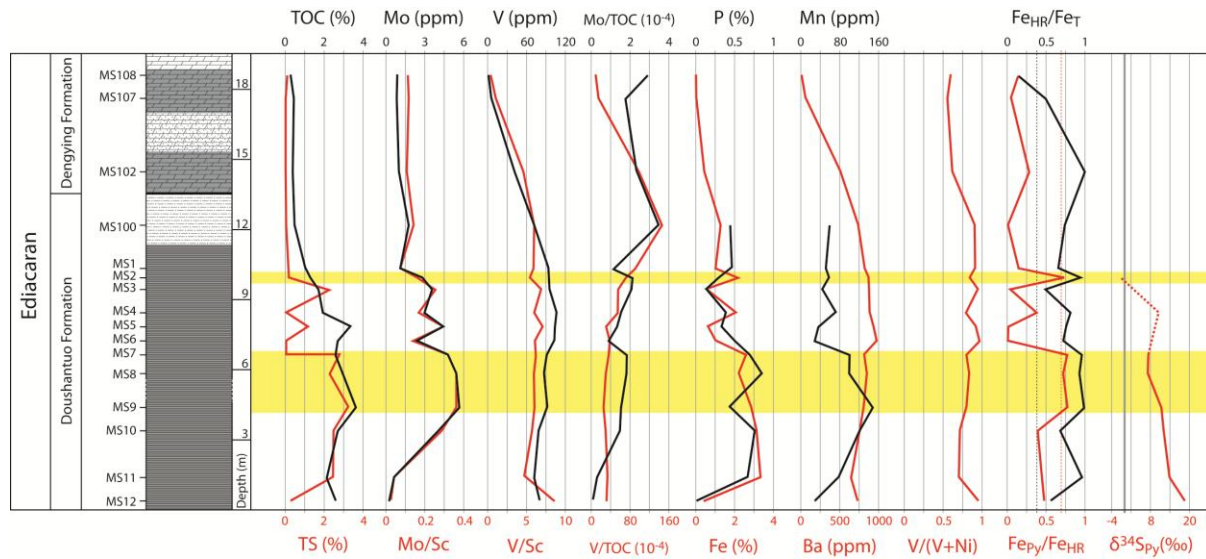


**Figure 5.2: The geochemical profile from the Doushantuo/Dengying boundary section at Maoshi. Yellow shaded intervals indicate intermittently euxinic conditions.**

## 5.2.2. The Doushantuo Formation in the Three Gorges Area, Hubei Province

### 5.2.2.1. The Member II at Jiulongwan

The profile starts about 1m above the cap carbonates from the lowermost Doushantuo Fm. and 1m below the onset of black shale deposition, where TOC and TS reach concentrations above 2% (see Fig. 5.3). For the rest of the succession, sulphur concentrations track TOC contents which vary between slightly below 1 and 2.7%. TS and pyrite sulphur correlate very well and there is a relatively consistent percentage of non-pyrite sulphur of about 20% except for a few samples with an overall low concentration of sulphur and analytical inaccuracies might play a role. Redox-sensitive trace-metals are within the range of UCC values or depleted throughout the section with maxima of Mo below 4.5 ppm, a maximum of V of 80 ppm and a U peak of 3.2 ppm. While some peaks occur concomitantly, such as at the base of the formation, Mo and V correlate only weakly and the best correlation is found between V and U. Other trace-metals such as Ni and Cu are almost exclusively depleted throughout. The Fe concentration pattern across the profile appears cyclical with values between 0.5 and 2.5% and

although there are significant interruptions in the stratigraphic column, it appears that variations in Fe content occur at an upwards diminishing frequency. Mn is enriched at the base of the Doushantuo Mb. II to concentrations of up to 2361 ppm and decreases stepwise to depleted values below 400 ppm. At that point, Ba concentrations increase over a few meters up to a maximum of 1075 ppm before decreasing slowly towards depleted values again further up the section. Mo/TOC ratios are very low and don't exceed  $4 \cdot 10^{-4}$  and the same applies to V/TOC ratios where a maximum of  $135.2 \cdot 10^{-4}$  is found. The Th/U ratio shows values above 5 in the first meter of the profile and then decreases to values below 2 for the rest of the sampled succession. Somehow contradictory, the V/(V+Ni) ratio shows higher values at the bottom of the section and then falls below 0.7 further up.

Iron speciation shows that  $Fe_{HR}/Fe_T$  ratios are mostly high and above 0.38 except in two isolated samples where we find ratios of 0.25 and 0.21. A few values exceed 1 which is probably due to a certain fraction of barely soluble iron phases (one ratio of above 3 was excluded from Fig. 5.3). Some  $Fe_{Py}/Fe_{HR}$  ratios attain values close to 0.7 at the base of the section and further up where a single value of 0.76 is found. Sulphur isotopes in pyrite are exclusively positive throughout the section exhibit significant variations between close to 0 and 22.9‰ (VCDT) with maxima at the base of the succession and on top within intervals with high  $Fe_{Py}/Fe_{HR}$  ratios.



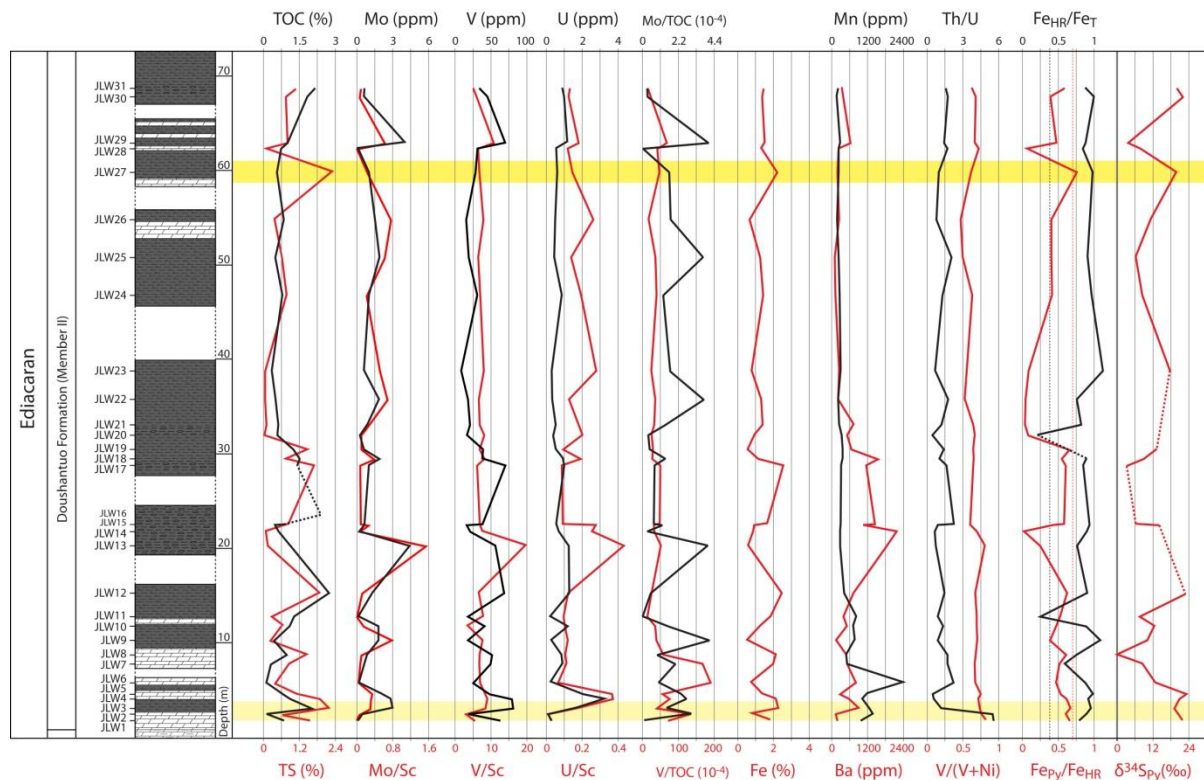


**Figure 5.3: The geochemical profile of parts of the Doushantuo Member II at Jiulongwan. Note that the disruptions in the stratigraphy are due to non-exposure of unknown lengths. The yellow shaded areas indicate sedimentation under euxinic conditions while the interval at the base of the section shows possibly euxinic conditions with  $Fe_{Py}/Fe_{HR}$  ratios of 0.66.**

#### 5.2.2.2. The Miaohu Member (Mb. IV) at Jiulongwan

A profile of about 20m length has been measured from the upper part of the Doushantuo Mb. III dolomites until the top of the black shales of the Miaohu Mb. at the boundary to the overlying Dengying Fm. (see Fig. 5.4). TOC contents gradually increase to values averaging more than 5% with a distinct peak of almost 15% a few decimetres below the Doushantuo/Dengying boundary. TS concentrations are more variable, rising to values above 2% at the base of the black shale, showing a distinct peak of 5.7% in the middle of the Miaohu Mb. and a decrease followed by a high concentration of 5.4% just below the Doushantuo/Dengying boundary. There is a weak negative correlation between TOC and TS whereby the highest TOC

contents at the top of the black shale correspond to low TS contents. TS and pyrite sulphur are well correlated with varying but minor amounts of non-pyrite sulphur. Mo concentrations are highest at the base of the black shale with 367.3 ppm and oscillate between 16.6 and 426.9 ppm further up towards the Dengying Fm. V concentration patterns are similar, with a maximum of 2404.8 ppm followed by variations between 171.1 and 2059.7 ppm. The U content varies between 3.2 and 31.5 ppm in the Miaohé Mb., the maximum value being found in the middle of the black shale succession. Normalization to Sc does not significantly affect sedimentary accumulation patterns. Other trace-metals, such as Ni and Cu are only moderately enriched except at the top of the Miaohé, where we find Ni and Cu depletion. Fe concentrations are very low within the uppermost Mb. III and increase to values between 2.3 and 3.9% within the Miaohé whereby values below 1% are attained at the top of the Miaohé before a maximum of 4.8% is seen just underneath the boundary to the overlying Dengying Fm. Mn is generally depleted with respect to UCC with one peak of 857.4 ppm within the middle part of the black shale which corresponds to relatively low trace-metal concentrations. Ba varies strongly between a few hundred and 4782.2 ppm. Mo, V and U correlate moderately with each other whereby the best covariation is seen between Mo and V ( $R^2 = 0.53$ ). There is no correlation between the analysed trace-metals and TOC or TS except for a weak negative correlation between V, Ni, Cu and TOC. Mn correlates weakly with Ni only, whereas the latter correlates moderately with Mo, V, U, Cu, Mn and Ba ( $R^2 \in [0.2, 0.4]$ ). Cu is moderately correlated to TS and Fe, Fe being negatively correlated to TOC. Mo/TOC ratios show a very high value of 181.2 at the base of the Miaohé Mb. and seem to decrease rapidly to values between 0.2 and 41.6. The V/TOC ratio as well is high at the base of the Miaohé Mb. (1186.4) and decreases to values between 11.3 and 493 within the overlying sediments.

Th/U ratios switch from values above 2 in the uppermost Mb. III to mainly very low values in the Miaohé except within the layer a few dm below the boundary to the overlying Dengying Fm.  $V/(V+Ni)$  ratios increase at the Mb. III/Miaohé boundary to values mostly above 0.9. Iron speciation data shows high  $Fe_{HR}/Fe_T$  ratios close to 1 throughout the profile while  $Fe_{Py}/Fe_{HR}$  ratios are above 0.7 about 4m below the Mb. III/Miaohé boundary followed by a short decrease to 0.44 before rising again towards very high ratios of between 0.7 and 1 in the

Miaohe black shale until another decrease to minimum of 0.57 less than 1m below the Doushantuo/Dengying boundary. The sample from the boundary interval shows again a  $Fe_{Py}/Fe_{HR}$  ratio of 0.86. Lower  $Fe_{Py}/Fe_{HR}$  ratios correspond to low  $Fe_T$  contents below 1% which might cause some unreliability.

Pyrite sulphur isotopic values are negative between -5.9‰ (VCDT) within the upper Mb. III and -19‰ (VCDT) on top of the Miaohe within an interval where TS contents and Th/U ratios track the isotopic record.

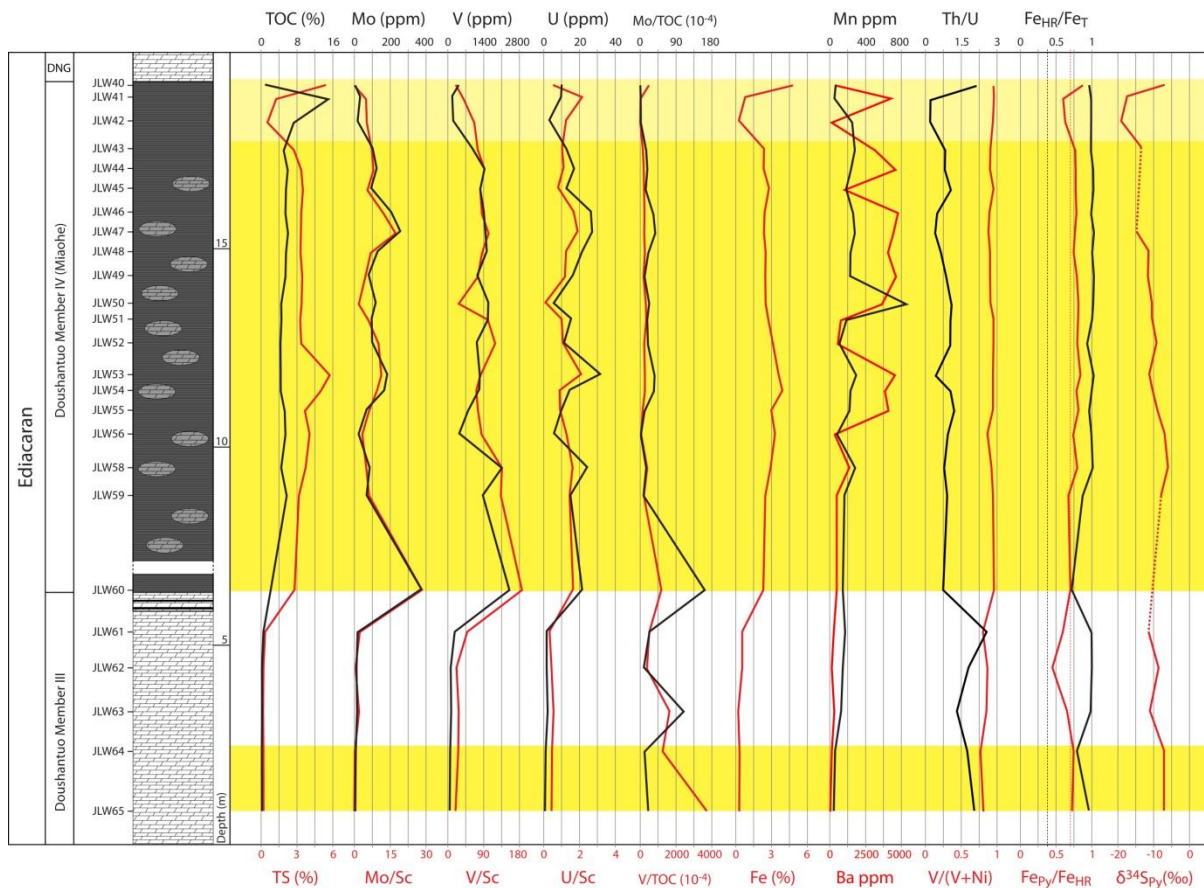
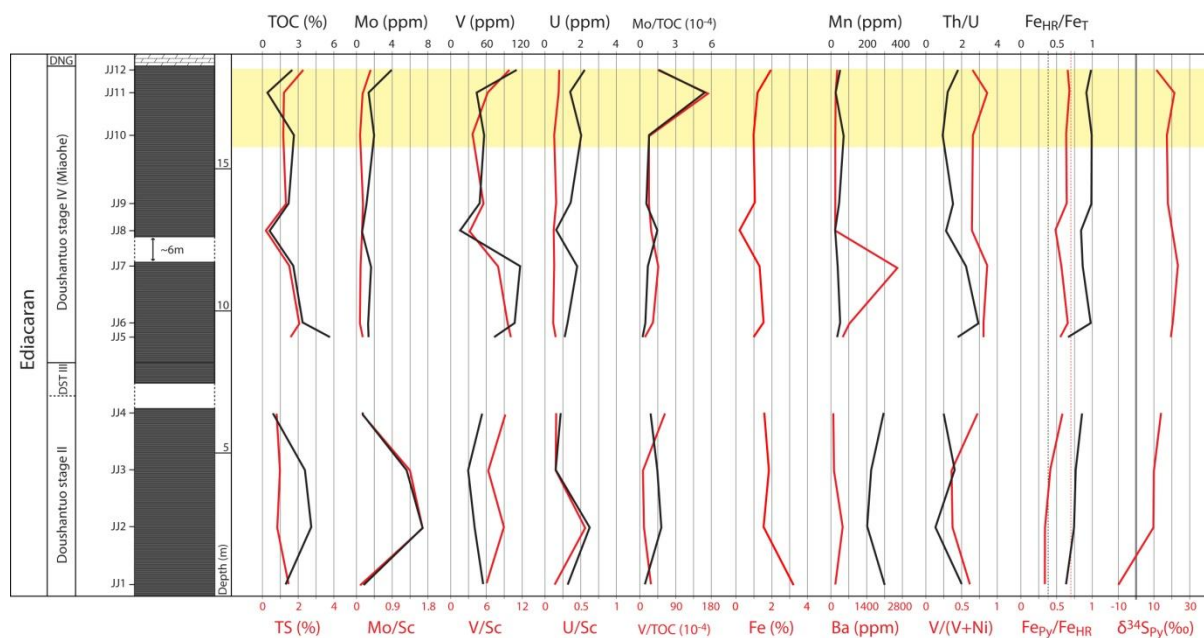


Figure 5.4: The geochemical profile from the upper part of Doushantuo Mb. III to the Doushantuo/Dengying boundary. Yellow shaded intervals represent euxinic depositional conditions and the lighter shaded interval at the top of the Miaohe Mb. suggests a short period of non-sulphidic conditions until the boundary.

### 5.2.2.3. Member II and the Miaohé Member at Jijiawan

Samples have been analysed for black shale intervals of the Mb. II and the Miaohé Mb. of the Doushantuo Fm. (see Fig. 5.5). TOC contents are variable between 0.8 and 4% and TS concentrations remain around 1% within Mb. II. In the Miaohé black shale, TOC concentrations are very high at the base with a maximum of 5.6% and remain largely below 3% for the rest of the succession. TS concentrations remain below 2% until the top of the Miaohé, shortly before the boundary to the overlying Dengying Fm. where a maximum of 2.3% is found. There is a good correlation between TS and pyrite sulphur with variable amounts of non-pyrite sulphur averaging about 40%. Mo concentrations are low throughout with the highest value of 7.3 ppm within Mb. II. The same applies to V with a maximum of 116.7 within the Miaohé and U with a maximum of 2.5 ppm within Mb. II. Ni and Cu are mostly below UCC values. The major elements Fe and Mn are also depleted with averages of 1.45% and 110.6 ppm respectively whereby the carbonates in Mb. II are less depleted in Mn but slightly more depleted in Fe. Within the Miaohé, moderate to good correlation is found between Mo, U, Ni, Cu and TS, whereby TS correlates well with redox-sensitive metals insoluble under reducing conditions such as Mn. In addition, good correlation ( $R^2 = 0.61$ ) is seen between V and Fe. Mn correlates moderately with U and Ni. Mo/TOC ratios are low throughout the section with a maximum of  $5.4 \times 10^{-4}$  on top of the Miaohé where a concomitant peak in V/TOC ratios of  $170.8 \times 10^{-4}$  is found. Th/U is below 2 within Mb. II and highest in the lower part of the Miaohé with a ratio of 2.9. V/(V+Ni) is mostly below 0.64 in Mb. II and increases in the Miaohé where ratios remain above 0.64.  $Fe_{HR}/Fe_T$  ratios are consistently above 0.38 in both members and  $Fe_{Py}/Fe_{HR}$  ratios vary between 0.49 and 0.69 within the Miaohé with the highest ratios on top.  $\delta^{34}S_{Pyrite}$  values are negative within the stratigraphically oldest sample (-10.5‰) but increase to positive values above 10‰ (VCDT) further up with a maximum of 23.2‰ within the Miaohé.



**Figure 5.5: Analytical results for the lower part of the Doushantuo Mb. II and the Miaohe Mb. at Jijiawan. Note that the gap between Mb. II and the Miaohe is unknown but in the range of a few tens of meters. The light yellow interval indicates deposition under possibly sulphidic conditions with  $Fe_{Py}/Fe_{HR}$  ratios between 0.63 and 0.69.**

### 5.2.3. Ocean chemistry and platform evolution in the Ediacaran

The short interval sampled from the Doushantuo Mb. II at Jijiawan is geochemically similar to the more extended profile analyzed at Jiulongwan, where we find no enrichment in redox-sensitive trace-metals, comparable TOC and TS contents, overall anoxic conditions and mostly positive  $\delta^{34}S_{Pyrite}$  values above 10‰ (VCDT). Past geochemical studies from the Jiulongwan section in the Three Gorges Area agree with our results (Bristow and Kennedy, 2009; Li et al., 2010) and suggest that low trace-metal concentrations are likely a widespread characteristic on the platform and margin during the deposition of the Doushantuo Mb. II. Low to moderate enrichment of Mo and V in Mb. II has been reported from slope and basin sections, where Mo concentrations can reach a few tens of ppm (Wallis, 2006; Guo et al., 2007). Although there are indications for intermittent euxinia in Mb. II at Jiulongwan, suggested by high  $Fe_{Py}/Fe_{HR}$  ratios close to 0.7, no Mo enrichment took place. Because Mo/TOC and V/TOC

ratios remain accordingly very low throughout the lower part of the Doushantuo Fm., a limited reservoir of Mo and V in the water column could have prevailed during the deposition of the Doushantuo Mb. II, which can either be due to globally reduced oceanic trace-metal budgets or to a certain extent of basin restriction, such as seen in the Black Sea today (Algeo and Lyons, 2006; Scott et al., 2008; Jiang et al., 2011). On the other hand, low H<sub>2</sub>S concentrations (below 11 μM: Helz et al., 1996) might have reduced the removal of redox-sensitive trace-metals, Mo in particular, from the water column. However, paleogeographical, sedimentological and carbon isotope studies support a rimmed platform margin and the formation of restricted basins on the Yangtze Platform (Jiang et al., 2003, 2008, 2011; Vernhet, 2007; Vernhet and Reijmer, 2010), indicating geographical barriers as main trace-metal limiting mechanism. However, Bristow and Kennedy (2009) recently carried out a study on Mb. II at Jiulongwan and found abundant saponite, a clay mineral predominantly formed under elevated pH (>9) in alkaline lakes and hypothesized that Mb. II could have been deposited in a non-marine environment without access to the open ocean. Furthermore, δ<sup>34</sup>S values in pyrite are very variable but generally enriched in <sup>34</sup>S resulting from quantitative sulphate-reduction and a sulphate-poor water column which could also result from restricted access to the open ocean. A further possibility would be widespread euxinia during the deposition of Mb. II, effectively depleting the oceanic reservoir of sulphate and redox-sensitive trace-metals but there is no evidence for long-lived and sustained euxinia neither on the Yangtze Platform nor elsewhere in the world during that time (Canfield et al., 2008). And, last but not least, low atmospheric oxygen levels prior to the NOE could have effectively limited oxidative weathering and the ocean would remain depleted in molybdate and sulphate during the Early Ediacaran. Such a scenario is enticing and may constrain the NOE better in time but Jiang et al. (2011) recently suggested that the platform margin developed into a rimmed-shelf relatively soon after the deposition of the cap carbonates ca. 635 Ma and would have possibly restricted the depositional environments north of the platform margin making the paleobathymetric setup the controlling parameter regarding trace-metal and sulphate availability (see Fig. 5.6).

The black shales from the Miaohu Mb. were clearly deposited under euxinic conditions at Jiulongwan. Euxinia is less well supported at Jijiawan where a maximum Fe<sub>Py</sub>/Fe<sub>HR</sub> ratio of

0.69 is observed. The geochemistry at Jijiawan might have been altered by weathering (see chapter 3.1.2.), resulting in oxidation and remobilization of redox-sensitive elements. Intermittently euxinic conditions are also indicated within the uppermost Doushantuo Fm. at Maoshi, which is about 530km south west of the Three Gorges Area, suggesting widespread euxinic conditions on the borders of the platform during deposition of the upper Doushantuo black shales. Element concentrations and sulphide isotopes are strikingly different between the Jiulongwan sections and both, Jijiawan and Maoshi sections. Whereas Mo, V, U and most other redox-sensitive metal concentrations are within the range of average shale (or UCC) values at Maoshi and Jijiawan, we find the highest Precambrian Mo concentrations (>300 ppm) so far on record within the Miaohe Mb. at Jiulongwan. Furthermore, while sulphide isotopes are exclusively and distinctively negative in the Miaohe black shale at Jiulongwan, averaging -11.2‰ (VCDT), we find mostly positive values at Maoshi, averaging 9.9‰, and at Jijiawan with an average of 18.4‰. The evolution of the Yangtze Platform margin during the deposition of the Ediacaran Doushantuo Fm. can tentatively be constrained in time and space on geochemical proxies alone if we assume a global oceanic Mo and sulphate reservoir in the range of modern magnitude.

The Nantuo Fm., deposited during the Marinoan Glaciation, represents the last stage of the rifting history of the Yangtze Platform and left the morphology with abundant horst and graben structures (see Fig. 3.3; Vernhet, 2007) onto which the sediments of the Doushantuo Fm. have been draped. A mosaic of different depositional environments can therefore be imagined which has been confirmed by studies demonstrating significant lateral facies variations, notably around the Three Gorges Area, including rims, protected shallow-water basins and intra-shelf basins (Fig. 5.6; Vernhet, 2007; Vernhet and Rejimer, 2010). A rising eustatic sea-level would have successively allowed these restricted or semi-restricted basins access to the open ocean and thus increased the availability of redox-sensitive trace-metals to be scavenged by anoxic and even sulphidic bottom waters (see Fig. 5.7). Low sulphate concentrations in the water column during the deposition of Mb. II were sufficiently counteracted by overall low Fe(II) concentrations to allow episodic euxinia to develop. The pronounced euxinic sediments of the Miaohe Mb. at the Jiulongwan section are accompanied by very high Mo/TOC ratios and

negative sulphide isotope values, suggesting an almost unlimited supply of redox-sensitive trace-metals and sulphate by the overlying shallow, oxic ocean and enhanced by the limited extent of the euxinic water masses, in the form of a sulphidic wedge, for instance, as proposed by Li et al. (2010). The Miaohe Mb. sediments at the Jijiawan section do not exhibit any enrichment of redox-sensitive trace-metals and pyrite is enriched in  $^{34}\text{S}$  and suggest that while depositional environments closer to the platform margin had unrestricted access to the open ocean, some intra-shelf basins remained isolated further within the inner platform. This also applies to the sediments deposited at the Maoshi section, which exhibits similarly low Mo, V and U enrichments along with positive sulphide isotope signatures (see Fig. 5.2 and 5.6c).

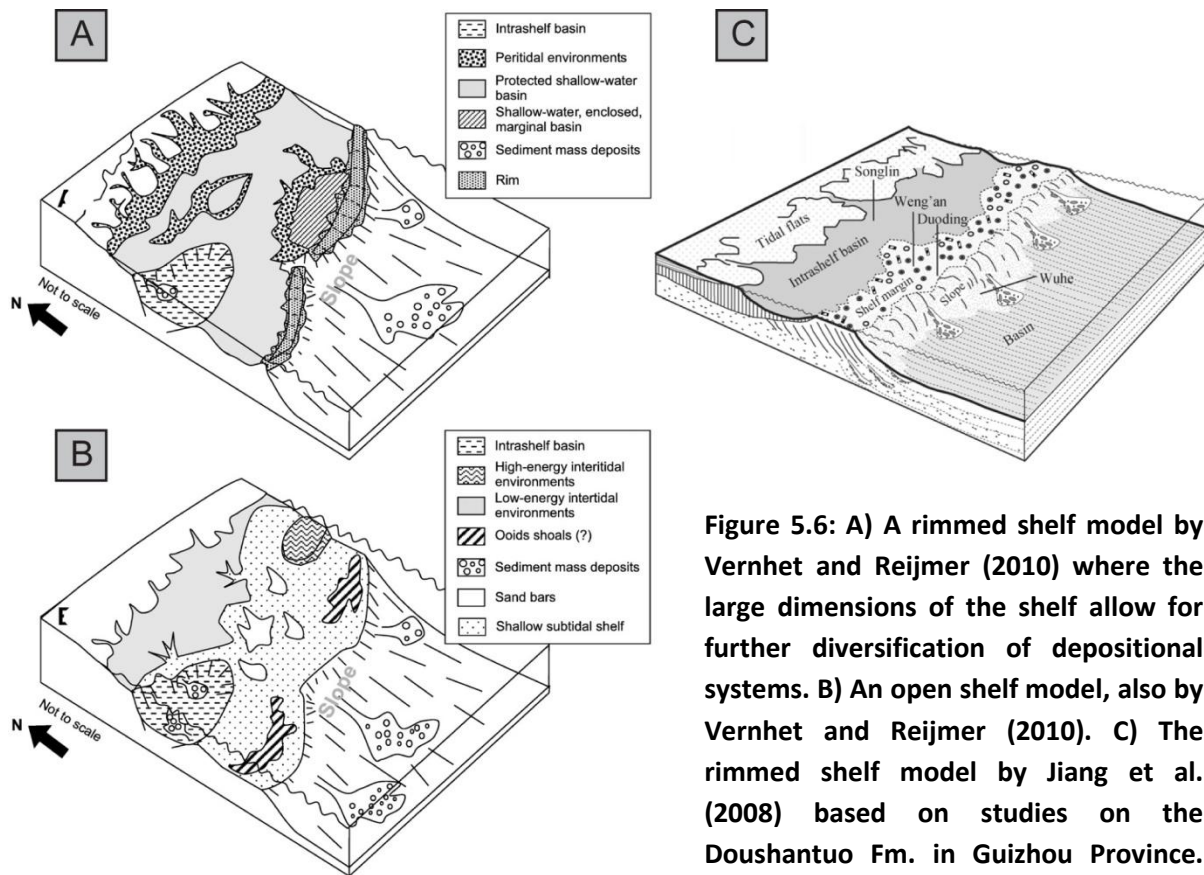


**Figure 5.6:** A) A rimmed shelf model by Vernhet and Reijmer (2010) where the large dimensions of the shelf allow for further diversification of depositional systems. B) An open shelf model, also by Vernhet and Reijmer (2010). C) The rimmed shelf model by Jiang et al. (2008) based on studies on the Doushantuo Fm. in Guizhou Province. The Maoshi section is located near Songlin, within the intra-shelf basin.



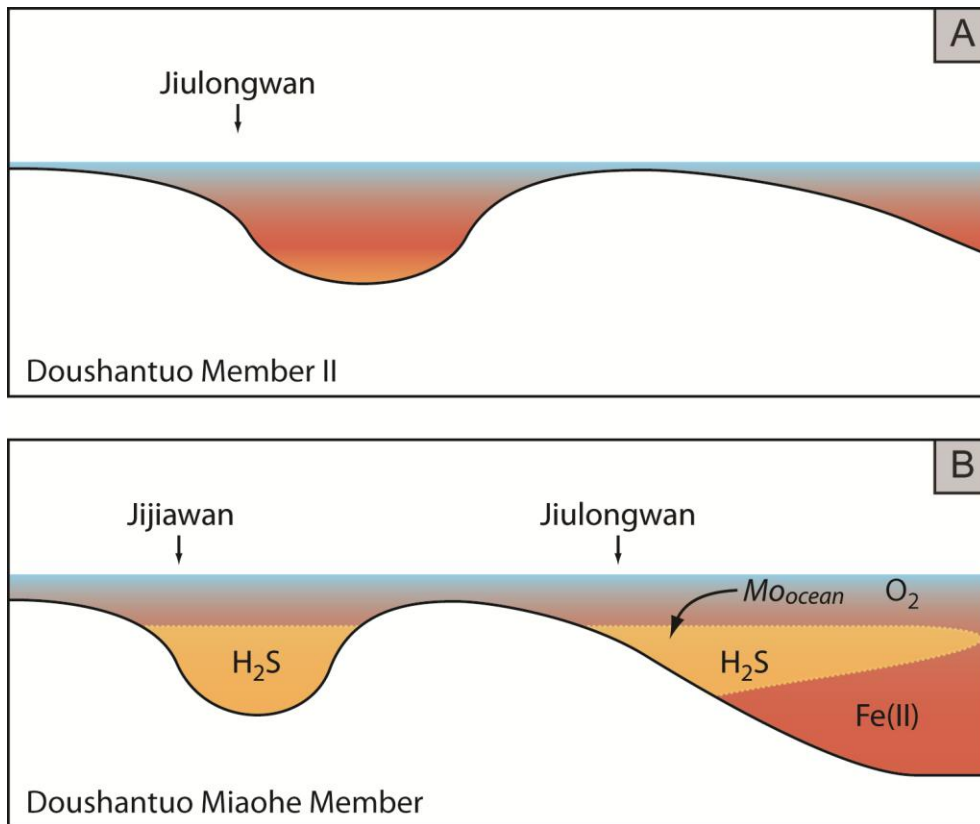


**Figure 5.7:** A) shows a restricted intra-shelf basin with a stratified water column including intermittent euxinic conditions such as might have been the case during the deposition of the Doushantuo Mb. II. B) A model schematically illustrating how the Miaohe Mb. might have been deposited in different environmental settings. The sulphidic wedge, analogous to modern oxygen-minimum zones, has been adopted from Li et al. (2010) to account for the very high enrichment in redox-sensitive trace-metals observed at Jiulongwan.

#### 5.2.4. A high-resolution profile from the top of the Miaohe Member at Jiulongwan

##### 5.2.4.1. Results

The ca. 80 cm long interval recovered from the upper part of the Miaohe Mb., about 20 cm below JLW42, consists of pyrite rich, finally laminated black shale whereby 7 individual blocks of 5cm length have been sawn out and subjected to Laser Ablation ICP-MS (see Fig. 4.4a).

The results have been averaged for each individual sample which is shown in figure 5.8 while the detailed results can be found in the appendix. Average Mo concentrations vary between 154 and 293 ppm, average V concentrations between 877 and 1429 ppm and average U concentrations between 26 and 40 ppm. There is no correlation between Mo and V but a moderate covariation is observed between Mo and U contents, exemplified by the minimum average Mo concentration occurring together with the minimum average U concentration but the maximum average V concentration. Mn contents are relatively low but gradually increase up-section to a maximum average of 810 ppm while a very high variability is observed for average Ba concentrations of between 543 and 9931 ppm which tend to be inversely correlated to Mo contents.

The high resolution profiles can be found in the appendix and only MI2, sampled about 25cm below JLW42, will be discussed further at this stage (see Fig. 5.9). Mo concentrations generally remain around 200 ppm but show a few pronounced peaks within the lower part of the profile, where three distinctively enriched horizons follow each other with Mo contents gradually increasing to over 1000 ppm. This interval correlates with elevated Mn contents and is between very high Ba concentrations up to several percent. Another single Mo peak with concentrations up to almost 2000 ppm within the upper part is again accompanied by a prominent Mn maximum of about 4000 ppm and preceded by high Ba concentrations which can attain over 3%. V contents are mostly between 750 and 1500 ppm with a few layers which can reach almost 3000 ppm but are not correlated with other elements analysed here. U concentrations are mostly below 100 ppm with a suite of higher contents of up to 200 ppm in the middle and single peak on top of the profile. Th/U ratios mostly remain well below 2 but show a few enriched layers with values between 2 and 8, first between the 2<sup>nd</sup> and 3<sup>rd</sup> Mo peak within the lower part and second, before and after the maximum Mo and Mn concentrations within the upper part.

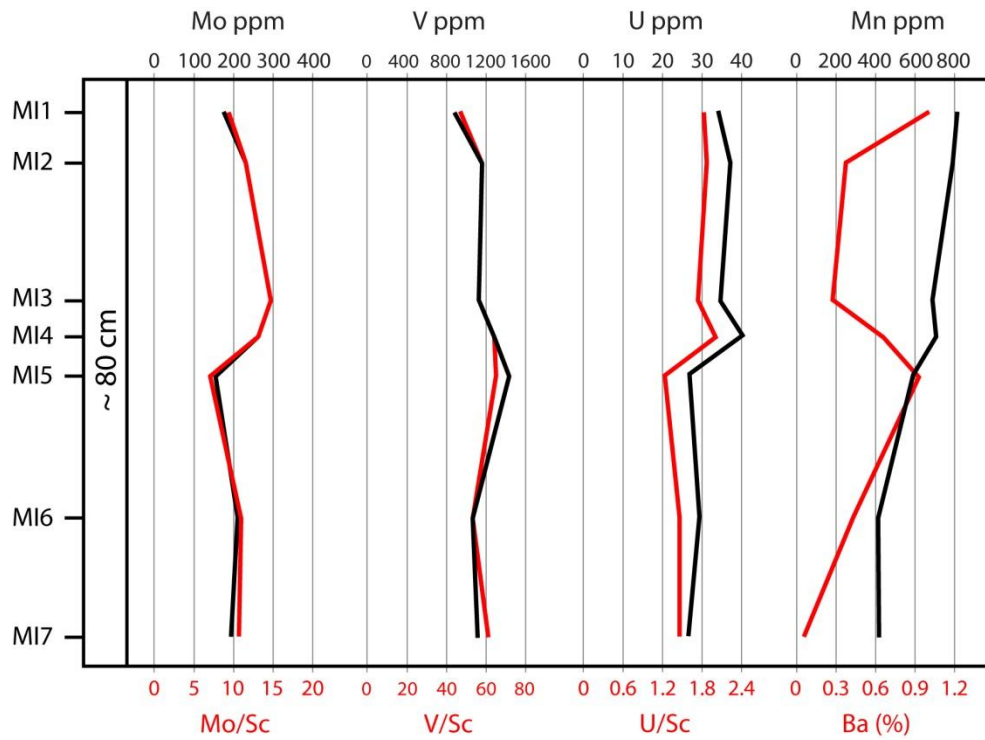


**Figure 5.8: Averaged redox-sensitive element concentrations from the LA-ICP-MS analysis performed on seven black shale samples from the uppermost Miaohé Mb. at Jiulongwan. Note that most concentrations are much higher than the bulk rock data in figure 5.4 which might result from particularly the unweathered and homogenous sample selection for the LA-ICP-MS.**

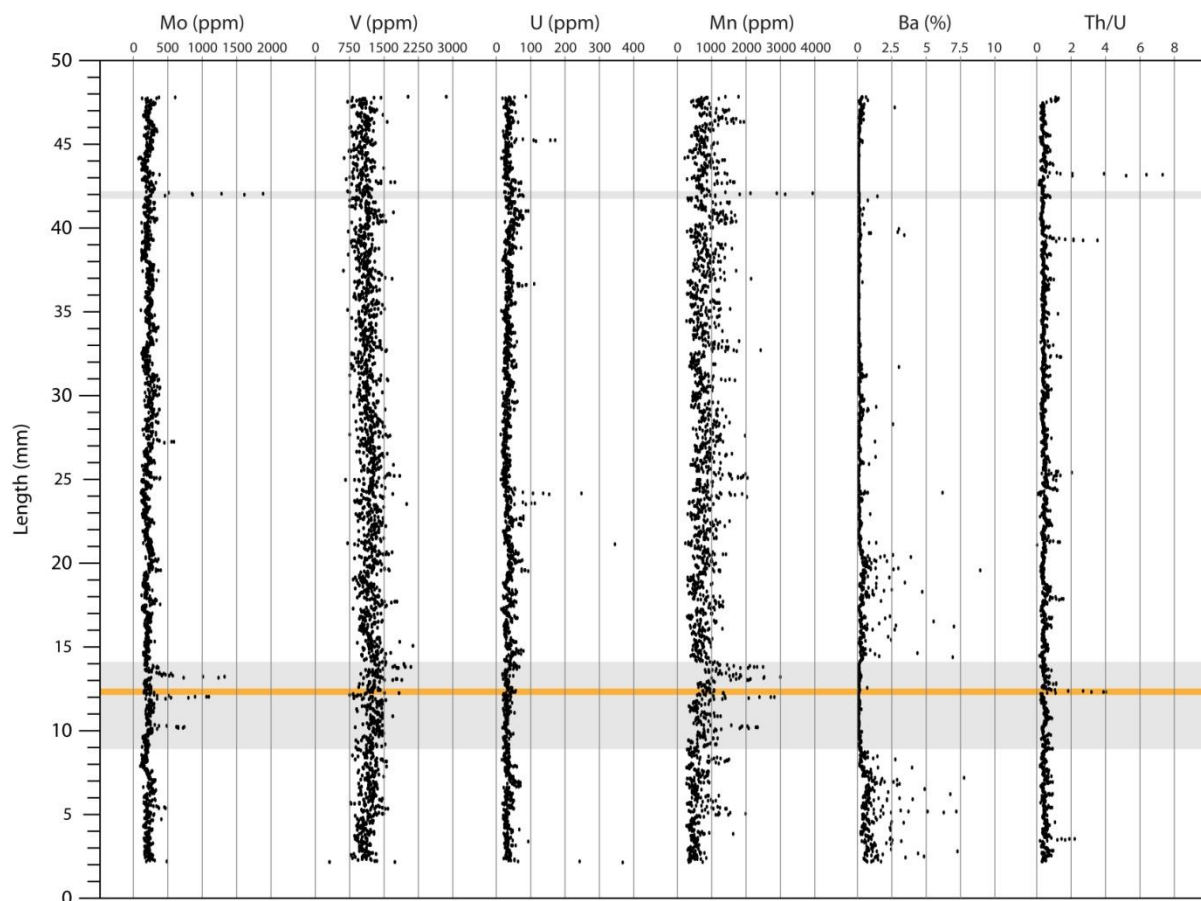


**Figure 5.9:** High resolution geochemical profile perpendicular to the lamination across MI2, a 5cm long sample from the uppermost Miaohe Mb. at Jiulongwan. The grey shaded areas indicate episodic Mo and Mn enrichment after and/or between two intervals of anomalously high Ba enrichment and the orange line indicates high Th/U ratios above 2 within the lower interval. Note that some isolated Ba concentrations significantly exceed 10% and are not shown here.

#### 5.2.4.2. Discussion

The consistently higher average concentrations from the LA-ICP-MS analysis compared to the bulk rock data, in particular for Mo and to a lesser extent for V, might result from a more careful selection of homogenous samples and polished surfaces. Alternatively, the calibration after the internal standard (Si), as outlined in chapter 4, might impact on the analytical results due to the mineralogical heterogeneity of the samples. However, even from a semi-quantitative

point of view the high-resolution profiles exhibit geochemical changes in the mm-scale and give insight into short term variations of the biogeochemical cycling of redox-sensitive trace-metals. The lowermost 2cm of sample MI2 in particular exhibits interesting and very sharp switches from Ba to Mo and back to Ba. This could suggest episodic blooms in productivity under oxygen depleted but non-sulphidic bottom water conditions followed by periods of intermittent euxinia which lead to enhanced Mo sequestration from the water column. But it is more likely to indicate a dynamic redoxcline with varying depth, leading to sulphate ( $\text{BaSO}_4$ ) precipitation when within the sediment and sulphide and concomitant Mo removal when bottom water euxinia developed. The fact that such changes are resolved within the range of a few millimetres is intriguing but element mapping of a small areas ( $900 \times 900 \mu\text{m}$ ) demonstrates large variability not only perpendicular to the lamination but also shows laterally limited features, such as inhomogeneous pyrite distribution and components very rich in vanadium (see Fig. 5.10). Nevertheless, this preliminary results are promising and further investigations, for instance by electron microscopy and high resolution studies on recent sediments, might shed light on mechanisms of diagenetic Mo fixation and even Mo sequestration within a multi-element framework.

The elevated Th/U ratios are mainly controlled by Th concentrations and do not indicate less reducing conditions or U remobilization, especially since U contents remain essentially constant. It can be assumed that high Ba concentrations indicate periods of elevated productivity which consequently causes enhanced sulphate-reduction and free  $\text{H}_2\text{S}$  in the water column scavenging dissolved Mo. This suggests a dynamic environment switching between periods of high surface productivity and sulphidic water masses causing bioessential trace-metals to become limiting nutrients over a relatively short time span.

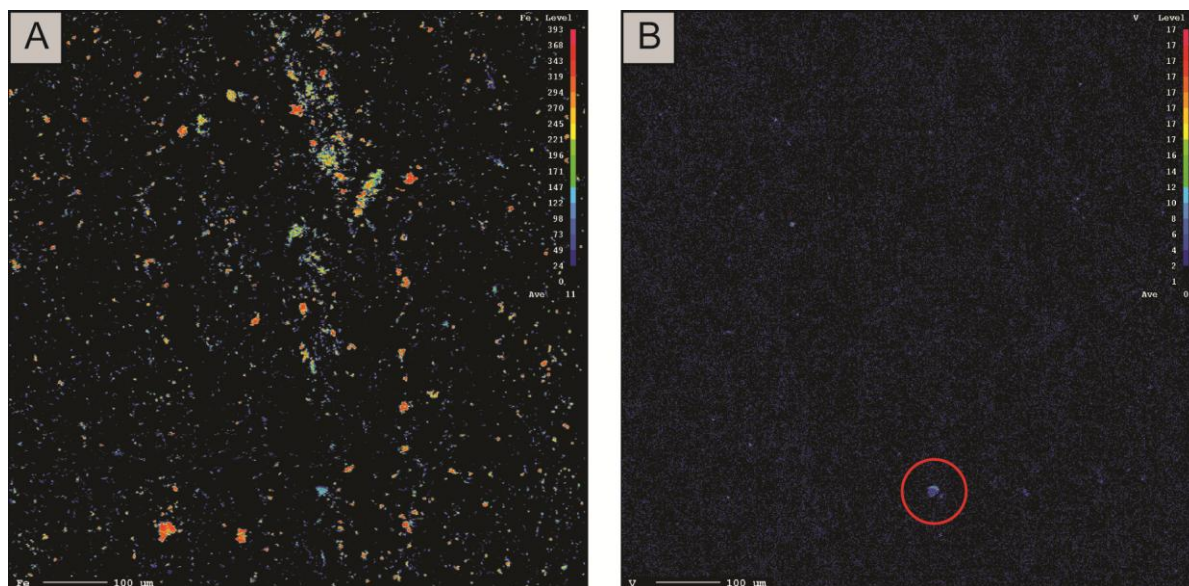


Figure 5.10: A) Element map showing intensities of Fe occurrence which is predominantly incorporated in pyrite. B) Element map of the same area indicating V occurrence. Due to the relatively high detection limit of the electron probe microanalyzer (ca. 1500 ppm), only exceptionally high V accumulation can be discerned, such as a highly enriched 'pebble' (red circle).

## 5.2.5. The Miaohe Member at Baiguoyuan, Hubei Province: A comparison

### 5.2.5.1. Results

Another well exposed outcrop of the Doushantuo Miaohe Mb. is located at Baiguoyuan, south of Jiulongwan on the eastern flank of the Huanglian Granite (see Fig. 3.2). The Miaohe Mb. is about 14m thick and has been sampled and geochemically analysed by Wallis (2006). The sedimentology of the succession presented in figure 5.11 is similar to the Miaohe at Jiulongwan but tends to have sandier black shales, in particular towards the upper part, and beds of silty dolomite are common. The TOC content is very high at the base (6.2%), decreases shortly before gradually rising again from 2.1 to 4.9% at the top. TS concentrations are below 0.2% throughout the Miaohe Mb. and correlate with very high Ba concentrations which attain a maximum of 1.3% but not with the low Fe concentrations of between 1 and 2.8%. Mo contents

remain between 4 and 45.7 while very high variations are seen for V concentrations which are 873 ppm at the base and have several peaks within the middle part of up to more than 1% (detection limit is at 9999 ppm) before decreasing again and reach 893 ppm on top of the Miaohe black shale. U concentrations as well tend to be lower at the base and the top while significant variations are seen in the middle part with a maximum of 23.3 ppm. There is a good correlation between V and U ( $R^2 = 0.71$ ), a weak correlation between V and Mo ( $R^2 = 0.29$ ) and a moderate correlation between Mo and U ( $R^2 = 0.46$ ). TS and TOC show no correlation with Mo, V or U. Mo/TOC and V/TOC ratios have been generated for samples with more than 1% TOC which lead to a maximum of  $17.3 \times 10^{-4}$  for Mo/TOC within the upper part of the black shale and  $3076.6 \times 10^{-4}$  for V/TOC in the middle of the black shale. Th/U ratios are relatively high at the base of the Miaohe Mb. with a ratio of 4.5 and gradually decrease to ratios close to 1. V/(V+Ni) ratios are mainly above 0.93 with one exception (0.84) within a carbonate bed.

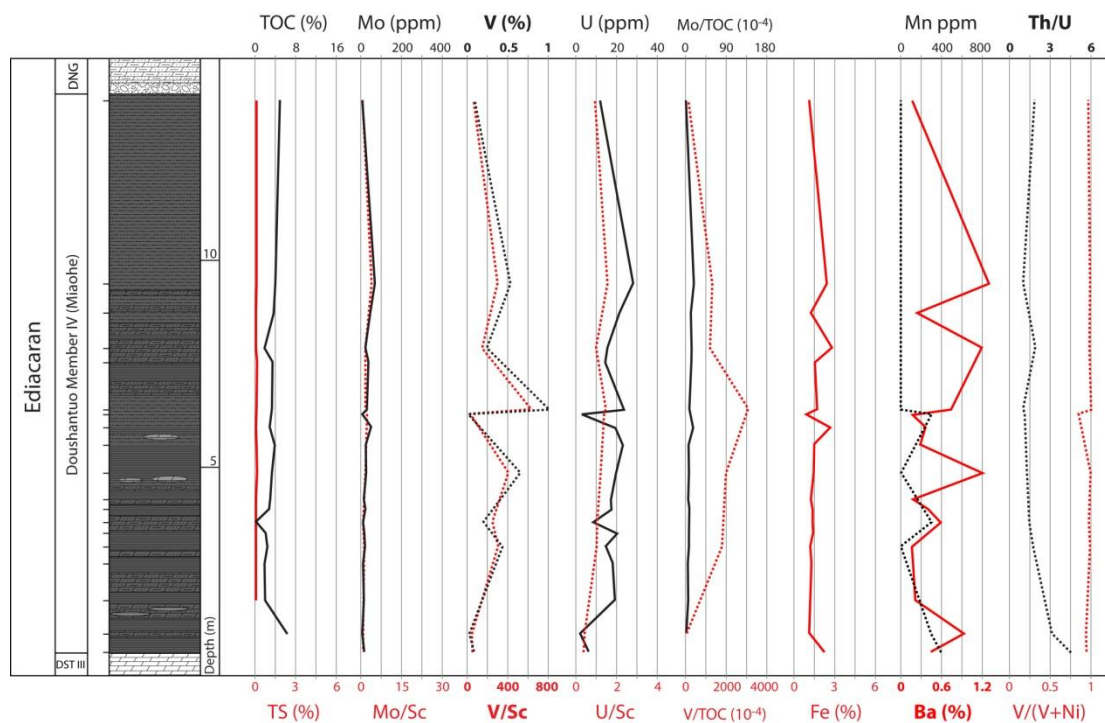


**Figure 5.11: The geochemical profile of the Miaoho Mb. at the Baiguoyuan section recorded by Wallis (2006). Dashed lines indicate lower sampling resolution than indicated on the stratigraphic column and where concentrations significantly exceed values found at Jiulongwan (see Fig. 5.4) the scale has been adjusted and labels are in bold.**

### 5.2.5.2. Discussion

The Baiguoyuan section is characterized by another unusual geochemistry and previous studies at Baiguoyuan have mainly focussed on the black shale hosted Ag-V ore deposit, generally thought to be of sedimentary-diagenetic origin (Chao and Fapeng, 1986; Qian et al., 1995; Zhuang et al., 1999). While TOC contents are within the same range at Jiulongwan, the Miaoho Mb. at Baiguoyuan is poor in TS which is likely to be mainly bound as barite. Comparing the covariation patterns of TOC and TS concentrations from the Miaoho Mb. at Maoshi, Jijiawan, Jiulongwan and Baiguoyuan (see Fig. 5.12), it can be observed that the TS vs. TOC covariation is significantly different at Baiguoyuan than in other Miaoho black shales which present values within a similar range. Sediments depleted in S with respect to TOC have previously been



interpreted as being non-marine (Berner and Raiswell, 1984) but the abundance of other redox-sensitive trace-elements suggests otherwise. Although Mo is still slightly enriched at Baiguoyuan with respect to average shale (or UCC) values, Mo concentrations do not exceed a tenth of the maximum content reached at Jiulongwan. On the other hand, V attains concentrations up to more than 1% at Baiguoyuan, which is about 5 times more than the maximum at Jiulongwan. Hence, there seems to be a strong geochemical gradient between the depositional environments at Jiulongwan and Baiguoyuan leading to a disparity between respective V/TOC ratios within the Miaohé Mb., particularly with respect to coeval Mo/TOC ratios. However, U concentrations are very similar within the Miaohé black shale at both sections, with an average of 15.8 ppm at Jiulongwan and 16.1 ppm at Baiguoyuan. A better estimate of authigenic U is given by correcting for detrital U input using the calculation  $U_{\text{aut}} = U_{\text{total}} - \text{Th}/4$  (see chapter 2.2.2.) and although Th contents are higher at Baiguoyuan,  $U_{\text{aut}}$  remain within a similar range at both sections (average of 12.9 ppm at Jiulongwan and 8.4 ppm at Baiguoyuan). Since authigenic U enrichment takes primarily place within the sediments and is decoupled from the amount of free  $\text{H}_2\text{S}$  in the water column, this leads to the suggestion that besides redox stratification, the biogeochemical cycling of sulphur played a crucial role in controlling the removal of Mo in combination with sulphide into the sediment, such as at Jiulongwan, and V together with elevated barite concentrations at Baiguoyuan.

In summary, while the availability of redox-sensitive trace-metals was geographically restricted at Maoshi and Jijiawan during the deposition of the Miaohé Mb., the redox conditions were broadly similar to Jiulongwan with euxinia clearly expressed at Maoshi and Jiulongwan. The depositional environment at Baiguoyuan and Jiulongwan were presumably subject to similar trace-metal availability but separated by a chemocline which limited sulphate-reduction and lead to preferential V over Mo mineralization at Baiguoyuan. Furthermore, it has been demonstrated that barite accumulation significantly depends of water-depth whereby detrital dilution and reductive dissolution tends to overprint primary Ba precipitation in shallow water environments and leads to greater enrichment in the deep sea (Von Breyman et al., 1992; Brumsack, 2006). Hence, the Miaohé Mb. at Baiguoyuan might have been deposited in a

deeper portion of the Yangtze Platform maybe even beneath a sulphidic wedge such as proposed by Li et al. (2010).

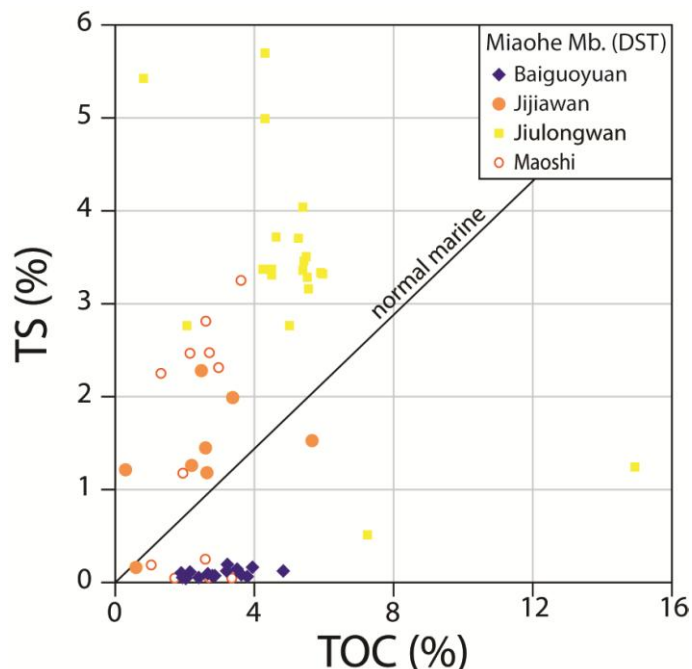


**Figure 5.12: Covariation patterns of TS vs. TOC from 4 different outcrops of the Doushantuo Miaohe Mb. Note that most values remain within an area above normal marine conditions (e.g. Berner and Raiswell, 1983) except for the Miaohe Mb. at Baiguoyuan where TS is significantly depleted with regard to TOC.**

## 5.2.6. The Dengying and Liuchapo formations

### 5.2.6.1. The geochemical profile at Wuhe (Shibantan Mb. of the Dengying Fm.)

At Wuhe, one sample from the uppermost Doushantuo Fm. and parts of the Shibantan Member of the Dengying Fm. have been analysed (see Fig. 5.13). The one sample from the Doushantuo reproduces element concentrations similar to the Jiulongwan section, which is not surprising due to the close vicinity of both sections in the Three Gorges Area (see Fig. 3.2). The Shibantan Mb. is predominantly composed of limestone with over 10% inorganic carbon and hence, due to significant dilution, very low trace- and major-element concentrations come as no surprise. The normalization of redox-sensitive trace-elements to Sc might represent a more accurate account of their respective depletion or enrichment but due to very low Sc concentrations below detection limit, element/Sc ratios exhibit a very different pattern compared to concentration profiles but are meaningless in this case. Nevertheless, TOC

contents of 1.7 and 2.6% are found at the base of the Shibantan limestone with little notable effect on TS and trace-metal concentrations although trace amounts of TOC further up correlate relatively well with trace-amounts of V, Mo, U, Ni, Cu, Mn, Ba and TS. Th/U ratios are very low, mostly due to Th concentrations below detection limit and  $V/(V+Ni)$  are between 0.57 and 0.76. Iron speciation analysis shows variable  $Fe_{HR}/Fe_T$  ratios between 0.24 and 0.79 but only very low  $Fe_T$  concentrations of below 0.1% are found within the Shibantan Mb.

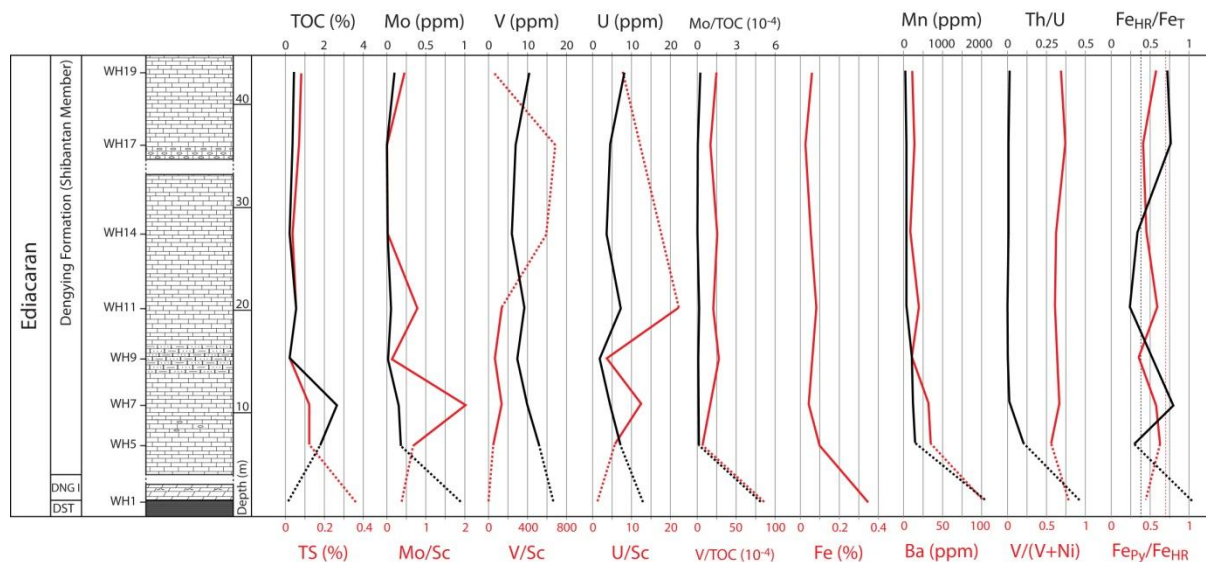


**Figure 5.13: Geochemical profile through the Dengying Fm. at Wuhe. The one sample from the uppermost Doushantuo Fm. invariably shows higher contents in redox-sensitive elements except for TOC. Normalizing them to Sc might represent a more accurate account of their respective depletion/enrichment but Sc contents are often below detection limit within the upper part of the Wuhe section which leads to unrealistically high V/Sc ratios (dashed interval is not to scale).**

### 5.2.6.2. The Huanglian section (Liuchapo and Jiumenchong formations)

The sampled interval at Huanglian consists of two black shale samples from Doushantuo Fm. and a continuous profile across the Liuchapo/Jiumenchong boundary. The two samples from the Doushantuo Fm., although stratigraphically poorly controlled, show TOC contents of up to 3.1% and most probably belong to the upper part of the formation (see Fig. 5.14). A

relatively high Mo concentration of 59 ppm and high V content of 1977.7 ppm together with depleted Ni and Cu concentrations support this interpretation. The silicified shales of the sampled Liuchapo succession all show very low concentrations of redox-sensitive trace-metals along with low Fe, Mn and Ba and, in particular, low TOC and TS contents. Across the Precambrian - Cambrian boundary, within the lowermost black shales of the Jiumenchong Fm., TOC contents increase to above 9% while TS remains relatively low at below 1%. 1-2m above the boundary, the V concentration increases to 9859.5 ppm before falling again to 3654.3 ppm 1m above. Mo gradually increases and attains 96.3 ppm on top of the sampled section. A Mo/TOC ratio of  $19 \times 10^{-4}$  is seen within the Doushantuo Fm. while the lower part of the Jiumenchong black shales is characterized by a gradual increase to up to  $10.1 \times 10^{-4}$ . V/TOC ratios are high within the Doushantuo interval but reach their maximum of  $1049.9 \times 10^{-4}$  at the base of the Jiumenchong Fm. Ni concentrations, with a maximum of 241 ppm, follow the concentration profile of V while Cu and other redox-sensitive redox-metals remain generally depleted. Ba increases into the percent range up to 1.3% in the lower Jiumenchong. V/(V+Ni) ratios vary between 0.8 and 0.99 throughout the section. Fe concentrations are very low in all samples and, except for 1.2% in one sample from the Doushantuo Fm., all below 0.7% and decrease within the upper Liuchapo Fm. before rising again at the base of the Jiumenchong Fm. Hence, Iron speciation data must be treated with caution due to probable analytical inaccuracies. P contents are depleted throughout the section with a maximum of 557 ppm within the Doushantuo Fm. and track Fe concentrations. Sulphide isotopes have only been measured in two samples, one from the Doushantuo Fm. and one from the Liuchapo Fm., and both have negative values of -4.3‰ and -6.3‰ (VCDT) respectively.

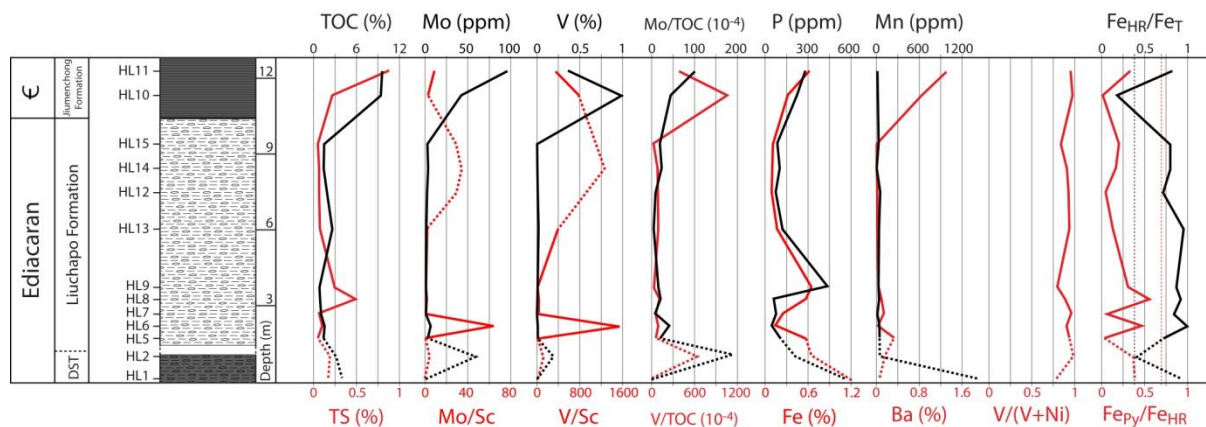


**Figure 5.14: Geochemical profile across the Liuchapo/Jiumenchong boundary at Huanglian, likely to be equivalent to the Precambrian – Cambrian boundary. Note that the two samples at the base of the section are from the uppermost Doushantuo Fm. without precise stratigraphic control.**

### 5.2.6.3. The Longbizui section (Liuchapo and Jiumenchong formations)

Within the predominantly cherty shales and chert beds of the Liuchapo Fm. a black shale interval is found where TOC and TS concentrations both attain over 3.1% within a thin horizon while Mo and U remain depleted and V is only slightly enriched to concentrations up to 338.8 ppm (see Fig. 5.15). Other trace-metals such as Ni and Cu are strongly depleted while Ba concentrations reach a peak of 2438.2 ppm.  $Fe_{Py}/Fe_{HR}$  ratios exceed 0.7 within an interval of 15cm just below and within that organic-rich horizon. Predominantly positive  $\delta^{34}S_{Pyrite}$  values attain a minimum of -0.38‰ (VCDT) 50cm below this horizon and are highly variable for the next few dm and reach 15.1‰ within the organic rich horizon itself. The following, predominantly cherty shales of the Liuchapo Fm. are characterized by TOC and TS contents under 1% and depleted trace-metal concentrations. In the overlying dark cherts and carbonate beds a significant increase in Ba concentrations to up to 2269.2 ppm takes place until the onset of the black shale succession at the Liuchapo/Jiumenchong boundary and decrease again in concert with strongly increasing trace-metal concentrations. V increases to 1936.8 ppm at the base of the black shale and decreases again within a few meters while Mo and U concentrations are still increasing to 107 and 51.6 ppm respectively before they fall again further up on top of

the sampled black shale, broadly tracking TOC and TS contents. TS contents correlate well with pyrite S although variable amounts of non-pyrite S averaging 50% of TS are observed. Fe concentrations vary between about 0.5 and 2.5% in the lower black shale horizon within the Liuchapo Fm. and remain relatively low further up until they increase again within the Jiumenchong black shales with a maximum of 3.6%. Mo/TOC ratios are low prior to the Jiumenchong Fm. where they reach values between 7 and  $15.8 \times 10^{-4}$ . V/TOC ratios on the other hand show a maximum of  $553.4 \times 10^{-4}$  just below the Jiumenchong black shales and decrease to low values between 26.4 and  $189.5 \times 10^{-4}$  further up. The maximum Mn concentration of 221 ppm is found just above the thin organic-rich interval and rapidly decreases to very low contents until a rise is seen again within the black shales.  $Fe_{HR}/Fe_T$  ratios indicate anoxic conditions throughout the section and  $Fe_{Py}/Fe_{HR}$  ratios between 0.7 and 0.8 suggest pronounced sulphidic conditions during extended intervals within the Jiumenchong black shale. Sulphide isotope values remain positive throughout the section,  $^{34}S$  being enriched in  $^{34}S$  by between 9.3 and 29.6‰ (VCDT).

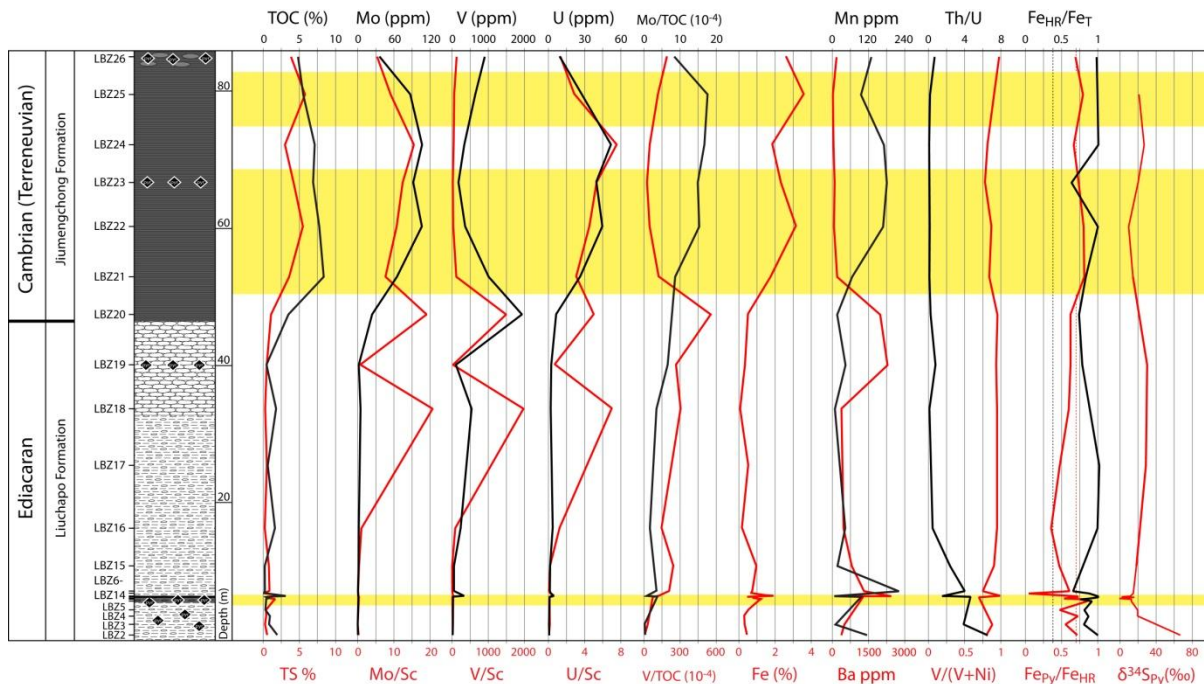


**Figure 5.15: The geochemical profile across the Precambrian – Cambrian boundary at Longbizui. The dataset including Mo, V, U, Sc, V and Ni has been kindly provided by Xi Chen (Nanjing University).**

#### 5.2.6.4. Discussion

The Longbizui section, our most complete Liuchapo/Jiumenchong boundary section, equivalent to the Precambrian – Cambrian boundary in the slope and basinal areas of the Yangtze Platform, records two euxinic events as indicated by iron speciation. The first one is indicated within a very limited interval of about 1m within the Liuchapo Fm. and a second one during the deposition of the massive black shale succession of the Jiumenchong Fm. ca. 30m above. The concentration of redox-sensitive trace-elements Mo and U remain low during the first euxinic interval but minor perturbations are observed for V, Fe, Mn, Ba and TOC contents, during the interval or right above. Although Mn concentrations attain a maximum just above the interval, concentrations are still significantly depleted as would be expected in a reducing environment and the fluctuations might be due to diagenetic remobilization and precipitation of trace-amounts of Mn-carbonate at a short-lived redoxcline. Higher V and Ba concentrations coincide with the significant increase in TOC contents within the euxinic interval due to their affinity to be fixed in the sediment in association with organic matter. The formation of significant amounts of pyrite is exemplified by comparatively elevated TS and Fe concentrations on top of the interval and coincides with highly variable sulphide isotope values whereby some are close to 0‰ and represent the lowest values found throughout the Longbizui section. This suggests episodic increases in seawater sulphate concentrations which caused euxinia to develop rapidly in an otherwise Fe(II)-limited environment. In other words, the sedimentary succession at Longbizui was deposited within a geochemically sensitive environment where minor changes in sulphate concentrations and/or organic matter delivery to the seafloor could trigger sulphidic conditions.

Within the upper black shale succession, TOC contents increase alongside redox-sensitive trace-metals, TS and Fe. While Mo and U concentrations remain enriched within the same range, V decreases soon afterwards but remains slightly enriched during the euxinic interval. The Ba enrichment within the chert beds underneath the black shales of the Jiumenchong Fm. might be used as a proxy for productivity in the photic zone as it can be assumed that sulphate-reduction did not lead to significant barite dissolution (e.g. van Os et al.,

1991; Torres et al., 1996). Thus, enhanced productivity during the Early Cambrian could have induced anoxic conditions and organic matter preservation in the deep sea which might have caused a rapid drawdown of V after an initial increase and enhanced sulphate-reduction would have remobilized Ba and ultimately lead to sulphidic conditions. Because Mo removal and fixation within the sediment mainly depends on significant concentrations of free H<sub>2</sub>S (e.g. Helz et al., 1996), one could hypothesize that reducing, anoxic environments were widespread at that time but euxinic only locally developed, which did not lead to a significantly depleted Mo reservoir during that time, additionally suggested by the undisturbed increase of Mo/TOC ratios.  $\delta^{34}\text{S}_{\text{py}}$  values remain positive but are inversely proportional to TS contents within the Jiumenchong black shale succession, indicating that fluctuating sulphate levels might have been decisive for the development of euxinia during a time of low seawater sulphate (see also above). However, several studies suggest low sulphate concentrations in the ocean of not more than 1-2 mM during most of the Precambrian until the late Neoproterozoic (see chapter 1.4; Shen et al., 2003; Canfield et al., 2004; Kah et al., 2004; Hurtgen et al., 2005; Johnston et al., 2006; Canfield and Farquhar, 2009; Ries et al., 2009), they are thought to have risen to values as high as 16mM during the Precambrian – Cambrian transition (Brennan et al., 2004). This makes sense when we consider that the black shales at the base of the Cambrian on the Yangtze Platform have often been deposited in a euxinic environment while ferruginous conditions probably dominated during the Neoproterozoic (Canfield et al., 2008; Poulton and Canfield, 2011). The apparent uniqueness of euxinic conditions on the Yangtze Platform indicates strong spatial variations in the timing of the oxygenation of the deep sea, where sulphide oxidation, possibly enhanced by the emergence of bioturbation (Canfield and Farquhar, 2009), led to globally increasing seawater sulphate concentrations and subsequently to enhanced sulphate-reduction which regionally led to increasing free H<sub>2</sub>S concentrations in the water column of the Yangtze Platform. Considering the pronounced euxinic conditions occurring during the deposition of the Miaohu Member of the Doushantuo Fm., we could hypothesize a gradual increase in oceanic sulphate levels causing euxinia on the shelf margin only (Li et al., 2010) which later, during the earliest Cambrian, developed towards the deeper portions of the basin. Alternatively, enhanced primary productivity and increasing export of organic matter to the



deep sea might have played an important role in fuelling sulphate reduction. Increased primary productivity could have caused the very high Ba contents found within the base of the Jiumenchong Fm. at Huanglian (Brumsack and Gieskes, 1983; Brumsack, 1986, 2006; Dymond et al., 1992; Tribovillard et al., 2006).

The Precambrian – Cambrian boundary section at Huanglian, ca. 70km southwest of Longbizui, exhibits a very similar geochemical profile regarding redox-sensitive trace-metals with rapidly increasing TOC, TS, Mo and V concentrations at the lowermost Jiumenchong black shale whereby V contents are rapidly falling afterwards. One major difference is that V concentrations attain almost 1% at Huanglian, which is about 5 times more than the maximum concentration measured at Longbizui while V/Sc ratios are even more than 10 times higher. V concentrations around and above 1% within basal Cambrian black shales deposited at deeper sections of the Yangtze Platform have been reported in other studies (Wallis, 2006; Guo et al., 2007). Along with an overall metal enrichment, the increase of Ba concentrations up to more than 1.3% is striking but agrees well with the occurrence of numerous Early Cambrian bedded barite deposits associated with black shales along the outer shelf parallel to the platform margin and along the northern border of the Yangtze Platform (see Fig. 5.16; Chen and Gao, 1984; Wang and Li, 1991; Maynard and Okita, 1991). The unusually abundant witherite ( $\text{BaCO}_3$ ) deposits occurring in Early Cambrian successions on the northern platform, which has not been investigated during the present study, have been interpreted as result of seawater sulphate depletion in conjunction with very high Ba concentrations (Lydon et al., 1985; Maynard and Okita, 1991). The high amount of non-pyrite sulphur within the Ba enriched horizon is enough to account for the sulphate that would be bound to 1.3% Ba (eq. to 2.2%  $\text{BaSO}_4$ ). Iron speciation analysis shows that contrary to the Jiumenchong black shale at Longbizui, euxinia was never reached at Huanglian and the high V enrichment, especially compared to Mo, indicates a dysoxic environment where sulphate-reduction played a minor role and thus barite could be preserved. A situation broadly similar between the Miaohe Mb. deposited at Jiulongwan and Bayguoyuan (see chapter 5.2.5.2.), where differences in paleo-depth have been suggested, meaning that Huanglian was deposited in deeper parts of the slope or basin with respect to Longbizui.

However, the use of Ba concentrations and barite abundance as paleoproductivity proxy has to be critically appreciated and even if sulphate-reducing conditions were not attained, high Ba enrichment might result from early diagenetic remobilization and, Ba migration through pore waters and re-precipitation where more oxidizing conditions are met (Van Os et al., 1991; Torres et al., 1996), a behaviour similar to Mn with which Ba can be involved (Dymond et al., 1992). Nevertheless, the very high TOC contents of above 9% at Huanglian might indicate that Ba can be used as a paleoproductivity proxy more confidently, especially since Mn concentrations show no correlation with Ba and both elements tend to exhibit mirroring concentrations profiles throughout the section. But from a qualitative point of view, considering the overall abundance of barite deposits on the Yangtze Platform, a significant increase in seawater sulphate concentrations and primary productivity is strongly suggested.

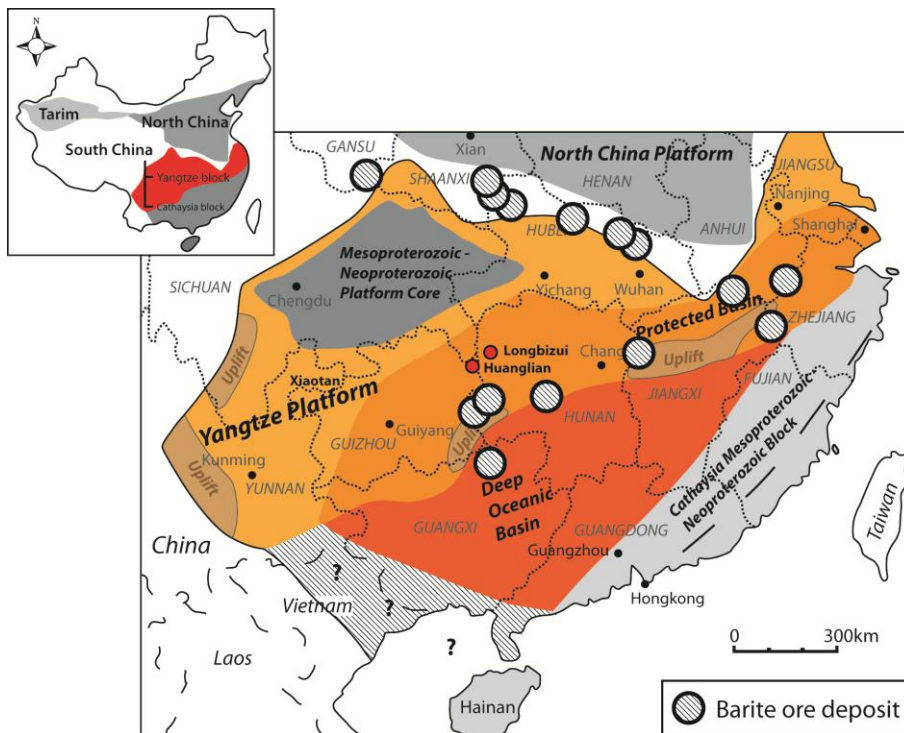


**Figure 5.16: Localities of the principal bedded barite deposits on the Yangtze Platform (modified from Wang and Li, 1991) from which the sections of Huanglian and Longbizui are slightly offset to the northwest.**

## 5.3. The Early Cambrian

### 5.3.1. The Early Cambrian in the Three Gorges Area (Shuijingtuo and Yangjiahe formations)

#### 5.3.1.1. The redox geochemistry during the Early Cambrian at the Jijiawan section

At Jijiawan, the lower Shuijingtuo has been sampled without precise stratigraphic control. However, TOC and TS contents increase stepwise towards the black shale and attain 5.8% TOC and 5.1% TS (see Fig. 5.17). There is moderate covariation between the high TOC and TS concentrations within the upper black shale, which averaging 5.1% and 3.5% respectively. TS and pyrite S correlate reasonably well although variable amounts of non-pyrite sulphur are observed, with maxima coinciding with high Ba contents of up to 4723.8 ppm. Mo and V concentrations show respective maxima of 212.8 ppm and 909.9 ppm within the lower black shale interval, where U contents also peak at 47.2 ppm. Whereas Mo and V concentrations decrease and stabilize around 40 ppm for Mo and 170 ppm for V within the upper black shale, U concentrations are more variable between 26.2 and 53.2 ppm. Ni concentrations show a broadly similar enrichment pattern whereas Cu is depleted throughout the section. Mo/TOC ratios remain below  $10 \times 10^{-4}$  throughout the section except in the metal-enriched horizon where they reach  $36.4 \times 10^{-4}$ . The V/TOC ratios behave similarly across the profile with a maximum of  $155.8 \times 10^{-4}$ . All redox-sensitive trace-metals show exhibit moderate to good correlation with TOC contents and moderate correlation with TS contents. Fe contents fluctuate between 0.3 and 2.3% prior to the onset of the black shale where a maximum of 3.5% is seen at the base and tend to decrease up-section but mostly remain above 2%. Mn is significantly depleted showing a maximum of 758.5 ppm within the same layer where U contents attain their maximum. Th/U ratios remain well below 1 and  $V/(V+Ni)$  values are highly variable below the black shale successions and remain between 0.5 and 0.68 within the overlying Shuijingtuo black shales. Iron speciation data shows high proportions of highly reactive iron with  $Fe_{HR}/Fe_T$  ratios close to 1 throughout the section while  $Fe_T$  concentrations are more variable and show low values of below 0.4% below the black shale successions where concentrations between

2.25 and 3.51% are found.  $Fe_{Py}/Fe_{HR}$  ratios have an average of 0.68 across the section whereby the lowest values are observed at the onset of the black shale intervals with a minimum of 0.56. There is a lack of sulphide isotope measurement and the only value of 18.6‰ (VCDT) has been obtained from a sample at the base of the sampled section underneath the black shales.

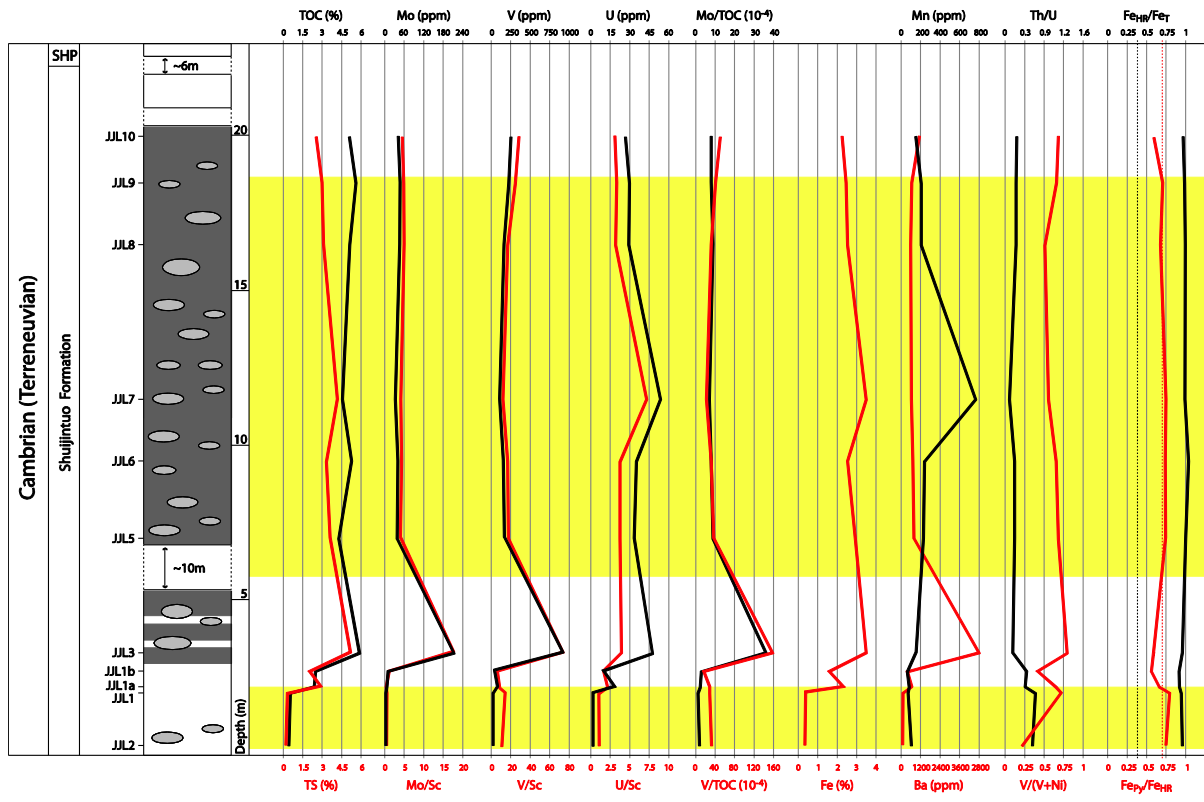


Figure 5.17: The geochemical profile analyzed from the Early Cambrian Shuijingtuo Fm. at the Jijiawan section. The yellow shaded intervals represent euxinic conditions as indicated by iron speciation.

### 5.3.1.2. The redox geochemistry during the Early Cambrian at the Wuhe section

At Wuhe, most of the Yangjiahe Fm. is poor in organic matter and redox-sensitive trace-elements (see Fig. 5.18). Within the phosphatic layer at the boundary to the overlying Shuijingtuo Fm., TOC contents increase to 2.3% together with the maximum V concentrations of 262.8 ppm. Other elements increase as well but reach their maximum more gradually further up. U reaches a maximum concentration of 119.3 ppm 1m above before decreasing again and

Mo peaks 4m above with 36.5 ppm, staying within the same range for the rest of the sampled section. The maximum Mo concentrations coincide with maximum TOC and TS contents of 3.4 and 4.4% respectively, a second peak in V content of 163 ppm, a maximum Ba concentration of 2570 ppm and peaks in Ni and Cu, although significant enrichment is not given. Fe concentrations are low within the Yangjiahe Fm. and peak at 3.5% within the black shale of the Shuijingtuo Fm. Mn contents show depleted values with a maximum within the Shuijingtuo black shale of 413 ppm. Although most of the sulphur measured throughout the section is non-pyritic, a good correlation exists between TS and pyrite S. Correlations between TOC and other elements are moderate and, considering the restricted dataset for the Wuhe section, are not significant. Mo/TOC ratios reach a maximum of  $31.5 \times 10^{-4}$  within the black shale on top of the sampled section while V/TOC ratios are very low within the black shales. Th/U ratios are well below 1 throughout the section although values are higher within the Yangjiahe Fm. and drop in the Shuijingtuo Fm. V/(V+Ni) values are variable and tend to be very low within the Shuijingtuo Fm. with a minimum of 0.32.

The  $Fe_{HR}/Fe_T$  ratios are high with a minimum of 0.66 in the uppermost sample and  $Fe_{Py}/Fe_{HR}$  ratios show a maximum of 0.71 just below the Yangjiahe/Shuijingtuo boundary. Sulphide isotopes show values below 10‰ (VCDT) until about 5m below the formations boundary and increase to values around 20‰ below the boundary around the interval with the highest  $Fe_{Py}/Fe_{HR}$  ratios. After the Yangjiahe/Shuijingtuo boundary,  $\delta^{34}S_{Pyrite}$  values decrease again and are between -4.9 and 0.1‰ (VCDT) within the lower Shuijingtuo Fm.

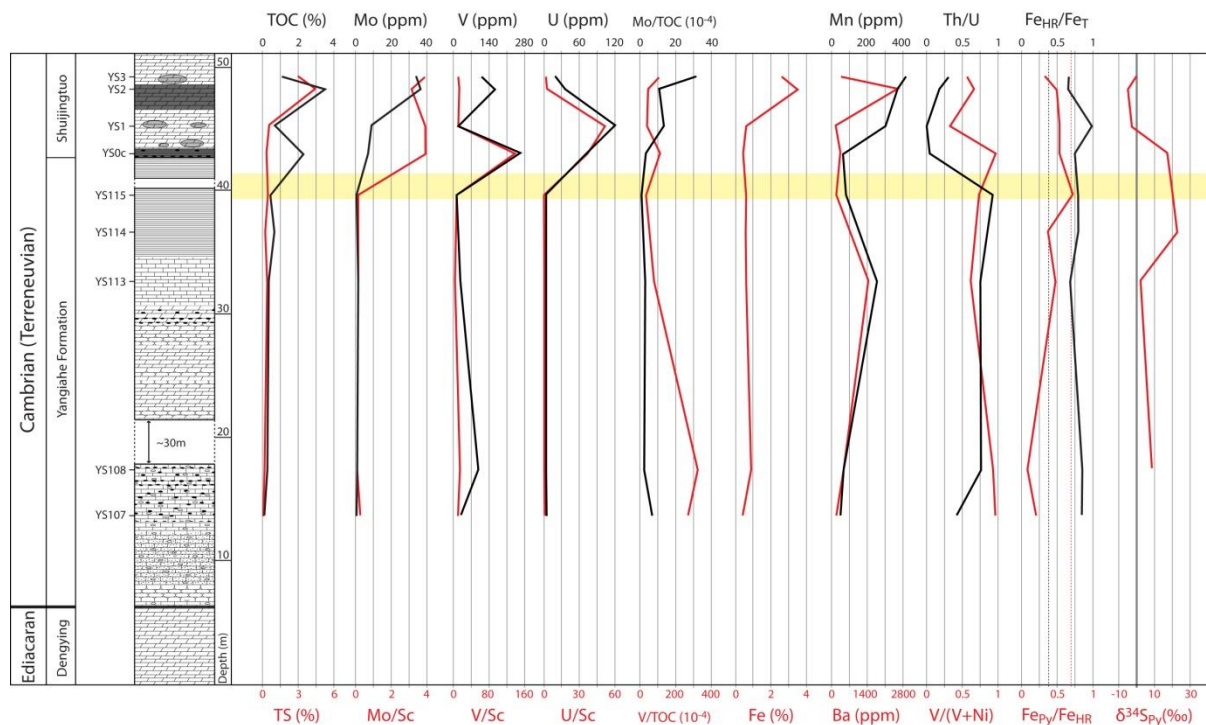


Figure 5.18: The geochemical profile across the Yangjiahe/Shuijingtuo boundary at the Wuhe section.

### 5.3.1.3. Ocean chemistry and platform evolution during the Early Cambrian:

#### The sequel

Although the stratigraphic correlation between the Early Cambrian Jijiawan and Wuhe sections is not straightforward, the enrichment pattern of the redox-sensitive trace-metals Mo, V and U are similar although with major differences in the extent, timing and the relative enrichments when compared to each other. While maximum Mo and V concentrations are between 5 and 10 times higher within the base of the Shuijingtuo Fm. at Jijiawan compared to Wuhe, it is the other way around when considering U concentrations, where maximum values are more than double at Wuhe compared to Jijiawan. At Jijiawan, the peak in Mo, V and U concentrations within the lower part of the Shuijingtuo black shale are coeval but while V contents return to values close to average shale (or UCC), Mo decreases as well but to values still significantly higher than in average shale and U remains within the same elevated range and even slightly increases further up in the black shale. One likely explanation is that euxinia

only marginally developed during the deposition of the Shuijingtuo black shale at Wuhe but happened to be pronounced at Jijiawan and that sulphidic conditions were the driving force in the removal of Mo from the water column and the preservation of organic matter along with associated V. Ba and Mn concentrations correlate well at the Wuhe section which illustrates the sometimes observed association between these two elements, probably caused by the remobilization of Ba alongside the reductive dissolution of Mn-oxyhydroxides which can lead to concomitant Ba enrichment when Mn-oxyhydroxides reprecipitate at the redoxcline (e.g. Dymond et al., 1992). At Jijiawan, maximum Ba concentrations are found within the short interval with low  $Fe_{Py}/Fe_{HR}$  which would additionally support minor sulphate-reduction.

Considering the study on the Doushantuo Fm. at the Jijiawan and Jiulongwan sections, the latter being close to Wuhe, an extended geochemical profile through the episodically occurring black shale successions can illustrate the dynamic changes in the biogeochemical cycling of redox-sensitive trace-elements and the coeval changes in the prevailing water column redox conditions (see Fig. 5.19). Iron speciation analysis shows that intermittent sulphidic conditions were common throughout the Precambrian – Cambrian transition at Jiulongwan but only appeared during the Early Cambrian at Jijiawan. While most of the analysed geochemical parameters differ significantly between Jiulongwan and Jijiawan during the deposition of the Miaohu Mb., we find similarities around the Early Cambrian Yangjiahe/Shuijingtuo boundary such as an increase of Mo/TOC ratios within the same range. It appears as if significantly increasing concentrations of dissolved redox-sensitive trace-metals and sulphate determined ocean chemistry at the end of the Doushantuo Fm. before 551 Ma leading to very high trace-metal accumulation and negative sulphide isotope signatures.

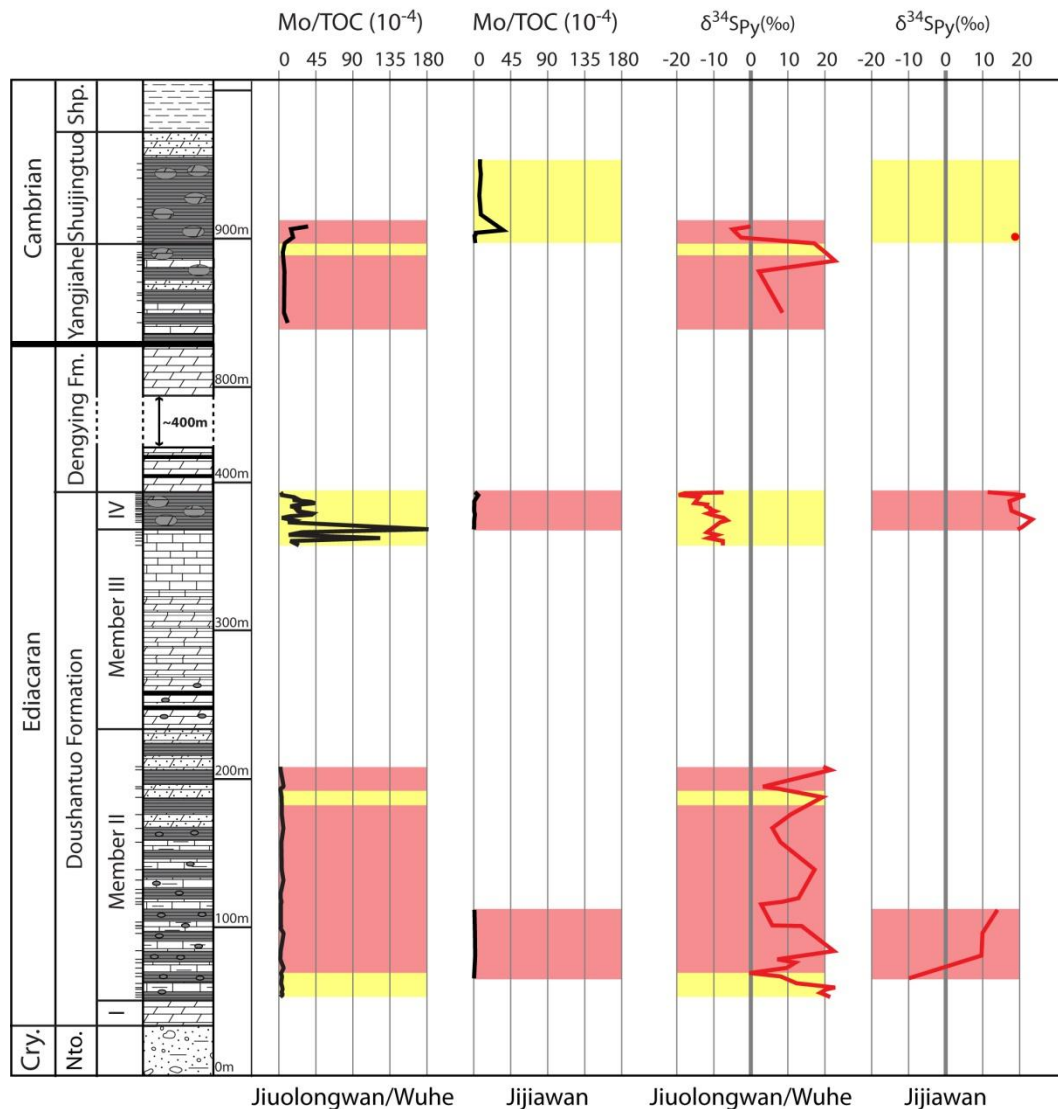


**Figure 5.19: Schematic stratigraphic profile as it appears in the Three Gorges Area, Hubei Province, with a considerably shortened Dengying Fm. for better display. The reddish shaded intervals indicate anoxic-ferruginous conditions and the yellow shaded intervals suggest a euxinic depositional environment.**

However, during the Early Cambrian, the Jiuolongwan (Wuhe) and Jijiawan depositional environments seem to have been connected and enjoyed similar seawater chemistry caused by the Yangtze Platform approaching open shelf geometry (see Fig. 5.6b). The more distally deposited Early Cambrian black shales at Huanglian and Longbizui as well exhibit Mo/TOC ratios



and sulphide isotope values similar to the sections around the Three Gorges Area and point to widespread euxinic conditions from the platform shelf down to the basin which consequently gave rise to increased pyrite burial and sulphate limitation. The increase in bio-available Mo and V in a dominantly ferruginous ocean might have triggered unprecedented primary production and organic matter delivery to the ocean floor, which on the one hand created conditions favourable for intensified sulphate-reduction and the diagenetic remobilization of Ba which reprecipitated as barite in deeper portions of the ocean (see chapter 5.2.3.), accelerating the seawater sulphate drawdown and suggesting non-euxinic conditions below an extended wedge of free H<sub>2</sub>S reaching towards the open ocean (see Fig. 5.20). However, a steady source of sulphate must have sustained euxinia and concomitant barite deposition over an extended amount of time. Canfield and Farquhar (2009) demonstrated that the emergence and intensification of bioturbation during the Precambrian – Cambrian transition (Martin et al., 2000) would have caused a several fold increase in seawater sulphate concentrations and initiated the extensive deposition of evaporite minerals throughout the Phanerozoic.

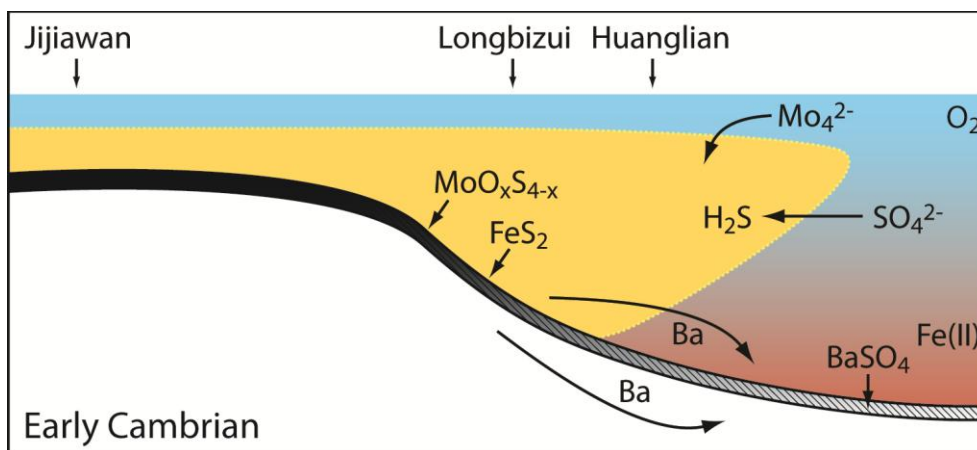


**Figure 5.20: Open shelf model showing how an enhanced source of sulphate to the water column would have widened a sulphidic wedge while sulphate-reduction played a minor role in the deeper parts of the ocean and thus allowing the accumulation of bedded barite deposits. A constant source of sulphate would have been required to sustain widespread euxinia and barite deposition which probably arose after the emergence and intensification of bioturbation (Canfield and Farquhar, 2009).**

### **5.3.2. The Zhongnan section (Niutitang Formation): A highly condensed succession on the platform margin**

#### **5.3.2.1. Geochemical analysis**

The sampled succession can be broadly subdivided into two parts (see Fig. 5.21). The lower part is predominantly composed of phosphate, with P contents of up to 15%, and poor in organic carbon (mostly less than 1%) and silicate (less than 20%). The upper part is composed by a black shale succession with high TOC content of up to 11%. The sulphide ore horizon is situated right above the lower phosphatic part and highly enriched in Fe, Mn, Cu, Ni, Ba, Zn and Mo but only Mn, Cu, Ni, Ba and Zn reach their maximum within this layer. Mo/TOC exhibits a prominent maximum peak at the sulphide ore layer while V/TOC is relatively high throughout the phosphorite until beyond the sulphide ore layer and varies considerably between 0 and 1600 within the remaining succession. Fe reaches its maximum of 16.1% about 15 cm above together with a peak in sulphur concentration. Although TS and pyrite S contents correlate very well throughout the section, there is significant non-pyrite S occurring within the ore layer which can be attributed to other metal sulphides. 5 cm above, TOC reaches its first peak with a concentration of 9.65%. With TOC, there is a concomitant rise in V content and a minor increase in Mo, Cu and Ni while Fe concentrations are very low again, down to around 1% and less. The decrease in TOC to below 2% 20 cm above is accompanied by a second peak in Cu, Mo and to a minor extent Zn content, and the first peak of V. 70 cm above, V decreases again to 487.3 ppm while other trace-metals show low and even depleted concentrations. The maximum TOC value within the recorded Zhongnan section of 11.08% is measured 35cm above and accompanied by concomitant peaks in Cu, Ni, Zn, Cr, Mo and V. The remaining 1.5m show an initial decrease in Mo and V before both concentrations rise again. There is an overall decrease in Cu, Ni and Zn and a slight increase in Ba in the uppermost 1.5m of the section. Mo/TOC ratios are extremely high within the ore horizon which is mostly due to very low TOC contents which mainly below 1%. Within the overlying black shales, Mo/TOC ratios are

relatively high with a peak of  $48.5 \times 10^{-4}$ . V/TOC ratios exhibit a similar pattern and correlate well with Mo/TOC ratios within the black shale above the ore layer ( $R^2 = 0.85$ ).

V/(V+Ni) varies between 0.75 and 0.99, exception made for a particularly low ratio of 0.42 within the sulphide ore layer. Iron speciation data shows lower  $Fe_{HR}/Fe_T$  ratio of 0.37 within the sulphide ore layer among generally high values which decrease upwards to values down to 0.3.  $Fe_{Py}/Fe_{HR}$  ratios reach values of over 0.8 just above the ore layer. Sulphide isotopes were measured for an interval of 20cm and show positive values above 4‰ (VCDT) including the sulphide ore layer where values peak at 11.1‰ (VCDT).

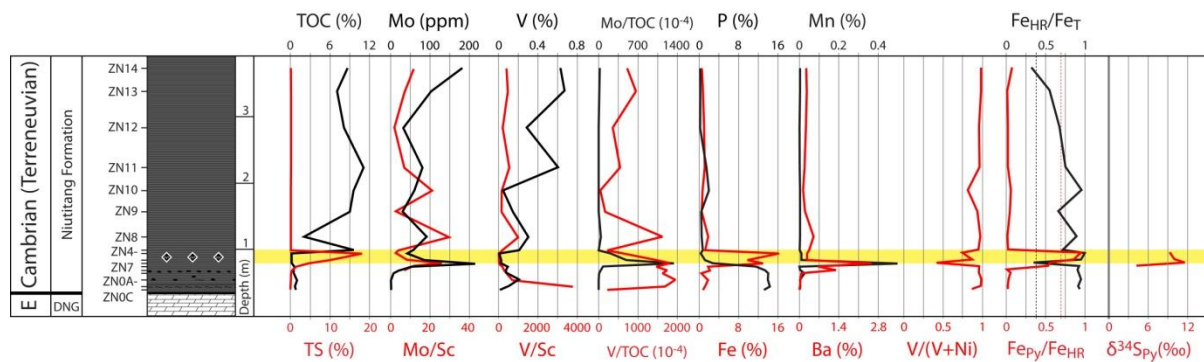


**Figure 5.21: The geochemical profile of the condensed Early Cambrian sedimentary succession at Zhongnan.**

### 5.3.2.2. Discussion

#### The phosphorite

P reaches the sediment via the deposition of organic material and is released as  $PO_4^{3-}$  during reductive dissolution of Fe-oxyhydroxides and/or organic matter remineralization and it either escapes back to the water column or precipitates within the sediment (e.g. Span et al., 1992; Louchouart et al., 1997; Kidder et al., 2003; Sannigrahi and Ingall, 2005; Ruttenger, 2003). Bacterial mediation plays a significant role in phosphogenesis, especially through sulphate reduction and fermentation (e.g. Tribovillard et al., 2006; Papineau, 2010). Under

anoxic conditions, P usually diffuses upwards from the sediment to the water column where it can return to the photic zone and further stimulate primary production or its concentration increases in the anoxic zone (Ruttenberg, 2003). P cycling being very efficient, Benitez-Nelson (2000) estimated that only 1% of organic P remains trapped within the sediments. Under certain conditions, mainly controlled by alkalinity, pH, Eh and bacterial activity (e.g. Benitez-Nelson, 2000), P remains in the sediment and authigenic P minerals can precipitate, principally apatite which explains the excellent covariation with Ca in our section. High P concentrations can be achieved by high organic matter supply but also in association with the redox cycling of Fe (Piper and Perkins, 2004; Algeo and Ingall, 2007) or Mn (Wang and Van Cappellen, 1996) and are therefore not necessarily indicative of a high organic matter flux (Tribovillard et al., 2006). In oxic environments, redox-cycling of Fe limits the diffusive flux of remineralized P to the surface and Fe-oxyhydroxides retain P within the sediment allowing enough time for the slow growth of authigenic P phases. In permanently anoxic environments with sulphidic bottom waters, Fe-oxyhydroxides do not precipitate within the sediments and P is therefore less likely to be retained. In order to form highly enriched phosphorite deposits such as in the Zhongnan section, hydrodynamically induced winnowing of sediments usually plays an important role. The extraordinary widespread occurrence and abundance of Early Cambrian phosphate deposits worldwide (Cook, 1992) are pointing to major changes in the biogeochemical cycling of phosphorus and are likely to pinpoint the transition from elevated oceanic P concentrations in the Precambrian to lower levels in the Phanerozoic (Planavsky et al., 2010), which together with favourable paleoceanographic constellation led to these massive phosphorite formations.

### **The Ni-Mo sulphide ore horizon**

The black shale associated Ni-Mo sulphide ore, which can contain Mo concentrations of up to several percent, has been reported from several locations along the platform margin within transgressional and highly condensed facies (Coveney and Chen, 1991; Lott et al., 1999; Steiner et al., 2001; Lehmann et al., 2007; Wille et al., 2008; Pašava et al., 2008; Chen et al., 2009; Wen and Carignan, 2011). Although metalliferous black shale successions are particularly

common during the Precambrian-Cambrian transition (e.g. Pašava et al., 2003; Lyons et al., 2006), the particular association of metals, including such anomalous enrichment in Mo, has provoked much controversy about the mechanism behind the origin of the Ni-Mo sulphide ore layer on the Yangtze Platform. While some advocate a sedimentary-exhalative (SEDEX) origin (Lott et al., 1999; Steiner et al., 2001; Pašava et al., 2004), others concluded that the metal enrichment derived directly from seawater (Mao et al., 2002; Lehman et al., 2007).

At Zhongnan, not all trace-metals are enriched within the ore horizon itself, i.e. Pb, Cr and V show higher concentrations within the phosphorite and above the ore layer where they are relatively depleted. This might on the one hand be related to the “open” structure of apatites, which allow many elements to substitute for Ca, PO<sub>4</sub> and F (e.g. Prévôt and Lucas, 1980; Jarvis et al., 1994; Tribovillard et al., 2006). However, it is difficult to explain why these particular elements have been enriched and not others, such as Zn and Mo, although they are likely to be affected by this substitution process as well. Nonetheless, the enrichment of Pb, Cr and V above the ore layer is concomitant with an almost two magnitude increase in TOC which might also have led to higher concentrations of other metals, in particular Fe and Ni.

Ni and Cu are predominantly delivered to the sediments in association with organic matter (Tribovillard et al., 2006) but only Ni exhibits a good covariation with TOC when the extremely high Ni content within the ore layer is excluded. The Mo vs. TOC plot exhibits no correlation at all and where sulphidic conditions are indicated through high Fe<sub>Py</sub>/Fe<sub>HR</sub> ratios, low TOC and moderate Mo contents represent somewhat counterintuitive results. Furthermore, the highest Mo concentrations are found in layers with the lowest Fe<sub>HR</sub>/Fe<sub>T</sub>. There is a good correlation between V and TOC concentrations prior to the increase of TOC contents to values above 2% but none within most of the organic rich black shales.

This contradictory behaviour of the investigated geochemical parameters does so far not support a seawater origin for the metal-enriched horizon which is itself neither enriched in TOC nor pyrite. Instead, a suite of a metal-rich horizon (Fe, Mn, Ba, Cu, Ni, Zn, Mo) followed by a pyrite layer and finally by a high TOC layer is observed while other trace metals (Pb, Cr and V) are enriched within the phosphorite). Such a successive suite of different metal-enrichment has not been reported from other occurrences of this Ni-Mo sulphide ore horizon and it might as

well represent an artefact which can arise from sampling or diagenetic mobilization and re-precipitation of redox-sensitive elements governed by steep redox-gradients.

### **5.3.3. The Xiaotan section**

#### **5.3.3.1. The redox geochemistry of its black shale successions**

Due to the extended character of the sampled Xiaotan section, the results have been subdivided into three black shale succession, the 1<sup>st</sup> and 2<sup>nd</sup> at the base and top of the Shiyantou Fm. and the 3<sup>rd</sup> in the lowermost Yuanshan Fm., whereby the last one includes the overlying organic poor sediments sampled at lower resolution until the overlying Canglangpu Fm.

#### **1<sup>st</sup> black shale (lower Shiyantou Fm.)**

The first black shale succession at the base of the Shiyantou Fm. is about 36 m thick and shows appreciable TOC concentrations with a maximum of 5.02% at the base and averaging 2.92%, while TS contents remain very low with a maximum of little over 0.3% (see Fig. 5.22). Mo concentrations are also very low, remaining close to average shale values except within the first black shale sample where it reaches a value of 20 ppm. V concentrations on the other hand reach a maximum value of 2147.9 ppm, over 21 times the average shale value, and are relatively high in the middle part of this first black shale succession. Such as in most previously discussed black shale successions, normalizing Mo and V contents to Sc does not significantly alter the overall pattern. There is no covariation between Mo and V, while very high V values tend to occur in samples where Mo concentrations are very low. Mo/TOC ratios show a peak at the beginning of the succession and then gradually rise towards the upper part of the black shale. Mo and TOC are only weakly correlated with  $R^2 = 0.36$ . V/TOC ratios can be relatively high and generally follow the same pattern as the V concentration profile. V correlates with TOC with  $R^2 = 0.32$ . Fe contents peak at the base of the Shiyantou Fm., decrease shortly after to

a minimum of 1.1% before an overall increasing trend across the black shale until Fe concentrations reach their maximum of 3.5% at the base of the overlying shales. P concentrations are highest (1%) within the boundary zone between the Dahai Mb. and the Shiyantou Fm. and remain variable for the next ca. 10m before stabilizing at lower values around 0.1% for the rest of the section. Mn contents show a maximum of 688.4 ppm at the boundary but decrease to low values between 40 and 200 ppm within the Shiyantou Fm., nonetheless describing a slightly increasing trend in concentrations, weakly mirroring Ba contents between a minimum of 384.7 ppm at the boundary and a maximum of 1310.2 ppm on top of the overlying black shale. The V/(V+Ni) yields values of mostly above 0.84. In this lowermost black shale succession,  $Fe_{HR}/Fe_T$  ratios remain above 0.38 but  $Fe_{Py}/Fe_{HR}$  close to 0, therefore indicating an anoxic, ferrous-iron rich water column without any significant amount of free H<sub>2</sub>S. A gradual decrease in  $Fe_{HR}/Fe_T$  as we move towards the top of the black shale can be observed while  $Fe_{Py}/Fe_{HR}$  ratios remain extremely low.

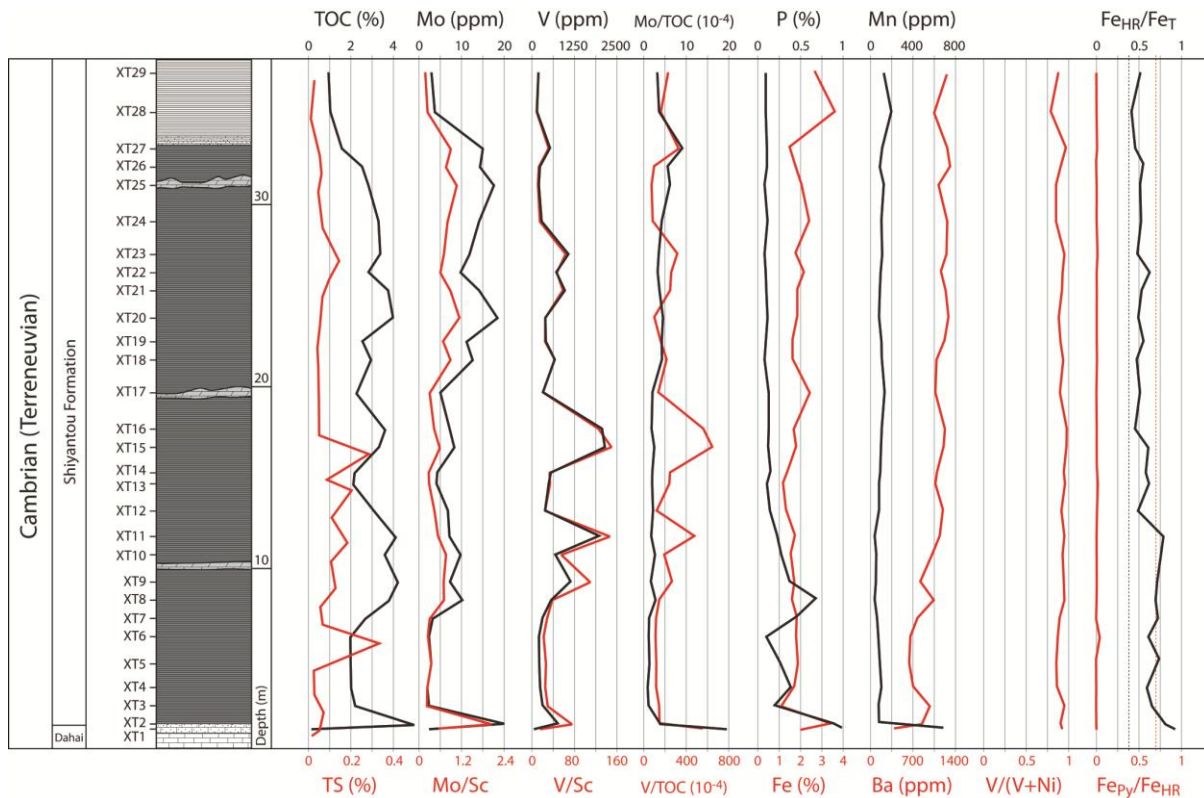


**Figure 5.22: The geochemical profile through the 1<sup>st</sup> black shale at the base of the Shiyantou Fm. at Xiaotan.**

### **2<sup>nd</sup> black shale succession (upper Shiyantou Fm.)**

The second black shale succession in the upper Shiyantou Fm. (XTY1-XTY30), with a thickness of about 39m, contains slightly lower TOC concentrations than in the previous black shale but sulphur contents are highly variable increasing to up to 1.52% in some layers within the upper half above a 2.5 m thick succession of more massive carbonate beds (see Fig. 5.23). Mo concentrations are still relatively low but slightly elevated in the upper part of the 2<sup>nd</sup> black shale, attaining a maximum of 18.95ppm. Fe concentrations are highly variable between 1.4 and 4.4%, increasing irregularly towards the upper part of the black shale. Mn contents are very low and fluctuate around 130 ppm until the onset of strongly metal-enriched black shale beds where a concentration of over 0.5% has been found together with pronounced, major enrichment of Ni (up to 556.8 ppm) and Zn (up to 1345.6 ppm) along with Li (251 ppm), Be (19.4 ppm) and Sc (185.4 ppm). V is markedly less enriched compared with the 1<sup>st</sup> black shale succession and does not exceed 306.4ppm. There is neither a correlation between Mo and V, nor between Mo and TOC, or V and TOC (see Fig. 5.24). Th/U ratios are mainly above 2 and V/(V+Ni) ratios average 0.82. An interesting feature is the very distinct peak in Ni concentrations, on top of the 2<sup>nd</sup> black shale, which increase from 36.5 to 285.5 up to 556.8 ppm before decreasing again to 28.1 ppm within only 3 m (see Fig. 5.25).  $Fe_{HR}/Fe_T$  values can be taken to indicate deposition under an anoxic-ferruginous water column although one value (0.36) is below the threshold of 0.38.  $Fe_{PY}/Fe_{HR}$  remains low but some peaks are clearly visible, sometimes concomitant with low  $Fe_{HR}/Fe_T$ , indicating that the proportion of pyrite iron sometimes accounts for most of the highly reactive iron. Sulphide isotopic values are negative throughout, with a maximum of -3.7‰ (VCDT), and tend to decrease towards to metal-enriched layer where a minimum of -17.5‰ (VCDT) is observed.



### 3<sup>rd</sup> black shale succession and beyond (Yuanshan Fm.)

The black shale succession at the base of the Yuanshan Fm., with a thickness of about 10m, begins with high TOC contents of up to 4.74% which rapidly decrease to moderate values and finally below 1% after 10 m for the rest of the section (see Fig. 5.23). Sulphur contents on the other hand remain below 0.5% at the base and increase to a maximum of 1.16% in the TOC poor carbonate/shale sediments, leading to a bimodal TOC and S covariation pattern for the Yuanshan Fm. (see Fig. 24). The Mo concentration profile begins with a maximum of 39.24 ppm which rapidly decreases and very closely follows the TOC content with  $\text{Mo (ppm)} = 8.6 \times \text{TOC (\%)}$  and  $R^2 = 0.98$ . V concentrations are slightly less well correlated with TOC ( $R^2 = 0.67$ ) and peaks a bit above the base of the Yuanshan black shale with 660.6 ppm. Vanadium decreases at a slower pace than Mo and shows greater variability throughout the succession while both, Mo and V, are correlated with each other with  $R^2 < 0.6$ . U, contrary to the previous black shale successions, also shows a moderate correlation with TOC with  $R^2 = 0.54$ . Fe concentrations increase at the onset of the black shale succession and reach a maximum of 5.3% after 3.3m and varies between 2.4 and 4.8% for the rest of the Yuanshan Fm. whereby minima correspond to maxima in Mn contents which fluctuate between a few hundreds to 2805 ppm and minima in Ba concentrations down to 644.6 ppm within the Yuanshan Fm. Both, Mn and Ba concentrations are otherwise uncorrelated to Fe contents. Mo/TOC ratios are higher than within the previous black shale successions but rather variable as well, peaking at a maximum of 20.47. V/TOC ratios are variable but show a gradual trend towards higher values at the top of the Yuanshan Fm. The redox proxy  $\text{V}/(\text{V}+\text{Ni})$  decreases from 0.95 to 0.78 towards the top of the Yuanshan Fm. and Th/U ratios show higher values (to a maximum of 6.39) in the sediments above the black shales. The  $\text{Fe}_{\text{HR}}/\text{Fe}_{\text{T}}$  ratio reaches values below 0.38 within the upper black shale and persists until the end of the Yuanshan Fm. while pyrite iron increases to a maximum of 50% highly reactive iron within the carbonate/shale sequence above the black shale.  $\delta^{34}\text{S}_{\text{py}}$  values are positive at the onset of the black shale succession with a value of 3.1‰ (VCDT) and decrease afterwards with some variations mostly within the negative range but with two

positive peaks of 1.5 and 12.6‰ (VCDT) which correspond to pronounced minima in TOC, V, Fe and Ba concentrations and maxima in Mn concentrations.

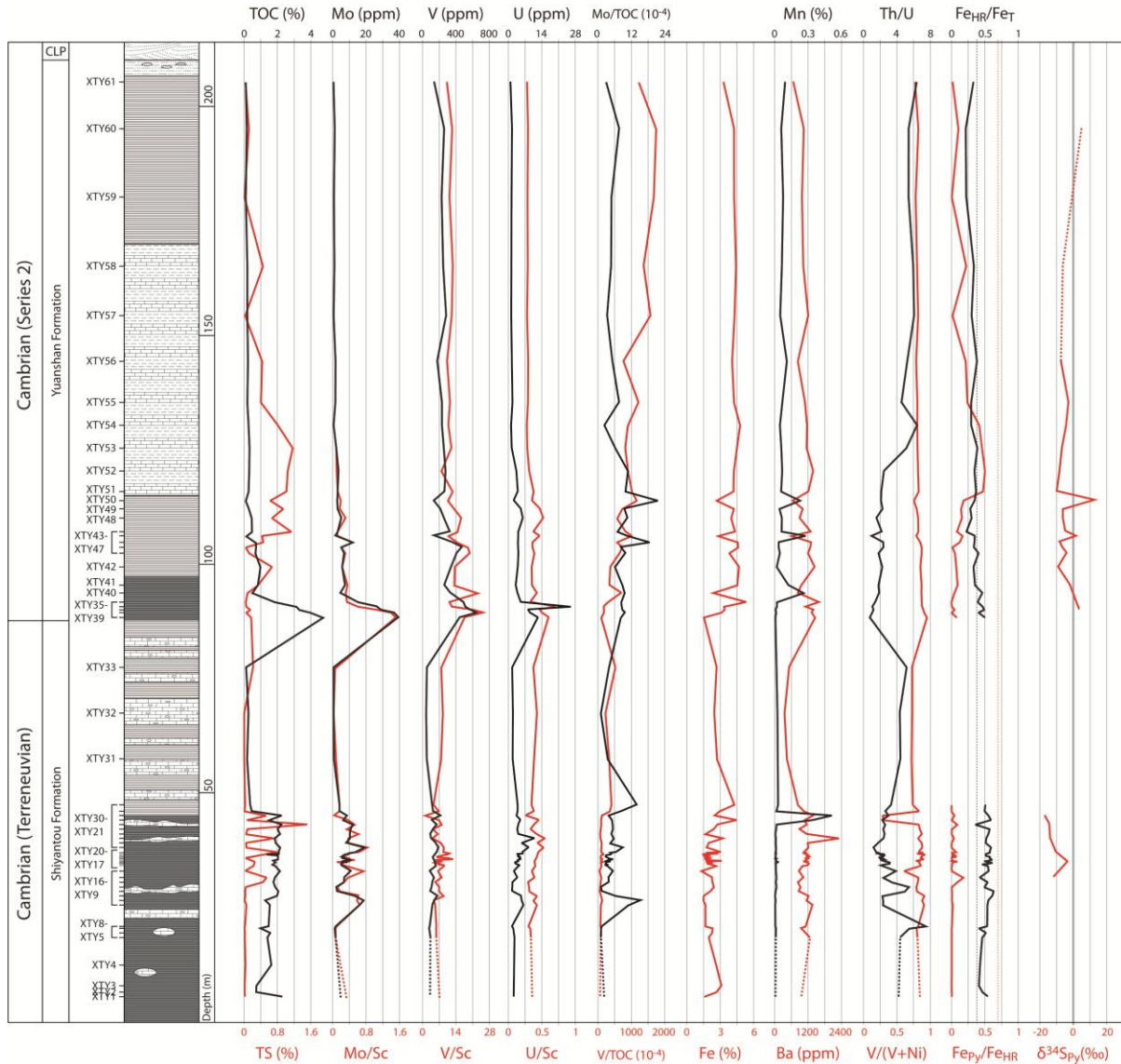


Figure 5.23: The geochemical profile across the Shiyantou/Yuanshan boundary, until the overlying Canglangpu Fm. (CLP), showing the 2<sup>nd</sup> and 3<sup>rd</sup> black shale succession.

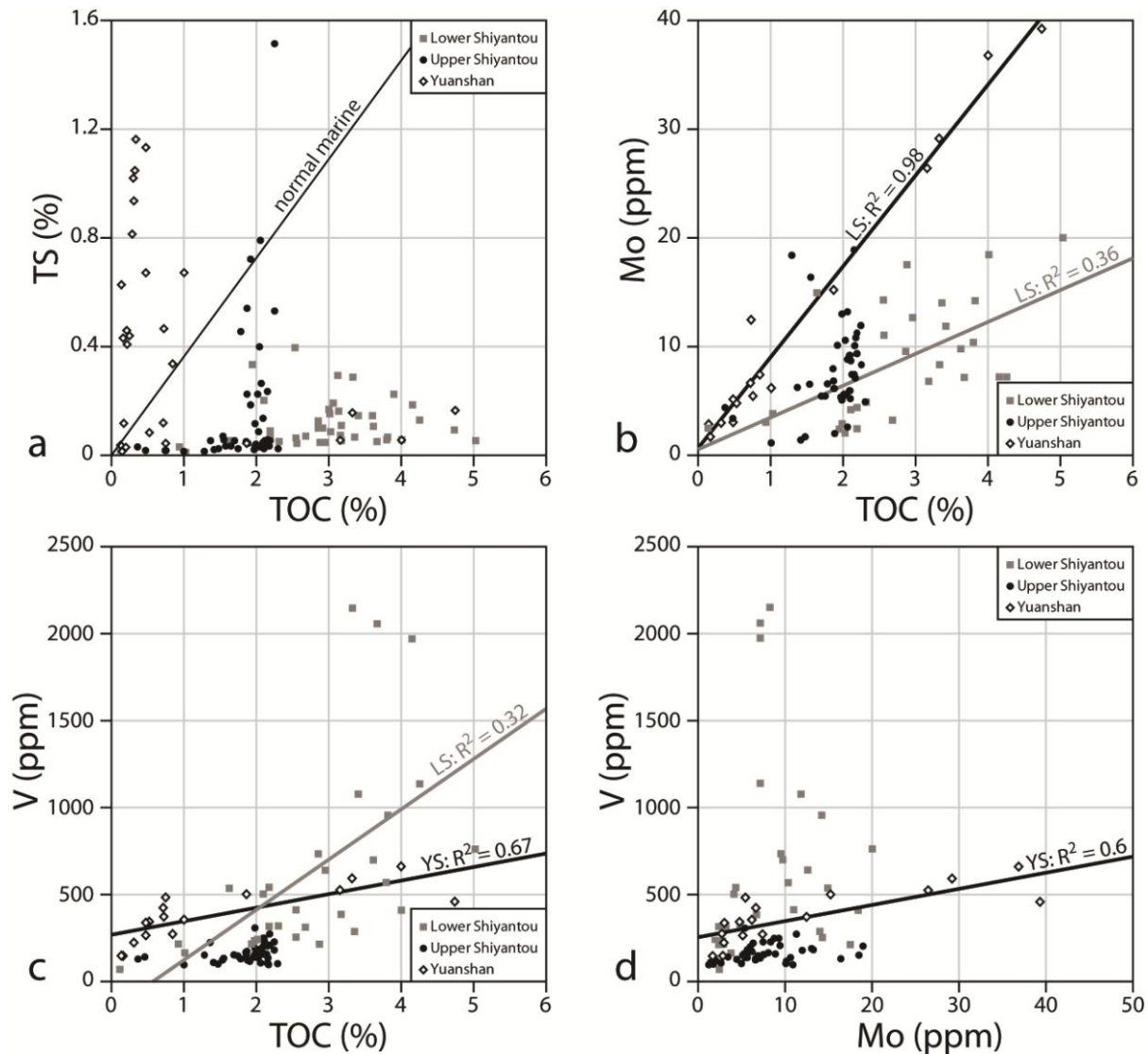


Figure 5.24: Covariation patterns between some geochemical parameters divided in the three black shale successions seen within the Early Cambrian black shales at Xiaotan.

### 5.3.3.2. High resolution sampling: results and discussion

The section sampled at higher resolution spanning part of the 1<sup>st</sup> black shale at the base of the Shiyantou Fm. (XTS1-14) shows generally more variability in the analysed geochemical parameters than the section sampled within the 2<sup>nd</sup> black shale at the top of the Shiyantou Fm. (see Fig. 5.25). For XTS1-14, note that within 1.2 m, TOC fluctuates between 2.53 and 4.74%

and TS between 0.05 and 0.39% while there is no or only negative correlation between the two parameters. Mo remains very low and varies between 3.41 and 14.53 ppm while V concentrations change within a large range of between 407.9 and 1574.74 ppm. There is no correlation between Mo and TOC, but instead for Mo and TS over that short distance, indicating incorporation of Mo into sulphurized organic matter (Tribovillard et al., 2004) and possibly also Mo fixation by adsorption onto pyrite surface (Huerta-Diaz and Morse, 1992; Helz et al., 1996; Bostick et al., 2002). V, on the other hand, follows the TOC profile more closely. Mo/TOC and V/TOC vary according to the trace metal pattern. In both intervals, Fe concentrations remain within a similar range of between 0.8 and 2.7% for the one within the lower Shiyantou and between 1.4 and 3.1% for the interval in the upper Shiyantou Fm. Mn and Ba concentrations are also varying within a similar range in both intervals, with Mn averaging 76.6 ppm within the lower interval and 149.6 ppm in the upper interval. Ba contents average 976.8 and 1171.7 ppm respectively. Iron speciation data confirm an anoxic-ferruginous depositional environment with  $Fe_{HR}/Fe_T$  fluctuating above 0.38 and  $Fe_{Py}/Fe_{HR}$  being close to zero. As already mentioned, the high resolution data from the 2<sup>nd</sup> black shale (XTY17-20) shows little variation with TOC contents averaging 2% while TS varies between 0.02 and 0.79 % at the top. Mo varies between 5.14 and 13.24 ppm and V remains closely around 190 ppm, Mo/TOC and V/TOC vary accordingly. Th/U shows an average of 2.35 but iron speciation suggests deposition under an anoxic-ferruginous water column while  $Fe_{Py}/Fe_{HR}$  remains close to zero.

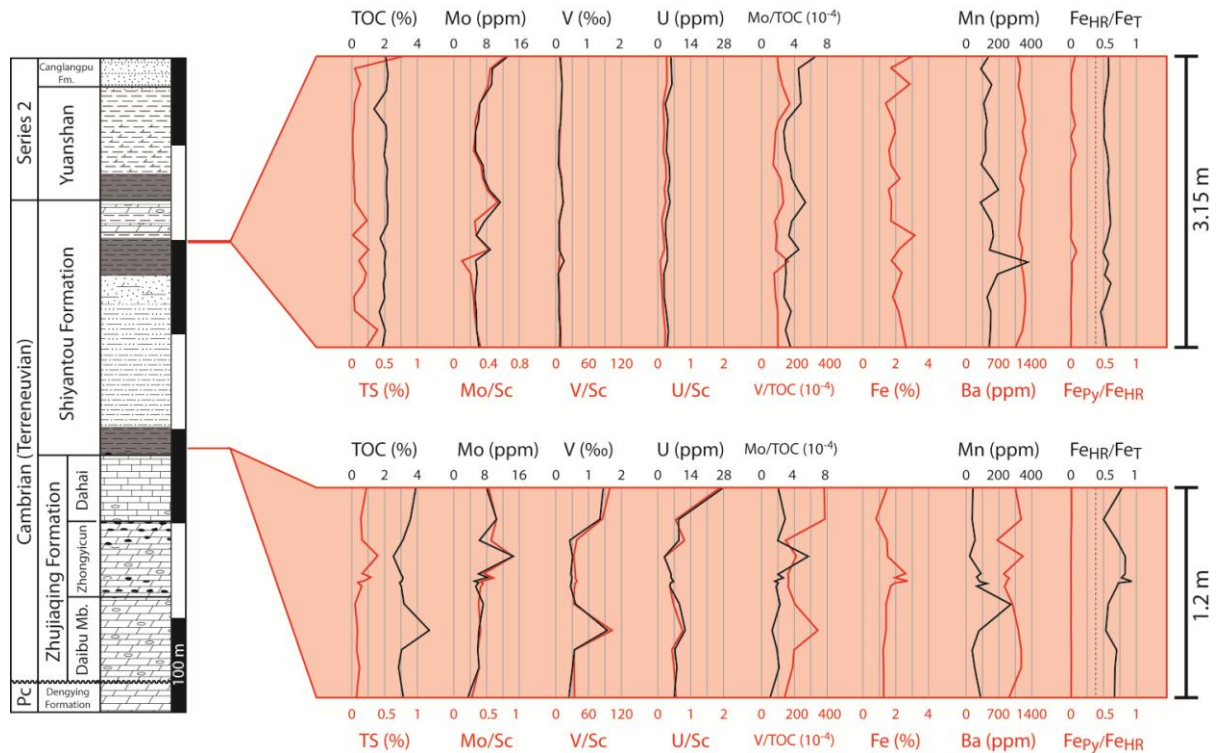


Figure 5.25: The geochemical profiles of higher resolution intervals taken within the lower and upper Shiyantou black shale successions.

### 5.3.4. Other Early Cambrian sections on the southwestern platform (Yunnan Province)

#### 5.3.4.1. The Deze Section (Zhongyicun Fm., Dahai Mb.)

The predominantly carbonatic lithology of the Dahai Mb. is TOC and TS poor throughout and accordingly depleted in redox-sensitive trace-metals as well as in Fe and Mn (see Fig. 5.26). Only Ba is significantly enriched with concentrations between 701.7 and 2163.2 ppm. Cu tracks TOC contents very well while Ni is only weakly correlated. A moderate correlation is seen between V and U and TOC but not between Mo and TOC. No covariation is found between TS, which is almost fully bound as pyrite S, and TOC contents. Th/U ratios are variable around 2 and  $V/(V+Ni)$  between 0.7 and 0.91. Iron speciation suggests anoxic-ferruginous conditions throughout the section with  $Fe_{HR}/Fe_T$  values close to 1 and  $Fe_{Py}/Fe_{HR}$  ratios below 0.5. A few

sulphide isotopic compositions have been measured and indicate pyrite enriched in  $^{34}\text{S}$  with  $\delta^{34}\text{S}$  values between 9.5 and 21.6‰ (VCDT).

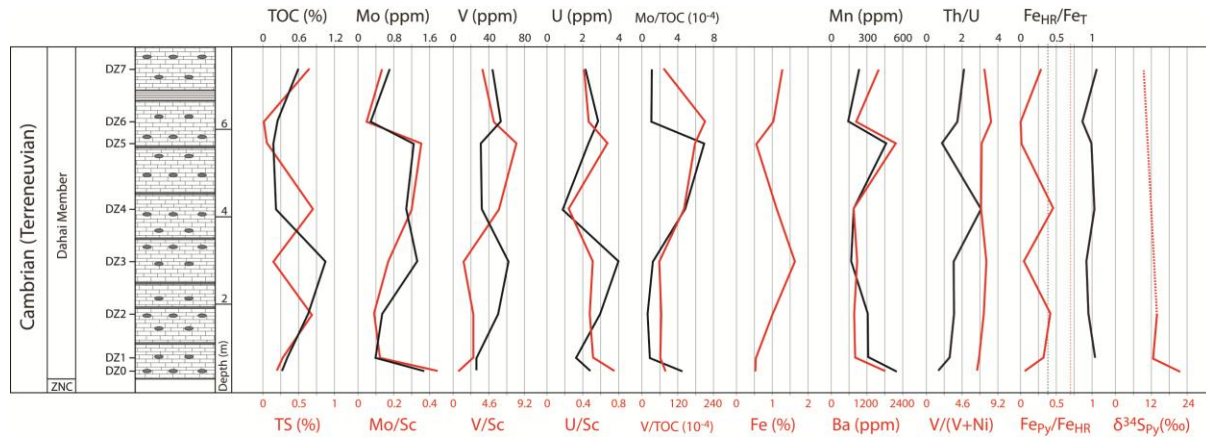


**Figure 5.26: The geochemical profile through the lower part of the Dahai Mb. (Zhujiqing Fm.) which is mainly composed of carbonates and some chert beds.**

#### 5.3.4.2. The Meishucun Section (lower Shiyantou Fm.)

The stratigraphically poorly correlated samples from the lower Shiyantou Fm. at Meishucun show moderate TOC contents, which correlate negatively with comparatively high TS concentrations reaching values of 2.36% (see Fig. 5.27). Mo varies between 3.7 and 9.44 ppm and correlates with V concentrations varying between 150.5 and 459.1 ppm. Only two samples have been analysed for U which remains around 10 ppm with Th/U ratios of 0.51 and 0.94. Mo/TOC ratios average 4.5 and V/TOC ratios fluctuate around 230, both being in the same range as the ratios found throughout Xiaotan. Fe concentrations tend to increase through the section from 2.2% to over 3%. Mn and Ba concentrations do not demonstrate enrichment but indicate a mirror pattern where the highest Mn content of 811.9 ppm coincides with the lowest Ba concentration of 270.8 ppm at the lowermost part of the section. In addition, no significant enrichment is seen for Ni and Cu with concentrations around average shale (or UCC) values but both elements correlate moderately well with TOC contents. Around the Shiyantou/Yuanshan boundary, overall low concentrations of trace-metals coincide with high TS concentrations of

up to 3.4% and very high P content of up to 10.8%. V/(V+Ni) values remain within a narrow range of between 0.71 and 0.88. Iron speciation analysis indicates anoxic-ferruginous conditions but rather high  $Fe_{Py}/Fe_{HR}$  ratios of up to 0.72 indicate intermittently euxinic conditions. Sulphide isotope analysis indicates variable  $\delta^{34}S_{Pyrite}$  values between -14.4 and 2.2‰ (VCDT).

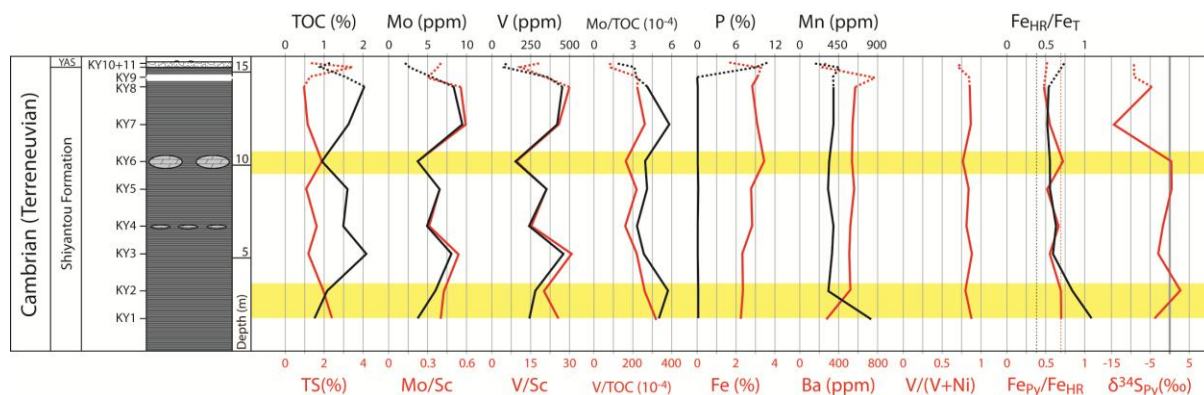


**Figure 5.27: A geochemical profile through an interval within the lower part of the Shiyantou black shale at Meishucun. Note that the Shiyantou/Yuanshan boundary is at an undefined stratigraphic height.**

### 5.3.5. Discussion: Biogeochemical cycling during the Early Cambrian on the southwestern Yangtze Platform

The present study demonstrates that the three black shale successions at Xiaotan exhibit rather different geochemical characteristics (see Fig. 5.28). Plotting TS vs. TOC (see Fig. 5.24a) shows that from the 1<sup>st</sup> black shale upwards, S/C ratios tend to increase without correlating, even while average TOC contents slightly decrease and average TS concentrations increase. From the 1<sup>st</sup> to the 3<sup>rd</sup> black shale succession we find clearly increasing average Fe, Mn and U concentrations and slightly increasing Ba and S concentrations. While Mo values are highest within the 3<sup>rd</sup> black shale succession, V contents are highest in the 1<sup>st</sup> black shale such as are TOC contents. Mo and V vs. TOC (see Fig. 5.24b) show moderate correlation in the 1<sup>st</sup> black shale and good correlation in the 3<sup>rd</sup> black shale succession. Other redox-sensitive trace-

metals such as Ni and Cu are depleted and exhibit no clear trend. While iron speciation data analysis suggests anoxic-ferruginous conditions throughout the deposition of the sampled section, we find  $Fe_{HR}/Fe_T$  ratios consistently below 0.38 above the last black shale in the Yuanshan Fm.

The Early Cambrian on the Yangtze Platform shows, at least in the South, significant differences in sediment thicknesses, which have also been demonstrated for the Ediacaran Doushantuo (Vernhet, 2007) and late Ediacaran Dengying formations (Steiner et al., 2007). And the Xiaotan section represents one of the most expanded and probably most complete section covering the Precambrian-Cambrian transition in South China or even worldwide. Increasing S/C ratios towards the Yuanshan Formation could imply a transition to more open marine conditions with increased circulation leading to increased concentrations of sulphate in the seawater intensifying sulphate-reduction and pyrite precipitation. Other studies have demonstrated a variable but generally low sulphate reservoir in the ocean across the Precambrian-Cambrian ocean which increased throughout the Phanerozoic (e.g. Canfield, 2004; Hurtgen et al., 2009). Recently, Canfield and Farquhar (2009) hypothesized that sulphate levels in the ocean significantly increased after the onset of bioturbation around 555 Ma (Martin et al., 2000). Alternatively, the upwelling of sulphide-rich water masses from deeper levels of the Yangtze Platform, which has been shown to have been at least intermittently euxinic in transitional settings on the platform margin, such as in Zhongnan and Meishucun (e.g. this study; Canfield et al., 2008), might explain the apparent decoupling of TOC and sulphur contents in the upper black shales. However, such a putative  $H_2S$  release to surface waters has been hypothesized by Wille et al. (2008) to explain transient Mo isotope signals in another Early Cambrian succession close to Zhongnan on the Yangtze Platform margin. Furthermore, total sulphur is increasingly equivalent to pyrite sulphur towards the top of the Yuanshan Formation (see Fig. 5.29) while an important fraction of TS in the lower black shales is mostly non-pyritic and probably represents sulphur bound to organic matter and other S phases. This might indicate that sulphate-reducing conditions were not met during the deposition of the earlier black shale successions, i.e. a reducing setting merely reaching denitrifying conditions, which is also supported by very high V enrichment and virtually no Mo enrichment in the 1<sup>st</sup> black shale.



However, such an explanation fails to explain why Mo, V and U are all not significantly enriched in the upper successions towards the Shiyantou/Yuanshan boundary, which might be due to anoxic draw down of the trace-metal reservoir which is indicated within the interval sampled at Meishucun, where minimum Mo and V concentrations are found within the euxinic intervals.

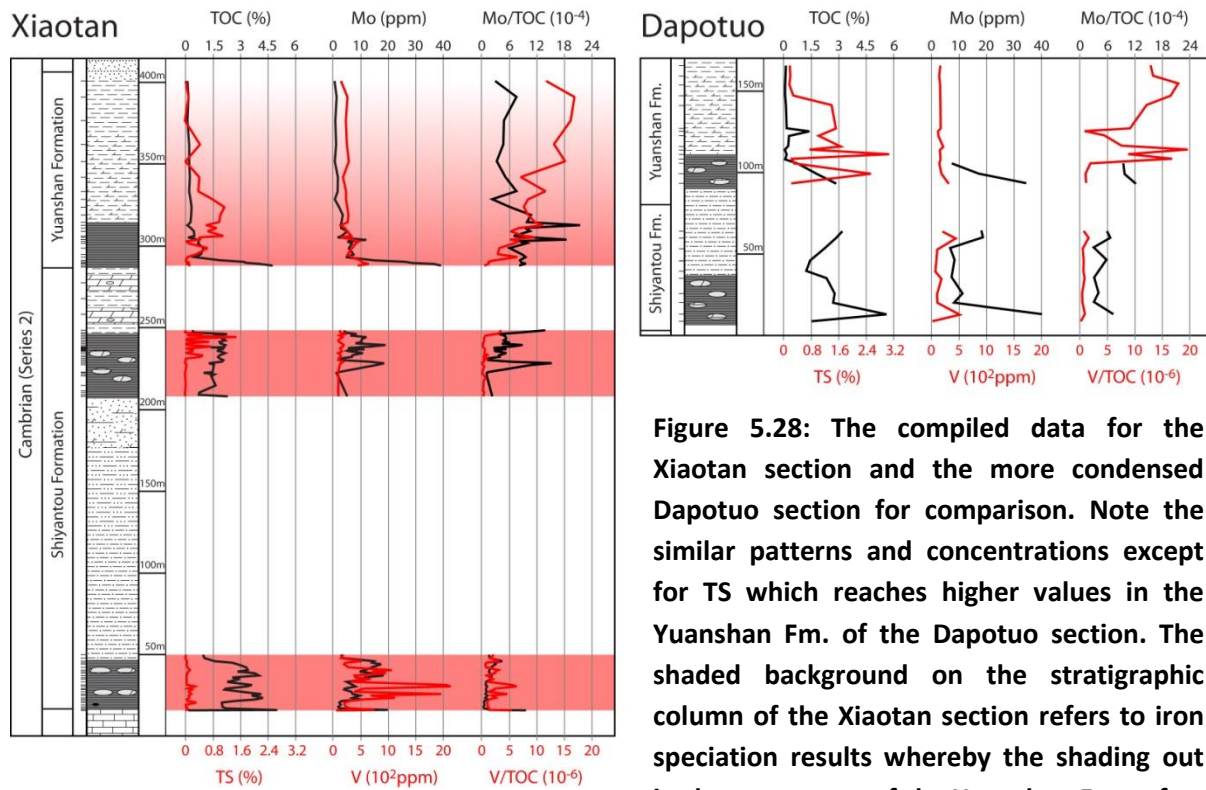


**Figure 5.28:** The compiled data for the Xiaotan section and the more condensed Dapotuo section for comparison. Note the similar patterns and concentrations except for TS which reaches higher values in the Yuanshan Fm. of the Dapotuo section. The shaded background on the stratigraphic column of the Xiaotan section refers to iron speciation results whereby the shading out in the upper part of the Yuanshan Fm. refers to  $Fe_{HR}/Fe_T$  ratios below the threshold firmly confirming anoxia of 0.38.

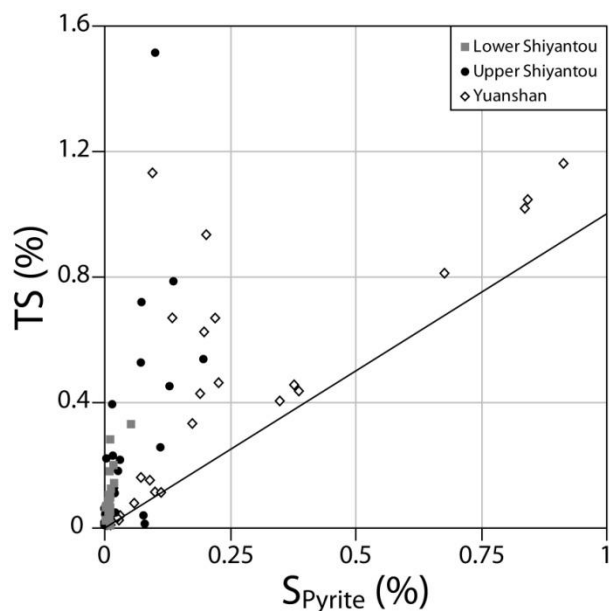


**Figure 5.29: There is significant non-pyrite sulphur in the lower two black shale members and good correlation and almost exclusively pyrite sulphur in the 3<sup>rd</sup> black shale succession in the Yuanshan Fm. The two data points below the 1:1 line represent measurements with very low sulphur content prone to inaccuracies.**

The transition to open marine conditions and increasing trace-metal availability is supported by overall increasing Mo/TOC ratios. But we must keep in mind that strictly speaking, the Mo/TOC ratio as proxy for Mo availability only applies in sediments deposited under euxinic conditions, where quantitative removal can be expected. Nevertheless, similar Mo/TOC ratios within the intermittently euxinic Shiyantou Fm. at Meishucun suggest that Mo might have been a limiting nutrient during the Early Cambrian on the southwestern platform. The perfect correlation between Mo and TOC in the black shale at the base of the Yuanshan Formation suggests a water column with more abundant Mo which leads to Mo removal at the same rate as organic matter burial or the transition from a weakly reducing depositional setting to sulphate-reducing conditions, evidenced by the increasing ratio of pyrite sulphur to total sulphur. Above the last black shale succession, Iron speciation and Th/U ratios suggest that bottom waters might have developed towards less reducing conditions, at Xiaotan but also at Dapotuo (see appendix for the detailed dataset).

Iron speciation data suggests intermittent euxinia during the deposition of the lower Shiyantou Fm. at Meishucun with very high sulphide contents. This either indicates highly variable redox conditions on the Yangtze Platform or, because the Meishucun samples have been collected in an actively exploited mine, that Xiaotan is weathered to some extent. On the other hand, the nearby Dapotuo section also exhibits high TS contents and suggests higher

sulphur/pyrite contents further south on the Platform. The use of V/TOC ratios to infer fluctuations of the V reservoir cannot necessarily be applied accordingly and we suggest that redox conditions are primarily controlling V accumulation in the sediment although it can be argued that the V reservoir is significantly affected by the early sequestration from denitrifying conditions already, which would lead to its depletion after the deposition of the 1<sup>st</sup> black shale.

The relative inconsistency of the different paleoredox proxies including V/(V+Ni), Th/U and iron speciation together with overall low trace-metal concentrations approaching average shale (except for V in the 1<sup>st</sup> black shale) are striking. V/(V+Ni) seems particularly inappropriate when used to infer sulphidic conditions. Several reasons have to be considered: (1) the probably restricted access to the open ocean of wide regions on the Yangtze Platform leading to suppressed trace-metal enrichment, (2) an overall transitional character of trace-metal geochemistry during the late Neoproterozoic and early Cambrian and (3) a likely sulphate-poor basin inhibiting sulphate-reduction and subsequent development of euxinic conditions. Consequently, the use of paleoredox proxies involving redox-sensitive trace-metals might be preferably restricted to Phanerozoic, post-Cambrian studies only.

A conspicuous Ni enrichment horizon occurs in the upper Shiyantou Fm. which despite the relatively coarsely resolved sampling shows a gradual increase within about 2m. We argue here that this Ni peak in Xiaotan might be correlated with the intensely studied Ni-Mo sulphide layer found along the platform margin. The origin of this unusual Ni and Mo enrichment found along the platform margin is still not agreed upon. Whereas some suggest a hydrothermal origin (e.g. SEDEX deposits: Lott et al., 1999; Steiner et al., 2001) others advocate a seawater origin (Mao et al., 2002; Lehmann et al., 2007) or multiple sources for the observed metal enrichment (Pašava et al., 2008). Age constraints are often imprecise: there exists a Pb-Pb age of 521±54 Ma for the metalliferous horizon itself and a Pb-Pb age of 531±24 Ma for the underlying black shales (Jiang et al., 2006). A more recent, more precise U-Pb SHRIMP age of 532.3±0.7 Ma from a volcanic ash bed between the phosphorites and the Ni-Mo layer (Jiang et al., 2009) sets a narrower timeframe and emphasizes the extremely condensed character of the early Cambrian sediments within the transitional belt but would not conflict with U-Pb ages set by Compston et al. (2008) for the middle Zhongyicun Mb. of 539.4±2.9 Ma and for the basal

Shiyantou Fm. of  $526.5 \pm 1.1$  Ma. There is a distinct possibility of two separate metal enrichments: an earlier one due to SEDEX-type mineralisation including Ni as a typical element and a second one due to redox processes leading to high TOC and Mo accumulation (see Fig. 5.30), which only appear to be coeval within the strongly condensed sedimentary successions at the platform margin. In addition, the high sulphide contents with concomitant low TOC levels and the inferred euxinic conditions at Zhongnan might well correspond to the elevated pyrite levels above the last black shale at the base of the Yuanshan Fm. at Xiaotan, where the strong bimodal covariation pattern of TOC and TS are also observed. Moreover, the earlier V enrichment seen in the bottom Shiyantou Fm. at Xiaotan, below the Ni-Mo horizon at Zhongnan and other Early Cambrian section, which can attain a few percent as well (e.g. Wallis, 2006; Guo et al., 2007), additionally supports a platform-wide correlation based on redox-sensitive trace-metals. The succession of Ni-Mo enrichment, pyrite horizons and high TOC contents has not been reported elsewhere and is probably due to diagenetic redistribution or, because of a certain conglomeratic character of the interval (see also Steiner et al., 2001), the sampling could have lead to a slightly altered rendition of the true geochemical situation to some extent.

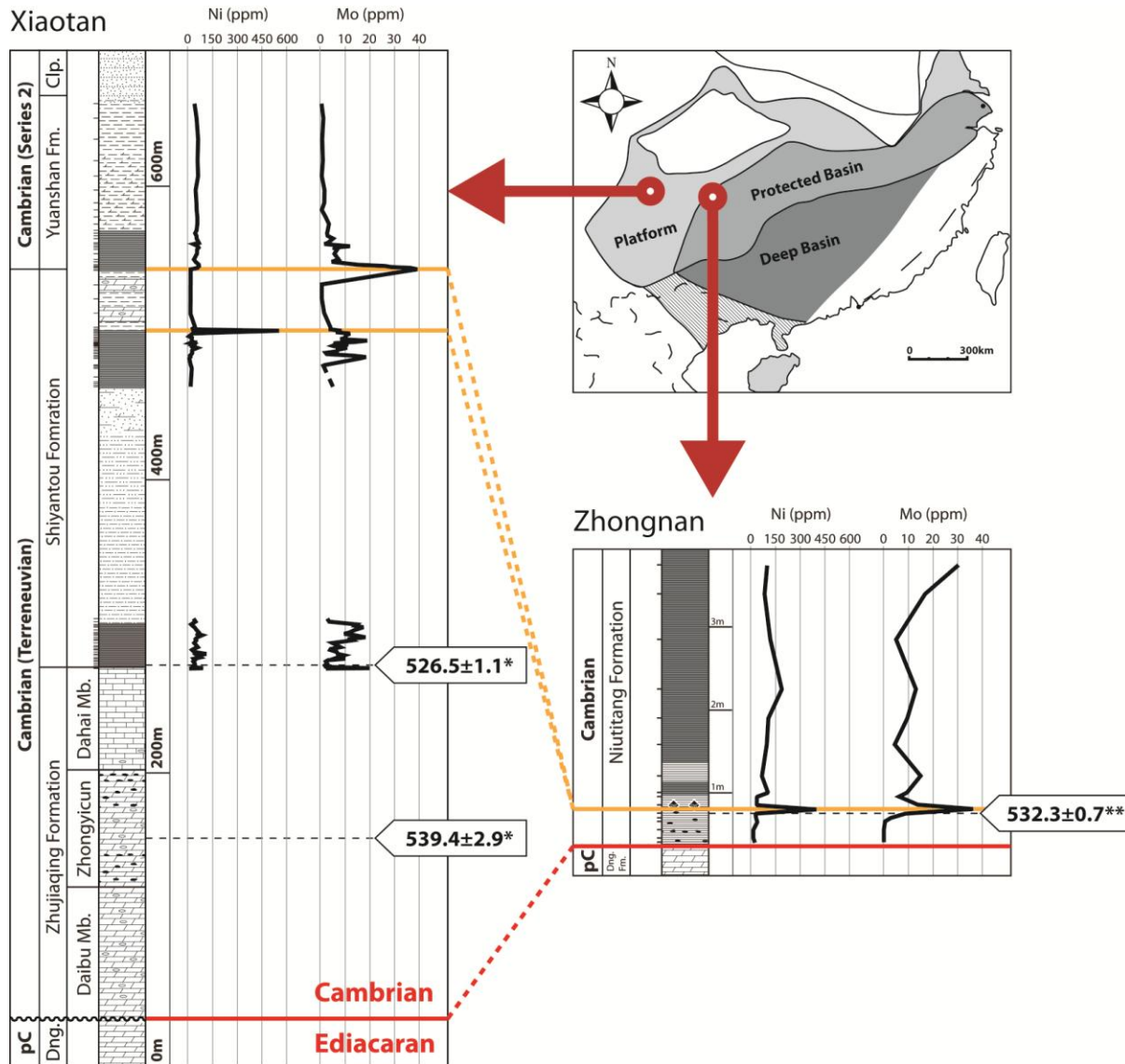


**Figure 5.30: A possible correlation can be established between the highly metalliferous black shales of the lower Niutitang Fm. in the transitional belt and the distinct Ni peak found within the upper Shiyantou Fm. Precise age constraints are sparse (\*Compston et al., 2008; \*\*Jiang et al., 2009: between the phosphorite and the ore layer) but do not contradict the possibility of such a geographically extensive geochemical Ni marker horizon.**

The present study shows that the geochemical record can be explained by invoking long and short-term water depth fluctuations indicating overall rising eustatic sea level leading to increased Mo/TOC ratios and subsequently to an influx of H<sub>2</sub>S from the adjacent deeper regions

and basin of the Yangtze Platform (see Fig. 5.31). The latter is suggested by dominantly low Mo enrichment at Xiaotan, significant occurrence of non-pyrite sulphur and bimodal TOC vs. TS covariation patterns which indicate low sulphate-reduction rates in the platform interior but upwelling of sulphide rich waters from the basin. Furthermore, the extensive and relatively undisturbed sedimentary successions at Xiaotan in comparison to the stratigraphy in the South of Yunnan Province suggest a deeper region on the Yangtze Platform around today's Xiaotan section. Furthermore, it is indicated that a peak of very high Nickel concentrations within the upper Shiyantou Fm. followed by elevated Mo enrichment several meters above can be correlated with the conspicuous Ni-Mo-sulphide ore horizon found along the platform margin where the stratigraphy is strongly condensed (see Fig. 5.30). This would successfully help to solve the mystery of coupled extreme Ni and Mo enrichment by attributing the Ni-sulphide ore to a sedimentary-exhalative process and the subsequent Mo enrichment to sequestration due to increased Mo reservoir and an anoxic water column. However, the depth of Xiaotan could not have sustained the benthic life found at the well preserved fossil deposits at Chengjiang, where bioturbation has been documented and indicates at least intermittently oxic bottom waters (Conway Morris, 1989; Dornbos et al., 2005) although the typical Chengjiang Biota most likely represents an assemblage transported away from a nearby, more life-prone environment (Zhang and Hou, 2007; Gaines and Droser, 2010). Increased access to the open ocean during the Early Cambrian could on one hand have led to the upwelling of nutrients onto the Yangtze Platform together with sulphide-rich water which would have immediately precipitated as pyrite due to Fe(II)-rich waters without leading to euxinic bottom waters in the Xiaotan region. The higher sulphur contents and the putative development of euxinic environments further south of the Yangtze Platform could suggest proximity to the open sea, and probably their position and depth with respect to upwelling nutrients. As euxinia has been demonstrated for Early Cambrian successions deposited in the basin (previous chapters; Canfield et al., 2008), a triangular model such as Li et al. (2010) proposed for the Late Ediacaran cannot be supported nor refuted by the situation found on the southwestern platform. On the other hand, the addition of large shallow-water continental margins would have made the colonisation by recently evolved metazoans possible while still maintaining an environment which would

favour fossil preservation under anoxic conditions as well as episodic extinction events. Widespread anoxic and even euxinic environments on the south-western Yangtze Platform, possibly represented in Meishucun, could provide necessary preservation traps which gave us the perfectly preserved Chengjiang Biota. While it is unclear how and whether the upwelling of sulphide-rich waters over a probably extended amount of time impacted on the biosphere it is nevertheless interesting to see that the deposition and preservation of the exceptional Chengjiang Biota on the Yangtze Platform closely followed this interval. Future studies will hopefully reveal whether the biological innovations witnessed in the fossil record at Chengjiang were delayed, preserved or even made possible through a fragile and diverse environment creating numerous niches of differing biogeochemical parameters and thus acting as an evolutionary laboratory.

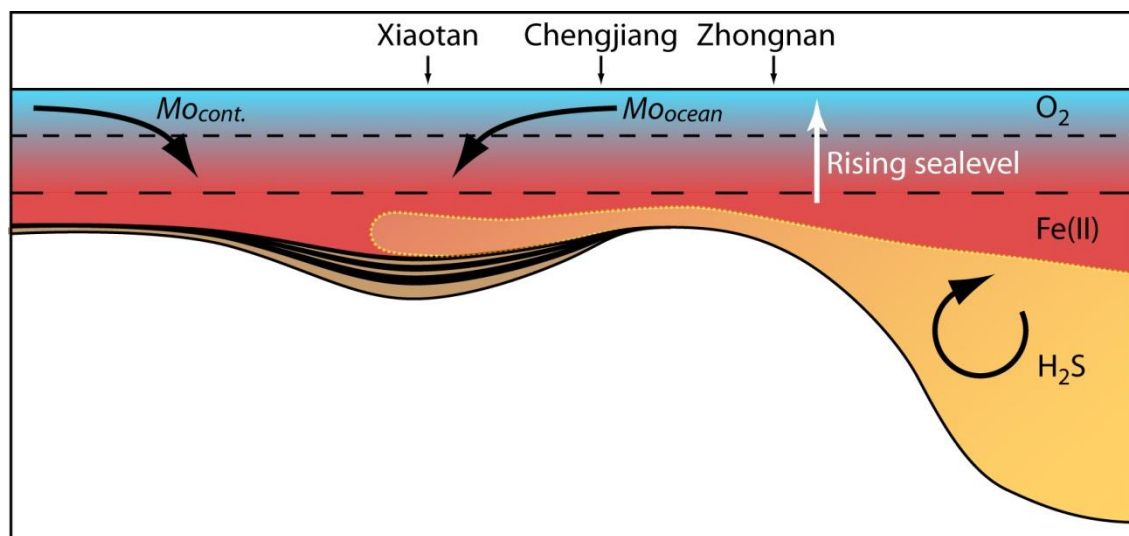


**Figure 5.31:** A possible model of the situation on the southwestern Yangtze platform with rising sea levels first leading to an increase in the Mo budget and subsequently to the upwelling of H<sub>2</sub>S into the inner platform. The position of the sections analyzed refers to their distance from the open ocean.

#### **5.4. Biogeochemical cycling across the Precambrian – Cambrian transition on the Yangtze Platform: a summary and global perspective**

The application of redox-sensitive trace-metals (Mo, V and U) have proven to be a valuable tool to infer paleoredox conditions in Phanerozoic marine sediments (see reviews by Tribouillard et al., 2006; Meyer and Kump, 2008; Lyons et al., 2009) when cautiously applied in combination with other, independent redox indicators such as stable isotopes and iron speciation and a good understanding of the architecture of the depositional environment with regard to physical barriers affecting trace-metal availability in the water column (e.g. Algeo and Lyons, 2006). This approach is more complicated for Precambrian sediments when low oxygen levels limited oxidative weathering, hence causing a limited renewal of the oceanic trace-metal reservoir from the continents, and widespread anoxic or even euxinic deep waters might have efficiently drawn down the seawater inventory of redox-sensitive trace-metals (e.g. Scott et al., 2008). The rise in atmospheric oxygen levels and the ventilation of the deep sea during the Neoproterozoic Oxygenation Event mark, amongst other major revolutions on the Earth surface, the transition from marine sediments predominantly poor in redox-sensitive elements to highly enriched black shales (see chapter 2). Regardless of the mechanism, it can be assumed that a significant increase in dissolved trace-metals concentrations in the ocean took place whereas the timing remains under debate and most likely did not follow a globally uniform pace, which can be illustrated by available data on Mo and V concentrations in black shales between 700 and 400 Ma (see Fig. 6.1 and 6.2). Although there is a scarcity of black shale data coming from localities outside the Yangtze Platform, we observe some enrichment within the interglacial Datangpo Fm. (~663 Ma) and then a gradual increase from lower Mo concentrations to a peak at the base of the Cambrian followed by a gradual decrease throughout the Paleozoic (see Fig. 6.1a). In addition to high Mo enrichment presented in this study, very high Mo concentrations are found within a black shale succession deposited around the Precambrian – Cambrian boundary within the Ara Group, Oman (Schröder and Grotzinger, 2007; Wille et al., 2008) while only minimal enrichment has been reported from basal Cambrian black shales from the Tarim Basin, Northwest China (Yu et al., 2009). However, variations of Mo/TOC ratios across the same



interval are clearly dominated by values reported from the Yangtze Platform and suggest an extraordinary and particularly efficient removal of Mo from the water column within the depositional environment on the Yangtze Platform. The temporal trends in V accumulation in black shales (see Fig. 6.2a) follow a similar pattern, describing a sharp rise from the late Ediacaran and a peak in the earliest Cambrian. Although concentrations decrease for the rest of the Paleozoic, values above 2000 ppm remain common. Apart from black shales from the Precambrian – Cambrian boundary on the Yangtze Platform, extremely high V concentrations of up to 1.2% have been observed within the Tarim Basin (Yu et al., 2009) while they remain moderate within the black shale succession in the Ara Group, Oman, according to the study by Schröder and Grotzinger (2007). The anomalously high Mo concentrations within the Ni-Mo sulphide ore layer in the lower Niutitang Fm. have to be critically appreciated since it represents a highly condensed section but very high Mo concentrations and Mo/TOC ratios occur already within the Miaohu Mb. of the Doushantuo Fm. at Jiulongwan ca. 551Ma, in the Jiumenchong Fm. within transitional and basin sections and within the Shuijingtuo Fm. on the northern Yangtze Platform. The same applies for V although the proportion with respect to Mo varies significantly and reflects differences in redox-sensitivity. Hence, exponentially increasing concentrations of redox-sensitive trace-metals from the Early Ediacaran towards the Early Cambrian can be firmly confirmed for the Yangtze Platform and preliminary data from the Tarim Basin (Yu et al., 2009) and the Ara Group in Oman (Schröder and Grotzinger, 2007) suggest that this increase was not limited to the depositional environments on Yangtze Platform.

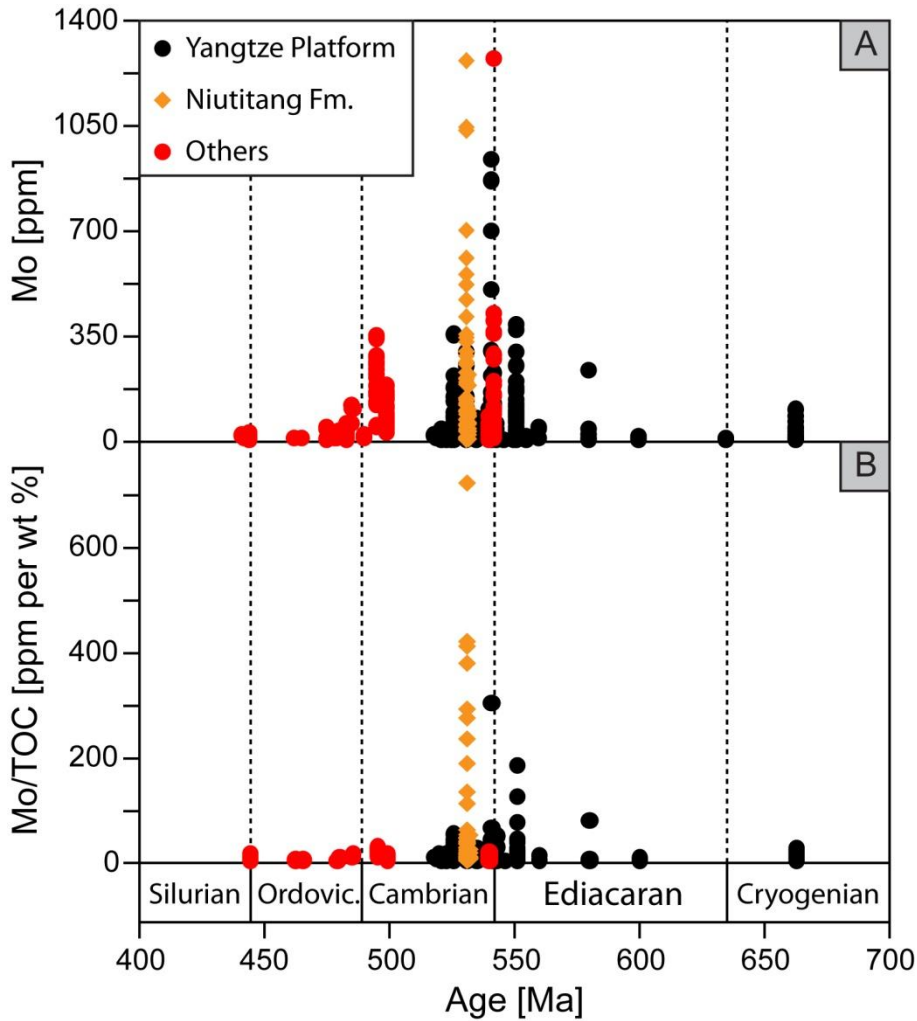


Figure 6.1: A) Mo concentrations in black shales from the 700 to 400 Ma (see also Fig. 2.2). Black dots represent data acquired from the Yangtze Platform, orange diamonds are specifically from the Niutitang Fm., and red dots show measurements reported from elsewhere. Anomalously high Mo concentrations from the Ni-Mo sulphide ore layer at the base of the Niutitang Fm. in the range of a few percent have been omitted here. B) Temporal trends in Mo/TOC ratios are from the same dataset and generated with TOC contents above 1% where available. While Mo concentrations increase and decrease gradually around a peak at the base of the Cambrian, Mo/TOC ratios are high in black shales deposited during the Precambrian – Cambrian transition on the Yangtze Platform but remain low in available analysed sediments deposited elsewhere.

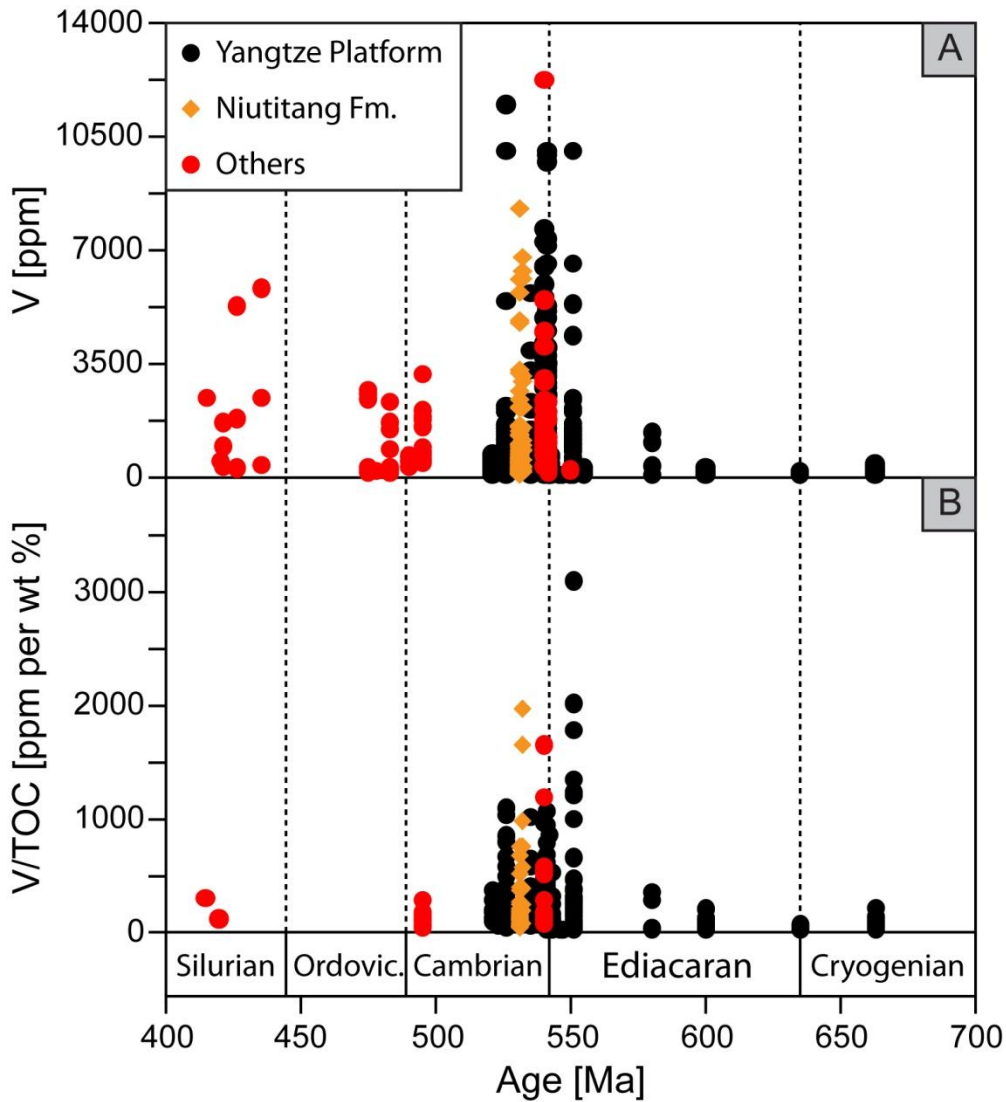
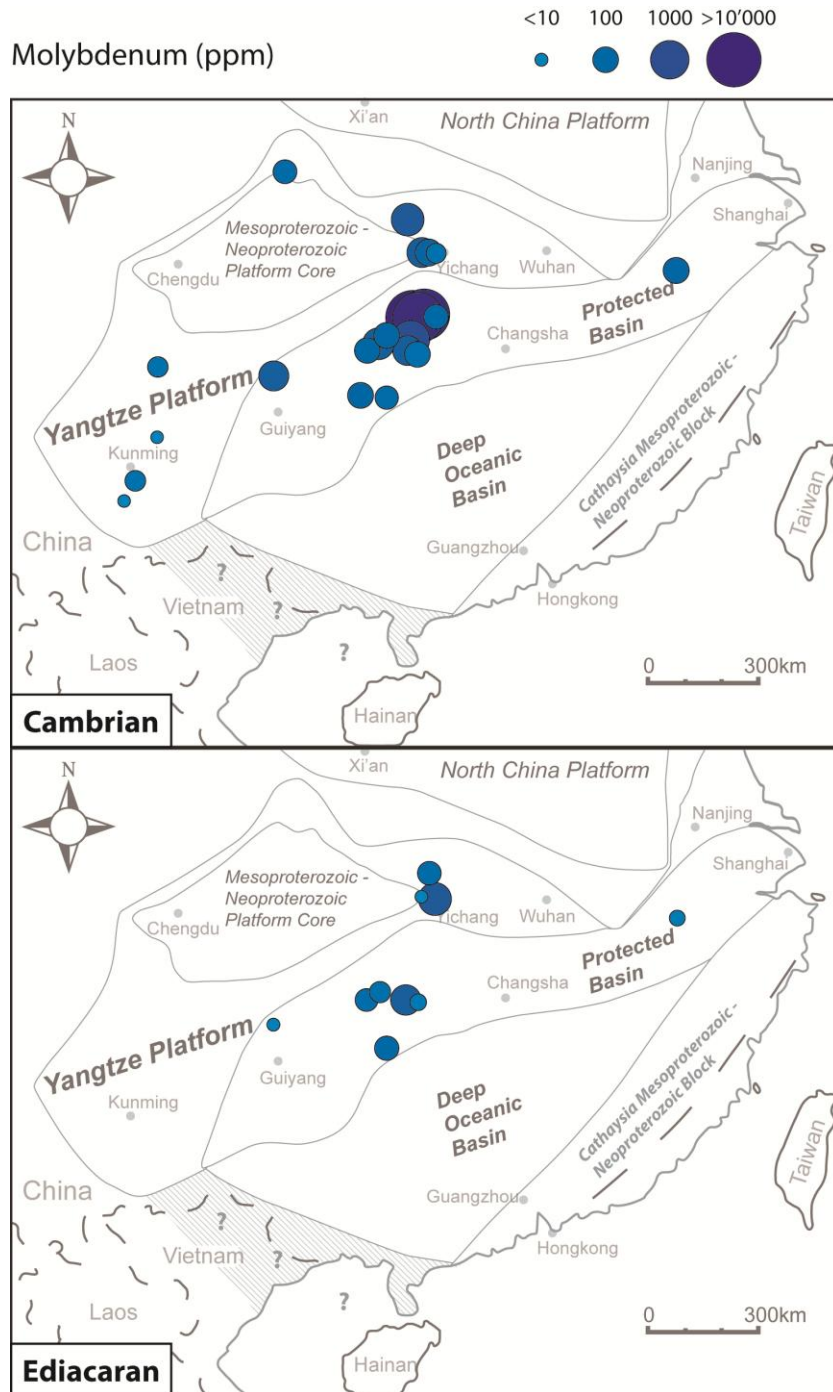


Figure 6.2: A) Temporal trends in V concentrations in black shales on the Yangtze Platform (black), specifically within the Niutitang Fm. (orange diamonds) and within black shales from other parts of the world (red dots). Note the exponential increase from the Early Ediacaran towards the Early Cambrian before V contents decrease again while maxima remain above 2000 ppm for the Paleozoic. B) V/TOC ratios, applying a TOC threshold of 1%, between 700 and 400 Ma demonstrate very high values during the Precambrian – Cambrian transition with a maximum within the Miaohé Mb. of the Doushantuo Fm. ca. 551 Ma and ratios below 500 for most of the Ediacaran and the Paleozoic.

Mo and V concentrations in black shales do not only vary globally but especially within the Yangtze Platform which has been demonstrated to depend on the access to the open ocean

for a given depositional environment. Figure 6.3 and 6.4 show maximum Mo and V concentrations by section locality whereby the vast datasets from Wallis (2006) and Guo et al. (2007) have been incorporated. Although there is a lack of sections exposing sedimentary successions across the Precambrian – Cambrian boundary and a quantitatively more important dataset covering the Early Cambrian, both trace-metals increase considerably from the Ediacaran to the Cambrian. High V concentrations are already found within some Ediacaran succession on the Northern platform while a more widespread distribution of V enriched black shales is seen during the Cambrian. The increase in maximum Mo concentrations is more pronounced and a greater disparity is observed regarding the depositional environment so that we find the highest enrichment within transitional and slope sections, moderate enrichment on the platform and particularly low concentrations on the Southwest platform. Although the patterns of element/Sc ratios rarely differed much from element concentrations alone throughout individual sections, normalizing trace-metal concentrations to a common denominator can enhance the comparability between the different depositional settings as shown in figure 6.5.



**Figure 6.3: Maximum Mo concentrations found within Late Ediacaran and Early Cambrian black shale successions on the Yangtze Platform. Besides the pronounced increase of Mo concentrations across the Precambrian – Cambrian boundary, significant differences are found amongst the investigated section (this study, Wallis, 2006; Guo et al., 2007), particularly during the Early Cambrian.**

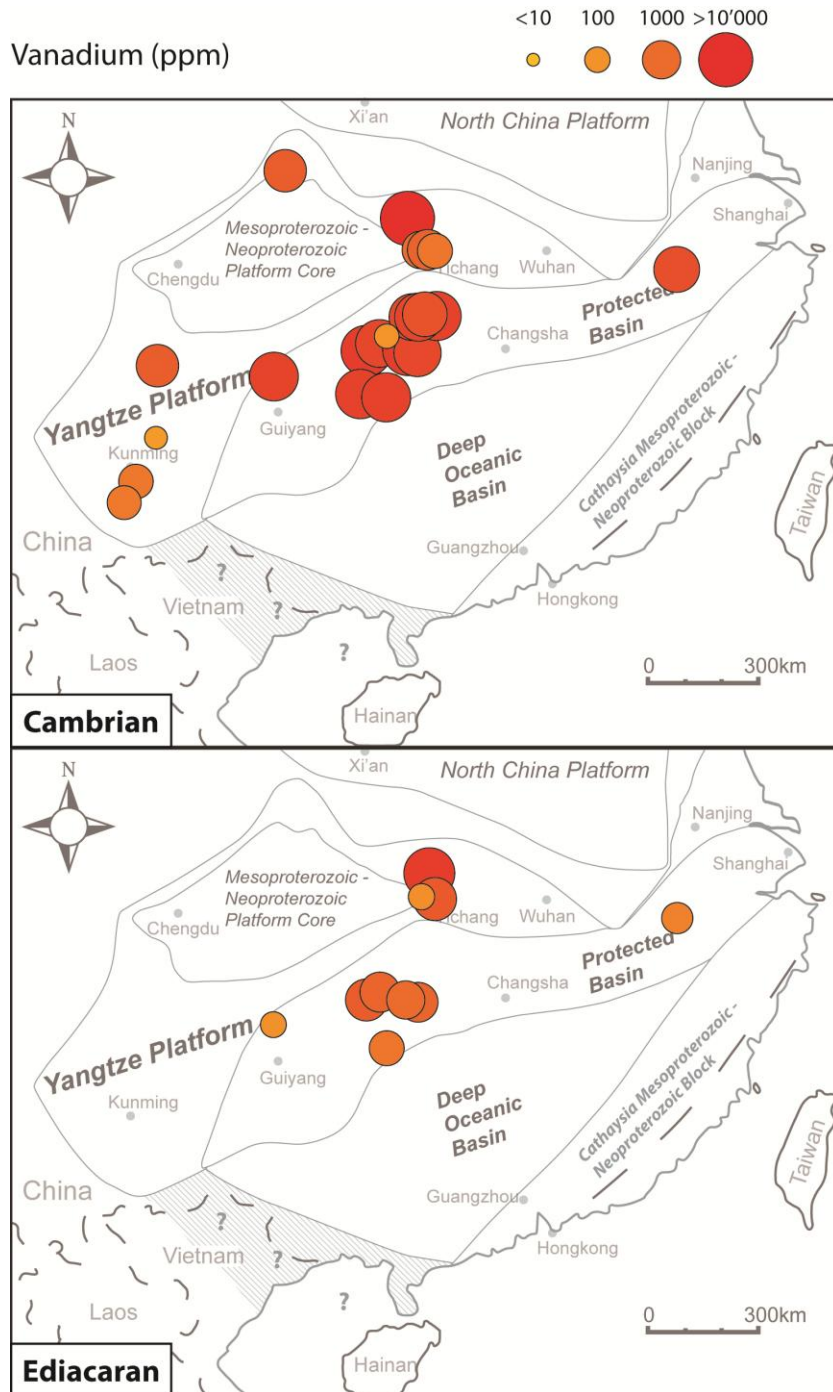
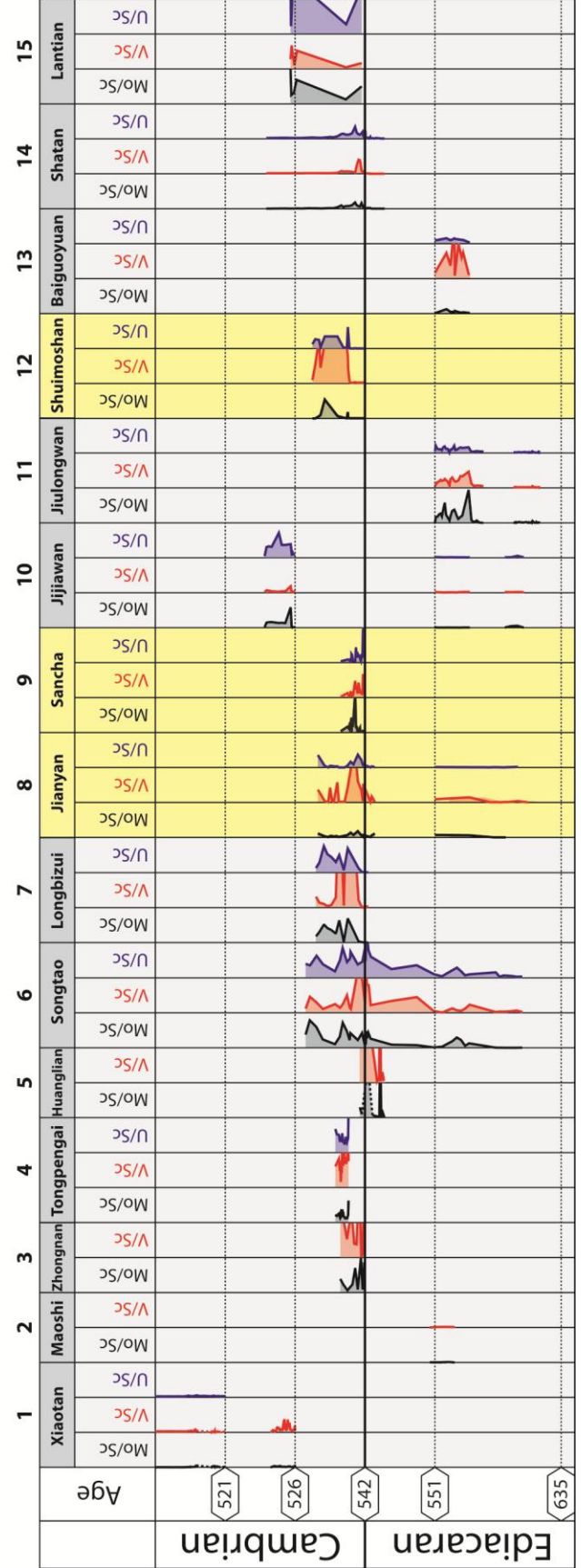
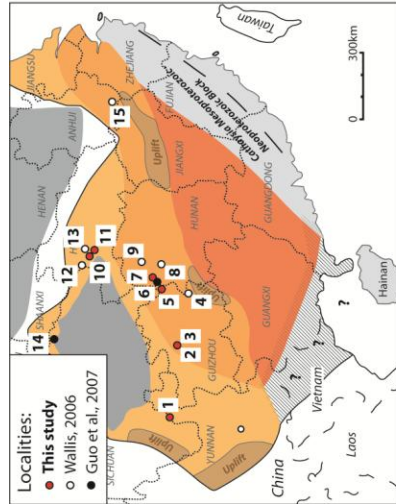


Figure 6.4: Maximum V concentrations in Late Ediacaran and Early Cambrian black shales on the Yangtze Platform including data from Wallis (2006) and Guo et al. (2007). Note that very high concentrations occur already during the Ediacaran but are more widespread after the Precambrian – Cambrian boundary.

Figure 6.5: Summary of normalized redox-sensitive trace-metals (Mo/Sc, V/Sc and U/Sc) from organic rich marine sediments deposited during the Precambrian – Cambrian transition on the Yangtze Platform (this study; Wallis, 2006; Guo et al., 2007). Grey shaded columns have a width of Mo/Sc = 30, V/Sc = 400 and U/Sc = 10 and yellow shaded columns, indicating particularly high contents in one or more trace-metals, have a width of Mo/Sc = 300, V/Sc = 1000 and U/Sc = 150. Very high ratios are attained in Late Ediacaran successions around the Three Gorges Area (Jiulongwan etc.) while Early Cambrian trace-metal enrichments are more widespread except on the south western Yangtze Platform (Yunnan Province).



According to Algeo and Lyons (2006), there is a nearly linear relationship between Mo concentrations in anoxic sediments and dissolved Mo concentrations in the overlying water column based on the degree of restriction of the subchemocline water mass affecting deepwater renewal. Based on these findings, it can be attempted to quantify temporal changes of Mo concentrations in seawater which prevailed in different depositional environments on the Yangtze Platform (see Fig. 6.7). However, while the difference in dissolved Mo is minimal between the modern Cariaco Basin and Saanich Inlet, Mo contents within the anoxic sediments of Saanich Inlet are about double the ones within the Cariaco Basin. Hence, it can be expected that Mo/TOC ratios exceeding 50 will even more diverge from a linear relationship. Nevertheless, according to the discussion in the previous chapter, physical barriers causing Mo limitation can be assumed for the intra-shelf basins and/or shelf lagoons during the deposition of the Late Ediacaran Miaohé Mb. at Maoshi and Jijiawan whereas oceanic Mo concentrations probably within today's magnitude lead to the enrichment and Mo/TOC ratios of over 180 seen in the Miaohé Mb. at Jiulongwan, which suggests an open connection to the global ocean and regular seawater renewal rates. Regarding Mb. II of the Doushantuo Fm. the situation is more complex; some advocate a restricted and even lacustrine environment (Bristow and Kennedy, 2008) and others demonstrated higher Mo/TOC ratios of up to 10 within the basal Doushantuo Fm. at Zhongling (ca. 100km south of Jiulongwan: Li et al., 2010), while Jiang et al. (2011) showed that a rimmed platform developed soon after the deposition of the cap carbonates (Doushantuo Mb. I), suggesting that paleobathymetry was already a parameter limiting Mo availability. Hence, it remains difficult to constrain the increase in the seawater inventory of redox-sensitive trace-metals in time, and it can merely be confirmed that it occurred prior to the deposition of the Miaohé Mb. ca. 551 Ma.

Mo/TOC ratios within the intermittently euxinic Early Cambrian successions at Meishucun, Longbizui, Zhongnan and Jijiawan show average Mo/TOC ratios between 4 and 14 but maxima above 30 for some horizons at Zhongnan and Jijiawan, similar to modern anoxic environments. Although a lack of precise paleogeographical studies of the Early Cambrian on the Yangtze Platform must be acknowledged, there is no indication for physical limitation of Mo availability going from the Jijiawan section in the North down to the Meishucun in the



Southwest and including the slope and basinal sections at Zhongnan and Longbizui stretching over more than 1000km and a redox-controlled widespread draw down of the seawater trace-metal inventory could account for predominantly low Mo/TOC ratios (see Fig. 6.6).

Although an overall increase in V/TOC across the Precambrian – Cambrian boundary can be observed (see Fig. 6.2b), the variation patterns amongst the investigated sections are very different from Mo/TOC ratios. V/TOC ratios remain within a narrow range throughout the Jijiawan section, from the lower part of the Doushantuo up to the Shuijingtuo Fm. There is significant variation within the Longbizui section but V/TOC averages within the Ediacaran Liuchapo and the Cambrian Jiumenchong remain virtually the same as opposed to the Huanglian section where low V/TOC ratios within the Liuchapo do not overlap with very high ratios of up to  $1050 \times 10^{-4}$  found within the Jiumenchong Fm. Furthermore, as already mentioned in chapter 5.3.3., V/TOC ratios are not following any clear trend at Xiaotan as opposed to the gradual increase of average Mo/TOC ratios but both ratios are similar between the Meishucun and Xiaotan sections, implying relatively uniform trace-metal concentrations on the south western Yangtze Platform.

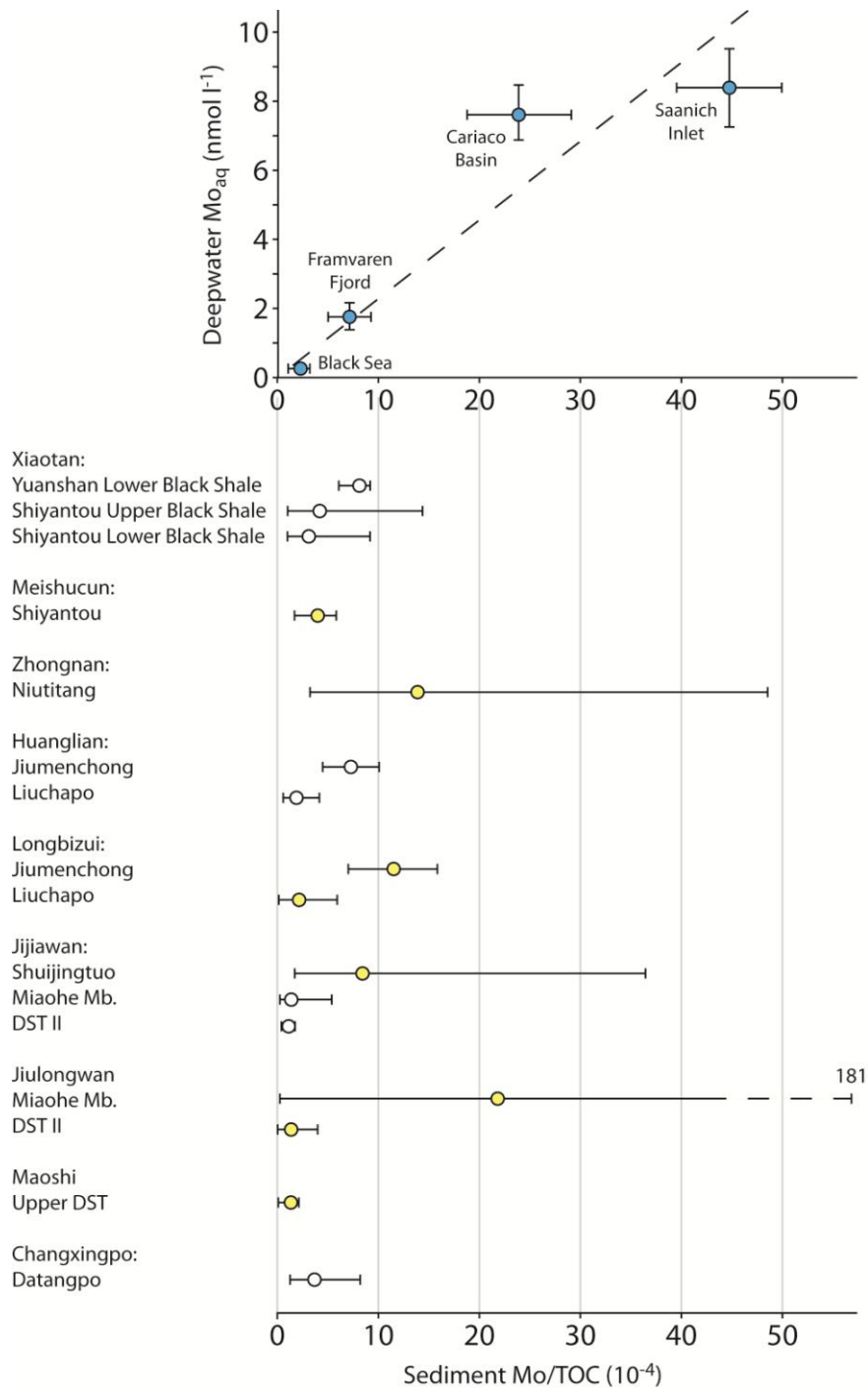
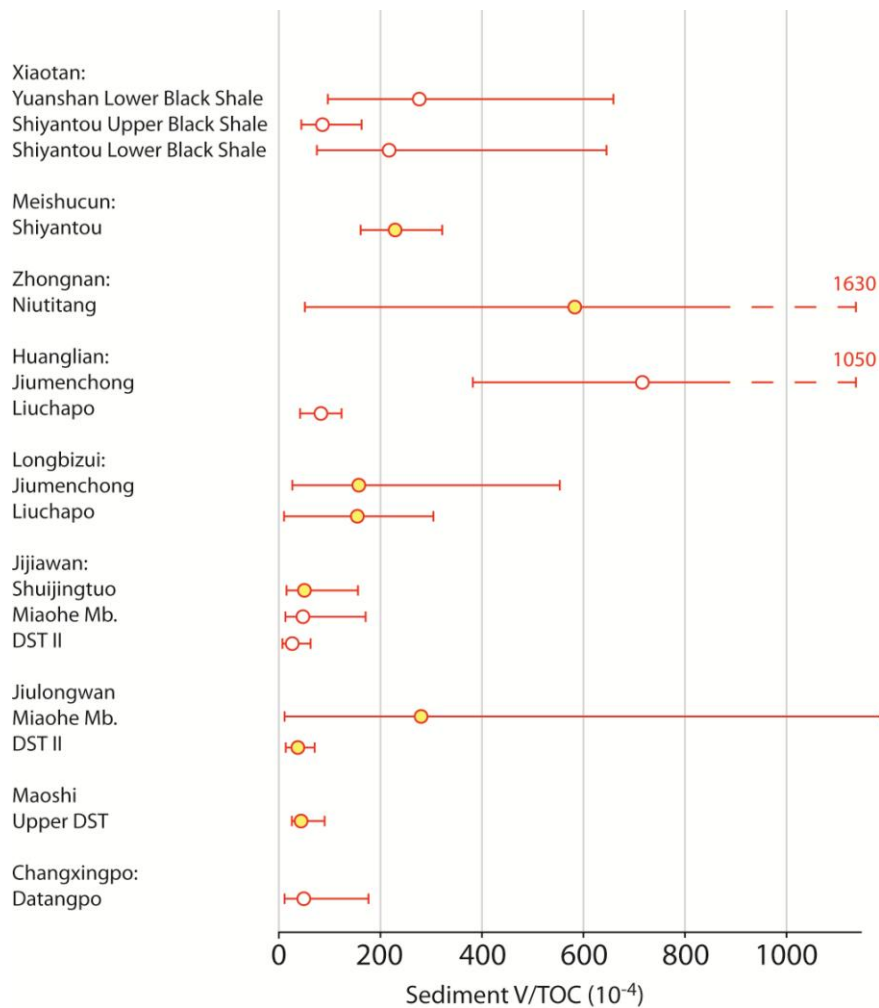


Figure 6.6: Range of Mo/TOC ratios from sections on the Yangtze Platform compared to modern anoxic environments (modified after Algeo and Lyons, 2006). Yellow coloured circles indicate intermittently euxinic sedimentary successions. A TOC threshold of 1% has been applied for the Zhongnan section due to unreasonably high Mo/TOC in within the organic-poor Ni-Mo sulphide horizon.



**Figure 6.7: Range of V/TOC ratios divided by section and geological formations. Intermittently euxinic formations are indicated by yellow circles.**

A more detailed illustration of Mo/TOC ratios and redox conditions based on iron speciation analysis is shown in figure 6.8. Although pronounced euxinic conditions, such as within the Miaohe Mb. and the Early Cambrian Jiumenchong Fm., suggest enhanced Mo removal from the water column, a systematic relationship between euxinia and Mo scavenging is not supported (e.g. Algeo and Lyons, 2006). On the other hand, it can be observed that Mo/TOC ratios above  $15 \cdot 10^{-4}$  occur exclusively within sedimentary successions where intermittent euxinia is indicated although not necessarily within the same horizon (see also Fig. 6.6). This suggests that the increase of molybdate and sulphate concentrations in seawater follow similar mechanisms (e.g. Algeo et al., 2007), which is also suggested by a similar patterns

of Mo/TOC and S/TOC ratios across the Precambrian – Cambrian transition (see Fig. 1.13). And while sulphidic environments represent conditions favourable for Mo sequestration it is primarily a question of an increasing Mo reservoir, together with increasing sulphate concentrations eventually leading to sulphidic environments, which lead to increasing Mo concentrations in black shales during the Neoproterozoic – Cambrian transition. The widespread sulphidic conditions seen during the Late Ediacaran ca. 551 Ma are accompanied by significant barite enrichment in deeper regions of the platform (e.g. Baiguoyuan) while probably more widespread sulphidic conditions during the Early Cambrian are contemporaneous to extended, massive barite deposits in the basin.

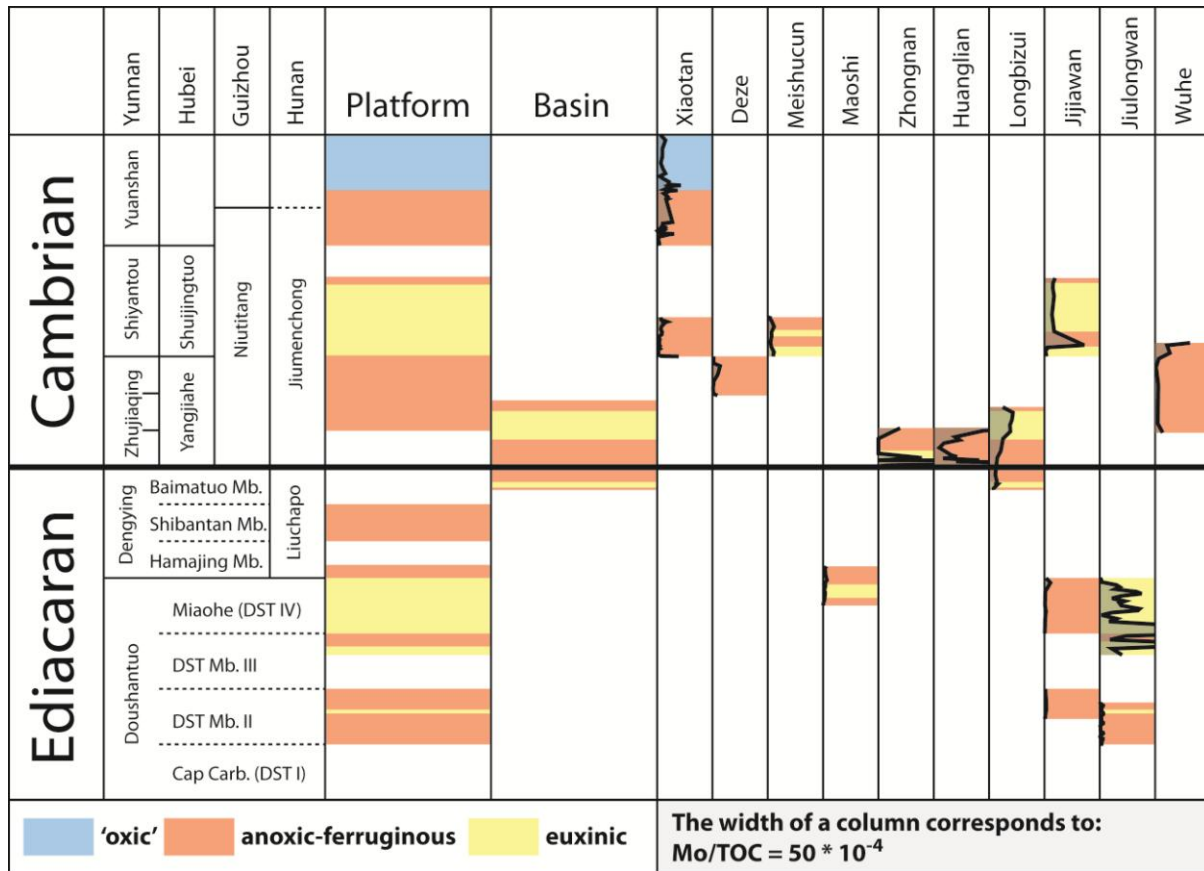


Figure 6.8: Summary of iron speciation and Mo/TOC ratios. Sections have been broadly subdivided into platform and basin whereby the transitional Zhongnan section has been included amongst the slope and/or basinal sections at Longbizui and Huanglian. Note that stratigraphic correlations across the platform are easily achieved for the Doushantuo Fm. and between the Early Cambrian formations in Yunnan and Hubei (Three Gorges Area) whereas the Niutitang and Jiumenchong Fm. are likely to have been deposited with significantly lower sedimentation rates and the upper Liuchapo Fm. possibly continued into the Cambrian (e.g. Wang et al., 1998).

## 6. Conclusions

### 6.1. The biogeochemical cycling of redox-sensitive trace-metals during the Precambrian – Cambrian transition on the Yangtze Platform

During the Precambrian –Cambrian transition we observe an exponential increase in redox-sensitive trace-metal concentrations in black shales by at least one magnitude, notably Mo, V and U, most likely caused by the Neoproterozoic Oxygenation Event which is likely to have occurred after the break-up up of the supercontinent Rodinia and the onset of major glaciations but before the late Ediacaran, where we find the oldest evidence for extreme Mo, V and U enrichment. The underlying cause for the enrichment is likely to be enhanced oxidative weathering and oxygenation of the sea floor, possibly by intensified reworking, which lead to an increasing Mo, V and U seawater inventory alongside with increasing sulphate concentrations in the ocean. There is no convincing evidence that a global retreat of anoxic-sulphidic conditions in the deep ocean lead to overall higher trace-metal concentrations in the ocean and, although available data based on iron speciation is sparse for the Early Neoproterozoic, it is likely that euxinic conditions were rare in a sulphate-poor, predominantly ferruginous Neoproterozoic ocean.

However, it has been demonstrated that redox-sensitive trace-metals can reflect paleoceanographic evolution from a regional point of view. During the sedimentation of the Ediacaran Doushantuo Fm. on the Yangtze Platform, the development of a rimmed shelf soon after the deposition of the cap carbonates led to trace-metal limitation within the shelf lagoon and numerous intra-shelf basins such as reflected by Mo/TOC ratios. Subsequent flooding of the inner platform and enhanced access to the open ocean increased trace-metal availability such as at Jiulongwan during the transition from Member II, with low trace-metal concentrations, to the Miaohu Member (Doushantuo Mb. IV), where the highest Precambrian Mo concentrations on record occur. Depositional basins further inside the platform, such as Jijiawan, do not exhibit elevated trace-metal concentrations during the Ediacaran and represent restricted depositional environments. During the Early Cambrian, the geochemical profiles at

Jiulongwan and Jijiawan exhibit a similar pattern indicating that open oceanic circulation extended further onto the platform. Sulphide isotope analysis supports this scenario and suggests that seawater sulphate concentrations increased alongside molybdate and other oxidized trace-metals while at the same time triggered euxinic conditions and Mo sequestration.

While euxinic conditions were widespread during the Early Cambrian, from the shelf to deeper parts of the Yangtze Platform, the southwestern inner platform remained anoxic-ferruginous except along the platform margin and the transitional zone, the latter being represented by the condensed Zhongnan section. The ubiquitous black shale associated Ni-Mo sulphide ore layer at Zhongnan can be correlated with the sedimentary succession at Xiaotan, more than 300km westwards on the shelf, where a thin Ni enriched horizon and a Mo enriched black shale succession a few meters further up have been found. This suggests that two separate mechanisms lead to the Ni-Mo ore horizon, which occurs along the transitional zone, notably a SEDEX-type mineralization resulting in high Ni concentrations and other associated metals followed by a redox driven Mo enrichment. This constrains the age of the Ni-Mo sulphide ore horizon at around 521 Ma and suggests that the biological innovations recorded in the fossil Lagerstätte at Chengjiang, also on the southwestern platform, might have emerged shortly after the retreat of widespread sulphidic conditions on the Yangtze Platform. Moreover, the pronounced euxinic conditions which seem to have prevailed during the Late Ediacaran and the Early Cambrian could be linked to the demise of the Ediacara Biota and the subsequent Cambrian Explosion.

## **6.2. A multi-proxy approach to investigate ancient paleoredox conditions**

The combined analysis of Mo, V and U concentrations in black shales demonstrated that it is possible to confidently differentiate redox conditions which prevailed during the deposition of the analysed sedimentary successions. At the Xiaotan section for example, elevated V and low Mo concentrations within the black shale succession in the lowermost Shiyantou Fm. indicate oxygen depletion without reaching sulphate-reducing conditions. This changed further up during the deposition of the lowermost Yuanshan Fm. where Mo enrichment takes place and

tracks organic carbon. On the other hand, it has been shown that higher U concentrations with respect to Mo concentrations, i.e. higher U/Mo ratios, point to strongly reducing conditions without the release of significant amount of free H<sub>2</sub>S, such as during the deposition of the black shale of the lower Shuijingtuo Fm. in the Early Cambrian.

It also became apparent that sulphidic conditions, indicated by iron speciation analysis, do not necessarily lead to coeval high Mo enrichment or elevated Mo/TOC ratios. However, sedimentary successions where intermittent euxinia occurs are the only ones where Mo/TOC ratios above  $15 \times 10^{-4}$  were observed at some point in the stratigraphy. Furthermore, the high resolution geochemical analysis of parts of the uppermost black shale of the Doushantuo Fm. (Miaohe Mb.) exhibits some cyclicity between Mo and Ba enrichment which could indicate dynamic changes in seawater chemistry involving episodic euxinia but it is startling that high Mo concentrations occur within the same zone as elevated Mn concentrations which might indicate Mo delivery to the seafloor by adsorption onto Mn-oxyhydroxides which is not considered to be an efficient enrichment mechanism. Barite within the sediment could have been reduced and lead to vertically very restricted thiomolybdate precipitation fronts.

### **6.3. Future challenges**

The biogeochemical cycling during the Precambrian – Cambrian transition on the Yangtze Platform is clearly intriguing and demonstrates a highly dynamic interval in Earth's history. Further studies outside the Yangtze Platform are needed to constrain the outlined geochemical changes from a global perspective and show whether the Yangtze Platform really experienced unique biogeochemical conditions or truly represents a unique sedimentary archive of the Precambrian – Cambrian transition. Moreover, there is a striking scarcity of geochemical investigations on sedimentary sequences prior to the Neoproterozoic glaciations predominantly due to preservational hiatuses created by major tectonic upheavals that occurred during the break-up of Rodinia. Concentrating on potentially available Early Neoproterozoic sedimentary successions would considerably improve our understanding of the Earth's surface chemistry and metazoan evolution.



Furthermore, the redox chemistry of molybdenum has to be better understood in particular with regard to pathways and mechanisms leading to molybdenum sequestration from the water column and fixation in marine sediments. Only few studies on Mo limitation as a trace nutrient have been conducted and further investigation should shed light on the connection between the biological innovations occurring during the Precambrian – Cambrian transition and the increased availability of redox-sensitive trace-metals in seawater.

And, last but not least, improved understanding of the consequences following the emergence of bioturbation is paramount in understanding the Neoproterozoic Oxygenation Event and in concert with improved age constraints, notably of the Early Cambrian on the Yangtze Platform, there is good potential to better understand the co-evolution of marine chemistry and the advent of architecturally more complex metazoans.

## **Formal Acknowledgements**

The present study has been made possible by the German Research Foundation (DFG) and the National Science Foundation of China (NSFC) through the Sino-German Research Project FOR 736. The geochemical analysis was carried out at the Royal Holloway, University of London (XRF and LA-ICP-MS), at the State Key Laboratory for Mineral Deposit Research, Nanjing University (ICP-MS), at the Civil Engineering and Geosciences Department, Newcastle University (iron speciation), at the Wolfson Laboratory, Birkbeck, University of London (C/S analysis), and at the Institute of Geology and Paleontology, University of Münster (sulphide isotope analysis).

## **Personal Acknowledgements**

I would like to express my deep gratitude to my supervisor Graham Shields-Zhou who accepted me as his student, let me work with a great deal of independence and took me out for a beer or two once in a while. His knowledge, enthusiasm and in particular his great personality made the past three years a pleasurable time. Great thanks also to Ying Shields-Zhou who was often a companion in the best of times and created space for good discussions and excellent fun. I will never forget the great dinners and the unforgettable Chinese New Years I had the opportunity to experience at their house. At this point, I would also like to express my appreciation for my colleague and friend Lorenzo with whom our road trips in China and elsewhere around the globe gained an extra value. Furthermore, I would like to thank Hongfei Ling, a superb person and scientist, for accompanying us in the Chinese countryside and for his overall helpfulness, from an academic and personal point of view. Great thanks are also due to my colleague Li Da, with whom most of my time in London would have been much sadder, and my colleague Chen Xi with his great humour and wit.

Great thanks to Christina Manning for her substantial help, advice and her very pleasant cheerfulness while I was doing less exciting sample preparations. Further thanks to Matthew Thirlwall and Wolfgang Müller for their inspiring attitude and great help. All three are at the

Royal Holloway, University of London. I'm also indebted to Tony Osborne from the Wolfson Laboratory, and Simon Poulton, Newcastle University, for letting me run riot in his lab.

Many, many thanks to my dear family for their great support and for their numerous visits while I was in London. And, last but not least, many thanks to my beloved Yilei for being there in great but also difficult times.

## References

- Abdelsalam, M.G. et al., 2003. Neoproterozoic deformation in the northeastern part of the Saharan Metacraton, northern Sudan. *Precambrian Research*, 123(2-4): 203-221.
- Adams, J.A.S. and Weaver, C.E., 1958. Thorium-to-uranium ratios as indicators of sedimentary processes: example of concept of geochemical facies. *AAPG Bulletin*, 42(2): 387.
- Algeo, T.J., 2004. Can marine anoxic events draw down the trace element inventory of seawater? *Geology*, 32(12): 1057-1060.
- Algeo, T.J. and Ingall, E., 2007. Sedimentary  $C_{org}:P$  ratios, paleocean ventilation, and Phanerozoic atmospheric  $pO_2$ . *Palaeogeography, Palaeoclimatology, Palaeoecology*, 256(3-4): 130-155.
- Algeo, T.J. and Tribouillard, N., 2009. Environmental analysis of paleoceanographic systems based on molybdenum-uranium covariation. *Chemical Geology*, 268(3-4): 211-225.
- Aller, R.C. and Rude, P.D., 1988. Complete oxidation of solid phase sulfides by manganese and bacteria in anoxic marine sediments. *Geochimica et Cosmochimica Acta*, 52(3): 751-765.
- Amthor, J.E. et al., 2003. Extinction of *Cloudina* and *Namacalathus* at the Precambrian-Cambrian boundary in Oman. *Geology*, 31(5): 431-434.
- Anbar, A.D., Knab, K.A. and Barling, J., 2001. Precise Determination of Mass-Dependent Variations in the Isotopic Composition of Molybdenum Using MC-ICPMS. *Analytical Chemistry*, 73(7): 1425-1431.
- Anders, E. and Grevesse, N., 1989. Abundances of the elements: Meteoritic and solar. *Geochimica et Cosmochimica Acta*, 53(1): 197-214.
- Anderson, L.A. and Sarmiento, J.L., 1994. Redfield ratios of remineralization determined by nutrient data analysis. *Global Biogeochem. Cycles*, 8(1): 65-80.
- Anderson, T.F. and Raiswell, R., 2004. Sources and mechanisms for the enrichment of highly reactive iron in euxinic Black Sea sediments. *Am J Sci*, 304(3): 203-233.
- Archer, C. and Vance, D., 2006. Coupled Fe and S isotope evidence for Archean microbial Fe(III) and sulfate reduction. *Geology*, 34(3): 153-156.
- Arnold, G.L., Anbar, A.D., Barling, J. and Lyons, T.W., 2004. Molybdenum Isotope Evidence for Widespread Anoxia in Mid-Proterozoic Oceans. *Science*, 304(5667): 87-90.
- Asmerom, Y., Jacobsen, S.B., Knoll, A.H., Butterfield, N.J. and Swett, K., 1991. Strontium isotopic variations of Neoproterozoic seawater: Implications for crustal evolution. *Geochimica et Cosmochimica Acta*, 55(10): 2883-2894.
- Aspler, L.B. and Chiarenzelli, J.R., 1998. Two Neoproterozoic supercontinents? Evidence from the Paleoproterozoic. *Sedimentary Geology*, 120(1-4): 75-104.
- Awramik, S.M., Schopf, J.W. and Walter, M.R., 1983. Filamentous fossil bacteria from the Archean of Western Australia. *Precambrian Research*, 20(2-4): 357-374.
- Awramik, S.M., Schopf, J.W. and Walter, M.R., 1988. Carbonaceous filaments from North Pole, Western Australia: Are they fossil bacteria in Archean stromatolites? A discussion. *Precambrian Research*, 39(4): 303-309.
- Babcock, L.E. and Peng, S., 2007. Cambrian chronostratigraphy: Current state and future plans. *Palaeogeography, Palaeoclimatology, Palaeoecology*, 254(1-2): 62-66.
- Babcock, L.E., Zhang, W. and Leslie, S.A., 2001. The Chengjiang Biota: record of the Early Cambrian diversification of life and clues to exceptional preservation of fossils. *GSA Today*, 11: 4-9.
- Banner, J.L., 2004. Radiogenic isotopes: systematics and applications to earth surface processes and chemical stratigraphy. *Earth-Science Reviews*, 65(3-4): 141-194.
- Bao, H., Lyons, J.R. and Zhou, C., 2008. Triple oxygen isotope evidence for elevated  $CO_2$  levels after a Neoproterozoic glaciation. *Nature*, 453(7194): 504-506.

- Barley, M.E., Bekker, A. and Krapez, B., 2005. Late Archean to Early Paleoproterozoic global tectonics, environmental change and the rise of atmospheric oxygen. *Earth and Planetary Science Letters*, 238(1-2): 156-171.
- Barling, J. and Anbar, A.D., 2004. Molybdenum isotope fractionation during adsorption by manganese oxides. *Earth and Planetary Science Letters*, 217(3-4): 315-329.
- Barling, J., Arnold, G.L. and Anbar, A.D., 2001. Natural mass-dependent variations in the isotopic composition of molybdenum. *Earth and Planetary Science Letters*, 193(3-4): 447-457.
- Barrow, J.D. and Tipler, F.J., 1986. *The Anthropoc Cosmological Principle*. Oxford University Press, New York.
- Bau, M., Romer, R.L. and Beukes, N.J., 1998. Increase of Oxygen in the Earth's Atmosphere and Hydrosphere between -2.5 and -2.4 Ga B.P. *Mineralogical Magazine*, 62A(1): 127-128.
- Bekker, A. et al., 2004. Dating the rise of atmospheric oxygen. *Nature*, 427: 117 - 120.
- Bekker, A., Holland, H.D., Young, G.M. and Nesbitt, H.W., 2003. Fe<sub>2</sub>O<sub>3</sub>/FeO ratio in average shale through time: a reflection of the stepwise oxidation of the atmosphere. *Geological Society of America Abstracts with programs*, 35(6): 83.
- Bell, R.T. and Jefferson, C.W., 1987. An hypothesis for an Australia-Canadian connection in the Late Proterozoic and the birth of the Pacific Ocean. *Proceedings of the Pacific Rim Congress*, 87: 39 - 50.
- Bengtson, S., 2002. Origins and early evolution of predation. *Paleontological Society Papers*, 8: 289 - 317.
- Bengtson, S. and Zhao, Y., 1992. Predatorial Borings in Late Precambrian Mineralized Exoskeletons. *Science*, 257(5068): 367-369.
- Benitez-Nelson, C.R., 2000. The biogeochemical cycling of phosphorus in marine systems. *Earth-Science Reviews*, 51(1-4): 109-135.
- Bergman, N.M., Lenton, T.M. and Watson, A.J., 2004. COPSE: A new model of biogeochemical cycling over Phanerozoic time. *American Journal of Science*, 304(5): 397-437.
- Berkner, L.V. and Marshall, L.C., 1965. On the Origin and Rise of Oxygen Concentration in the Earth's Atmosphere. *Journal of the Atmospheric Sciences*, 22(3): 225-261.
- Berner, R., 2004. *The Phanerozoic carbon cycle: CO<sub>2</sub> and O<sub>2</sub>*. Oxford University Press, Oxford, UK.
- Berner, R.A., 1970. Sedimentary pyrite formation. *American Journal of Science*, 268(1): 1-23.
- Berner, R.A., 2006. GEOCARBSULF: A combined model for Phanerozoic atmospheric O<sub>2</sub> and CO<sub>2</sub>. *Geochimica et Cosmochimica Acta*, 70(23): 5653-5664.
- Berner, R.A., Beerling, D.J., Dudley, R., Robinson, J.M. and Wildman, R.A., 2003. Phanerozoic atmospheric oxygen. *Annual Review of Earth and Planetary Sciences*, 31(1): 105-134.
- Berner, R.A. and Canfield, D.E., 1989. A new model for atmospheric oxygen over Phanerozoic time. *American Journal of Science*, 289(4): 333-361.
- Berner, R.A. and Raiswell, R., 1983. Burial of organic carbon and pyrite sulfur in sediments over phanerozoic time: a new theory. *Geochimica et Cosmochimica Acta*, 47(5): 855-862.
- Berner, R.A. and Raiswell, R., 1984. C/S method for distinguishing freshwater from marine sedimentary rocks. *Geology*, 12(6): 365-368.
- Berrang, P.G. and Grill, E.V., 1974. The effect of manganese oxide scavenging on molybdenum in saanich inlet, British Columbia. *Marine Chemistry*, 2(2): 125-148.
- Berry, W.B.N. and Wilde, P., 1978. Progressive ventilation of the oceans; an explanation for the distribution of the lower Paleozoic black shales. *American Journal of Science*, 278(3): 257-275.
- Bertine, K.K. and Turekian, K.K., 1973. Molybdenum in marine deposits. *Geochimica et Cosmochimica Acta*, 37(6): 1415-1434.
- Bertrand-Sarfati, J., Moussine-Pouchkine, A., Amard, B. and Aït Kaci Ahmed, A., 1995. First Ediacaran fauna found in western Africa and evidence for an Early Cambrian glaciation. *Geology*, 23(2): 133-136.

- Beukes, N.J., Dorland, H., Gutzmer, J., Nedachi, M. and Ohmoto, H., 2002. Tropical laterites, life on land, and the history of atmospheric oxygen in the Paleoproterozoic. *Geology*, 30(6): 491-494.
- Beukes, N.J. and Lowe, D.R., 1989. Environmental control on diverse stromatolite morphologies in the 3000 Myr Pongola Supergroup, South Africa. *Sedimentology*, 36(3): 383-397.
- Bickle, M.J., 1994. The role of metamorphic decarbonation reactions in returning strontium to the silicate sediment mass. *Nature*, 367(6465): 699-704.
- Billings, E., 1872. On some fossils from the Primordial rocks of Newfoundland. *Canadian Naturalist*, 6: 465 - 479.
- Bishop, J.K.B., 1988. The barite-opal-organic carbon association in oceanic particulate matter. *Nature*, 332(6162): 341-343.
- Björkman, O., 1966. The Effect of Oxygen Concentration on Photosynthesis in Higher Plants. *Physiologia Plantarum*, 19(3): 618-633.
- Blackship, R.E., Sadekaar, S. and Raymond, J., 2007. *Evolution of Primary Producers in the Sea*. Elsevier Academic Press, New York.
- Blackship, R.E. and Hartman, H., 1998. The origin and evolution of oxygenic photosynthesis. *Trends in Biochemical Sciences*, 23(3): 94-97.
- Bleeker, W., 2003. The late Archean record: a puzzle in ca. 35 pieces. *Lithos*, 71(2-4): 99-134.
- Boger, S.D. and Miller, J.M., 2004. Terminal suturing of Gondwana and the onset of the Ross-Delamerian Orogeny: the cause and effect of an Early Cambrian reconfiguration of plate motions. *Earth and Planetary Science Letters*, 219(1-2): 35-48.
- Bond, G.C., Nickeson, P.A. and Kominz, M.A., 1984. Breakup of a supercontinent between 625 Ma and 555 Ma: new evidence and implications for continental histories. *Earth and Planetary Science Letters*, 70(2): 325-345.
- Bonnoit-Courtois, C. and Flicoteaux, R., 1989. Distribution of rare-earth and some trace elements in Tertiary phosphorites from the Senegal Basin and their weathering products. *Chemical Geology*, 75(4): 311-328.
- Bostick, B.C., Fendorf, S. and Helz, G.R., 2003. Differential Adsorption of Molybdate and Tetrathiomolybdate on Pyrite (FeS<sub>2</sub>). *Environmental Science & Technology*, 37(2): 285-291.
- Bottomley, D.J., Veizer, J., Nielsen, H. and Moczydlowska, M., 1992. Isotopic composition of disseminated sulfur in Precambrian sedimentary rocks. *Geochimica et Cosmochimica Acta*, 56(8): 3311-3322.
- Bowring, S.A. and Erwin, D.H., 1998. A new look at evolutionary rates in deep time uniting paleontology and high-precision geochronology. *GSA Today*, 8: 1-8.
- Bowring, S.A., Myrow, P., Landing, E. and Ramenzani, J., 2003. Geochronological constraints on terminal Neoproterozoic events and the rise of Metazoan. EGS - AGU - EUG Joint Assembly, Abstracts from the meeting held in Nice, France, 6 - 11 April 2003.
- Bradley, D.C., 2008. Passive margins through earth history. *Earth-Science Reviews*, 91(1-4): 1-26.
- Brasier, M., Cowie, J. and Taylor, M., 1994. Decision on the Precambrian-Cambrian boundary stratotype. *Episodes*, 17(1 & 2): 3-8.
- Brasier, M. and Lindsay, J.F., 2001. Did supercontinental amalgamation trigger the "Cambrian explosion"? In: A.Y. Zhuravlev and R. Riding (Editors), *The Ecology of the Cambrian Radiation*. Columbia University Press, New York, pp. 173-199.
- Brasier, M. et al., 2000. New U-Pb zircon dates for the Neoproterozoic Ghubrah glaciation and for the top of the Huqf Supergroup, Oman. *Geology*, 28(2): 175-178.
- Brasier, M., McLoughlin, N., Green, O. and Wacey, D., 2006. A fresh look at the fossil evidence for early Archaean cellular life. *Philosophical Transactions of the Royal Society B: Biological Sciences*, 361(1470): 887-902.

- Brasier, M.D. and Lindsay, J.F., 1998. A billion years of environmental stability and the emergence of eukaryotes; new data from northern Australia. *Geology*, 26(6): 555-558.
- Brennan, S.T., Lowenstein, T.K. and Horita, J., 2004. Seawater chemistry and the advent of biocalcification. *Geology*, 32(6): 473-476.
- Bristow, T.F. et al., 2009. Mineralogical constraints on the paleoenvironments of the Ediacaran Doushantuo Formation. *Proceedings of the National Academy of Sciences*, 106(32): 13190-13195.
- Brocks, J.J., Buick, R., Summons, R.E. and Logan, G.A., 2003. A reconstruction of Archean biological diversity based on molecular fossils from the 2.78 to 2.45 billion-year-old Mount Bruce Supergroup, Hamersley Basin, Western Australia. *Geochimica et Cosmochimica Acta*, 67(22): 4321-4335.
- Brocks, J.J., Logan, G.A., Buick, R. and Summons, R.E., 1999. Archean Molecular Fossils and the Early Rise of Eukaryotes. *Science*, 285(5430): 1033-1036.
- Brocks, J.J. et al., 2005. Biomarker evidence for green and purple sulphur bacteria in a stratified Palaeoproterozoic sea. *Nature*, 437(7060): 866-870.
- Broecker, W.S. and Peng, T.H., 1982. *Tracers in the Sea*. Eldigio Press, Columbia University, Palisades, NY, 689 pp.
- Brookins, D.G., 1989. Aqueous geochemistry of rare earth elements. *Reviews in Mineralogy and Geochemistry*, 21(1): 201-225.
- Brown, A.C., 1984. Oxygen diffusion into the foot of the whelk *Bullia digitalis* (Dillwyn) and its possible significance in respiration. *Journal of Experimental Marine Biology and Ecology*, 79(1): 1-7.
- Bruland, K.W., 1983. Trace elements in sea-water. *Chemical oceanography*, 8: 157-220.
- Brumsack, H.-J., 2006. The trace metal content of recent organic carbon-rich sediments: Implications for Cretaceous black shale formation. *Palaeogeography, Palaeoclimatology, Palaeoecology*, 232(2-4): 344-361.
- Brumsack, H.J., 1986. The inorganic geochemistry of Cretaceous black shales (DSDP Leg 41) in comparison to modern upwelling sediments from the Gulf of California. Geological Society, London, Special Publications, 21(1): 447-462.
- Brumsack, H.J. and Gieskes, J.M., 1983. Interstitial water trace-metal chemistry of laminated sediments from the Gulf of California, Mexico. *Marine Chemistry*, 14(1): 89-106.
- Brunner, B. and Bernasconi, S.M., 2005. A revised isotope fractionation model for dissimilatory sulfate reduction in sulfate reducing bacteria. *Geochimica et Cosmochimica Acta*, 69(20): 4759-4771.
- Buchan, K., Mortensen, J., Card, K. and Percival, J., 1998. Paleomagnetism and U-Pb geochronology of diabase dyke swarms of Minto block, Superior Province, Quebec, Canada. *Canadian Journal of Earth Sciences*, 35(9): 1054-1069.
- Budd, G.E., 2008. The earliest fossil record of the animals and its significance. *Philosophical Transactions of the Royal Society B: Biological Sciences*, 363: 1425-1434.
- Budd, G.E. and Jensen, S., 2000. A critical reappraisal of the fossil record of the bilaterian phyla. *Biological Reviews*, 75: 253 - 295.
- Buick, R., 1992. The antiquity of oxygenic photosynthesis: evidence from stromatolites in sulphate-deficient Archean lakes. *Science*, 255(5040): 74-77.
- Buick, R., Des Marais, D.J. and Knoll, A.H., 1995. Stable isotopic compositions of carbonates from the Mesoproterozoic Bangemall group, northwestern Australia. *Chemical Geology*, 123(1-4): 153-171.
- Burns, S.J. and Matter, A., 1993. Carbon isotopic record of the latest Proterozoic from Oman. *Eclogae Geologicae Helveticae*, 86(2): 595-607
- Butterfield, N.J., 2001. Ecology and evolution of Cambrian plankton. In: A.Y. Zhuravlev and R. Riding (Editors), *The Ecology of the Cambrian Radiation*. Columbia University Press, pp. 200 - 216.

- Butterfield, N.J., 2004. A vaucheriacean alga from the middle Neoproterozoic of Spitsbergen: implications for the evolution of Proterozoic eukaryotes and the Cambrian explosion. *Paleobiology*, 30(2): 231-252.
- Butterfield, N.J., 2005a. Probable Proterozoic fungi. *Paleobiology*, 31(1): 165-182.
- Butterfield, N.J., 2005b. Reconstructing a complex early Neoproterozoic eukaryote, Wynniatt Formation, arctic Canada. *Lethaia*, 38(2): 155-169.
- Butterfield, N.J., Knoll, A.H. and Swett, K., 1994. Paleobiology of the Neoproterozoic Svanbergfjellet Formation, Spitsbergen. *Lethaia*, 27(1): 76-76.
- Butterfield, N.J. and Rainbird, R.H., 1998. Diverse organic-walled fossils, including "possible dinoflagellates," from the early Neoproterozoic of arctic Canada. *Geology*, 26(11): 963-966.
- Calver, C.R., 2000. Isotope stratigraphy of the Ediacarian (Neoproterozoic III) of the Adelaide Rift Complex, Australia, and the overprint of water column stratification. *Precambrian Research*, 100(1-3): 121-150.
- Calver, C.R., Black, L.P., Everard, J.L. and Seymour, D.B., 2004. U-Pb zircon age constraints on late Neoproterozoic glaciation in Tasmania. *Geology*, 32(10): 893-896.
- Calvert, S.E. and Pedersen, T.F., 1996. Sedimentary geochemistry of manganese; implications for the environment of formation of manganese black shales. *Economic Geology*, 91(1): 36-47.
- Cameron, E.M., 1982. Sulphate and sulphate reduction in early Precambrian oceans. *Nature*, 296(5853): 145-148.
- Cameron, E.M. and Hattori, K., 1987. Archean sulphur cycle: Evidence from sulphate minerals and isotopically fractionated sulphides in superior province, Canada. *Chemical Geology: Isotope Geoscience section*, 65(3-4): 341-358.
- Campbell, I.H. and Allen, C.M., 2008. Formation of supercontinents linked to increases in atmospheric oxygen. *Nature Geoscience*, 1(8): 554-558.
- Campbell, I.H. and Squire, R.J., 2010. The mountains that triggered the Late Neoproterozoic increase in oxygen: The Second Great Oxidation Event. *Geochimica et Cosmochimica Acta*, 74(15): 4187-4206.
- Campbell, J.A. and Yeats, P.A., 1981. Dissolved chromium in the northwest Atlantic Ocean. *Earth and Planetary Science Letters*, 53(3): 427-433.
- Canfield, D.E., 1989. Reactive iron in marine sediments. *Geochimica et Cosmochimica Acta*, 53(3): 619-632.
- Canfield, D.E., 1998. A new model for Proterozoic ocean chemistry. *Nature*, 396(6710): 450-453.
- Canfield, D.E., 2004. The evolution of the Earth surface sulfur reservoir. *Am J Sci*, 304(10): 839-861.
- Canfield, D.E., 2005. The Early History of Atmospheric Oxygen: Homage to Robert M. Garrels. *Annual Review of Earth and Planetary Sciences*, 33(1): 1-36.
- Canfield, D.E., Farquhar, J. and Zerkle, A.L., 2010. High isotope fractionations during sulfate reduction in a low-sulfate euxinic ocean analog. *Geology*, 38(5): 415-418.
- Canfield, D.E., Lyons, T.W. and Raiswell, R., 1996. A model for iron deposition to euxinic Black Sea sediments. *American Journal of Science*, 296(7): 818-834.
- Canfield, D.E. et al., 2008. Ferruginous Conditions Dominated Later Neoproterozoic Deep-Water Chemistry. *Science*, 321(5891): 949-952.
- Canfield, D.E., Poulton, S.W. and Narbonne, G.M., 2007. Late-Neoproterozoic Deep-Ocean Oxygenation and the Rise of Animal Life. *Science*, 315(5808): 92-95.
- Canfield, D.E. and Raiswell, R., 1999. The evolution of the sulfur cycle. *American Journal of Science*, 299(7-9): 697-723.
- Canfield, D.E., Raiswell, R. and Bottrell, S.H., 1992. The reactivity of sedimentary iron minerals toward sulfide. *American Journal of Science*, 292(9): 659-683.



- Canfield, D.E., Raiswell, R., Westrich, J.T., Reaves, C.M. and Berner, R.A., 1986. The use of chromium reduction in the analysis of reduced inorganic sulfur in sediments and shales. *Chemical Geology*, 54(1-2): 149-155.
- Canfield, D.E. and Teske, A., 1996. Late Proterozoic rise in atmospheric oxygen concentration inferred from phylogenetic and sulphur-isotope studies. *Nature*, 382(6587): 127-132.
- Canuto, V.M., Levine, J.S., Augustsson, T.R., Imhoff, C.L. and Giampapa, M.S., 1983. The young Sun and the atmosphere and photochemistry of the early Earth. *Nature*, 305(5932): 281-286.
- Caplan, M.L. and Bustin, R.M., 1998. Sedimentology and sequence stratigraphy of Devonian-Carboniferous strata, southern Alberta. *Bulletin of Canadian Petroleum Geology*, 46(4): 487-514.
- Castresana, J. and Saraste, M., 1995. Evolution of energetic metabolism: the respiration-early hypothesis. *Trends in Biochemical Sciences*, 20(11): 443-448.
- Catling, D.C. and Claire, M.W., 2005. How Earth's atmosphere evolved to an oxic state: A status report. *Earth and Planetary Science Letters*, 237(1-2): 1-20.
- Catling, D.C., Glein, C.R., Zahnle, K.J. and McKay, C.P., 2005. Why O<sub>2</sub> Is Required by Complex Life on Habitable Planets and the Concept of Planetary "Oxygenation Time". *Astrobiology*, 5(3): 415-438.
- Cavalier-Smith, T., 2002. The neomuran origin of archaeobacteria, the negibacterial root of the universal tree and bacterial megaclassification. *International Journal of Systematic and Evolutionary Microbiology*, 52(1): 7-76.
- Cawood, P.A., Kröner, A. and Pisarevsky, S., 2006. Precambrian plate tectonics: Criteria and evidence. *GSA Today*, 16(7): 4-11.
- Cawood, P.A. and Pisarevsky, S.A., 2006. Was Baltica right-way-up or upside-down in the Neoproterozoic? *Journal of the Geological Society*, 163(5): 753-759.
- Chaillou, G., Anschutz, P., Lavaux, G., Schäfer, J. and Blanc, G., 2002. The distribution of Mo, U, and Cd in relation to major redox species in muddy sediments of the Bay of Biscay. *Marine Chemistry*, 80(1): 41-59.
- Chao, C. and Fapeng, X., 1986. An account of the Baiguoyuan black shale type silver-vanadium deposit. *Mineral Deposits*, 1.
- Chen, D., Wang, J., Qing, H., Yan, D. and Li, R., 2009. Hydrothermal venting activities in the Early Cambrian, South China: Petrological, geochronological and stable isotopic constraints. *Chemical Geology*, 258(3-4): 168-181.
- Chen, D.F., Dong, W.Q., Qi, L., Chen, G.Q. and Chen, X.P., 2003. Possible REE constraints on the depositional and diagenetic environment of Doushantuo Formation phosphorites containing the earliest metazoan fauna. *Chemical Geology*, 201: 103-118.
- Chen, J.-Y. et al., 2000. Precambrian animal diversity: Putative phosphatized embryos from the Doushantuo Formation of China. *Proceedings of the National Academy of Sciences of the United States of America*, 97(9): 4457-4462.
- Chen, M., Chen, Y. and Qian, Y., 1981. Some tubular fossils from Sinian-Lower Cambrian boundary sequences, Yangtze Gorge. *Bulletin, Tianjin Institute of Geology and Mineral Resources*, 3: 117-124.
- Chen, X. and Gao, J., 1984. Geology-geochemistry of barite in China. In: G. Tu (Editor), *Developments in geoscience*. Beijing Science Press, pp. 375-384.
- Chen, X., Li, D., Ling, H.-F. and Jiang, S.-Y., 2008. Carbon and sulfur isotopic compositions of basal Datangpo Formation, northeastern Guizhou, South China: Implications for depositional environment. *Progress in Natural Science*, 18(4): 421-429.
- Clemmey, H. and Badham, N., 1982. Oxygen in the Precambrian atmosphere: An evaluation of the geological evidence. *Geology*, 10(3): 141-146.
- Cloud, P., 1972. A working model of the primitive Earth. *American Journal of Science*, 272(6): 537-548.

- Cloud, P.E., Jr., 1968. Atmospheric and Hydrospheric Evolution on the Primitive Earth: Both secular accretion and biological and geochemical processes have affected earth's volatile envelope. *Science*, 160(3829): 729-736.
- Cohen, P.A. et al., 2009. Tubular Compression Fossils from the Ediacaran Nama Group, Namibia. *Journal of Paleontology*, 83(1): 110-122.
- Coleman, A., 1926. *Ice Ages, recent and ancient*. Macmillan, London, 296 pp.
- Collier, R. and Edmond, J., 1984. The trace element geochemistry of marine biogenic particulate matter. *Progress In Oceanography*, 13(2): 113-199.
- Collier, R.W., 1985. Molybdenum in the Northeast Pacific Ocean *Limnology and Oceanography* 30(6): 1351 - 1354.
- Collins, A.S. and Pisarevsky, S.A., 2005. Amalgamating eastern Gondwana: The evolution of the Circum-Indian Orogens. *Earth-Science Reviews*, 71(3-4): 229-270.
- Compston, W., Williams, I.S., Kirschvink, J.L., Zichao, Z. and Guogan, M.A., 1992. Zircon U-Pb ages for the Early Cambrian time-scale. *Journal of the Geological Society*, 149(2): 171-184.
- Compston, W., Zhang, Z., Cooper, J.A., Ma, G. and Jenkins, R.J.F., 2008. Further SHRIMP geochronology on the early Cambrian of South China. *American Journal of Science*, 308(4): 399-420.
- Condie, K.C., Des Marais, D.J. and Abbott, D., 2001. Precambrian superplumes and supercontinents: a record in black shales, carbon isotopes, and paleoclimates. *Precambrian research*, 106(3-4): 22.
- Condon, D. et al., 2005. U-Pb Ages from the Neoproterozoic Doushantuo Formation, China. *Science*, 308(5718): 95-98.
- Conway Morris, S., 1989. The persistence of Burgess Shale-type faunas: implications for the evolution of deeper-water faunas. *Transactions of the Royal Society of Edinburgh: Earth Sciences*, 80(3-4): 271-283.
- Conway Morris, S., 1992. Burgess Shale-type faunas in the context of the 'Cambrian explosion': a review. *Journal of the Geological Society*, 149(4): 631-636.
- Conway Morris, S., 2006. Darwin's dilemma: the realities of the Cambrian 'explosion'. *Philosophical Transactions of the Royal Society B: Biological Sciences*, 361(1470): 1069-1083.
- Cook, P.J., 1992. Phosphogenesis around the Proterozoic-Phanerozoic transition. *Journal of the Geological Society*, 149(4): 615-620.
- Cook, P.M. and Shergold, J.H., 1986. *Phosphate Deposits of the World: Proterozoic and Cambrian phosphorites*. Phosphate Deposits of the World, 1. Cambridge University Press, Cambridge, UK.
- Cornwell, J.C. and Morse, J.W., 1987. The characterization of iron sulfide minerals in anoxic marine sediments. *Marine Chemistry*, 22(2-4): 193-206.
- Corsetti, F.A., Awramik, S.M. and Pierce, D., 2003. A complex microbiota from snowball Earth times: Microfossils from the Neoproterozoic Kingston Peak Formation, Death Valley, USA. *Proceedings of the National Academy of Sciences of the United States of America*, 100(8): 4399-4404.
- Corsetti, F.A. and Kaufman, A.J., 2003. Stratigraphic investigations of carbon isotope anomalies and Neoproterozoic ice ages in Death Valley, California. *Geological Society of America Bulletin*, 115(8): 916-932.
- Corsetti, F.A. and Kaufman, A.J., 2005. The relationship between the Neoproterozoic Noonday Dolomite and the Ibex Formation: New observations and their bearing on [']snowball Earth'. *Earth-Science Reviews*, 73(1-4): 63-78.
- Corsetti, F.A., Olcott, A.N. and Bakermans, C., 2006. The biotic response to Neoproterozoic snowball Earth. *Palaeogeography, Palaeoclimatology, Palaeoecology*, 232(2-4): 114-130.
- Coveney, R.M. and Chen, N., 1991. Ni-Mo-PGE-Au-rich ores in Chinese black shales and speculations on possible analogues in the United States. *Mineralium Deposita*, 26(2): 83-88.
- Cowie, J., 1985. Continuing work on the Precambrian-Cambrian boundary. *Episodes*, 8(2): 93-97.

- Crusius, J., Calvert, S., Pedersen, T. and Sage, D., 1996. Rhenium and molybdenum enrichments in sediments as indicators of oxic, suboxic and sulfidic conditions of deposition. *Earth and Planetary Science Letters*, 145(1-4): 65-78.
- Cuney, M., 2010. Evolution of Uranium Fractionation Processes through Time: Driving the Secular Variation of Uranium Deposit Types. *Economic Geology*, 105(3): 553-569.
- Dalziel, I.W.D., 1991. Pacific margins of Laurentia and East Antarctica-Australia as a conjugate rift pair; evidence and implications for an Eocambrian supercontinent. *Geology*, 19(6): 598-601.
- Danovaro, R. et al., 2010. The first metazoa living in permanently anoxic conditions. *BMC Biology*, 8(1): 30.
- Darwin, C.R., 1859. *On the Origin of the Species*. Murray, London, 502 pp.
- Davies, G.F., 1992. On the emergence of plate tectonics. *Geology*, 20(11): 963-966.
- Davy, R., 1983. A geochemical study of the Mount McRae shale and the upper part of the Mount Sylvia Formation in Core RD1, Rhodes Ridge, Western Australia. *Geological Survey of Western Australia Record*, 3.
- Derry, L.A., 2010. A burial diagenesis origin for the Ediacaran Shuram-Wonoka carbon isotope anomaly. *Earth and Planetary Science Letters*, 294(1-2): 152-162.
- Derry, L.A., Kaufman, A.J. and Jacobsen, S.B., 1992. Sedimentary Cycling and Environmental-Change in the Late Proterozoic - Evidence from Stable and Radiogenic Isotopes. *Geochimica et Cosmochimica Acta*, 56(3): 1317-1329.
- Des Marais, D.J., 1985. Carbon exchange between the mantle and the crust, and its effect upon the atmosphere - Today compared to Archean time. In: E.T. Sundquist and W.S. Broecker (Editors), *The Carbon Cycle and Atmospheric CO<sub>2</sub>: Natural Variations Archean to Present*. American Geophysical Union Washington DC, pp. 602-611.
- Des Marais, D.J., 1997. Isotopic evolution of the biogeochemical carbon cycle during the Proterozoic Eon. *Organic Geochemistry*, 27(5-6): 185-193.
- Des Marais, D.J., 2001. Isotopic Evolution of the Biogeochemical Carbon Cycle During the Precambrian. *Reviews in Mineralogy and Geochemistry*, 43(1): 555-578.
- Des Marais, D.J., Strauss, H., Summons, R.E. and Hayes, J.M., 1992. Carbon isotope evidence for the stepwise oxidation of the Proterozoic environment. *Nature*, 359(6396): 605-609.
- Di Giulio, M., 2003. The ancestor of the Bacteria domain was a hyperthermophile. *Journal of Theoretical Biology*, 224(3): 277-283.
- Dimroth, E. and Kimberley, M.M., 1976. Precambrian atmospheric oxygen: evidence in the sedimentary distributions of carbon, sulfur, uranium, and iron. *Canadian Journal of Earth Sciences*, 13(9): 1161-1185
- Ding, L. et al., 1996. *Sinian Miaohu Biota*. Geological Publishing House, Beijing.
- Ding, L., Zhang, L., Li, Y. and Dong, J., 1992. *The Study of the Late Sinian-Early Cambrian Biotas from the Northern Margin of the Yangtze Platform*. Scientific and Technical Documents Publishing House, Beijing, 135.
- Doolittle, R.F., Feng, D.-F., Tsang, S., Cho, G. and Little, E., 1996. Determining Divergence Times of the Major Kingdoms of Living Organisms with a Protein Clock. *Science*, 271(5248): 470-477.
- Dornbos, S.Q., Bottjer, D.J. and Chen, J.-Y., 2005. Paleoecology of benthic metazoans in the Early Cambrian Maotianshan Shale biota and the Middle Cambrian Burgess Shale biota: evidence for the Cambrian substrate revolution. *Palaeogeography, Palaeoclimatology, Palaeoecology*, 220(1-2): 47-67.
- Douzery, E.J.P., Snell, E.A., Baptiste, E., Delsuc, F.d.r. and Philippe, H., 2004. The timing of eukaryotic evolution: Does a relaxed molecular clock reconcile proteins and fossils? *Proceedings of the National Academy of Sciences of the United States of America*, 101(43): 15386-15391.

- Drever, J., Li, Y. and Maynard, J., 1988. Geochemical cycles: the continental crust and the oceans. In: C.B. Gregor (Editor), *Chemical Cycles in the Evolution of the Earth*. John Wiley, New York, pp. 17–53.
- Droser, M.L., Jensen, S. and Gehling, J.G., 2002. Trace fossils and substrates of the terminal Proterozoic-Cambrian transition: Implications for the record of early bilaterians and sediment mixing. *Proceedings of the National Academy of Sciences of the United States of America*, 99(20): 12572-12576.
- Dymond, J., Suess, E. and Lyle, M., 1992. Barium in Deep-Sea Sediment: A Geochemical Proxy for Paleoproductivity. *Paleoceanography*, 7(2): 163-181.
- Eady, R.R., 1996. Structure-Function Relationships of Alternative Nitrogenases. *Chemical Reviews*, 96(7): 3013-3030.
- Eisbacher, G.H., 1985. Late proterozoic rifting, glacial sedimentation, and sedimentary cycles in the light of windermere deposition, Western Canada. *Palaeogeography, Palaeoclimatology, Palaeoecology*, 51(1-4): 231-254.
- Elie, M., Nogueira, A.C.R., Nédélec, A., Trindade, R.I.F. and Kenig, F., 2007. A red algal bloom in the aftermath of the Marinoan Snowball Earth. *Terra Nova*, 19(5): 303-308.
- Ellis, A.S., Johnson, T.M. and Bullen, T.D., 2002. Chromium Isotopes and the Fate of Hexavalent Chromium in the Environment. *Science*, 295(5562): 2060-2062.
- Ellis, R.J., 1979. The most abundant protein in the world. *Trends in Biochemical Sciences*, 4(11): 241-244.
- Emerson, S.R. and Huested, S.S., 1991. Ocean anoxia and the concentrations of molybdenum and vanadium in seawater. *Marine Chemistry*, 34(3-4): 177-196.
- Erickson, B.E. and Helz, G.R., 2000. Molybdenum(VI) speciation in sulfidic waters:: Stability and lability of thiomolybdates. *Geochimica et Cosmochimica Acta*, 64(7): 1149-1158.
- Ernst, R.E., Wingate, M.T.D., Buchan, K.L. and Li, Z.X., 2008. Global record of 1600-700 Ma Large Igneous Provinces (LIPs): Implications for the reconstruction of the proposed Nuna (Columbia) and Rodinia supercontinents. *Precambrian Research*, 160(1-2): 159-178.
- Ernst, W.G., 2003. High-pressure and ultrahigh-pressure metamorphic belts- Subduction, recrystallization, exhumation, and significance for ophiolite study. *Special Paper: Ophiolite concept and the evolution of geological thought*, 373(0): 365-384.
- Ernst, W.G., 2007. Speculations on evolution of the terrestrial lithosphere-asthenosphere system-- Plumes and plates. *Gondwana Research*, 11(1-2): 38-49.
- Ernst, W.G. and Peacock, S.M., 1996. A thermotectonic model for preservation of ultrahigh pressure phases in metamorphosed continental crust. In: G.E. Bebout, et al. (Editor), *Subduction: Top to bottom*. Geophysical Monograph. American Geophysical Union.
- Erwin, D.H., 2006. Dates and Rates: Temporal Resolution in the Deep Time Stratigraphic Record\*. *Annual Review of Earth and Planetary Sciences*, 34(1): 569-590.
- Erwin, D.H. and Davidson, E.H., 2002. The last common bilaterian ancestor. *Development*, 129(13): 3021-3032.
- Evans, D.A., Beukes, N.J. and Kirschvink, J.L., 1997. Low-latitude glaciation in the Palaeoproterozoic era. *Nature*, 386(6622): 262-266.
- Evans, D.A.D., 2003a. A fundamental Precambrian-Phanerozoic shift in earth's glacial style? *Tectonophysics*, 375(1-4): 353-385.
- Evans, D.A.D., 2003b. True polar wander and supercontinents. *Tectonophysics*, 362(1-4): 303-320.
- Eyles, N. and Januszczak, N., 2004. 'Zipper-rift': a tectonic model for Neoproterozoic glaciations during the breakup of Rodinia after 750 Ma. *Earth-Science Reviews*, 65(1-2): 1-73.
- Falkowski, P.G. and Godfrey, L.V., 2008. Electrons, life and the evolution of Earth's oxygen cycle. *Philosophical Transactions of the Royal Society B: Biological Sciences*, 363: 2705-2716.
- Fairchild, I.J. and Kennedy, M.J., 2007. Neoproterozoic glaciation in the Earth System. *Journal of the Geological Society*, 164(5): 895-921.

- Falkowski, P.G. and Godfrey, L.V., 2008. Electrons, life and the evolution of Earth's oxygen cycle. *Philosophical Transactions of the Royal Society B: Biological Sciences*, 363(1504): 2705-2716.
- Fanning, C.M. and Link, P.K., 2004. U-Pb SHRIMP ages of Neoproterozoic (Sturtian) glaciogenic Pocatello Formation, southeastern Idaho. *Geology*, 32(10): 881-884.
- Farquhar, J. and Wing, B.A., 2003. Multiple sulfur isotopes and the evolution of the atmosphere. *Earth and Planetary Science Letters*, 213(1-2): 1-13.
- Farquhar, J., Wu, N., Canfield, D.E. and Oduro, H., 2010a. Connections between Sulfur Cycle Evolution, Sulfur Isotopes, Sediments, and Base Metal Sulfide Deposits. *Economic Geology*, 105(3): 509-533.
- Farquhar, J., Zerkle, A. and Bekker, A., 2010b. Geological constraints on the origin of oxygenic photosynthesis. *Photosynthesis Research*: 1-26.
- Faure, G., 1986. *Principles of isotope geology*. Second edition. John Wiley and Sons Inc., New York, NY, United States, Pages: 592 pp.
- Fee, J.A., 1982. Is superoxide important in oxygen poisoning? *Trends in Biochemical Sciences*, 7(3): 84-86.
- Felitsyn, S. and Morad, S., 2002. REE patterns in latest Neoproterozoic-early Cambrian phosphate concretions and associated organic matter. *Chemical Geology*, 187(3-4): 257-265.
- Fendorf, S.E., 1995. Surface reactions of chromium in soils and waters. *Geoderma*, 67(1-2): 55-71.
- Feng, L.-J., Chu, X.-L., Huang, J., Zhang, Q.-R. and Chang, H.-J., 2010. Reconstruction of paleo-redox conditions and early sulfur cycling during deposition of the Cryogenian Datangpo Formation in South China. *Gondwana Research*, 18(4): 632-637.
- Fennel, K., Follows, M. and Falkowski, P.G., 2005. The co-evolution of the nitrogen, carbon and oxygen cycles in the Proterozoic ocean. *American Journal of Science*, 305(6-8): 526-545.
- Ferreira, K.N., Iverson, T.M., Maghlaoui, K., Barber, J. and Iwata, S., 2004. Architecture of the Photosynthetic Oxygen-Evolving Center. *Science*, 303(5665): 1831-1838.
- Fischer, W.W., Summons, R.E. and Pearson, A., 2005. Targeted genomic detection of biosynthetic pathways: anaerobic production of hopanoid biomarkers by a common sedimentary microbe. *Geobiology*, 3(1): 33-40.
- Fitton, G., 1997. X-ray fluorescence spectrometry. In: R. Gill (Editor), *Modern analytical geochemistry: an introduction to quantitative chemical analysis techniques for earth, environmental and materials scientists*. Longman, Harlow, UK, pp. 87-115.
- François, L.M. and Walker, J.C.G., 1992. Modelling the Phanerozoic carbon cycle and climate; constraints from the  $^{87}\text{Sr}/^{86}\text{Sr}$  isotopic ratio of seawater. *American Journal of Science*, 292(2): 81-135.
- Frimmel, H.E., 2008. An evaporitic facies in Neoproterozoic post-glacial carbonates: The Gifberg Group, South Africa. *Gondwana Research*, 13(4): 453-468.
- Froelich, P.N., Bender, M.L., Luedtke, N.A., Heath, G.R. and DeVries, T., 1982. The marine phosphorus cycle. *American Journal of Science*, 282(4): 474-511.
- Fry, B., Ruf, W., Gest, H. and Hayes, J.M., 1988. Sulfur isotope effects associated with oxidation of sulfide by O<sub>2</sub> in aqueous solution. *Chemical Geology: Isotope Geoscience section*, 73(3): 205-210.
- Gagnon, C., Mucci, A. and Pelletier, É., 1995. Anomalous accumulation of acid-volatile sulphides (AVS) in a coastal marine sediment, Saguenay Fjord, Canada. *Geochimica et Cosmochimica Acta*, 59(13): 2663-2675.
- Gaillardet, J., Dupré, B., Louvat, P. and Allègre, C.J., 1999. Global silicate weathering and CO<sub>2</sub> consumption rates deduced from the chemistry of large rivers. *Chemical Geology*, 159(1-4): 3-30.
- Gaines, R.R. and Droser, M.L., 2010. The paleoredox setting of Burgess Shale-type deposits. *Palaeogeography, Palaeoclimatology, Palaeoecology*, 297(3-4): 649-661.
- Garrels, R.M. and Perry, E.A., 1974. Cycling of carbon, sulfur and oxygen through geological time. In: E.D. Goldberg (Editor), *The Sea*. Wiley Interscience, New York, pp. 303-16.
- Garrels, R.M., Perry, E.A. and Mackenzie, F.T., 1973. Genesis of Precambrian Iron-Formations and the Development of Atmospheric Oxygen. *Economic Geology*, 68(7): 1173-1179.

- Gehling, J.G., 1999. Microbial mats in terminal Proterozoic siliciclastics; Ediacaran death masks. *PALAIOS*, 14(1): 40-57.
- Gellatly, A.M. and Lyons, T.W., 2005. Trace sulfate in mid-Proterozoic carbonates and the sulfur isotope record of biospheric evolution. *Geochimica et Cosmochimica Acta*, 69(15): 3813-3829.
- German, C.R. and Elderfield, H., 1990. Application of the Ce Anomaly as a Paleoredox Indicator: The Ground Rules. *Paleoceanography*, 5.
- Giddings, J.A. and Wallace, M.W., 2009. Facies-dependent  $\delta^{13}\text{C}$  variation from a Cryogenian platform margin, South Australia: Evidence for stratified Neoproterozoic oceans? *Palaeogeography, Palaeoclimatology, Palaeoecology*, 271(3-4): 196-214.
- Glaessner, M.F., 1959. The oldest fossil faunas of South Australia. *International Journal of Earth Sciences*, 47(2): 522-531.
- Glass, J.B., Wolfe-Simon, F. and Anbar, A.D., 2009. Coevolution of metal availability and nitrogen assimilation in cyanobacteria and algae. *Geobiology*, 7(2): 100-123.
- Godfrey, L.V. and Falkowski, P.G., 2009. The cycling and redox state of nitrogen in the Archaean ocean. *Nature Geoscience*, 2: 725-729
- Goldstein, S.L., 1988. Decoupled evolution of Nd and Sr isotopes in the continental crust and the mantle. *Nature*, 336(6201): 733-738.
- Gorjan, P., Veevers, J.J. and Walter, M.R., 2000. Neoproterozoic sulfur-isotope variation in Australia and global implications. *Precambrian Research*, 100(1-3): 151-179.
- Gorjan, P., Walter, M.R. and Swart, P.K., 2003. Global Neoproterozoic (Sturtian) post-glacial sulfide-sulfur isotope anomaly recognised in Namibia. *Journal of African Earth Sciences*, 36(1-2): 89-98
- Gould, S.J., 1989. *Wonderful life: the Burgess Shale and the nature of history*. Norton, New York.
- Grant, S.W.F., 1990. Shell structure and distribution of Cloudina, a potential index fossil for the terminal Proterozoic. *American Journal of Science*, 290-A: 261-294.
- Grantham, P., Lijmbach, G., Posthuma, J., Clarke, M. and Willink, R., 1988. Origin of crude oils in Oman. *Journal of Petroleum Geology*, 11: 61-80.
- Grazhdankin, D., 2004. Patterns of distribution in the Ediacaran biotas: facies versus biogeography and evolution. *Paleobiology*, 30(2): 203-221.
- Grey, K., Walter, M.R. and Calver, C.R., 2003. Neoproterozoic biotic diversification: Snowball Earth or aftermath of the Acraman impact? *Geology*, 31(5): 459-462.
- Grotzinger, J.P. and Kasting, J.F., 1993. New Constraints on Precambrian Ocean Composition. *The Journal of Geology*, 101(2): 235-243.
- Grotzinger, J.P. and Knoll, A.H., 1995. Anomalous carbonate precipitates; is the Precambrian the key to the Permian? *Palaaios*, 10(6): 578-596.
- Grotzinger, J.P. and Knoll, A.H., 1999. Stromatolites in Precambrian carbonates: Evolutionary Mileposts or Environmental Dipsticks? *Annual Review of Earth and Planetary Sciences*, 27(1): 313-358.
- Grotzinger, J.P., Watters, W.A. and Knoll, A.H., 2000. Calcified Metazoans in Thrombolite-Stromatolite Reefs of the Terminal Proterozoic Nama Group, Namibia. *Paleobiology*, 26(3): 334-359.
- Guo, Q. et al., 2007. Trace element chemostratigraphy of two Ediacaran-Cambrian successions in South China: Implications for organosedimentary metal enrichment and silicification in the Early Cambrian. *Palaeogeography, Palaeoclimatology, Palaeoecology*, 254(1-2): 194-216.
- Habicht, K.S., Gade, M., Thamdrup, B., Berg, P. and Canfield, D.E., 2002. Calibration of Sulfate Levels in the Archean Ocean. *Science*, 298(5602): 2372-2374.
- Hagadorn, J.W., 2002. Chengjiang: early record of the Cambrian explosion. In: D.J. Bottjer, W. Etter, J.W. Hagadorn and C.M. Tang (Editors), *Exceptional Fossil Preservation: A Unique View on the Evolution of Marine Life*. Columbia University Press, New York, pp. 35-60.

- Halverson, G., 2006. A Neoproterozoic Chronology, Neoproterozoic Geobiology and Paleobiology, pp. 231-271.
- Halverson, G.P., Dudás, F.Ö., Maloof, A.C. and Bowring, S.A., 2007. Evolution of the  $^{87}\text{Sr}/^{86}\text{Sr}$  composition of Neoproterozoic seawater. *Palaeogeography, Palaeoclimatology, Palaeoecology*, 256(3-4): 103-129.
- Halverson, G.P., Hoffman, P.F., Schrag, D.P., Maloof, A.C. and Rice, A.H.N., 2005. Toward a Neoproterozoic composite carbon-isotope record. *Geological Society of America Bulletin*, 117(9): 1181-1207.
- Halverson, G.P. and Hurtgen, M.T., 2007. Ediacaran growth of the marine sulfate reservoir. *Earth and Planetary Science Letters*, 263(1-2): 32-44.
- Hambrey, M.J. and Harland, W.B., 1981. *Earth's pre-Pleistocene glacial record*. Cambridge University Press.
- Haq, B.U. and Schutter, S.R., 2008. A Chronology of Paleozoic Sea-Level Changes. *Science*, 322(5898): 64-68.
- Hatch, J.R. and Leventhal, J.S., 1992. Relationship between inferred redox potential of the depositional environment and geochemistry of the Upper Pennsylvanian (Missourian) Stark Shale Member of the Dennis Limestone, Wabaunsee County, Kansas, U.S.A. *Chemical Geology*, 99(1-3): 65-82.
- Hayashi, K.-I., Fujisawa, H., Holland, H.D. and Ohmoto, H., 1997. Geochemistry of ~1.9 Ga sedimentary rocks from northeastern Labrador, Canada. *Geochimica et Cosmochimica Acta*, 61(19): 4115-4137.
- Hayes, J.M., Strauss, H. and Kaufman, A.J., 1999. The abundance of  $^{13}\text{C}$  in marine organic matter and isotopic fractionation in the global biogeochemical cycle of carbon during the past 800 Ma. *Chemical Geology*, 161(1-3): 103-125.
- Hayes, J.M. and Waldbauer, J.R., 2006. The carbon cycle and associated redox processes through time. *Philosophical Transactions of the Royal Society B: Biological Sciences*, 361(1470): 931-950.
- Hazen, R.M. et al., 2008. Mineral evolution. *American Mineralogist*, 93(11-12): 1693-1720.
- Heaman, L., 1997. Global mafic magmatism at 2.45 Ga: Remnants of an ancient large igneous province? *Geology*, 25(4): 299-302.
- Heckman, D.S. et al., 2001. Molecular Evidence for the Early Colonization of Land by Fungi and Plants. *Science*, 293(5532): 1129-1133.
- Hedges, S., Blair, J., Venturi, M. and Shoe, J., 2004. A molecular timescale of eukaryote evolution and the rise of complex multicellular life. *BMC Evolutionary Biology*, 4(1): 2.
- Helz, G.R. et al., 1996. Mechanism of molybdenum removal from the sea and its concentration in black shales: EXAFS evidence. *Geochimica et Cosmochimica Acta*, 60(19): 3631-3642.
- Hill, A.C. and Walter, M.R., 2000. Mid-Neoproterozoic (~830-750 Ma) isotope stratigraphy of Australia and global correlation. *Precambrian Research*, 100: 181-211.
- Ho, T.-Y. et al., 2003. The elemental composition of some marine phytoplankton. *Journal of Phycology*, 39(6): 1145-1159.
- Hoashi, M. et al., 2009. Primary haematite formation in an oxygenated sea 3.46 billion years ago. *Nature Geoscience*, 2(4): 301-306.
- Hoffman, P.F., 1991. Did the Breakout of Laurentia Turn Gondwanaland Inside-Out? *Science*, 252(5011): 1409-1412.
- Hoffman, P.F., 1997. Tectonic genealogy of North America. In: B.A. van der Pluum and S. Marshak (Editors), *Earth Structure: An Introduction to Structural Geology and Tectonics*. , McGraw-Hill, New York, pp. 459-464.
- Hoffman, P.F., 2009. Pan-glacial - a third state in the climate system. *Geology Today*, 25(3): 100-107.
- Hoffman, P.F. et al., 2007. Are basal Ediacaran (635 Ma) post-glacial "cap dolostones" diachronous? *Earth and Planetary Science Letters*, 258(1-2): 114-131.

- Hoffman, P.F., Kaufman, A.J., Halverson, G.P. and Schrag, D.P., 1998. A Neoproterozoic Snowball Earth. *Science*, 281(5381): 1342-1346.
- Hoffman, P.F. and Li, Z.-X., 2009. A palaeogeographic context for Neoproterozoic glaciation. *Palaeogeography, Palaeoclimatology, Palaeoecology*, 277(3-4): 158-172.
- Hoffman, P.F. and Schrag, D.P., 2002. The snowball Earth hypothesis: testing the limits of global change. *Terra Nova*, 14(3): 129-155.
- Hoffmann, K.-H., Condon, D.J., Bowring, S.A. and Crowley, J.L., 2004. U-Pb zircon date from the Neoproterozoic Ghaub Formation, Namibia: Constraints on Marinoan glaciation. *Geology*, 32(9): 817-820.
- Hofmann, H.J. and Mountjoy, E.W., 2001. Namacalathus-Cloudina assemblage in Neoproterozoic Miette Group (Byng Formation), British Columbia: Canada's oldest shelly fossils. *Geology*, 29(12): 1091-1094.
- Hofmann, H.J., Narbonne, G.M. and Aitken, J.D., 1990. Ediacaran remains from intertillite beds in northwestern Canada. *Geology*, 18(12): 1199-1202.
- Holland, H.D., 1984. *The Chemical Evolution of the Atmosphere and Oceans*. Princeton University Press, Princeton, NY, pp. 582.
- Holland, H.D., 1994. Early Proterozoic atmospheric change. In: S. Bengtson (Editor), *Early Life on Earth*. Columbia University Press, New York, pp. 237-244.
- Holland, H.D., 2002. Volcanic gases, black smokers, and the great oxidation event. *Geochimica et Cosmochimica Acta*, 66(21): 3811-3826.
- Holland, H.D., 2004. The Geologic History of Seawater. In: H.D. Holland and K.K. Turekian (Editors), *Treatise on Geochemistry*. Elsevier, Oxford, pp. 583 - 625.
- Holland, H.D., 2006. The oxygenation of the atmosphere and oceans. *Philosophical Transactions of the Royal Society B: Biological Sciences*, 361(1470): 903-915.
- Holland, H.D., 2009. Why the atmosphere became oxygenated: A proposal. *Geochimica et Cosmochimica Acta*, 73(18): 5241-5255.
- Holser, W.T., 1997. Evaluation of the application of rare-earth elements to paleoceanography. *Palaeogeography, Palaeoclimatology, Palaeoecology*, 132(1-4): 309-323.
- Horodyski, R.J. and Knauth, L.P., 1994. Life on Land in the Precambrian. *Science*, 263(5146): 494-498.
- Hou, X., Ramsköld, L. and Bergström, J., 1991. Composition and preservation of the Chengjiang fauna - a Lower Cambrian soft-bodied biota. *Zoologica Scripta*, 20(4): 395-411.
- Howard, J.B. and Rees, D.C., 1996. Structural Basis of Biological Nitrogen Fixation. *Chemical Reviews*, 96(7): 2965-2982.
- Hsü, K.J. et al., 1985. 'Strangelove ocean' before the Cambrian explosion. *Nature*, 316(6031): 809-811.
- Hua, H., Pratt, B.R. and Zhang, Y.-L., 2003. Borings in Cloudina Shells: Complex Predator-Prey Dynamics in the Terminal Neoproterozoic. *PALAIOS*, 18(4): 454-459.
- Huerta-Diaz, M.A. and Morse, J.W., 1992. Pyritization of trace metals in anoxic marine sediments. *Geochimica et Cosmochimica Acta*, 56(7): 2681-2702.
- Hurtgen, M.T., Arthur, M.A. and Halverson, G.P., 2005. Neoproterozoic sulfur isotopes, the evolution of microbial sulfur species, and the burial efficiency of sulfide as sedimentary pyrite. *Geology*, 33(1): 41-44.
- Hurtgen, M.T., Pruss, S.B. and Knoll, A.H., 2009. Evaluating the relationship between the carbon and sulfur cycles in the later Cambrian ocean: An example from the Port au Port Group, western Newfoundland, Canada. *Earth and Planetary Science Letters*, 281(3-4): 288-297.
- Hyde, W.T., Crowley, T.J., Baum, S.K. and Peltier, W.R., 2000. Neoproterozoic 'snowball Earth' simulations with a coupled climate/ice-sheet model. *Nature*, 405(6785): 425-429.



- Ishikawa, T. et al., 2008. Carbon isotope chemostratigraphy of a Precambrian/Cambrian boundary section in the Three Gorge area, South China: Prominent global-scale isotope excursions just before the Cambrian Explosion. *Gondwana Research*, 14(1-2): 193-208.
- Isley, A.E. and Abbott, D.H., 1999. Plume-related mafic volcanism and the deposition of banded iron formation. *Journal of Geophysical Research*, 104(15): 461 - 15 477.
- Izbicki, J.A., Ball, J.W., Bullen, T.D. and Sutley, S.J., 2008. Chromium, chromium isotopes and selected trace elements, western Mojave Desert, USA. *Applied Geochemistry*, 23(5): 1325-1352.
- Jacobs, J. and Thomas, R.J., 2004. Himalayan-type indenter-escape tectonics model for the southern part of the late Neoproterozoic-early Paleozoic East African- Antarctic orogen. *Geology*, 32(8): 721-724.
- Jacobsen, S.B., 1988. Isotopic constraints on crustal growth and recycling. *Earth and Planetary Science Letters*, 90(3): 315-329.
- Jacobsen, S.B. and Kaufman, A.J., 1999. The Sr, C and O isotopic evolution of Neoproterozoic seawater. *Chemical Geology*, 161(1-3): 37-57.
- Jahn, B.-M., Caby, R. and Monie, P., 2001. The oldest UHP eclogites of the World: age of UHP metamorphism, nature of protoliths and tectonic implications. *Chemical Geology*, 178(1-4): 143-158.
- James, N.P., Narbonne, G.M., Dalrymple, R.W. and Kyser, T.K., 2005. Glendonites in Neoproterozoic low-latitude, interglacial, sedimentary rocks, northwest Canada: Insights into the Cryogenian ocean and Precambrian cold-water carbonates. *Geology*, 33(1): 9-12.
- James, N.P., Narbonne, G.M. and Kyser, T.K., 2001. Late Neoproterozoic cap carbonates: Mackenzie Mountains, northwestern Canada: precipitation and global glacial meltdown. *Canadian Journal of Earth Sciences*, 38(8): 1229-1262
- Jarvis, I. et al., 1994. Phosphorite geochemistry: state-of-the-art and environmental concerns. *Eclogae Geologicae Helveticae*, 87(3): 643-700.
- Jarvis, K.E., 1997. Inductively coupled plasma-mass spectrometry. In: R. Gill (Editor), *Modern analytical geochemistry: an introduction to quantitative chemical analysis techniques for earth, environmental and materials scientists*. Longman, Harlow, UK, pp. 87-115.
- Jenkins, R.J.F., Cooper, J.A. and Compston, W., 2002. Age and biostratigraphy of Early Cambrian tuffs from SE Australia and southern China. *Journal of the Geological Society*, 159(6): 645-658.
- Jensen, S., Gehling, J.G. and Droser, M.L., 1998. Ediacara-type fossils in Cambrian sediments. *Nature*, 393(6685): 567-569.
- Jiang, G., Kaufman, A.J., Christie-Blick, N., Zhang, S. and Wu, H., 2007a. Carbon isotope variability across the Ediacaran Yangtze platform in South China: Implications for a large surface-to-deep ocean  $\delta^{13}\text{C}$  gradient. *Earth and Planetary Science Letters*, 261(1-2): 303-320.
- Jiang, G., Kennedy, M.J. and Christie-Blick, N., 2003a. Stable isotopic evidence for methane seeps in Neoproterozoic postglacial cap carbonates. *Nature*, 426(6968): 822-826.
- Jiang, G., Kennedy, M.J., Christie-Blick, N., Wu, H. and Zhang, S., 2006a. Stratigraphy, Sedimentary Structures, and Textures of the Late Neoproterozoic Doushantuo Cap Carbonate in South China. *JOURNAL OF SEDIMENTARY RESEARCH*, 76(7): 978-995.
- Jiang, G., Shi, X., Zhang, S., Wang, Y. and Xiao, S., 2011. Stratigraphy and paleogeography of the Ediacaran Doushantuo Formation (ca. 635-551 Ma) in South China. *Gondwana Research*, In Press, Corrected Proof.
- Jiang, G., Sohl, L.E. and Christie-Blick, N., 2003b. Neoproterozoic stratigraphic comparison of the Lesser Himalaya (India) and Yangtze block (south China): Paleogeographic implications. *Geology*, 31(10): 917-920.

- Jiang, G., Zhang, S., Shi, X. and Wang, X., 2008. Chemocline instability and isotope variations of the Ediacaran Doushantuo basin in South China. *Science in China Series D: Earth Sciences*, 51(11): 1560-1569.
- Jiang, S.-Y. et al., 2006b. Trace- and rare-earth element geochemistry and Pb–Pb dating of black shales and intercalated Ni–Mo–PGE–Au sulfide ores in Lower Cambrian strata, Yangtze Platform, South China. *Mineralium Deposita*, 41(5): 453-467.
- Jiang, S.-Y. et al., 2007b. Extreme enrichment of polymetallic Ni-Mo-PGE-Au in Lower Cambrian black shales of South China: An Os isotope and PGE geochemical investigation. *Palaeogeography, Palaeoclimatology, Palaeoecology*, 254(1-2): 217-228.
- Johnston, D.T. et al., 2005. Multiple sulfur isotope fractionations in biological systems: A case study with sulfate reducers and sulfur disproportionators. *American Journal of Science*, 305(6-8): 645-660.
- Johnston, D.T. et al., 2006. Evolution of the oceanic sulfur cycle at the end of the Paleoproterozoic. *Geochimica et Cosmochimica Acta*, 70(23): 5723-5739.
- Johnston, D.T., Wolfe-Simon, F., Pearson, A. and Knoll, A.H., 2009. Anoxygenic photosynthesis modulated Proterozoic oxygen and sustained Earth's middle age. *Proceedings of the National Academy of Sciences*, 106(40): 16925-16929.
- Jones, B. and Manning, D.A.C., 1994. Comparison of geochemical indices used for the interpretation of palaeoredox conditions in ancient mudstones. *Chemical Geology*, 111(1-4): 111-129.
- Kah, L.C., Sherman, A.G., Narbonne, G.M., Knoll, A.H. and Kaufman, A.J., 1999.  $\delta^{13}\text{C}$  stratigraphy of the Proterozoic Bylot Supergroup, Baffin Island, Canada: Implications for regional lithostratigraphic correlations. *Canadian Journal of Earth Sciences*, 36: 313-332.
- Karhu, J.A., 1993. Paleoproterozoic evolution of the carbon isotope ratios of sedimentary carbonates in the Fennoscandian Shield. *Bulletin - Geological Survey of Finland*, 371: 87.
- Karhu, J.A. and Holland, H.D., 1996. Carbon isotopes and the rise of atmospheric oxygen. *Geology*, 24(10): 867-870.
- Kasemann, S.A., Hawkesworth, C.J., Prave, A.R., Fallick, A.E. and Pearson, P.N., 2005. Boron and calcium isotope composition in Neoproterozoic carbonate rocks from Namibia: evidence for extreme environmental change. *Earth and Planetary Science Letters*, 231(1-2): 73-86.
- Kasting, J.F., 1987. Theoretical constraints on oxygen and carbon dioxide concentrations in the Precambrian atmosphere. *Precambrian Research*, 34(3-4): 205-229.
- Kasting, J.F., Egger, D.H. and Raeburn, S.P., 1993. Mantle redox evolution and the oxidation state of the Archean atmosphere. *The Journal of Geology*, 101(2): 245-57.
- Kasting, J.F. and Ono, S., 2006. Palaeoclimates: the first two billion years. *Philosophical Transactions of the Royal Society B: Biological Sciences*, 361(1470): 917-929.
- Kasting, J.F., Pavlov, A.A. and Siefert, J.L., 2001. A Coupled Ecosystem-Climate Model for Predicting the Methane Concentration in the Archean Atmosphere. *Origins of Life and Evolution of Biospheres*, 31(3): 271-285.
- Kato, Y., Yamaguchi, K.E. and Ohmoto, H., 2006. Rare earth elements in Precambrian banded iron formations: Secular changes of Ce and Eu anomalies and evolution of atmospheric oxygen. *Memoir 198: Evolution of Early Earth's Atmosphere, Hydrosphere, and Biosphere - Constraints from Ore Deposits*, 198(0): 269-289.
- Kaufman, A. and Xiao, S., 2003. High  $\text{CO}_2$  levels in the Proterozoic atmosphere estimated from analyses of individual microfossils. *Nature*, 425(6955): 279-282.
- Kaufman, A.J. and Knoll, A.H., 1995. Neoproterozoic variations in the C-isotopic composition of seawater: stratigraphic and biogeochemical implications. *Precambrian Research*, 73(1-4): 27-49.
- Kaufman, A.J., Knoll, A.H. and Narbonne, G.M., 1997. Isotopes, ice ages, and terminal Proterozoic Earth history. *Proceedings of the National Academy of Sciences of the United States of America*, 94(13): 6600-6605.

- Kendall, B. et al., 2010. Pervasive oxygenation along late Archaean ocean margins. *Nature Geoscience*, 3: 647-652.
- Kennedy, M., Droser, M., Mayer, L.M., Pevear, D. and Mrofka, D., 2006. Late Precambrian Oxygenation; Inception of the Clay Mineral Factory. *Science*, 311(5766): 1446-1449.
- Kennedy, M.J., 1996. Stratigraphy, sedimentology, and isotopic geochemistry of Australian Neoproterozoic postglacial cap dolostones; deglaciation, delta 13 C excursions, and carbonate precipitation. *Journal of Sedimentary Research*, 66(6): 1050-1064.
- Kennedy, M.J., Christie-Blick, N. and Sohl, L.E., 2001. Are Proterozoic cap carbonates and isotopic excursions a record of gas hydrate destabilization following Earth's coldest intervals? *Geology*, 29(5): 443-446.
- Kennedy, M.J., Pevear, D.R. and Hill, R.J., 2002. Mineral Surface Control of Organic Carbon in Black Shale. *Science*, 295(5555): 657-660.
- Kennedy, M.J., Runnegar, B., Prave, A.R., Hoffmann, K.H. and Arthur, M.A., 1998. Two or four Neoproterozoic glaciations? *Geology*, 26(12): 1059-1063.
- Kenny, R. and Knauth, L.P., 2001. Stable isotope variations in the Neoproterozoic Beck Spring Dolomite and Mesoproterozoic Mescal Limestone paleokarst: Implications for life on land in the Precambrian. *Geological Society of America Bulletin*, 113(5): 650-658.
- Khain, E.V. et al., 2002. The most ancient ophiolite of the Central Asian fold belt: U-Pb and Pb-Pb zircon ages for the Dunzhugur Complex, Eastern Sayan, Siberia, and geodynamic implications. *Earth and Planetary Science Letters*, 199(3-4): 311-325.
- Kidder, D.L., Krishnaswamy, R. and Mapes, R.H., 2003. Elemental mobility in phosphatic shales during concretion growth and implications for provenance analysis. *Chemical Geology*, 198(3-4): 335-353.
- Kimura, H. and Watanabe, Y., 2001. Oceanic anoxia at the Precambrian-Cambrian boundary. *Geology*, 29(11): 995-998.
- Kirschvink, J., 1992. Late Proterozoic low-latitude global glaciation: The snowball Earth. In: J.W. Schopf and C. Klein (Editors), *The Proterozoic Biosphere*. Cambridge University Press, pp. 51-52.
- Kirschvink, J.L. et al., 2000. Paleoproterozoic snowball Earth: Extreme climatic and geochemical global change and its biological consequences. *Proceedings of the National Academy of Sciences of the United States of America*, 97(4): 1400-1405.
- Kirschvink, J.L. and Raub, T.D., 2003. A methane fuse for the Cambrian explosion: carbon cycles and true polar wander. *Comptes Rendus Geosciences*, 335(1): 65-78.
- Kirschvink, J.L., Ripperdan, R.L. and Evans, D.A., 1997. Evidence for a Large-Scale Reorganization of Early Cambrian Continental Masses by Inertial Interchange True Polar Wander. *Science*, 277(5325): 541-545.
- Klinkhammer, G.P. and Palmer, M.R., 1991. Uranium in the oceans: Where it goes and why. *Geochimica et Cosmochimica Acta*, 55(7): 1799-1806.
- Knauth, L.P. and Kennedy, M.J., 2009. The late Precambrian greening of the Earth. *Nature*, 460(7256): 728-732.
- Knoll, A.H., 2000. Learning to tell Neoproterozoic time. *Precambrian Research*, 100(1-3): 3-20.
- Knoll, A.H., 2003. *Life on a Young Planet; The First Three Billion Years of Evolution on Earth*. Princeton Univ. Press, Princeton/Oxford, 277 pp.
- Knoll, A.H. and Carroll, S.B., 1999. Early Animal Evolution: Emerging Views from Comparative Biology and Geology. *Science*, 284(5423): 2129-2137.
- Knoll, A.H., Hayes, J.M., Kaufman, A.J., Swett, K. and Lambert, I.B., 1986. Secular variation in carbon isotope ratios from Upper Proterozoic successions of Svalbard and East Greenland. *Nature*, 321(6073): 832-838.

- Knoll, A.H., Javaux, E.J., Hewitt, D. and Cohen, P., 2006. Eukaryotic organisms in Proterozoic oceans. *Philosophical Transactions of the Royal Society B: Biological Sciences*, 361(1470): 1023-1038.
- Knoll, A.H. and Walter, M.R., 1992. Latest Proterozoic stratigraphy and Earth history. *Nature*, 356(6371): 673-678.
- Knudsen, A.C. and Gunter, M.E., 2002. Sedimentary Phosphorites--An Example: Phosphoria Formation, Southeastern Idaho, U.S.A. *Reviews in Mineralogy and Geochemistry*, 48(1): 363-389.
- Komiya, T. et al., 2008. Evolution of the composition of seawater through geologic time, and its influence on the evolution of life. *Gondwana Research*, 14(1-2): 159-174.
- Kopp, R.E., Kirschvink, J.L., Hilburn, I.A. and Nash, C.Z., 2005. The Paleoproterozoic snowball Earth: A climate disaster triggered by the evolution of oxygenic photosynthesis. *Proceedings of the National Academy of Sciences of the United States of America*, 102(32): 11131-11136.
- Kump, L.R. and Barley, M.E., 2007. Increased subaerial volcanism and the rise of atmospheric oxygen 2.5 billion years ago. *Nature*, 448(7157): 1033-1036.
- Landing, E., 1994. Precambrian-Cambrian boundary global stratotype ratified and a new perspective of Cambrian time. *Geology*, 22(2): 179-182.
- Le Guerroué, E., Allen, P.A., Cozzi, A., Etienne, J.L. and Fanning, M., 2006. 50Myr recovery from the largest negative  $\delta^{13}\text{C}$  excursion in the Ediacaran ocean. *Terra Nova*, 18(2): 147-153.
- Le Hir, G. et al., 2009. The snowball Earth aftermath: Exploring the limits of continental weathering processes. *Earth and Planetary Science Letters*, 277(3-4): 453-463.
- Lee, J.S. and Chao, Y.T., 1924. Geology of the Gorge district of the Yangtze from Ichang to Tzehui, with special reference to the development of the Gorges. *Bulletin Geological Society of China* 3(3-4): 351-391.
- Lehmann, B. et al., 2007. Highly metalliferous carbonaceous shale and Early Cambrian seawater. *Geology*, 35(5): 403-406.
- Lenton, T.M. and Watson, A.J., 2000. Redfield Revisited 1. Regulation of Nitrate, Phosphate, and Oxygen in the Ocean. *Global Biogeochem. Cycles*, 14(1): 225 - 248.
- Lenton, T.M. and Watson, A.J., 2004. Biotic enhancement of weathering, atmospheric oxygen and carbon dioxide in the Neoproterozoic. *Geophysical Research Letters*, 31.
- Leventhal, J.S., 1991. Comparison of organic geochemistry and metal enrichment in two black shales: Cambrian Alum Shale of Sweden and Devonian Chattanooga Shale of United States. *Mineralium Deposita*, 26(2): 104-112.
- Lewan, M.D., 1984. Factors controlling the proportionality of vanadium to nickel in crude oils. *Geochimica et Cosmochimica Acta*, 48(11): 2231-2238.
- Li, C.-W., Chen, J.-Y. and Hua, T.-E., 1998. Precambrian Sponges with Cellular Structures. *Science*, 279(5352): 879-882.
- Li, D. et al., 2009. New carbon isotope stratigraphy of the Ediacaran-Cambrian boundary interval from SW China: implications for global correlation. *Geological Magazine*, 146(4): 465-484.
- Li, G. and Xiao, S., 2004. Tannuolina and Micrina (Tannuolinidae) from the Lower Cambrian of eastern Yunnan, South China, and their scleritome reconstruction. *Journal of Paleontology*, 78(5): 900-913.
- Li, R. et al., 1999a. Spatial and temporal variations in carbon and sulfur isotopic compositions of Sinian sedimentary rocks in the Yangtze platform, South China. *Precambrian Research*, 97(1-2): 59-75.
- Li, W., Li, X. and Li, Z., 2005. Neoproterozoic bimodal magmatism in the Cathaysia Block of South China and its tectonic significance. *Precambrian Research*, 136(1): 51-66.
- Li, X.H. et al., 2003a. Neoproterozoic granitoids in South China: crustal melting above a mantle plume at ca. 825 Ma? *Precambrian Research*, 122: 45-83.

- Li, Y., 1986. Regional review: China. In: P.J. Cook and J.H. Shergold (Editors), *Phosphate Deposits of the World: Proterozoic and Cambrian Phosphorites*. Cambridge University Press, Cambridge, UK, pp. 42-62.
- Li, Y. et al., 2008a. Vase-shaped microfossils from the Ediacaran Weng'an biota, Guizhou, South China. *Gondwana Research*, 14(1-2): 263-268.
- Li, Z.-X., Zhang, L. and Powell, C.M., 1995. South China in Rodinia: Part of the missing link between Australia 鈥掳ast Antarctica and Laurentia? *Geology*, 23(5): 407-410.
- Li, Z.-X.A. and Lee, C.-T.A., 2004. The constancy of upper mantle  $fO_2$  through time inferred from V/Sc ratios in basalts. *Earth and Planetary Science Letters*, 228(3-4): 483-493.
- Li, Z., Li, X., Zhou, H. and Kinny, P., 2002. Grenvillian continental collision in south China: New SHRIMP U-Pb zircon results and implications for the configuration of Rodinia: *Geology*, v. 30. doi, 10: 0091-7613.
- Li, Z.X. et al., 2008b. Assembly, configuration, and break-up history of Rodinia: A synthesis. *Precambrian Research*, 160(1-2): 179-210.
- Li, Z.X., Evans, D.A.D. and Zhang, S., 2004. A 90° spin on Rodinia: possible causal links between the Neoproterozoic supercontinent, superplume, true polar wander and low-latitude glaciation. *Earth and Planetary Science Letters*, 220(3-4): 409-421.
- Li, Z.X., Li, X.H., Kinny, P.D. and Wang, J., 1999b. The breakup of Rodinia: did it start with a mantle plume beneath South China? *Earth and Planetary Science Letters*, 173(3): 171-181.
- Li, Z.X. et al., 2003b. Geochronology of Neoproterozoic syn-rift magmatism in the Yangtze Craton, South China and correlations with other continents: evidence for a mantle superplume that broke up Rodinia. *Precambrian Research*, 122(1-4): 85-109.
- Lindsay, J.F. and Brasier, M.D., 2002. Did global tectonics drive early biosphere evolution? Carbon isotope record from 2.6 to 1.9 Ga carbonates of Western Australian basins. *Precambrian Research*, 114(1-2): 1-34.
- Lindsay, J.F. et al., 1996. Facies and sequence controls on the appearance of the Cambrian biota in southwestern Mongolia; implications for the Precambrian-Cambrian boundary. *Geological Magazine*, 133(4): 417-428.
- Ling, H.-F., Chen, X., Li, D. and Jiang, S.-Y., 2009. Rise of oxygen in Ediacaran shallow sea. *Geochimica et Cosmochimica Acta*, 73(13, Supplement 1): A769.
- Ling, H.F. et al., 2007. Carbon isotope variation through the Neoproterozoic Doushantuo and Dengying Formations, South China: Implications for chemostratigraphy and paleoenvironmental change. *Palaeogeography, Palaeoclimatology, Palaeoecology*, 254(1-2): 158-174.
- Liou, J., Tsujimori, T., Zhang, R., Katayama, I. and Maruyama, S., 2004. Global UHP Metamorphism and Continental Subduction/Collision: The Himalayan Model. *International Geology Review*, 46(1): 1-27.
- Liu, T.-b., Maynard, J.B. and Alten, J., 2006. Superheavy S isotopes from glacier-associated sediments of the Neoproterozoic of south China: Oceanic anoxia or sulfate limitation? *Memoir 198: Evolution of Early Earth's Atmosphere, Hydrosphere, and Biosphere - Constraints from Ore Deposits*, 198(0): 205-222.
- Liu, T., 1990. CS relationships in shales hosting manganese ores from Mexico, China, and Newfoundland; implications for depositional environment and mineralization. *Ore Geology Reviews*, 5: 325-340.
- Logan, G.A., Hayes, J.M., Hieshima, G.B. and Summons, R.E., 1995. Terminal Proterozoic reorganization of biogeochemical cycles. *Nature*, 376(6535): 53-56.
- Lord III, C.J., 1982. A selective and precise method for pyrite determination in sedimentary materials. *JOURNAL OF SEDIMENTARY RESEARCH*, 52(2): 664-666.
- Lott, D.A., Coveney, R.M., Murowchick, J.B. and Grauch, R.I., 1999. Sedimentary exhalative nickel-molybdenum ores in South China. *Economic Geology*, 94(7): 1051-1066.

- Louchouart, P., Lucotte, M., Duchemin, E. and de Vernal, A., 1997. Early diagenetic processes in recent sediments of the Gulf of St-Lawrence: phosphorus, carbon and iron burial rates. *Marine Geology*, 139(1-4): 181-200.
- Loukola-Ruskeeniemi, K., 1991. Geochemical evidence for the hydrothermal origin of sulphur, base metals and gold in Proterozoic metamorphosed black shales, Kainuu and Outokumpu areas, Finland. *Mineralium Deposita*, 26(2): 152-164.
- Love, G.D. et al., 2009. Fossil steroids record the appearance of Demospongiae during the Cryogenian period. *Nature*, 457(7230): 718-721.
- Lüning, S. and Kolonic, S., 2003. Uranium spectral gamma-ray response as a proxy for organic richness in black shales: Applicability and limitations. *Journal of Petroleum Geology*, 26(2): 153-174.
- Luo, H. et al., 1992. A Further Research on the Precambrian-Cambrian Boundary at Meishucun Section of Jinning, Yunnan, China. *Acta Geologica Sinica*, 5(2): 197-207.
- Luo, H. et al., 1982. The Sinian–Cambrian Boundary in Eastern Yunnan, China. Peoples' Publishing House of Yunnan, Kunming, Yunnan.
- Luo, H. et al., 1984. Sinian–Cambrian Boundary Stratotype Section at Meishucun, Jinning, Yunnan, China. People's Publishing House of Yunnan, Kunming, Yunnan.
- Lydon, J., Goodfellow, W. and Jonasson, I., 1985. A general genetic model for stratiform baritic deposits of the Selwyn Basin, Yukon Territory and District of Mackenzie. *Current Research Part A: Geological Survey of Canada Paper*: 651–660.
- Lyons, T.W., Anbar, A.D., Severmann, S., Scott, C. and Gill, B.C., 2009. Tracking Euxinia in the Ancient Ocean: A Multiproxy Perspective and Proterozoic Case Study. *Annual Review of Earth and Planetary Sciences*, 37(1): 507.
- Lyons, T.W., Gellatly, A.M., McGoldrick, P.J. and Kah, L.C., 2006. Proterozoic sedimentary exhalative (SEDEX) deposits and links to evolving global ocean chemistry. *Geological Society of America Memoirs*, 198: 169-184.
- Lyons, T.W. and Gill, B.C., 2010. Ancient Sulfur Cycling and Oxygenation of the Early Biosphere. *Elements*, 6(2): 93-99.
- Lyons, T.W. and Severmann, S., 2006. A critical look at iron paleoredox proxies: New insights from modern euxinic marine basins. *Geochimica et Cosmochimica Acta*, 70(23): 5698-5722.
- Lyons, T.W., Werne, J.P., Hollander, D.J. and Murray, R.W., 2003. Contrasting sulfur geochemistry and Fe/Al and Mo/Al ratios across the last oxic-to-anoxic transition in the Cariaco Basin, Venezuela. *Chemical Geology*, 195(1-4): 131-157.
- Ma, G., Lee, H. and Zhang, Z.F., 1984. An investigation of the age limits of the Sinian System in South China (in Chinese with English abstract). *Bull. Yichang Inst. Geol. Miner. Res.*, 8: 1-29.
- Macdonald, F.A. et al., 2010. Calibrating the Cryogenian. *Science*, 327(5970): 1241-1243.
- Maloof, A.C. et al., 2006. Combined paleomagnetic, isotopic, and stratigraphic evidence for true polar wander from the Neoproterozoic Akademikerbreen Group, Svalbard, Norway. *Geological Society of America Bulletin*, 118(9-10): 1099-1124.
- Maloof, A.C. et al., 2010. The earliest Cambrian record of animals and ocean geochemical change. *Geological Society of America Bulletin*, 122(11-12): 1731-1774.
- Marino, R., Howarth, R.W., Chan, F., Cole, J.J. and Likens, G.E., 2003. Sulfate inhibition of molybdenum-dependent nitrogen fixation by planktonic cyanobacteria under seawater conditions: a non-reversible effect. *Hydrobiologia*, 500(1): 277-293.
- Marshall, H.G., Walker, J.C.G. and Kuhn, W.R., 1988. Long-term climate change and the geochemical cycle of carbon. *Journal of Geophysical Research*, 93(D1): 791-801.
- Marshall, J.D., 1992. Climatic and oceanographic isotopic signals from the carbonate rock record and their preservation. *Geological Magazine*, 129(2): 143-160.

- Martin, M.W. et al., 2000. Age of Neoproterozoic Bilatarian Body and Trace Fossils, White Sea, Russia: Implications for Metazoan Evolution. *Science*, 288(5467): 841-845.
- Maruyama, S., Liou, J.G. and Terabayashi, M., 1996. Blueschists and eclogites of the world and their exhumation. *International Geology Review*, 38: 485 - 594.
- März, C. et al., 2008. Redox sensitivity of P cycling during marine black shale formation: Dynamics of sulfidic and anoxic, non-sulfidic bottom waters. *Geochimica et Cosmochimica Acta*, 72(15): 3703-3717.
- Maynard, J., 1991. Iron: Syngenetic deposition controlled by the evolving ocean-atmosphere system. Sedimentary and diagenetic mineral deposits: a basin analysis approach to exploration 5. Soc. of Economic Geologists Reviews in Economic Geology, El Paso, Texas, 141-145 pp.
- Maynard, J.B., 2010. The Chemistry of Manganese Ores through Time: A Signal of Increasing Diversity of Earth-Surface Environments. *Economic Geology*, 105(3): 535-552.
- Maynard, J.B. and Okita, P.M., 1991. Bedded barite deposits in the United States, Canada, Germany, and China; two major types based on tectonic setting. *Economic Geology*, 86(2): 364-376.
- McArthur, J.M. and Walsh, J.N., 1984. Rare-earth geochemistry of phosphorites. *Chemical Geology*, 47(3-4): 191-220.
- McCall, G.J.H., 2006. The Vendian (Ediacaran) in the geological record: Enigmas in geology's prelude to the Cambrian explosion. *Earth-Science Reviews*, 77(1-3): 1-229.
- McCay, G.A., Prave, A.R., Alsop, G.I. and Fallick, A.E., 2006. Glacial trinity: Neoproterozoic Earth history within the British-Irish Caledonides. *Geology*, 34(11): 909-912.
- McCulloch, M.T., 1993. The role of subducted slabs in an evolving Earth. *Earth and Planetary Science Letters*, 115(1-4): 89-100.
- McFadden, K., 2008. Integrated High-resolution Stratigraphy of the Doushantuo Formation, South China.
- McFadden, K.A. et al., 2008. Pulsed oxidation and biological evolution in the Ediacaran Doushantuo Formation. *Proceedings of the National Academy of Sciences*, 105(9): 3197-3202.
- McKeague, J.A. and Day, J.H., 1966. Dithionite and oxalate extractable Fe and ai as aids in differentiating various classes of soils. *Canadian journal of soil science*, 46: 13-21.
- McKenzie, D. and Bickle, M.J., 1988. The Volume and Composition of Melt Generated by Extension of the Lithosphere. *Journal of Petrology*, 29(3): 625-679.
- McLennan, S.M., 2001. Relationships between the trace element composition of sedimentary rocks and upper continental crust. *Geochemistry, Geophysics, Geosystems*, 2.
- McLennan, S.M. and Taylor, S.R., 1980. Th and U in sedimentary rocks: crustal evolution and sedimentary recycling. *Nature*, 285(5767): 621-624.
- McManus, J., Berelson, W.M., Klinkhammer, G.P., Hammond, D.E. and Holm, C., 2005. Authigenic uranium: Relationship to oxygen penetration depth and organic carbon rain. *Geochimica et Cosmochimica Acta*, 69(1): 95-108.
- McManus, J. et al., 1998. Geochemistry of barium in marine sediments: implications for its use as a paleoproxy. *Geochimica et Cosmochimica Acta*, 62(21-22): 3453-3473.
- McManus, J. et al., 2006. Molybdenum and uranium geochemistry in continental margin sediments: Paleoproxy potential. *Geochimica et Cosmochimica Acta*, 70(18): 4643-4662.
- McManus, J., Nägler, T., Siebert, C., Wheat, C. and Hammond, D., 2002. Oceanic molybdenum isotope fractionation: Diagenesis and hydrothermal ridge-flank alteration. *Geochemistry, Geophysics, Geosystems*, 3(12): 1078.
- McMenamin, M.A.S. and McMenamin, D.L.S., 1990. The Emergence of Animals: The Cambrian Breakthrough. p. 217.
- Meert, J.G., 2003. A synopsis of events related to the assembly of eastern Gondwana. *Tectonophysics*, 362(1-4): 1-40.

- Meert, J.G. and Lieberman, B.S., 2008. The Neoproterozoic assembly of Gondwana and its relationship to the Ediacaran-Cambrian radiation. *Gondwana Research*, 14(1-2): 5-21.
- Meert, J.G. and van der Voo, R., 1994. The Neoproterozoic (1000-540 Ma) glacial intervals: No more snowball earth? *Earth and Planetary Science Letters*, 123(1-3): 1-13.
- Mehra, O.P. and Jackson, M.L., 1960. Iron oxide removal from soils and clays by a dithionite-citrate system buffered with sodium bicarbonate. National conference on clays and minerals proceedings: 317-327.
- Melezhik, V., Fallick, A.E. and Pokrovsky, B.G., 2005a. Enigmatic nature of thick sedimentary carbonates depleted in  $^{13}\text{C}$  beyond the canonical mantle value: The challenges to our understanding of the terrestrial carbon cycle. *Precambrian Research*, 137(3-4): 131-165.
- Melezhik, V.A., Fallick, A.E., Filippov, M.M. and Larsen, O., 1999a. Karelian shungite--an indication of 2.0-Ga-old metamorphosed oil-shale and generation of petroleum: geology, lithology and geochemistry. *Earth-Science Reviews*, 47(1-2): 1-40.
- Melezhik, V.A. et al., 2009. Petroleum surface oil seeps from a Palaeoproterozoic petrified giant oilfield. *Terra Nova*, 21(2): 119-126.
- Melezhik, V.A. et al., 2005b. Emergence of an aerobic biosphere during the Archean-Proterozoic transition: Challenges of future research. *GSA Today*, 15(11): 4-11.
- Melezhik, V.A., Fallick, A.E., Makarikhin, V.V. and Lyubtsov, V.V., 1997. Links between Palaeoproterozoic palaeogeography and rise and decline of stromatolites: Fennoscandian Shield. *Precambrian Research*, 82(3-4): 311-348.
- Melezhik, V.A., Fallick, A.E., Medvedev, P.V. and Makarikhin, V.V., 1999b. Extreme  $^{13}\text{C}_{\text{carb}}$  enrichment in ca. 2.0 Ga magnesite-stromatolite-dolomite-'red beds' association in a global context: a case for the world-wide signal enhanced by a local environment. *Earth-Science Reviews*, 48(1-2): 71-120.
- Melezhik, V.A., Fallick, A.E., Rychanchik, D.V. and Kuznetsov, A.B., 2005c. Palaeoproterozoic evaporites in Fennoscandia: implications for seawater sulphate, the rise of atmospheric oxygen and local amplification of the  $\delta^{13}\text{C}$  excursion. *Terra Nova*, 17(2): 141-148.
- Meyer, K.M. and Kump, L.R., 2008. Oceanic Euxinia in Earth History: Causes and Consequences. *Annual Review of Earth and Planetary Sciences*, 36(1): 251-288.
- Miller, K.G. et al., 2005. The Phanerozoic Record of Global Sea-Level Change. *Science*, 310(5752): 1293-1298.
- Moczydlowska, M., 2008. The Ediacaran microbiota and the survival of Snowball Earth conditions. *Precambrian Research*, 167(1-2): 1-15.
- Moffett, J.W., 1990. Microbially mediated cerium oxidation in sea water. *Nature*, 345(6274): 421-423.
- Mojzsis, S.J. et al., 1996. Evidence for life on Earth before 3,800 million years ago. *Nature*, 384(6604): 55-59.
- Moore, E.M., 1991. Southwest U.S.-East Antarctic (SWEAT) connection; a hypothesis. *Geology*, 19(5): 425-428.
- Moore, E.M., 2002. Pre- 1 Ga (pre-Rodinian) ophiolites: Their tectonic and environmental implications. *Geological Society of America Bulletin*, 114(1): 80-95.
- Morford, J.L. and Emerson, S., 1999. The geochemistry of redox sensitive trace metals in sediments. *Geochimica et Cosmochimica Acta*, 63(11-12): 1735-1750.
- Morford, J.L., Russell, A.D. and Emerson, S., 2001. Trace metal evidence for changes in the redox environment associated with the transition from terrigenous clay to diatomaceous sediment, Saanich Inlet, BC. *Marine Geology*, 174: 355-369.
- Morse, J.W. and Luther, G.W., 1999. Chemical influences on trace metal-sulfide interactions in anoxic sediments. *Geochimica et Cosmochimica Acta*, 63(19-20): 3373-3378.
- Müller, A., 2002. Pyritization of iron and trace metals in anoxic fjord sediments (Nordåsvannet fjord, western Norway). *Applied Geochemistry*, 17(7): 923-933.



- Müller, W., Shelley, M., Miller, P. and Broude, S., 2009. Initial performance metrics of a new custom-designed ArF excimer LA-ICPMS system coupled to a two-volume laser-ablation cell. *Journal of Analytical Atomic Spectrometry*, 24: 209-214.
- Nägler, T.F., Siebert, C., Lüschen, H. and Böttcher, M.E., 2005. Sedimentary Mo isotope record across the Holocene fresh-brackish water transition of the Black Sea. *Chemical Geology*, 219(1-4): 283-295.
- Nagy, R.M., Porter, S.M., Dehler, C.M. and Shen, Y., 2009. Biotic turnover driven by eutrophication before the Sturtian low-latitude glaciation. *Nature Geoscience*, 2(6): 415-418.
- Narbonne, G.M., 2005. The Ediacara Biota: Neoproterozoic Origin of Animals and Their Ecosystems. *Annual Review of Earth and Planetary Sciences*, 33(1): 421-442.
- Narbonne, G.M. and Gehling, J.G., 2003. Life after snowball: The oldest complex Ediacaran fossils. *Geology*, 31(1): 27-30.
- Narbonne, G.M., Kaufman, A.J. and Knoll, A.H., 1994. Integrated chemostratigraphy and biostratigraphy of the Windermere Supergroup, northwestern Canada: Implications for Neoproterozoic correlations and the early evolution of animals. *Geological Society of America Bulletin*, 106(10): 1281-1292.
- Nisbet, E.G. and Sleep, N.H., 2001. The habitat and nature of early life. *Nature*, 409(6823): 1083-1091.
- Nothold, A.J.G. and Sheldon, R.P., 1986. Chapter 2. In: P.J. Cook and J.H. Shergold (Editors), *Phosphate deposits of the world: Proterozoic and Cambrian phosphorites* Cambridge University Press, Cambridge, UK.
- Nursall, J.R., 1959. Oxygen as a Prerequisite to the Origin of the Metazoa. *Nature*, 183(4669): 1170-1172.
- O'Leary, M.H., 1981. Carbon isotope fractionation in plants. *Phytochemistry*, 20(4): 553-567.
- Ohmoto, H., 1997. When did the Earth's atmosphere become oxic? *Geochemical News*, 93: 12-27.
- Ohno, T., Komiya, T., Ueno, Y., Hirata, T. and Maruyama, S., 2008. Determination of  $^{88}\text{Sr}/^{86}\text{Sr}$  mass-dependent isotopic fractionation and radiogenic isotope variation of  $^{87}\text{Sr}/^{86}\text{Sr}$  in the Neoproterozoic Doushantuo Formation. *Gondwana Research*, 14(1-2): 126-133.
- Okita, P.M., 1992. Manganese carbonate mineralization in the Molango District, Mexico. *Economic Geology*, 87(5): 1345.
- Olcott, A.N., Sessions, A.L., Corsetti, F.A., Kaufman, A.J. and de Oliveira, T.F., 2005. Biomarker Evidence for Photosynthesis During Neoproterozoic Glaciation. *Science*, 310(5747): 471-474.
- Ort, D., Yocum, C. and Heichel, I., 1996. *Oxygenic photosynthesis: the light reactions*. Kluwer Academic Publishers.
- Oze, C., Bird, D.K. and Fendorf, S., 2007. Genesis of hexavalent chromium from natural sources in soil and groundwater. *Proceedings of the National Academy of Sciences*, 104(16): 6544-6549.
- Pace, N.R., 1997. A Molecular View of Microbial Diversity and the Biosphere. *Science*, 276(5313): 734-740.
- Paikaray, S., Banerjee, S. and Mukherji, S., 2008. Geochemistry of shales from the Paleoproterozoic to Neoproterozoic Vindhyan Supergroup: Implications on provenance, tectonics and paleoweathering. *Journal of Asian Earth Sciences*, 32(1): 34-48.
- Papineau, D., 2010. Global Biogeochemical Changes at Both Ends of the Proterozoic: Insights from Phosphorites. *Astrobiology*, 10(2): 165-181.
- Papineau, D. et al., 2009. High primary productivity and nitrogen cycling after the Paleoproterozoic phosphogenic event in the Aravalli Supergroup, India. *Precambrian Research*, 171(1-4): 37-56.
- Pašava, J., Barnes, S.-J. and Vymazalová, A., 2003. The use of mantle normalization and metal ratios in the identification of the sources of platinum-group elements in various metal-rich black shales. *Mineralium Deposita*, 38(6): 775-783.
- Pašava, J. et al., 2008. Multiple Sources of Metals of Mineralization in Lower Cambrian Black Shales of South China: Evidence from Geochemical and Petrographic Study. *Blackwell Publishing Asia*, pp. 25-42.

- Paulsson, O. and Andreasson, P.-G., 2002. Attempted break-up of Rodinia at 850 Ma: geochronological evidence from the Seve-Kalak Superterrane, Scandinavian Caledonides. *Journal of the Geological Society*, 159(6): 751-761.
- Pavlov, A.A., Hurtgen, M.T., Kasting, J.F. and Arthur, M.A., 2003. Methane-rich Proterozoic atmosphere? *Geology*, 31(1): 87-90.
- Pavlov, A.A. and Kasting, J.F., 2002. Mass-Independent Fractionation of Sulfur Isotopes in Archean Sediments: Strong Evidence for an Anoxic Archean Atmosphere. *Astrobiology*, 2(1): 27-41.
- Payne, J. et al., 2009. Two-phase increase in the maximum size of life over 3.5 billion years reflects biological innovation and environmental opportunity. *Proceedings of the National Academy of Sciences*, 106(1): 24.
- Pearce, C.R., Cohen, A.S., Coe, A.L. and Burton, K.W., 2008. Molybdenum isotope evidence for global ocean anoxia coupled with perturbations to the carbon cycle during the Early Jurassic. *Geology*, 36(3): 231-234.
- Pease, V., Scott, R. and Eliaeson, K., 2006. A Baltica province for the Kara terrane. *Bulletin of the Geological Society of Finland*, 121.
- Pell, S.D., McKirdy, D.M., Jansyn, J. and Jenkins, R.J.F., 1993. Ediacaran carbon isotope stratigraphy of South Australia - An initial study. *Transactions of the Royal Society of South Australia*, 117(4): 153-161.
- Peterson, K.J. and Davidson, E.H., 2000. Regulatory evolution and the origin of the bilaterians. *Proceedings of the National Academy of Sciences of the United States of America*, 97(9): 4430-4433.
- Peterson, K.J. et al., 2004. Estimating metazoan divergence times with a molecular clock. *Proceedings of the National Academy of Sciences of the United States of America*, 101(17): 6536-6541.
- Peterson, K.J., McPeck, M.A. and Evans, D.A.D., 2005. Tempo and mode of early animal evolution: inferences from rocks, Hox, and molecular clocks. *Paleobiology*, 31(2\_Suppl): 36-55.
- Phillips, E.J.P. and Lovley, D.R., 1987. Determination of Fe(III) and Fe(II) in oxalate extracts of sediment. *Soil Science Society of America journal*, 51(4): 938-941.
- Piepgras, D.J. and Jacobsen, S.B., 1992. The behavior of rare earth elements in seawater: Precise determination of variations in the North Pacific water column. *Geochimica et Cosmochimica Acta*, 56(5): 1851-1862.
- Piper, D.Z., 1994. Seawater as the source of minor elements in black shales, phosphorites and other sedimentary rocks. *Chemical Geology*, 114(1-2): 95-114.
- Piper, D.Z. and Calvert, S.E., 2009. A marine biogeochemical perspective on black shale deposition. *Earth-Science Reviews*, 95(1-2): 63-96.
- Piper, D.Z. and Perkins, R.B., 2004. A modern vs. Permian black shale--the hydrography, primary productivity, and water-column chemistry of deposition. *Chemical Geology*, 206(3-4): 177-197.
- Piper, J.D.A., 2000. The Neoproterozoic Supercontinent: Rodinia or Palaeopangaea? *Earth and Planetary Science Letters*, 176(1): 131-146.
- Piper, J.D.A., Beckmann, G.E.J. and Badham, J.P.N., 1976. Palaeomagnetic Evidence for a Proterozoic Super-Continent [and Discussion]. *Philosophical Transactions of the Royal Society of London. Series A, Mathematical and Physical Sciences (1934-1990)*, 280(1298): 469-490.
- Pisarevsky, S.A., Murphy, J.B., Cawood, P.A. and Collins, A.S., 2008. Late Neoproterozoic and Early Cambrian palaeogeography: models and problems. *Geological Society, London, Special Publications*, 294(1): 9-31.
- Planavsky, N.J. et al., 2010. The evolution of the marine phosphate reservoir. *Nature*, 467(7319): 1088-1090.
- Pollack, H.N., 1997. Thermal characteristics of the Archaean. In: M.J. De Wit and L.D. Ashwal (Editors), *Greenstone belts: Oxford Monographs on Geology and Geophysics*, pp. 223-232.

- Porter, S.M., Knoll, A.H. and Affaton, P., 2004. Chemostratigraphy of Neoproterozoic cap carbonates from the Volta Basin, West Africa. *Precambrian Research*, 130(1-4): 99-112.
- Poulson, R.L., Siebert, C., McManus, J. and Berelson, W.M., 2006. Authigenic molybdenum isotope signatures in marine sediments. *Geology*, 34(8): 617-620.
- Poulton, S.W., Bottrell, S.H. and Underwood, C.J., 1998. Porewater sulphur geochemistry and fossil preservation during phosphate diagenesis in a Lower Cretaceous shelf mudstone. *Sedimentology*, 45(5): 875-887.
- Poulton, S.W. and Canfield, D.E., 2005. Development of a sequential extraction procedure for iron: implications for iron partitioning in continentally derived particulates. *Chemical Geology*, 214(3-4): 209-221.
- Poulton, S.W. and Canfield, D.E., 2011. Ferruginous oceanic conditions: a dominant feature of the ocean through Earth's history. *Elements*.
- Poulton, S.W., Fralick, P.W. and Canfield, D.E., 2004a. The transition to a sulphidic ocean ~1.84 billion years ago. *Nature*, 431(7005): 173-177.
- Poulton, S.W., Fralick, P.W. and Canfield, D.E., 2010. Spatial variability in oceanic redox structure 1.8 billion years ago. *Nature Geoscience*, 3(7): 486-490.
- Poulton, S.W., Krom, M.D. and Raiswell, R., 2004b. A revised scheme for the reactivity of iron (oxyhydr)oxide minerals towards dissolved sulfide. *Geochimica et Cosmochimica Acta*, 68(18): 3703-3715.
- Poulton, S.W. and Raiswell, R., 2002. The low-temperature geochemical cycle of iron: From continental fluxes to marine sediment deposition. *American Journal of Science*, 302(9): 774-805.
- Pratt, B.R., 2001. Septarian concretions: internal cracking caused by synsedimentary earthquakes. *Sedimentology*, 48(1): 189-213.
- Prave, A.R., 2002. Life on land in the Proterozoic: Evidence from the Torridonian rocks of northwest Scotland. *Geology*, 30(9): 811-814.
- Prévôt, L. and Lucas, J., 1980. Behaviour of some trace elements in phosphatic sedimentary formations. In: Y.K. Bendor (Editor), *Marine Phosphorites*. Soc. Econ. Paleont. Miner. Spec. Publ., pp. 31-39.
- Qian, Y. and Bengtson, S., 1989. Palaeontology and biostratigraphy of the Early Cambrian Meishucunian Stage in Yunnan Province, South China. *Fossils and Strata*, 24(1): 1-156.
- Qian, Z., Zhensheng, D. and Xinzhi, Z., 1995. Geochemical characteristics of Baiguoyuan black shale-type Ag-V deposit in Western Hubei Province. *Acta Mineralogica Sinica*, 2.
- Quan, T.M., van de Schootbrugge, B., Field, M.P., Rosenthal, Y. and Falkowski, P.G., 2008. Nitrogen isotope and trace metal analyses from the Mingolsheim core (Germany): Evidence for redox variations across the Triassic-Jurassic boundary. *Global Biogeochem. Cycles*, 22.
- Raiswell, R. and Al-Biatty, H.J., 1989. Depositional and diagenetic C-S-Fe signatures in early Paleozoic normal marine shales. *Journal Name: Geochimica et Cosmochimica Acta; (USA); Journal Volume: 53:5: Medium: X; Size: Pages: 1147-1152.*
- Raiswell, R. and Anderson, T.F., 2005. Reactive iron enrichment in sediments deposited beneath euxinic bottom waters: constraints on supply by shelf recycling. *Geological Society, London, Special Publications*, 248(1): 179-194.
- Raiswell, R. and Berner, R.A., 1985. Pyrite formation in euxinic and semi-euxinic sediments. *American Journal of Science*, 285(8): 710-724.
- Raiswell, R. and Berner, R.A., 1986. Pyrite and organic matter in Phanerozoic normal marine shales. *Geochimica et Cosmochimica Acta*, 50(9): 1967-1976.
- Raiswell, R., Buckley, F., Berner, R.A. and Anderson, T.F., 1988. Degree of pyritization of iron as a paleoenvironmental indicator of bottom-water oxygenation. *Journal of Sedimentary Research*, 58(5): 812-819.

- Raiswell, R., Canfield, D. and Berner, R., 1994. A comparison of iron extraction methods for the determination of degree of pyritisation and the recognition of iron-limited pyrite formation. *Chemical Geology*, 111(1-4): 101-110.
- Raiswell, R. and Canfield, D.E., 1996. Rates of reaction between silicate iron and dissolved sulfide in Peru Margin sediments. *Geochimica et Cosmochimica Acta*, 60(15): 2777-2787.
- Raiswell, R. and Canfield, D.E., 1998. Sources of iron for pyrite formation in marine sediments. *American Journal of Science*, 298(3): 219-245.
- Raiswell, R., Newton, R. and Wignall, P.B., 2001. An Indicator of Water-Column Anoxia: Resolution of Biofacies Variations in the Kimmeridge Clay (Upper Jurassic, U.K.). *Journal of Sedimentary Research*, 71(2): 286-294.
- Raiswell, R. et al., 2006. Contributions from glacially derived sediment to the global iron (oxyhydr)oxide cycle: Implications for iron delivery to the oceans. *Geochimica et Cosmochimica Acta*, 70(11): 2765-2780.
- Rasmussen, B. and Buick, R., 1999. Redox state of the Archean atmosphere: Evidence from detrital heavy minerals in ca. 3250-2750 Ma sandstones from the Pilbara Craton, Australia. *Geology*, 27(2): 115-118.
- Reddy, S.M. and Evans, D.A.D., 2009. Palaeoproterozoic supercontinents and global evolution: correlations from core to atmosphere. Geological Society, London, Special Publications, 323(1): 1-26.
- Redfield, A.C., 1934. On the proportions of organic derivatives in sea water and their relation to the composition of plankton, James Johnstone Memorial Volume. Univ. Liverpool, pp. 176-192.
- Rees, C.E., Jenkins, W.J. and Monster, J., 1978. The sulphur isotopic composition of ocean water sulphate. *Geochimica et Cosmochimica Acta*, 42(4): 377-381.
- Reinhard, C.T., Raiswell, R., Scott, C., Anbar, A.D. and Lyons, T.W., 2009. A Late Archean Sulfidic Sea Stimulated by Early Oxidative Weathering of the Continents. *Science*, 326(5953): 713-716.
- Retallack, G.J., 2007. Growth, decay and burial compaction of *Dickinsonia*, an iconic Ediacaran fossil. *Alcheringa: An Australasian Journal of Palaeontology*, 31(3): 215 - 240.
- Richter, F.M., Rowley, D.B. and DePaolo, D.J., 1992. Sr isotope evolution of seawater: the role of tectonics. *Earth and Planetary Science Letters*, 109(1-2): 11-23.
- Ridgwell, A.J., Kennedy, M.J. and Caldeira, K., 2003. Carbonate Deposition, Climate Stability, and Neoproterozoic Ice Ages. *Science*, 302(5646): 859-862.
- Ries, J.B., Fike, D.A., Pratt, L.M., Lyons, T.W. and Grotzinger, J.P., 2009. Superheavy pyrite ( $\delta^{34}\text{C}_{\text{pyr}} > \delta^{34}\text{S}_{\text{CAS}}$ ) in the terminal Proterozoic Nama Group, southern Namibia: A consequence of low seawater sulfate at the dawn of animal life. *Geology*, 37(8): 743-746.
- Rimmer, S.M., 2004. Geochemical paleoredox indicators in Devonian-Mississippian black shales, Central Appalachian Basin (USA). *Chemical Geology*, 206(3-4): 373-391.
- Rogers, J.J.W. and Santosh, M., 2002. Configuration of Columbia, a Mesoproterozoic Supercontinent. *Gondwana Research*, 5(1): 5-22.
- Rosing, M.T., 1999.  $^{13}\text{C}$ -Depleted Carbon Microparticles in >3700-Ma Sea-Floor Sedimentary Rocks from West Greenland. *Science*, 283(5402): 674-676.
- Rosing, M.T. and Frei, R., 2004. U-rich Archean sea-floor sediments from Greenland - indications of >3700 Ma oxygenic photosynthesis. *Earth and Planetary Science Letters*, 217(3-4): 237-244.
- Roy, S., 1997. Genetic diversity of manganese deposition in the terrestrial geological record. Geological Society, London, Special Publications, 119(1): 5-27.
- Roy, S., 2006. Sedimentary manganese metallogenesis in response to the evolution of the Earth system. *Earth-Science Reviews*, 77(4): 273-305.

- Rudnicki, M.D., Elderfield, H. and Spiro, B., 2001. Fractionation of sulfur isotopes during bacterial sulfate reduction in deep ocean sediments at elevated temperatures. *Geochimica et Cosmochimica Acta*, 65(5): 777-789.
- Runnegar, B., 1982. Oxygen requirements, biology and phylogenetic significance of the late Precambrian worm *Dickinsonia*, and the evolution of the burrowing habit. *Alcheringa: An Australasian Journal of Palaeontology*, 6(3): 223 - 239.
- Runnegar, B., 1991. Precambrian oxygen levels estimated from the biochemistry and physiology of early eukaryotes. *Global and Planetary Change*, 5(1-2): 97-111.
- Ruttenberg, K.C., Heinrich, D.H. and Karl, K.T., 2003. *The Global Phosphorus Cycle, Treatise on Geochemistry*. Pergamon, Oxford, pp. 585-643.
- Rye, R. and Holland, H.D., 1998. Paleosols and the evolution of atmospheric oxygen; a critical review. *American Journal of Science*, 298(8): 621-672.
- Saltzman, M.R., 2005. Phosphorus, nitrogen, and the redox evolution of the Paleozoic oceans. *Geology*, 33(7): 573-576.
- Samuelsson, J. and Butterfield, N.J., 2001. Neoproterozoic fossils from the Franklin Mountains, northwestern Canada: stratigraphic and palaeobiological implications. *Precambrian Research*, 107: 235-251.
- Sannigrahi, P. and Ingall, E., 2005. Polyphosphates as a source of enhanced P fluxes in marine sediments overlain by anoxic waters: Evidence from <sup>31</sup>P NMR. *Geochemical Transactions*, 6(3): 52.
- Sass, B.M. and Rai, D., 1987. Solubility of amorphous chromium(III)-iron(III) hydroxide solid solutions. *Inorganic Chemistry*, 26(14): 2228-2232.
- Saul, J.M., 2009. Did detoxification processes cause complex life to emerge? *Lethaia*, 42(2): 179-184.
- Saul, J.M. and Schwartz, L., 2007. Cancer as a consequence of the rising level of oxygen in the Late Precambrian. *Lethaia*, 40(3): 211-220.
- Saylor, B.Z., Kaufman, A.J., Grotzinger, J.P. and Urban, F., 1998. A composite reference section for terminal Proterozoic strata of southern Namibia. *Journal of Sedimentary Research*, 68(6): 1223-1235.
- Schenau, S.J., Passier, H.F., Reichart, G.J. and de Lange, G.J., 2002. Sedimentary pyrite formation in the Arabian Sea. *Marine Geology*, 185(3-4): 393-402.
- Schidlowski, M., 1988. A 3,800-million-year isotopic record of life from carbon in sedimentary rocks. *Nature*, 333(6171): 313-318.
- Schopf, J. and Packer, B., 1987. Early Archean (3.3-billion to 3.5-billion-year-old) microfossils from Warrawoona Group, Australia. *Science*, 237(4810): 70-73.
- Schopf, J.W., 1993. Microfossils of the Early Archean Apex Chert: New Evidence of the Antiquity of Life. *Science*, 260(5108): 640-646.
- Schopf, J.W., 2006. Fossil evidence of Archaean life. *Philosophical Transactions of the Royal Society B: Biological Sciences*, 361(1470): 869-885.
- Schrag, D.P., Berner, R.A., Hoffman, P.F. and Halverson, G.P., 2002. On the initiation of a snowball Earth. *Geochemistry, Geophysics, Geosystems*, 3(6): 1 pp.
- Scotese, C.R., 2004. *A Continental Drift Flipbook*. *The Journal of Geology*, 112(6): 729-741.
- Scott, C. et al., 2008. Tracing the stepwise oxygenation of the Proterozoic ocean. *Nature*, 452(7186): 456-460.
- Seilacher, A., 1984. Late Precambrian and Cambrian Metazoa; preservational or real extinctions? In: H.D. Holland and A.F. Trendall (Editors), *Patterns of Change in Earth Evolution*, Berlin: Fed. Republic Ger., pp. 159 - 168.
- Sharp, Z., 2007. *Principles of stable isotope geochemistry*. Pearson Education, Upper Saddle River, NJ.

- Shen, B., Xiao, S., Zhou, C. and Yuan, X., 2009. *Yangtziramulus Zhangi* New Genus and Species, a Carbonate-hosted Macrofossil from the Ediacaran Dengying Formation in the Yangtze Gorges Area, South China. *Journal of Paleontology*, 83(4): 575-587.
- Shen, Y. and Buick, R., 2004. The antiquity of microbial sulfate reduction. *Earth-Science Reviews*, 64(3-4): 243-272.
- Shen, Y., Canfield, D.E. and Knoll, A.H., 2002. Middle Proterozoic ocean chemistry: Evidence from the McArthur Basin, northern Australia. *American Journal of Science*, 302(2): 81-109.
- Shen, Y., Knoll, A.H. and Walter, M.R., 2003. Evidence for low sulphate and anoxia in a mid-Proterozoic marine basin. *Nature*, 423(6940): 632-5.
- Shen, Y. and Schidlowski, M., 2000. New C isotope stratigraphy from southwest China: Implications for the placement of the Precambrian-Cambrian boundary on the Yangtze Platform and global correlations. *Geology*, 28(7): 623-626.
- Shen, Y., Zhang, T. and Chu, X., 2005. C-isotopic stratification in a Neoproterozoic postglacial ocean. *Precambrian Research*, 137(3-4): 243-251.
- Sherwood, B.A., Sager, S.L. and Holland, H.D., 1987. Phosphorus in foraminiferal sediments from North Atlantic Ridge cores and in pure limestones. *Geochimica et Cosmochimica Acta*, 51(7): 1861-1866.
- Shields, G., 1999. Working towards a new stratigraphic calibration scheme for the Neoproterozoic-Cambrian. *Eclogae Geologicae Helvetiae* 92: 221-233.
- Shields, G., Stille, P., Brasier, M.D. and Atudorei, N.-V., 1997. Stratified oceans and oxygenation of the late Precambrian environment: a post glacial geochemical record from the Neoproterozoic of W. Mongolia. *Terra Nova*, 9(5-6): 218-222.
- Shields, G.A., 2002. 'Molar-tooth microspar': a chemical explanation for its disappearance ~750 Ma. *Terra Nova*, 14(2): 108-113.
- Shields, G.A., 2005. Neoproterozoic cap carbonates: a critical appraisal of existing models and the *plumeworld* hypothesis. *Terra Nova*, 17(4): 299-310.
- Shields, G.A., 2007. A normalised seawater strontium isotope curve: possible implications for Neoproterozoic-Cambrian weathering rates and the further oxygenation of the Earth. *eEarth*, 2(2): 35-42.
- Shields, G.A., Strauss, H., Howe, S.S. and Siegmund, H., 1999. Sulphur isotope compositions of sedimentary phosphorites from the basal Cambrian of China: implications for Neoproterozoic-Cambrian biogeochemical cycling. *Journal of the Geological Society*, 156(5): 943-955.
- Sholkovitz, E. and Shen, G.T., 1995. The incorporation of rare earth elements in modern coral. *Geochimica et Cosmochimica Acta*, 59(13): 2749-2756.
- Shu, L. and Charvet, J., 1996. Kinematics and geochronology of the Proterozoic Dongxiang-Shexian ductile shear zone: with HP metamorphism and ophiolitic melange (Jiangnan Region, South China). *Tectonophysics*, 267(1-4): 291-302.
- Siebert, C., Kramers, J.D., Meisel, T., Morel, P. and Nägler, T.F., 2005. PGE, Re-Os, and Mo isotope systematics in Archean and early Proterozoic sedimentary systems as proxies for redox conditions of the early Earth. *Geochimica et Cosmochimica Acta*, 69(7): 1787-1801.
- Siebert, C., McManus, J., Bice, A., Poulson, R. and Berelson, W.M., 2006. Molybdenum isotope signatures in continental margin marine sediments. *Earth and Planetary Science Letters*, 241(3-4): 723-733.
- Siebert, C., Nägler, T.F., von Blanckenburg, F. and Kramers, J.D., 2003. Molybdenum isotope records as a potential new proxy for paleoceanography. *Earth and Planetary Science Letters*, 211(1-2): 159-171.
- Signor, P.W. and Lipps, J.H., 1992. Origin and early radiation of the Metazoa. In: J.H. Lipps and P.W. Signor (Editors), *Origin and Early Evolution of the Metazoa*. Plenum Press, New York, pp. 3-23.

- Sikora, E.R., Johnson, T.M. and Bullen, T.D., 2008. Microbial mass-dependent fractionation of chromium isotopes. *Geochimica et Cosmochimica Acta*, 72(15): 3631-3641.
- Slack, J.F., Grenne, T., Bekker, A., Rouxel, O.J. and Lindberg, P.A., 2007. Suboxic deep seawater in the late Paleoproterozoic: Evidence from hematitic chert and iron formation related to seafloor-hydrothermal sulfide deposits, central Arizona, USA. *Earth and Planetary Science Letters*, 255(1-2): 243-256.
- Sleep, N.H., 1992. Archean plate tectonics: what can be learned from continental geology? *Canadian Journal of Earth Sciences*, 29(10): 2066–2071
- Sleep, N.H., 2000. Evolution of the mode of convection within terrestrial planets. *Journal of Geophysical Research*, 105(E7): 563 - 578.
- Sleep, N.H. and Zahnle, K., 2001. Carbon dioxide cycling and implications for climate on ancient Earth. *Journal of Geophysical Research*, 106(E1): 1373–1399.
- Smithies, R.H., Champion, D.C. and Cassidy, K.F., 2003. Formation of Earth's early Archaean continental crust. *Precambrian Research*, 127(1-3): 89-101.
- Span, D., Dominik, J., Loizeau, J.L., Belzile, N. and Vernet, J.P., 1992. Phosphorus trapping by turbidites in deep-lake sediments. *Chemical Geology*, 102(1-4): 73-82.
- Spencer, A.M., 1971. Late Pre-Cambrian Glaciation in Scotland. *Memoirs of the Geological Society*, London, 6.
- Sprigg, R.C., 1947. Early Cambrian (?) jellyfishes from the Flinders ranges, South Australia. *Transactions of the Royal Society of South Australia*, 71 (Pt. 2): 212 - 224.
- Sprigg, R.C., 1949. Early Cambrian "jellyfishes" of Ediacara, South Australia and Mount John, Kimberley District, Western Australia. *Transactions of the Royal Society of South Australia*, 73 (Pt. 1): 72 - 99.
- Squire, R.J., Campbell, I.H., Allen, C.M. and Wilson, C.J.L., 2006. Did the Transgondwanan Supermountain trigger the explosive radiation of animals on Earth? *Earth and Planetary Science Letters*, 250(1-2): 116-133.
- Stanley, S.M., 1976. Ideas on the timing of metazoan diversification. *Paleobiology*, 2(3): 209-219.
- Staudigel, H., Hart, S.R., Schmincke, H.-U. and Smith, B.M., 1989. Cretaceous ocean crust at DSDP Sites 417 and 418: Carbon uptake from weathering versus loss by magmatic outgassing. *Geochimica et Cosmochimica Acta*, 53(11): 3091-3094.
- Stein, R., 1990. Organic carbon content/sedimentation rate relationship and its paleoenvironmental significance for marine sediments. *Geo-Marine Letters*, 10(1): 37-44.
- Steiner, M., 1994. Die Neoproterozoischen Megalgen Sudchinas. *Berliner Geowissenschaftliche Abhandlungen*, 15: 1-146.
- Steiner, M., 2001. Die fazielle Entwicklung und Fossilverbreitung auf der Yangtze Plattform (Südchina) im Neoproterozoikum/frühesten Kambrium. *Freiberger Forschungshefte*, 492: 1-26.
- Steiner, M., Li, G., Qian, Y., Zhu, M. and Erdtmann, B.-D., 2007. Neoproterozoic to Early Cambrian small shelly fossil assemblages and a revised biostratigraphic correlation of the Yangtze Platform (China). *Palaeogeography, Palaeoclimatology, Palaeoecology*, 254(1-2): 67-99.
- Steiner, M., Mehl, D., Reitner, J. and Erdtmann, B., 1993. Oldest entirely preserved sponges and other fossils from the Lowermost Cambrian and a new facies reconstruction of the Yangtze Platform (China). *Berliner Geowissenschaftliche Abhandlungen (E)*, 9: 293-329.
- Steiner, M., Wallis, E., Erdtmann, B.-D., Zhao, Y. and Yang, R., 2001a. Submarine-hydrothermal exhalative ore layers in black shales from South China and associated fossils -- insights into a Lower Cambrian facies and bio-evolution. *Palaeogeography, Palaeoclimatology, Palaeoecology*, 169(3-4): 165-191.
- Steiner, M., Zhu, M., Weber, B. and Geyer, G., 2001b. The Lower Cambrian of eastern Yunnan: trilobite-based biostratigraphy and related faunas. *Acta Palaeontologica Sinica*, 40(SUPP): 63-79.

- Stern, R.J., 1994. Arc-assembly and continental collision in the Neoproterozoic East African Orogen; implications for the consolidation of Gondwanaland. *Annual Review of Earth and Planetary Sciences*, 22: 319-351.
- Stern, R.J., 2005. Evidence from ophiolites, blueschists, and ultrahigh-pressure metamorphic terranes that the modern episode of subduction tectonics began in Neoproterozoic time. *Geology*, 33(7): 557-560.
- Stern, R.J., 2008. Neoproterozoic crustal growth: The solid Earth system during a critical episode of Earth history. *Gondwana Research*, 14(1-2): 33-50.
- Stern, R.J., Avigad, D., Miller, N. and Beyth, M., 2008. From Volcanic Winter to Snowball Earth: An Alternative Explanation for Neoproterozoic Biosphere Stress, Links Between Geological Processes, Microbial Activities&Evolution of Life, pp. 313-337.
- Stille, P. et al., 2003. REE mobility in groundwater proximate to the natural fission reactor at Bangombé (Gabon). *Chemical Geology*, 198(3-4): 289-304.
- Strauss, H., 2004. 4 Ga of seawater evolution: Evidence from the sulfur isotopic composition of sulfate. *Geological Society of America Special Papers*, 379: 195-205.
- Strauss, H., Bengtson, S., Myrow, P.M. and Vidal, G., 1992. Stable isotope geochemistry and palynology of the late Precambrian to Early Cambrian sequence in Newfoundland. *Canadian Journal of Earth Sciences*, 29(8): 1662-1673.
- Summons, R.E., Jahnke, L.L., Hope, J.M. and Logan, G.A., 1999. 2-Methylhopanoids as biomarkers for cyanobacterial oxygenic photosynthesis. *Nature*, 400(6744): 554-557.
- Sun, W., 1986. Late precambrian pennatulids (sea pens) from the eastern Yangtze Gorge, China: *Paracharnia* gen. nov. *Precambrian Research*, 31(4): 361-375.
- Sverjensky, D.A. and Lee, N., 2010. The Great Oxidation Event and Mineral Diversification. *Elements*, 6(1): 31-36.
- Tajika, E., 2003. Faint young Sun and the carbon cycle: implication for the Proterozoic global glaciations. *Earth and Planetary Science Letters*, 214(3-4): 443-453.
- Tang, S. and Liu, T., 1999. Origin of the early Sinian Minle manganese deposit, Hunan Province, China. *Ore Geology Reviews*, 15(1-3): 71-78.
- Taylor, S.R. and McLennan, S.M., 1985. *The continental crust: Its composition and evolution*. Blackwell Scientific Publications, Palo Alto, CA, 328 pp.
- Tessier, A., Campbell, P.G.C. and Bisson, M., 1979. Sequential extraction procedure for the speciation of particulate trace metals. *Analytical Chemistry*, 51(7): 844-851.
- Thompson, M.D. and Bowring, S.A., 2000. Age of the Squantum "tillite," Boston Basin, Massachusetts; U-Pb zircon constraints on terminal Neoproterozoic glaciation. *American Journal of Science*, 300(8): 630-655.
- Tice, M.M. and Lowe, D.R., 2004. Photosynthetic microbial mats in the 3,416-Myr-old ocean. *Nature*, 431(7008): 549-552.
- Torres, M.E., Brumsack, H.J., Bohrmann, G. and Emeis, K.C., 1996. Barite fronts in continental margin sediments: a new look at barium remobilization in the zone of sulfate reduction and formation of heavy barites in diagenetic fronts. *Chemical Geology*, 127(1-3): 125-139.
- Tosca, N.J. et al., 2010. Clay mineralogy, organic carbon burial, and redox evolution in Proterozoic oceans. *Geochimica et Cosmochimica Acta*, 74(5): 1579-1592.
- Towe, K.M., 1981. Biochemical keys to the emergence of complex life. In: J. Billingham (Editor), *Life in the Universe*. MIT Press, Cambridge, MA, pp. 297-305.
- Tribovillard, N., Riboulleau, A., Lyons, T. and Baudin, F., 2004. Enhanced trapping of molybdenum by sulfurized marine organic matter of marine origin in Mesozoic limestones and shales. *Chemical Geology*, 213(4): 385-401.



- Tricca, A. et al., 1999. Rare earth elements and Sr and Nd isotopic compositions of dissolved and suspended loads from small river systems in the Vosges mountains (France), the river Rhine and groundwater. *Chemical Geology*, 160(1-2): 139-158.
- Trompette, R., 1997. Neoproterozoic (~600 Ma) aggregation of Western Gondwana: a tentative scenario. *Precambrian Research*, 82: 101-112.
- Turchyn, A.V. and Schrag, D.P., 2004. Oxygen Isotope Constraints on the Sulfur Cycle over the Past 10 Million Years. *Science*, 303(5666): 2004-2007.
- Ugidos, J.M., Armenteros, I., Barba, P., Valladares, M.I. and Colmenero, J.R., 1997a. Geochemistry and petrology of recycled orogen-derived sediments: a case study from Upper Precambrian siliciclastic rocks of the Central Iberian Zone, Iberian Massif, Spain. *Precambrian Research*, 84(3-4): 163-180.
- Ugidos, J.M. et al., 1997b. Provenance of Upper Precambrian-Lower Cambrian shales in the Central Iberian Zone, Spain: evidence from a chemical and isotopic study. *Chemical Geology*, 136(1-2): 55-70.
- Valentine, J.W., 1980. Determinants of diversity in higher taxonomic categories. *Paleobiology*, 6(4): 444-450.
- Valentine, J.W., 1992. The macroevolution of phyla. In: J.H. Lipps and P.W. Signor (Editors), *Origin and Early Evolution of the Metazoa*. Plenum Press, New York, pp. 535-553.
- Valentine, J.W., 2002. Prelude to the Cambrian Explosion. *Annual Review of Earth and Planetary Sciences*, 30(1): 285-306.
- Valentine, J.W. and Moores, E.M., 1970. Plate-tectonic Regulation of Faunal Diversity and Sea Level: a Model. *Nature*, 228(5272): 657-659.
- Valentine, J.W. and Walker, T.D., 1986. Diversity trends within a model taxonomic hierarchy. *Physica D: Nonlinear Phenomena*, 2(1-3): 31-42.
- Van Cappellen, P. and Ingall, E.D., 1994. Benthic Phosphorus Regeneration, Net Primary Production, and Ocean Anoxia: A Model of the Coupled Marine Biogeochemical Cycles of Carbon and Phosphorus. *Paleoceanography*, 9.
- Van der Weijden, C.H., 2002. Pitfalls of normalization of marine geochemical data using a common divisor. *Marine Geology*, 184(3-4): 167-187.
- van Os, B.J.H., Middelburg, J.J. and de Lange, G.J., 1991. Possible diagenetic mobilization of barium in sapropelic sediment from the eastern Mediterranean. *Marine Geology*, 100(1-4): 125-136.
- Vargas, M., Kashafi, K., Blunt-Harris, E.L. and Lovley, D.R., 1998. Microbiological evidence for Fe(III) reduction on early Earth. *Nature*, 395(6697): 65-67.
- Veevers, J.J., 2004. Gondwanaland from 650-500 Ma assembly through 320 Ma merger in Pangea to 185-100 Ma breakup: supercontinental tectonics via stratigraphy and radiometric dating. *Earth-Science Reviews*, 68(1-2): 1-132.
- Veizer, J., 1989. Strontium Isotopes in Seawater through Time. *Annual Review of Earth and Planetary Sciences*, 17(1): 141-167.
- Veizer, J. et al., 1999.  $^{87}\text{Sr}/^{86}\text{Sr}$ ,  $\delta^{13}\text{C}$  and  $\delta^{18}\text{O}$  evolution of Phanerozoic seawater. *Chemical Geology*, 161(1-3): 59-88.
- Veizer, J., Godderis, Y. and Francois, L.M., 2000. Evidence for decoupling of atmospheric  $\text{CO}_2$  and global climate during the Phanerozoic eon. *Nature*, 408(6813): 698-701.
- Veizer, J., Mackenzie, F.T., Heinrich, D.H. and Karl, K.T., 2003. *Evolution of Sedimentary Rocks, Treatise on Geochemistry*. Pergamon, Oxford, pp. 369-407.
- Vernhet, E., 2007. Paleobathymetric influence on the development of the late Ediacaran Yangtze platform (Hubei, Hunan, and Guizhou provinces, China). *Sedimentary Geology*, 197(1-2): 29-46.

- Vernhet, E., Heubeck, C., Zhu, M. and Zhang, J., 2006. Large-scale slope instability at the southern margin of the Ediacaran Yangtze platform (Hunan province, central China). *Precambrian Research*, 148(1-2): 32-44.
- Vernhet, E. and Reijmer, J.J.G., 2010. Sedimentary evolution of the Ediacaran Yangtze platform shelf (Hubei and Hunan provinces, Central China). *Sedimentary Geology*, 225(3-4): 99-115.
- Von Breyman, M.T., Emeis, K.-C. and Suess, E., 1992. Water depth and diagenetic constraints on the use of barium as a palaeoproductivity indicator. Geological Society, London, Special Publications, 64(1): 273-284.
- Vorliceck, T.P. and Helz, G.R., 2002. Catalysis by mineral surfaces: Implications for Mo geochemistry in anoxic environments. *Geochimica et Cosmochimica Acta*, 66(21): 3679-3692.
- Vorliceck, T.P., Kahn, M.D., Kasuya, Y. and Helz, G.R., 2004. Capture of molybdenum in pyrite-forming sediments: role of ligand-induced reduction by polysulfides. *Geochimica et Cosmochimica Acta*, 68(3): 547-556.
- Walcott, C.D., 1899. Precambrian fossiliferous formations. *Bulletin of the Geological Society of America*, 10: 199-204.
- Walker, J.C.G., 1977. *Evolution of the atmosphere*. Macmillan, New York.
- Walker, J.C.G., Hays, P.B. and Kasting, J.F., 1981. A negative feedback mechanism for the long-term stabilization of the earth's surface temperature. *Journal of Geophysical Research*, 86(C10): 9776-9782.
- Wallis, E., 2006. The climatic and environmental history of the south Chinese Yangtze platform during the Neoproterozoic and early Cambrian: hydrothermally active and salinity stratified epicontinental basins, a key for understanding the „Cambrian Explosion“? Doctoral Thesis Thesis, TU Berlin, Berlin, 227 pp.
- Walter, M.R., Veevers, J.J., Calver, C.R., Gorjan, P. and Hill, A.C., 2000. Dating the 840-544 Ma Neoproterozoic interval by isotopes of strontium, carbon, and sulfur in seawater, and some interpretative models. *Precambrian Research*, 100: 371-433.
- Wang, H.-Z. and Mo, X.-X., 1995. An outline of the tectonic evolution of China. *Episodes*, 18: 6-16.
- Wang, J. and Li, Z.X., 2003. History of Neoproterozoic rift basins in South China: implications for Rodinia break-up. *Precambrian Research*, 122: 141-158.
- Wang, K. et al., 1993. The great latest Ordovician extinction on the South China Plate: Chemostratigraphic studies of the Ordovician-Silurian boundary interval on the Yangtze platform. *Palaeogeography, Palaeoclimatology, Palaeoecology*, 104(1-4): 61-79.
- Wang, X.F., Erdtmann, B.-D., Chen, X.H. and Mao, X.D., 1998. Integrated sequence-, bio- and chemostratigraphy of the terminal Proterozoic to Lowermost Cambrian "black rock series" from central South China. *Episodes*, 21(3): 12.
- Wang, Y. and Van Cappellen, P., 1996. A multicomponent reactive transport model of early diagenesis: Application to redox cycling in coastal marine sediments. *Geochimica et Cosmochimica Acta*, 60(16): 2993-3014.
- Wang, Z. and Li, G., 1991. Barite and witherite deposits in Lower Cambrian shales of South China; stratigraphic distribution and geochemical characterization. *Economic Geology*, 86(2): 354-363.
- Warburg, O., 1920. Über die Geschwindigkeit der photochemischen Kohlensäurezersetzung in lebenden Zellen II. *Biochemische Zeitschrift*, 103: 188-217.
- Wasylenki, L.E., Anbar, A.D. and Gordon, G.W., 2006. Temperature dependence of Mo isotope fractionation during adsorption to  $\Delta$ -MnO<sub>2</sub>: Implications for the paleoredox proxy. *Geochimica et Cosmochimica Acta*, 70(18, Supplement 1): A691-A691.
- Watanabe, Y., Klarke, A.I., Poulson, S. and Ohmoto, H., 2005. The absence of mass independent sulfur isotope fractionation in Archean sedimentary rocks: evidence for an oxic atmosphere? , *Earth System Processes 2*, Calgary, Alberta, Canada.

- Weaver, C.E., 1967. Potassium, illite and the ocean. *Geochimica et Cosmochimica Acta*, 31(11): 2181-2196.
- Weaver, C.E., 1989. *Clays, Muds, and Shales. Developments in Sedimentology*, 44. Elsevier, Amsterdam, 819 pp.
- Wedepohl, K.H., 1971. Environmental influences on the chemical composition of shales and clays. *Physics and Chemistry of The Earth*, 8: 305-333.
- Wedepohl, K.H., 1995. The composition of the continental crust. *Geochimica et Cosmochimica Acta*, 59(7): 1217-1232.
- Weisfogh, T., 1964. Diffusion in Insect Wing Muscle, the Most Active Tissue Known. *Journal of Experimental Biology*, 41(2): 229-256.
- Wen, H. and Carignan, J., 2011. Selenium isotopes trace the source and redox processes in the black shale-hosted Se-rich deposits in China. *Geochimica et Cosmochimica Acta*, In Press, Accepted Manuscript.
- Werne, J.P., Lyons, T.W., Hollander, D.J., Formolo, M.J. and Sinninghe Damsté, J.S., 2003. Reduced sulfur in euxinic sediments of the Cariaco Basin: sulfur isotope constraints on organic sulfur formation. *Chemical Geology*, 195(1-4): 159-179.
- Werne, J.P., Sageman, B.B., Lyons, T.W. and Hollander, D.J., 2002. An integrated assessment of a "type euxinic" deposit: Evidence for multiple controls on black shale deposition in the middle Devonian Oatka Creek formation. *American Journal of Science*, 302(2): 110-143.
- Wetherill, G.W., Mark, R. and Lee-Hu, C., 1973. Chondrites: Initial Strontium-87/Strontium-86 Ratios and the Early History of the Solar System. *Science*, 182(4109): 281-283.
- Wijsman, J.W.M., Middelburg, J.J., Herman, P.M.J., Böttcher, M.E. and Heip, C.H.R., 2001. Sulfur and iron speciation in surface sediments along the northwestern margin of the Black Sea. *Marine Chemistry*, 74(4): 261-278.
- Wille, M., Nagler, T.F., Lehmann, B., Schroder, S. and Kramers, J.D., 2008. Hydrogen sulphide release to surface waters at the Precambrian/Cambrian boundary. *Nature*, 453(7196): 767-769.
- Williams, D.M., Kasting, J.F. and Frakes, L.A., 1998. Low-latitude glaciation and rapid changes in the Earth's obliquity explained by obliquity-oblateness feedback. *Nature*, 396(6710): 453-455.
- Williams, G. and Wallace, M., 2003. The Acraman asteroid impact, South Australia: magnitude and implications for the late Vendian environment. *Journal of the Geological Society*, 160(4): 545-554.
- Williams, G.E., 1975. Late Precambrian glacial climate and the Earth's obliquity. *Geological Magazine*, 112(5): 441-465.
- Williams, G.E., 1993. History of the earth's obliquity. *Earth-Science Reviews*, 34(1): 1-45.
- Williams, G.E., 2008. Proterozoic (pre-Ediacaran) glaciation and the high obliquity, low-latitude ice, strong seasonality (HOLIST) hypothesis: Principles and tests. *Earth-Science Reviews*, 87(3-4): 61-93.
- Windley, B.F., 1995. Uniformitarianism today: plate tectonics is the key to the past. *Geological Society, London, Memoirs*, 16(1): 11-23.
- Woese, C.R., 1987. Bacterial evolution. *Microbiology and Molecular Biology Reviews*, 51(2): 221-271.
- Woodhead, J.D., Hellstrom, J., Hergt, J.M., Greig, A. and Maas, R., 2007. Isotopic and Elemental Imaging of Geological Materials by Laser Ablation Inductively Coupled Plasma-Mass Spectrometry. *Geostandards and Geoanalytical Research*, 31(4): 331-343.
- Worsley, T.R. and Kidder, D.L., 1991. First-order coupling of paleogeography and CO<sub>2</sub>, with global surface temperature and its latitudinal contrast. *Geology*, 19(12): 1161-1164.
- Wortmann, U.G., Bernasconi, S.M. and Böttcher, M.E., 2001. Hypersulfidic deep biosphere indicates extreme sulfur isotope fractionation during single-step microbial sulfate reduction. *Geology*, 29(7): 647-650.

- Xiao, S., 2004. New Multicellular Algal Fossils and Acritarchs in Doushantuo Chert Nodules (Neoproterozoic; Yangtze Gorges, South China). *Journal of Paleontology*, 78(2): 393-401.
- Xiao, S. and Knoll, A.H., 2000. Phosphatized animal embryos from the Neoproterozoic Doushantuo Formation at Weng'an, Guizhou, South China. *Journal of Paleontology*, 74(5): 767-788.
- Xiao, S., Zhang, Y. and Knoll, A.H., 1998. Three-dimensional preservation of algae and animal embryos in a Neoproterozoic phosphorite. *Nature*, 391(6667): 553-558.
- Yamaguchi, K., 2002. Geochemistry of Archean Paleoproterozoic black shales: the early evolution of the atmosphere, oceans, and biosphere. PhD thesis Thesis, The Pennsylvania State University.
- Yamaguchi, K., 2003. Evolution of the atmospheric oxygen in the early Precambrian: An updated review of geological "evidence". *Frontier Research on Earth evolution*, 2: 9.
- Yang, A., Zhu, M., Zhang, J. and Li, G., 2003. Early Cambrian eodiscoid trilobites of the Yangtze Platform and their stratigraphic implications \*. *Progress in Natural Science*, 13: 861-866.
- Yang, J.-D., Sun, W.-G., Wang, Z.-Z. and Wang, Y.-X., 1996. Sm-Nd isotopic age of Precambrian-Cambrian boundary in China. *Geological Magazine*, 133(01): 53-61.
- Yang, J., Sun, W., Wang, Z., Xue, Y. and Tao, X., 1999. Variations in Sr and C isotopes and Ce anomalies in successions from China: evidence for the oxygenation of Neoproterozoic seawater? *Precambrian Research*, 93: 215-233.
- Yang, W.B. and Holland, H.D., 2003. The Hekpoort paleosol profile in Strata 1 at Gaborone, Botswana: soil formation during the Great Oxidation Event. *American Journal of Science*, 303(3): 187.
- Yin, C. et al., 2003. Lower boundary age of the Nanhua System and the Gucheng glacial stage: Evidence from SHRIMP II dating. *Chinese Science Bulletin*, 48(16): 1657-1662.
- Yin, L. et al., 2007. Doushantuo embryos preserved inside diapause egg cysts. *Nature*, 446(7136): 661-663.
- Yoon, H.S., Hackett, J.D., Ciniglia, C., Pinto, G. and Bhattacharya, D., 2004. A Molecular Timeline for the Origin of Photosynthetic Eukaryotes. *Molecular Biology and Evolution*, 21(5): 809-818.
- Young, G.M., von Brunn, V., Gold, D.J.C. and Minter, W.E.L., 1998. Earth's Oldest Reported Glaciation: Physical and Chemical Evidence from the Archean Mozaan Group (~2.9 Ga) of South Africa. *The Journal of Geology*, 106(5): 523-538.
- Yu, B., Dong, H., Widom, E., Chen, J. and Lin, C., 2009. Geochemistry of basal Cambrian black shales and cherts from the Northern Tarim Basin, Northwest China: Implications for depositional setting and tectonic history. *Journal of Asian Earth Sciences*, 34(3): 418-436.
- Yudovich, Y.E. and Ketris, M., 1994. *Elements in Black Shales*. Nauka, Ekaterinburg, 303 pp.
- Zartman, R.E. and Richardson, S.H., 2005. Evidence from kimberlitic zircon for a decreasing mantle Th/U since the Archean. *Chemical Geology*, 220(3-4): 263-283.
- Zerkle, A.L., House, C.H., Cox, R.P. and Canfield, D.E., 2006. Metal limitation of cyanobacterial N<sub>2</sub> fixation and implications for the Precambrian nitrogen cycle. *Geobiology*, 4(4): 285-297.
- Zhang, S., Jiang, G., Dong, J., Han, Y. and Wu, H., 2008a. New SHRIMP U-Pb age from the Wuqiangxi Formation of Banxi Group: Implications for rifting and stratigraphic erosion associated with the early Cryogenian (Sturtian) glaciation in South China. *Science in China Series D: Earth Sciences*, 51(11): 1537-1544.
- Zhang, S., Jiang, G. and Han, Y., 2008b. The age of the Nantuo Formation and Nantuo glaciation in South China. *Terra Nova*, 20(4): 289-294.
- Zhang, S. et al., 2005. U-Pb sensitive high-resolution ion microprobe ages from the Doushantuo Formation in south China: Constraints on late Neoproterozoic glaciations. *Geology*, 33(6): 473-476.
- Zhang, S., Li, Z.-X. and Wu, H., 2006. New Precambrian palaeomagnetic constraints on the position of the North China Block in Rodinia. *Precambrian Research*, 144(3-4): 213-238.

- Zhang, X.G. and Hou, X.G., 2007. Gravitational constraints on the burial of Chengjiang fossils. *Palaios*, 22(4): 448-453.
- Zhang, Y., Yin, L., Xiao, S. and Knoll, A., 1998. Permineralized fossils from the terminal Proterozoic Doushantuo Formation, south China. *Memoir (The Paleontological Society)*, 50: 1-52.
- Zhao, G., Cawood, P., Wilde, S. and Sun, M., 2002. Review of global 2.1–1.8 Ga orogens: Implications for a pre-Rodinia supercontinent. *Earth Science Reviews*, 59(1-4): 125-162.
- Zhao, G., Sun, M., Wilde, S. and Li, S., 2004. A Paleo-Mesoproterozoic supercontinent: assembly, growth and breakup. *Earth Science Reviews*, 67(1-2): 91-123.
- Zhao, J.-H., Zhou, M.-F., Yan, D.-P., Zheng, J.-P. and Li, J.-W., 2011. Reappraisal of the ages of Neoproterozoic strata in South China: No connection with the Grenvillian orogeny. *Geology*, 39(4): 299-302.
- Zhao, Z. et al., 1988. *The Sinian System of Hubei*. China University of Geosciences Press, Wuhan.
- Zheng, Y.-F. et al., 2004. Zircon U-Pb and oxygen isotope evidence for a large-scale  $^{18}\text{O}$  depletion event in igneous rocks during the Neoproterozoic. *Geochimica et Cosmochimica Acta*, 68(20): 4145-4165.
- Zheng, Y., Anderson, R.F., van Geen, A. and Kuwabara, J., 2000. Authigenic molybdenum formation in marine sediments: a link to pore water sulfide in the Santa Barbara Basin. *Geochimica et Cosmochimica Acta*, 64(24): 4165-4178.
- Zhou, C. et al., 2004a. New constraints on the ages of Neoproterozoic glaciations in south China. *Geology*, 32(5): 437-440.
- Zhou, C. and Xiao, S., 2007. Ediacaran  $\delta^{13}\text{C}$  chemostratigraphy of South China. *Chemical Geology*, 237(1-2): 89-108.
- Zhou, C., Xie, G., McFadden, K.A., Xiao, S. and Yuan, X., 2007. The diversification and extinction of Doushantuo-Pertatataka acritarchs in South China: causes and biostratigraphic significance. *Geological Journal*, 42(3-4): 229-262.
- Zhou, J., Wang, X., Qiu, J. and Gao, J., 2004b. Geochemistry of Meso- and Neoproterozoic mafic-ultramafic rocks from northern Guangxi, China: Arc or plume magmatism? *GEOCHEMICAL JOURNAL-JAPAN*, 38(2): 139-152.
- Zhou, M., Kennedy, A., Sun, M., Malpas, J. and Lesher, C., 2002a. Neoproterozoic arc-related mafic intrusions along the northern margin of South China: Implications for the accretion of Rodinia. *The Journal of Geology*, 110(5): 611-618.
- Zhou, M., Yan, D., Kennedy, A., Li, Y. and Ding, J., 2002b. SHRIMP U-Pb zircon geochronological and geochemical evidence for Neoproterozoic arc-magmatism along the western margin of the Yangtze Block, South China. *Earth and Planetary Science Letters*, 196(1-2): 51-67.
- Zhu, M., 1997. Precambrian-Cambrian trace fossils from eastern Yunnan, China: implications for Cambrian explosion. *Bull. Nat. Mus. Nat. Sci*, 10: 275-312.
- Zhu, M. et al., 2001. Early Cambrian stratigraphy of east Yunnan, southwestern China: a synthesis. *Acta Palaeontologica Sinica*, 40(SUPP): 4-39.
- Zhu, M.Y. et al., 2003. Sinian-Cambrian stratigraphic framework for shallow- to deep-water environments of the Yangtze platform: an integrated approach. *Progress in Natural Science*, 13(12): 951-960.
- Zhuang, H. et al., 1999. Evidence for transforming mineralization of Baiguoyuan silver-vanadium deposit hosted in black shale in Hubei, China. *Chinese Science Bulletin*, 44(3): 263-267.
- Zhuravlev, A.Y., 2001. Biotic diversity and structure during the Neoproterozoic-Ordovician transition. In: A.Y. Zhuravlev and R. Riding (Editors), *The Ecology of the Cambrian Radiation*. Columbia University Press, New York, pp. 173-199.

## References used for the trace-metal, TOC and S compilations (chapters 1 and 2)

- Alberdi-Genolet, M. and Tocco, R., 1999. Trace metals and organic geochemistry of the Machiques Member (Aptian-Albian) and La Luna Formation (Cenomanian-Campanian), Venezuela. *Chemical Geology*, 160(1-2): 19-38.
- Anbar, A.D. et al., 2007. A Whiff of Oxygen Before the Great Oxidation Event? *Science*, 317(5846): 1903-1906.
- Böning, P. et al., 2004. Geochemistry of Peruvian near-surface sediments. *Geochimica et Cosmochimica Acta*, 68(21): 4429-4451.
- Brumsack, H.-J., 1991. Inorganic geochemistry of the German "Posidonia Shale": palaeoenvironmental consequences. Geological Society, London, Special Publications, 58(1): 353-362.
- Canfield, D.E. and Farquhar, J., 2009. Animal evolution, bioturbation, and the sulfate concentration of the oceans. *Proceedings of the National Academy of Sciences*, 106(20): 8123-8127.
- Caplan, M.L. and Bustin, R.M., 1998. Sedimentology and sequence stratigraphy of Devonian-Carboniferous strata, southern Alberta. *Bulletin of Canadian Petroleum Geology*, 46(4): 487-514.
- Claypool, G.E., Holser, W.T., Kaplan, I.R., Sakai, H. and Zak, I., 1980. The age curves of sulfur and oxygen isotopes in marine sulfate and their mutual interpretation. *Chemical Geology*, 28: 199-260.
- Coveney, J.R.M. and Glascock, M.D., 1989. A review of the origins of metal-rich Pennsylvanian black shales, central U.S.A., with an inferred role for basinal brines. *Applied Geochemistry*, 4(4): 347-367.
- Dabard, M.-p. and Paris, F., 1986. Palaeontological and geochemical characteristics of Silurian black shale formations from the Central Brittany Domain of the Armorican Massif (northwest France). *Chemical Geology*, 55(1-2): 17-29.
- Dahl, T.W. et al., 2010. Devonian rise in atmospheric oxygen correlated to the radiations of terrestrial plants and large predatory fish. *Proceedings of the National Academy of Sciences*, 107(42): 17911-17915.
- Fox, J.S. and Videtich, P.E., 1997. Revised estimate of  $\delta^{34}\text{S}$  for marine sulfates from the Upper Ordovician: data from the Williston Basin, North Dakota, U.S.A. *Applied Geochemistry*, 12(1): 97-103.
- Fyffe, L. and Pickerill, R., 1993. Geochemistry of Upper Cambrian-Lower Ordovician black shale along a northeastern Appalachian transect. *Geological Society of America Bulletin*, 105(7): 897.
- Gellatly, A.M. and Lyons, T.W., 2005. Trace sulfate in mid-Proterozoic carbonates and the sulfur isotope record of biospheric evolution. *Geochimica et Cosmochimica Acta*, 69(15): 3813-3829.
- Gill, B.C. et al., 2011. Geochemical evidence for widespread euxinia in the Later Cambrian ocean. *Nature*, 469(7328): 80-83.
- Goldberg, T., Poulton, S.W. and Strauss, H., 2005. Sulphur and oxygen isotope signatures of late Neoproterozoic to early Cambrian sulphate, Yangtze Platform, China: Diagenetic constraints and seawater evolution. *Precambrian Research*, 137(3-4): 223-241.
- Gorjan, P., Walter, M.R. and Swart, P.K., 2003. Global Neoproterozoic (Sturtian) post-glacial sulfide-sulfur isotope anomaly recognised in Namibia. *Journal of African Earth Sciences*, 36(1-2): 89-98
- Guo, Q. et al., 2007. Trace element chemostratigraphy of two Ediacaran-Cambrian successions in South China: Implications for organosedimentary metal enrichment and silicification in the Early Cambrian. *Palaeogeography, Palaeoclimatology, Palaeoecology*, 254(1-2): 194-216.

- Hatch, J.R. and Leventhal, J.S., 1992. Relationship between inferred redox potential of the depositional environment and geochemistry of the Upper Pennsylvanian (Missourian) Stark Shale Member of the Dennis Limestone, Wabaunsee County, Kansas, U.S.A. *Chemical Geology*, 99(1-3): 65-82.
- Hirner, A.V. and Xu, Z., 1991. Trace metal speciation in Julia Creek oil shale. *Chemical Geology*, 91(2): 115-124.
- Holser, W.T. and Kaplan, I.R., 1966. Isotope geochemistry of sedimentary sulfates. *Chemical Geology*, 1: 93-135.
- Hough, M.L. et al., 2006. A major sulphur isotope event at c. 510 Ma: a possible anoxia-extinction-volcanism connection during the Early-Middle Cambrian transition? *Terra Nova*, 18(4): 257-263.
- Hurtgen, M.T., Arthur, M.A. and Halverson, G.P., 2005. Neoproterozoic sulfur isotopes, the evolution of microbial sulfur species, and the burial efficiency of sulfide as sedimentary pyrite. *Geology*, 33(1): 41-44.
- Hurtgen, M.T., Arthur, M.A. and Prave, A.R., 2004. The sulfur isotope composition of carbonate-associated sulfate in Mesoproterozoic to Neoproterozoic carbonates from Death Valley, California. *Geological Society of America Special Papers*, 379: 177-194.
- Hurtgen, M.T., Arthur, M.A., Suits, N.S. and Kaufman, A.J., 2002. The sulfur isotopic composition of Neoproterozoic seawater sulfate: implications for a snowball Earth? *Earth and Planetary Science Letters*, 203(1): 413-429.
- Jenkyns, H.C., 1988. The early Toarcian (Jurassic) anoxic event; stratigraphic, sedimentary and geochemical evidence. *American Journal of Science*, 288(2): 101-151.
- Jiang, S.-Y. et al., 2006. Trace- and rare-earth element geochemistry and Pb–Pb dating of black shales and intercalated Ni–Mo–PGE–Au sulfide ores in Lower Cambrian strata, Yangtze Platform, South China. *Mineralium Deposita*, 41(5): 453-467.
- Jones, B. and Manning, D.A.C., 1994. Comparison of geochemical indices used for the interpretation of palaeoredox conditions in ancient mudstones. *Chemical Geology*, 111(1-4): 111-129.
- Kah, L.C., Lyons, T.W. and Frank, T.D., 2004. Low marine sulphate and protracted oxygenation of the Proterozoic biosphere. *Nature*, 431(7010): 834-838.
- Kendall, B., Creaser, R.A., Gordon, G.W. and Anbar, A.D., 2009. Re-Os and Mo isotope systematics of black shales from the Middle Proterozoic Velkerri and Wollongorang Formations, McArthur Basin, northern Australia. *Geochimica et Cosmochimica Acta*, 73(9): 2534-2558.
- Kendall, B. et al., 2010. Pervasive oxygenation along late Archaean ocean margins. *Nature Geoscience*, 3: 647-652.
- Leventhal, J.S., 1991. Comparison of organic geochemistry and metal enrichment in two black shales: Cambrian Alum Shale of Sweden and Devonian Chattanooga Shale of United States. *Mineralium Deposita*, 26(2): 104-112.
- Lewis, S., Henderson, R., Dickens, G., Shields, G. and Coxhell, S., 2010. The geochemistry of primary and weathered oil shale and coquina across the Julia Creek vanadium deposit (Queensland, Australia). *Mineralium Deposita*, 45(6): 599-620.
- Liu, T.-b., Maynard, J.B. and Alten, J., 2006. Superheavy S isotopes from glacier-associated sediments of the Neoproterozoic of south China: Oceanic anoxia or sulfate limitation? *Memoir 198: Evolution of Early Earth's Atmosphere, Hydrosphere, and Biosphere - Constraints from Ore Deposits*, 198(0): 205-222.
- Loukola-Ruskeeniemi, K., 1991. Geochemical evidence for the hydrothermal origin of sulphur, base metals and gold in Proterozoic metamorphosed black shales, Kainuu and Outokumpu areas, Finland. *Mineralium Deposita*, 26(2): 152-164.
- Lyons, T.W., Luepke, J.J., Schreiber, M.E. and Zieg, G.A., 2000. Sulfur geochemical constraints on mesoproterozoic restricted marine deposition: lower Belt Supergroup, northwestern United States. *Geochimica et Cosmochimica Acta*, 64(3): 427-437.

- Lyons, T.W., Werne, J.P., Hollander, D.J. and Murray, R.W., 2003. Contrasting sulfur geochemistry and Fe/Al and Mo/Al ratios across the last oxic-to-anoxic transition in the Cariaco Basin, Venezuela. *Chemical Geology*, 195(1-4): 131-157.
- Manikyamba, C. and Kerrich, R., 2006. Geochemistry of black shales from the Neoproterozoic Sandur Superterrane, India: First cycle volcanogenic sedimentary rocks in an intraoceanic arc-trench complex. *Geochimica et Cosmochimica Acta*, 70(18): 4663-4679.
- Manikyamba, C., Kerrich, R., González-Álvarez, I., Mathur, R. and Khanna, T.C., 2008. Geochemistry of Paleoproterozoic black shales from the Intracontinental Cuddapah basin, India: implications for provenance, tectonic setting, and weathering intensity. *Precambrian Research*, 162(3-4): 424-440.
- Meyer, F.M. and Robb, L.J., 1996. The geochemistry of black shales from the Chuniespoort Group, Transvaal Sequence, eastern Transvaal, South Africa. *Economic Geology*, 91(1): 111-121.
- Misi, A. and Veizer, J., 1998. Neoproterozoic carbonate sequences of the Una Group, Irece Basin, Brazil: chemostratigraphy, age and correlations. *Precambrian Research*, 89: 87-100.
- Montoya-Pino, C. et al., 2010. Global enhancement of ocean anoxia during Oceanic Anoxic Event 2: A quantitative approach using U isotopes. *Geology*, 38(4): 315-318.
- Mossman, D.J., Gauthier-Lafaye, F., Nagy, B. and Rigali, M.J., 1998. Geochemistry of Organic-Rich Black Shales Overlying the Natural Nuclear Fission Reactors of Oklo, Republic of Gabon. *Energy Sources, Part A: Recovery, Utilization, and Environmental Effects*, 20(6): 521 - 539.
- Paikaray, S., Banerjee, S. and Mukherji, S., 2008. Geochemistry of shales from the Paleoproterozoic to Neoproterozoic Vindhyan Supergroup: Implications on provenance, tectonics and paleoweathering. *Journal of Asian Earth Sciences*, 32(1): 34-48.
- Pancost, R.D. et al., 2004. Further evidence for the development of photic-zone euxinic conditions during Mesozoic oceanic anoxic events. *Journal of the Geological Society*, 161(3): 353-364.
- Pašava, J., Oszczepalski, S. and Du, A., 2010. Re-Os age of non-mineralized black shale from the Kupferschiefer, Poland, and implications for metal enrichment. *Mineralium Deposita*, 45(2): 189-199.
- Peryt, T.M., Halas, S., Kovalevych, V.M., Petrychenko, O.Y. and Dzhinoridze, N.M., 2005. The sulphur and oxygen isotopic composition of Lower Cambrian anhydrites in East Siberia. *Geological Quarterly*, 49(2): 235-242.
- Prokoph, A., Shields, G.A. and Veizer, J., 2008. Compilation and time-series analysis of a marine carbonate  $\delta^{18}\text{O}$ ,  $\delta^{13}\text{C}$ ,  $^{87}\text{Sr}/^{86}\text{Sr}$  and  $\delta^{34}\text{S}$  database through Earth history. *Earth Science Reviews*, 87(3-4): 113-133.
- Quan, T.M., van de Schootbrugge, B., Field, M.P., Rosenthal, Y. and Falkowski, P.G., 2008. Nitrogen isotope and trace metal analyses from the Mingolsheim core (Germany): Evidence for redox variations across the Triassic-Jurassic boundary. *Global Biogeochem. Cycles*, 22.
- Raiswell, R. and Berner, R.A., 1986. Pyrite and organic matter in Phanerozoic normal marine shales. *Geochimica et Cosmochimica Acta*, 50(9): 1967-1976.
- Ries, J.B., Fike, D.A., Pratt, L.M., Lyons, T.W. and Grotzinger, J.P., 2009. Superheavy pyrite ( $\delta^{34}\text{S}_{\text{pyr}} > \delta^{34}\text{S}_{\text{CAS}}$ ) in the terminal Proterozoic Nama Group, southern Namibia: A consequence of low seawater sulfate at the dawn of animal life. *Geology*, 37(8): 743-746.
- Romer, R.L. and Hahne, K., 2010. Life of the Rheic Ocean: Scrolling through the shale record. *Gondwana Research*, 17(2-3): 236-253.
- Sageman, B.B. et al., 2003. A tale of shales: the relative roles of production, decomposition, and dilution in the accumulation of organic-rich strata, Middle-Upper Devonian, Appalachian basin. *Chemical Geology*, 195(1-4): 229-273.



- Scheiderich, K., Zerkle, A.L., Helz, G.R., Farquhar, J. and Walker, R.J., 2010. Molybdenum isotope, multiple sulfur isotope, and redox-sensitive element behavior in early Pleistocene Mediterranean sapropels. *Chemical Geology*, 279(3-4): 134-144.
- Schröder, S. and Grotzinger, J.P., 2007. Evidence for anoxia at the Ediacaran-Cambrian boundary: the record of redox-sensitive trace elements and rare earth elements in Oman. *Journal of the Geological Society*, 164(1): 175-187.
- Scott, C. et al., 2008. Tracing the stepwise oxygenation of the Proterozoic ocean. *Nature*, 452(7186): 456-460.
- Scott, C.T. et al., 2011. Late Archean euxinic conditions before the rise of atmospheric oxygen. *Geology*, 39(2): 119-122.
- Shen, Y., Canfield, D.E. and Knoll, A.H., 2002. Middle Proterozoic ocean chemistry: Evidence from the McArthur Basin, northern Australia. *American Journal of Science*, 302(2): 81-109.
- Shen, Y., Schidlowski, M. and Chu, X., 2000. Biogeochemical approach to understanding phosphogenic events of the terminal Proterozoic to Cambrian. *Palaeogeography, Palaeoclimatology, Palaeoecology*, 158(1-2): 99-108.
- Shields, G., Kimura, H., Yang, J. and Gammon, P., 2004. Sulphur isotopic evolution of Neoproterozoic-Cambrian seawater: new francolite-bound sulphate  $\delta^{34}\text{S}$  data and a critical appraisal of the existing record. *Chemical Geology*, 204(1-2): 163-182.
- Shields, G.A., Strauss, H., Howe, S.S. and Siegmund, H., 1999. Sulphur isotope compositions of sedimentary phosphorites from the basal Cambrian of China: implications for Neoproterozoic-Cambrian biogeochemical cycling. *Journal of the Geological Society*, 156(5): 943-955.
- Siebert, C., Kramers, J.D., Meisel, T., Morel, P. and Nägler, T.F., 2005. PGE, Re-Os, and Mo isotope systematics in Archean and early Proterozoic sedimentary systems as proxies for redox conditions of the early Earth. *Geochimica et Cosmochimica Acta*, 69(7): 1787-1801.
- Tayel El-Hasan, A.-K., 2008. Geochemistry of redox-sensitive trace elements and its implication on the mode of formation of the Upper Cretaceous oil shales, Central Jordan. *Neues Jahrbuch fuer Geologie und Palaeontologie - Abhandlungen*, 249: 333-344.
- Tribovillard, N.-P. et al., 1994. Geochemical study of organic-matter rich cycles from the Kimmeridge Clay Formation of Yorkshire (UK): productivity versus anoxia. *Palaeogeography, Palaeoclimatology, Palaeoecology*, 108(1-2): 165-181.
- Ugidos, J.M., Armenteros, I., Barba, P., Valladares, M.I. and Colmenero, J.R., 1997. Geochemistry and petrology of recycled orogen-derived sediments: a case study from Upper Precambrian siliciclastic rocks of the Central Iberian Zone, Iberian Massif, Spain. *Precambrian Research*, 84(3-4): 163-180.
- Strauss, H., 1993. The sulfur isotopic record of Precambrian sulfates: new data and a critical evaluation of the existing record. *Precambrian Research*, 63(3-4): 225-246.
- Strauss, H., 1999. Geological evolution from isotope proxy signals - sulfur. *Chemical Geology*, 161(1-3): 89-101.
- Strauss, H., Banerjee, D.M. and Kumar, V., 2001. The sulfur isotopic composition of Neoproterozoic to early Cambrian seawater -- evidence from the cyclic Hanseran evaporites, NW India. *Chemical Geology*, 175(1-2): 17-28.
- Walter, M.R., Veevers, J.J., Calver, C.R., Gorjan, P. and Hill, A.C., 2000. Dating the 840-544 Ma Neoproterozoic interval by isotopes of strontium, carbon, and sulfur in seawater, and some interpretative models. *Precambrian Research*, 100: 371-433.
- Wallis, E., 2006. The climatic and environmental history of the south Chinese Yangtze platform during the Neoproterozoic and early Cambrian: hydrothermally active and salinity stratified epicontinental basins, a key for understanding the „Cambrian Explosion“? Doctoral Thesis Thesis, TU Berlin, Berlin, 227 pp.

- Werne, J.P., Sageman, B.B., Lyons, T.W. and Hollander, D.J., 2002. An integrated assessment of a "type euxinic" deposit: Evidence for multiple controls on black shale deposition in the middle Devonian Oatka Creek formation. *American Journal of Science*, 302(2): 110-143.
- Wille, M. et al., 2007. Evidence for a gradual rise of oxygen between 2.6 and 2.5 Ga from Mo isotopes and Re-PGE signatures in shales. *Geochimica et Cosmochimica Acta*, 71(10): 2417-2435.
- Yu, B., Dong, H., Widom, E., Chen, J. and Lin, C., 2009. Geochemistry of basal Cambrian black shales and cherts from the Northern Tarim Basin, Northwest China: Implications for depositional setting and tectonic history. *Journal of Asian Earth Sciences*, 34(3): 418-436.